UNIVERSITY
OF HULL

Investigation and characterization of MP derived from media conditioned by various cancer cell lines and their effect on *human umbilical vein endothelial cells* (HUVECs) under static and flow conditions.

being a thesis submitted in fulfilment of the

requirements for the degree of

Doctor of

Philosophy in Medical Sciences

in the University of Hull

by

Abdulrahman Eid Saeed Algarni

February 2020

Dedication

Firstly, I dedicate this thesis to my mother, Gharsah. Without her support, advice and pray, I would not complete this work. Secondly, I would like to dedicate this work to my beloved wife, Badriah, for her persistent support and patience. Third, I dedicate this thesis to my beautiful daughter, Danah, for helping me and understand my long hours in University to complete this work. Finally, I dedicate this work to my sweetheart Jasmine thank you for your love and affection.

Acknowledgements

First and foremost, I would like to express my sincere gratitude to Allah and praise him for helping me to complete this work. I would like to express my deepest appreciation to my supervisor Dr. Leigh Madden who has supported me through my research. Without his patience, knowledge and guidance, I wouldn't be able to complete this project. Many thanks also for his significant comments which helped me to finalise the thesis. I am very grateful to him, who has provided insightful comments about the project results and has offered much advice and useful comments. I would like also to extend my gratitude to Professor John Greenman for his support and guidance throughout my research project. Special thanks go to Dr. Alex and Linsey Malcolm for their assistance and training during my project.

I must convey my very special thanks to my best friend Dr. Ibrahim Al-Harthi for continuing listening to any complaints I had throughout the project and for his special assistance through my study. Also, I must convey my special thanks to my colleague Dr Farouq Garada, Dr. Meftah Mehdawi, and Dr. Anwar Fanan, and for their support and encouragement throughout my project. I also would like to thank my brother Dr. Saad Alahmari. Also, a very special thanks to Dr. Abdullah Shwish Al-Dwaihy and Dr. Abdullah Aloufi.

Finally, I would like to express my deepest gratitude to my family for supporting me during all my studies at University. Special gratitude to my mother and all my brothers specially Abdullah and Ali and sisters and a very special appreciation to my wife Badriah and my daughters Danah and Jasmine for their support and encouragement throughout my studies. Last but not least, I would like to thank the Saudi cultural bureau and higher ministry of education in Saudi Arabia for their continual financial support.

Publications and Conferences

Published Articles:

Algarni, A., Greenman, J. & Madden, L. A. (2019) Procoagulant tumour microvesicles attach to endothelial cells on biochips under microfluidic flow. *Biomicrofluidics*, 13(6), 064124.

Algarni, A., Greenman, J. and Madden, L.A., 2020. Doxorubicin Enhances Procoagulant Activity of Endothelial Cells after Exposure to Tumour Microparticles on Microfluidic Devices. *Bloods—International Open Access Journal of Hematology*, 1(1), pp.23-34.

Posters presentations:

Algarni, A., Greenman, J. and Madden, L.A., 2016. PO-48-Assessment of the procoagulant potential state of tumour-MP in cancer patients. *Thrombosis research*, *140*, p.S194.

Algarni, A., Greenman, J. and Madden, L.A., 2017. Tumour microvesicles interact with endothelial cells under venous flow in *vitro*. (Poster presented at ISTH2017, 2324—PB, Germany).

Abstract

Microparticles (MP) are procoagulant due to tissue factor and phospholipid exposure on the surface. MP are tumour-derived and can be a beneficial biomarker of cancer to recognize individuals who are susceptible to venous thrombosis. The aim of the presented work was to develop and validate an *in vitro* microfluidic system consisting of two distinct microfluidic biochips to enable the investigation of the relationship between tumour MP and endothelial cells *in vitro*. Firstly, a range of tumour cell lines were assessed for procoagulant activity (PCA) of the cells and also MP released into the media. Pancreatic AsPC-1, human glioma U87 ovarian ES-2 and SKOV-3, were found to have the highest PCA in both cell suspension and cell-free media, while pancreatic MIAPaCa-2 and ovarian A2780 had a lower PCA. Cell lines were then investigated as to whether or not they could form stable spheroids in 3D cell culture U87, AsPC-1 and ES-2 produced the most compact spheroids and had the fastest PCA. In contrast, PANC-1, MIAPaCa-2 and A2780 formed loose shaped spheroids and slower PCA. However, SKOV-3 showed small compact spheroid and slower PCA. Following the application of media flow, ES-2 and U87 were selected and transferred into the developed dual microfluidic biochips model. Labelled MP were quantified via flow cytometry and this showed MP concentration reduced over time suggesting attachment of tumour MP to HUVECs. This reduction in MP was further reflected with a loss of PCA associated with the media. The effect of Doxorubicin on tumour spheroids resulted in an increased PCA of an endothelial cell layer under flow condition. In conclusion, in this study a microfluidic two-chip dynamic model mimics the interstitial fluid flow showed that tumour MPs released from tumour spheroids attach to endothelial cells and potentially could be a mechanism of clot formation in cancer patients.

Contents

List of Figures

List of Tables

List of abbreviations

ATCC	American Type Culture Collection
ADP	Adenosine diphosphate
AML	Acute myeloid leukemia
APC	Activated protein C
asTF	Alternative spliced isoform Tissue Factor
bFGF	Fibroblast growth factor
BSA	Bovine serum albumin
Ca^{2+}	Calcium ion
$CaCl_2$	Calcium chloride
CD	Cluster of differentiation
CFSE	Carboxyfluorescein diacetate N-hydroxysuccinimidyl ester
CHA	chromogenic assay
CO_2	Carbone dioxide
CP	Cancer Procaogulant
CTCs	Circulating tumour cells
CTs	Clotting time in seconds
CVCs	Central venous catheters
dH_2O	Distilled water
DMEM	Dulbecco's Modified Eagle Medium
DMSO	Dimethyl sulfoxide
DNA	Deoxyribonucleic acid
DOX	Doxorubicin
DVT	Deep vein thrombosis
ECACC	European Collection of Cell Cultures
ECGM	Endothelial cell growth medium
ECM	Extracellular matrix
ECs	Endothelial cells
EDTA	Ethylenediaminetetraacetic acid
ELISA	Enzyme-linked immunosorbent assay

EMEM	Eagle's Minimum Essential Medium
EPCAM	Epithelial cell adhesion molecule
EPCR	Endothelial protein C receptor
EVs	Extracellular vesicles
FACS	Fluorescence-activated cell sorting
FBS	Foetal bovine serum
FITC	Fluorescein isothiocyanate
flTF	Full-length Tissue Factor
FSC	Forward scattering
GFP	Green fluorescent protein
GP	Glycoprotein
HCL	Hydrochloric acid
HEPES	4-(2-hydroxyethyl) -1-piperazineethanesulfonic acid)
HRP	Streptavidin- horseradish peroxidase
HUVECs	Human Umbilical Vein Endothelial Cells
ICAMs	Intercellular adhesion molecules
IMDM	Iscove's Modified Dulbecco's Medium
KCL	Potassium chloride
KDa	Kilodaltons
LOC	Lab-on-a-chip
MAPK	Mitogen-activated protein kinase
MCTS	Multicellular tumour spheroids
Ml	Millilitre
Mm	Millimolar
µL	Microliter
µS	Microsiemens
MP	Microparticles
MTS	(3- [4,5, dimethylthiazol-2-yl]-5-[3-carboxymethoxy-phenyl]-2- [4 sulfophenyl]-2H-tetrazolium, inner salt)
MV	Microvesicles

NK	Natural killer
Nm	Nanometre
Mm	Micrometre
NTPDase1	Nucleoside triphosphate diphosphohydrolase 1
O_2	Oxygen
P/S	Penicillin/streptomycin
PARs	Protease-activated receptors
PBS	Phosphate buffered saline
PCA	Procoagulant activity
PDMS	Poly-dimethylsiloxane
PE	Pulmonary embolism
PI3K	Phosphoinositide-3 kinase
PMMA	Poly methylmethacrylate
POC	Point-of-care
PolyHEMA	Poly-2-hydroxyethyl methacrylate
PS	Phosphatidylserine
PSGL-1	P-selectin glycoprotein ligand-1
PT	Prothrombin Time
RBC	red blood cells
RD	Reagent diluent
RNA	Ribonucleic acid
rpm	revolutions per minute
SSC	side scattering
TF	Tissue Factor
TFPI	TF pathway inhibitor
TM	Thrombomodulin
TNF- α	Tumour necrosis factor
TXA2	Thromboxane A2
UM-SCC-81B	University of Michigan-Squamous Cell Carcinoma-81B
V/V	volume/volume

VCAM-1	vascular cell adhesion molecule
VEGF	Vascular endothelial growth factor
VTE	Venous thromboembolism
VWF	von Willebrand factor

Chapter 1 General introduction

1.1 Cancer-associated Thrombosis (VTE)

Venous thromboembolism (VTE) is a condition associated with the formation of blood clots. VTE includes deep vein thrombosis (DVT) and pulmonary embolism (PE), and has an estimated annual incidence range from 104 to 183 per 100,000 persons among people of European ancestry (Heit, 2015). The association between cancer and VTE is well established. Up to 20% of adult cancer patients develop VTE during the course of their disease, which is recognized to be one of the leading causes of death in these patients (Brose & Lee, 2008; Khorana et al, 2007). The incidence rate of VTE in all cancers was 13.9 per 1,000 person-years in another study from the United Kingdom (Walker et al, 2013) (Table 1.1).

Table1.1: VTE incidence in UK.

Cancer type	Incidence rate per 1000 people	95% confidence interval (CI)
All cancers	14	13-14
pancreatic cancer	98	80-119
lung cancer	44	39-48
stomach cancer	37	31-45
ovarian cancer	31	27-36
uterine cancer	11	9-14
breast cancer	9	8-10

However, Horsted et al., 2012. systematic review data show somewhat higher incidences for the following cancer types: pancreatic cancer: 102/1000 (95% CI 70 to 151); lung cancer: 52/1000 (95% CI 38 to 70); breast cancer: 21/1000 (95% CI 10 to 41) and colorectal cancer: 33/1000 (95% CI 21 to 53) (Horsted et al, 2012; Walker et al, 2013).

VTE is a common cardiovascular disease and not unique to cancer. However, there is a considerable body of evidence that asserts that VTE is a frequent complication or comorbidity of malignancy and a significant contributor to mortality in cancer patients, with attribution of the association commonly attributed to French physician Armand Trousseau in 1865(Connolly & Francis, 2013; Connolly & Khorana, 2009; Hron et al, 2007).

VTE has been studied in variety of cancers including gastrointestinal (Khorana et al, 2006; Metcalf et al, 2017), breast (Levine et al, 1988; Mandala et al, 2009), pancreatic (Khorana et al, 2006; Mandalà et al, 2007), prostate (Ording et al, 2015; Secin et al, 2008), lung (Otten et al,

2004), liver (Rand et al, 2006), cerebral (Martinelli & De Stefano, 2010), ovarian (Otten et al, 2004; Tateo et al, 2005), brain (Brandes et al, 1997; Khorana et al, 2006), kidney (Falanga & Russo, 2012), uterine (Gonik et al, 2010; Rodriguez et al, 2011), and colorectal (Alcalay et al, 2006; Thaler et al, 2012a). Some cancers show higher incidences of VTE than others, particularly those related to hematological malignancies (Date et al, 2013; Geddings & Mackman, 2013). VTE occurs in cancer patients of all ages (Goldenberg et al, 2014). Cancer patients who experience VTE also experience poorer prognoses compared to individuals who have cancer without VTE (Caine et al, 2002; Carrier et al, 2015; Khorana, 2012; Tesselaar et al, 2007; Timp et al, 2013). Approximately 4–20% of cancer patients are expected to experience VTE at some point, the prevalence being the highest in the initial period of diagnosis. Annually, 0.5 % of patients with cancer would experience thrombosis compared to 0.1 % in the general population (Razak et al, 2018).

1.2 Cancer-induced hypercoagulability

VTE is considered a multifactorial disorder, due to the combination of genetic, acquired, and environmental factors (Manly et al, 2011). The pathogenesis of the cancer-associated coagulopathy is similarly complex and multifactorial. Most importantly, tumour cells gain the capacity to activate the host haemostatic system, and this phenomenon is driven by the same oncogenes responsible for the cellular neoplastic transformation. By this process, cancer tissues become capable of expressing different procoagulant proteins (i.e. Tissue Factor [TF], Cancer Procoagulant [CP], Factor VII), which contribute to the occurrence of the overt symptomatic coagulopathy in *vivo* (Falange et al, 2017). Malignancy appears to contribute to the hypercoagulable state through two main forms of interaction: firstly, its capacity to create and promote procoagulant and fibrinolytic activities, and secondly, its interactions with different kinds of blood cells such as endothelial cells, platelets, and monocytes (Caine et al, 2002; Date et al, 2017; Date et al, 2013; Seaman et al, 2014; Tesselaar et al, 2007). Recently platelets have received more attention for their role in cancer-associated VTE, with researchers noting that elevated platelet count is associated with an increased risk of cancer-associated thrombosis as a result of the presence of malignancy-activated platelets (Connolly et al, 2014; Mege et al, 2019) (Figure 1.1).

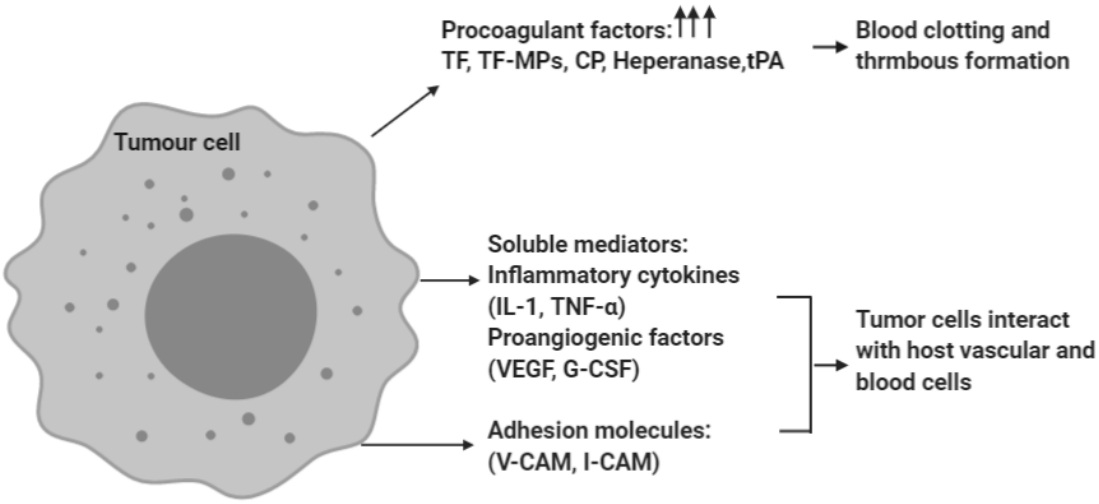

Figure 1.1: Image showing the principal mechanisms of hypercoagulability in cancer.
Tumour cells interact with haemostasis system via different pathways. Tumour cells can secret different procoagulant factors that activate blood coagulation system and impaired fibrinolysis activity. Also, tumour cells can secret different soluble cytokines and proangiogenic that interact with host normal cells such as endothelial cells, platelets and leukocytes and activate the expression of their procoagulant phonotype. Tumour cell also can interact with host cells via the adhesion molecules and this activate their procoagulant activity. Tissue factor (TF), Tissue Factor -bearing MP (TFMP) cancer procoagulant (CP), Interleukin-1 (IL-1), vascular endothelial growth factor (VEGF), Granulocyte-colony stimulating factor (G-CSF), vascular cell adhesion molecule (VCAM), Intercellular Adhesion Molecule (ICAM-1), Tumour Necrosis Factor alpha (TNF-a), Tissue plasminogen activator (tPA).

The shedding of procoagulant microparticles [MP] is also regulated by oncogenic events and further adds to the pathogenesis of the cancer-associated hypercoagulable state. MP are circulating, phospholipid-rich, particles of <1 μm diameter released from the membranes of platelets, endothelial cells, leucocytes and erythrocytes (Bucciarelli et al, 2012). In the past these MP were regarded as “cellular dust” resulting from apoptosis (Wolf, 1967) but research has demonstrated that MP actually serve many different functions including playing a role in inflammation, coagulation, vascular function, apoptosis, and cell proliferation and differentiation, depending on the constituents of the particle (Campello et al, 2011; Morel et al, 2011).

Tumours themselves can also produce substances which create the ideal conditions for the development of thrombosis. Davila et al. (2008) observed that malignant cells overexpress several different substances which activate the coagulation cascade – these substances include inflammatory cytokines, cancer procoagulant (a cysteine protease) and TF. With particular regard to TF, which will be examined more closely later in this introduction. Malignancies are able to promote hypercoagulability while simultaneously inhibiting anticoagulant activities and substances, as well as interfering with fibrinolysis, the processes by which blood clots are broken down (Date et al, 2013).

TF has been particularly implicated in cancer-induced VTE since malignancies have the ability to express TF and in the context of malignancies expression is significantly increased, enhancing the effects of TF-related hypercoagulability (Geddings & Mackman, 2013; Seaman et al, 2014). Aside from its traditional haemostatic role, surface TF is thought to further potentiate cancer progression, through an enhancement of angiogenesis and by facilitating metastasis, and possesses roles in primary tumour growth. *In vitro*, high levels of surface TF expression have been further correlated with cell invasion in pancreatic cancer cell lines (Date et al, 2013).

Malignancy appears to contribute to the hypercoagulable state through complex mechanisms. The principal mechanisms include the expression of procoagulant factors including: procoagulant proteins, such as TF and CP, MP, adhesion molecules and cytokines (Falanga et al, 2013). Another procoagulant protein is CPs, a cysteine protease that directly activates factor X independently of factor VII. CP is synthesized by malignant cells, and its activity has been found in extracts of different tumour (Donati et al, 1986; Mielicki et al, 1990). Another mechanism is elevation of coagulation factor levels (V, VIII, IX, and XI) (Edwards et al, 1987). In addition, circulating tumour cells possess the ability to adhere to endothelium through integrin and selectin adhesion molecules, therefore damage the endothelial cell anticoagulant mechanisms and promoting thrombogenesis (Giavazzi et al, 1993).

In addition, tumour cells may also release inflammatory cytokines (i.e. TNF-α, IL-1β) and proangiogenic factors (i.e. vascular endothelial growth factor [VEGF], basic fibroblast growth factor [bFGF]), that activate and induce the expression of a procoagulant phenotype by normal monocytes and Endothelium (Falanga et al, 2013; Folkman et al, 1988). Finally, the changes in the stromal cells of the tumour “niche” induced by tumour provide new evidence of the influence of the haemostasis system on cancer development (Falange et al, 2017).

1.3 VTE risk factors in cancer

There are several risk factors related to VTE which have been characterized as patient-related, cancer-related, and treatment-related risk factors (Khorana, 2012). These risks represent the demographic, disease, and management dimensions that can contribute to VTE. Patient-related risks include age, race/ethnicity, and comorbid conditions (Connolly & Francis, 2013; Khorana, 2012; Lee, 2010; Seaman et al, 2014; Timp et al, 2013). Though paediatric cancer patients can develop VTE (Goldenberg et al, 2014), the risk of VTE increases with age 60 years or older (OR 2.6; 95% CI1.2–5.7), (Khorana, 2012; Lee, 2010). And just as certain races/ethnicities are more prone to certain cancers, certain races/ethnicities are more prone

to VTE. African-Americans, for example, are at higher risk than Asian individuals (Khorana, 2012). Other risk factors, major surgery, trauma, malignancy or pregnancy, are responsible for development of VTE (Marik & Cavallazzi, 2015). Patients with a prior history of VTE unrelated to cancer are also at much higher risk (a 6- to 7-fold) for VTE in cancer than those cancer patients without such a history (Connolly & Francis, 2013).

While the incidence of cancer-associated VTE is reported as 1 in 200, which is four- to five-fold higher than that of the general population. Date et al. (2013) report that this risk is not uniformly distributed across difference cancer types. Although many kinds of cancer have already been studied and their related VTE risk measured, these results are contradictory, as the studies differ in relation to patient population, treatment protocols, follow-up length, research period and the detection and reporting method of VTE. (Date et al, 2013). Therefore, in terms of cancer-related factors, the type of cancer can either increase or decrease the risk of VTE. Certain kinds of cancer seem to more frequently facilitate the development of VTE; these include pancreatic, uterine, stomach, brain, kidney, lung, ovarian, and haematological cancers have higher rates of VTE (Connolly & Francis, 2013; Date et al, 2013; Khorana, 2012). On other hand, low risks (~10/1000 person-years (PY)) are generally seen in patients with breast or prostate cancer (Timp et al, 2013).This suggests that the site of cancer can increase the risk of VTE (Caine et al, 2002; Connolly & Francis, 2013; Connolly & Khorana, 2009; Faiz et al, 2015; Lee, 2010). The stage of the cancer can also make a difference; the more advanced the stage of the cancer, the higher the risk of VTE (Caine et al, 2002; Khorana, 2012; Timp et al, 2013).

In terms of treatment-related risk factors of VTE, surgery, chemotherapy, hormonal therapy, antiangiogenic agents, central venous catheters (CVCs), the utilization of erythropoiesis stimulating agents, and blood product transfusion are the primary causes (Caine et al, 2002; Connolly & Khorana, 2009; Khorana, 2012; Lee, 2010; Timp et al, 2013). Chemotherapy in particular has been implicated as a key factor in the development of VTE and this will be discussed later in the introduction (Blann & Dunmore, 2011; Connolly & Francis, 2013; Connolly & Khorana, 2009; Faiz et al, 2015; Falanga & Zacharski, 2005; Seaman et al, 2014). Surgery is also considered a significant risk increaser of VTE (Connolly & Francis, 2013; Khorana, 2012; Lee, 2010; Timp et al, 2013).

1.4 Venous Thrombosis

1.4.1 Mechanisms of hypercoagulability in cancer

Thrombosis occurs in cancer as a result of interference with the haemostatic system with particular regard to clotting mechanisms (Falanga et al, 2015). It accomplishes this interference

through the body's response to the tumour or through the processes of the tumour itself. Cytokines – responsible for the body's inflammatory response to invading bodies – have been connected to coagulation and present a good example of the mechanisms which can promote thrombosis in cancer. Demetz and Ott (2012) report that protease-activated receptors (PARs) mediate several different cell reactions, including those related to activated coagulation factors, as well as cytokine release, expression of adhesion molecules, cell migrations or proliferation, a finding echoed by Date et al. (2013) (Demetz & Ott, 2012). Therefore, when a malignancy prompts the body's inflammatory response, it automatically stimulates certain procoagulant activities which enable hypercoagulability which in turn promotes VTE. Additionally, as Caine et al. (2002) note, many elements of the other immune responses to malignancies including acute phase reactants, abnormal protein metabolism, necrosis, and hemodynamic rearrangements have the capacity to stimulate abnormal coagulant activity in cancer patients. Raised D-dimer or fibrin degradation product levels are also considered as indication of haemostatic system activation (Dikshit, 2015). In addition, some changes in the haemostatic system have been reported to contribute to cancer associated thrombosis that include activation of platelets and direct factor X, and the subsequent decrease in hepatic anticoagulant synthesis accompanied by reduced hepatic clearance of coagulation factors and presence of antiphospholipid antibodies (Noble & Pasi, 2010). Upregulation of TF due to activation of the proto-oncogene K-ras and mutation of the tumour suppression gene p53, is considered to play an important role in cancer associated thrombosis via promotion of the tumour growth and metastasis (Sheth et al, 2017). Microparticles bearing TF are shed from platelets, erythrocytes, tumour cells, endothelial cells, monocytes and lymphocytes. MP bearing TF can provide the anionic phospholipid surface required to promote coagulation (Davila et al, 2008; Lacroix & Dignat-George, 2012a; Manly et al, 2011; Nomura & Shimizu, 2015).

1.5 Haemostatic system and cancer

1.5.1 Background

The pathophysiology of VTE involves endothelial damage, blood stasis, and hypercoagulability (Chirinos et al, 2005). Cancer is able to disrupt the haemostatic system which in essence creates a chain reaction, prompting the activation of the coagulation protease cascade (Langer et al, 2008). The main points at which cancer contributes to haemostatic disruption and in turn to VTE are primary and secondary haemostasis.

1.5.2 Primary haemostasis

Primary haemostasis is the initial phase of platelet plugs formation. In a normal, non-injured state, platelets will not stick to cell surfaces or each other (Broos et al, 2011). This is because the endothelium in the vessels maintains an anticoagulant surface that serves to maintain blood in its fluid state (Gale, 2011). In the absence of injury, these anticoagulants include thrombomodulin and Tissue factor pathway inhibitor (TFPI), heparin-like proteoglycans and endothelial protein C receptor. When injury occurs the platelets "are exposed to subendothelial matrix, and adhesion and activation of platelets begins," with the platelets adhering to both the site of the injury in the endothelium and to each other (Gale, 2011; Ruggeri, 1997).

Platelets have multiple receptors on their surfaces which facilitate adhesion through targeting by several adhesive proteins (Gale, 2011). In order to prevent adhesion at other sites beyond the injury, the receptors are restricted through the proteins that bind with one another and to the platelet receptors. For example, binding between receptor GPIb-IX-V and immobilized von Willebrand factor (VWF) is facilitated via an interaction between GPIbα and the A1 domain of VWF" but soluble VWF in the circulation does not bind with high affinity to GPIbα (Gale, 2011; Hoffbrand & Steensma, 2019).

Platelet adherence and aggregation are strengthened through platelet-to-platelet connections as a result of αIIbβ3 binding to fibrinogen, VWF, fibronectin, or vitronectin; this can also be accomplished through αvβ3 binding to victronectin or thrombospondin; there is also some evidence that suggests that α5β1-fibronectin and α6β1-laminin interactions may play parts in the process. The interaction of integrin α2β1 and collagen strengthen adherence to the subendothelial collagen (Gale, 2011; McMichael, 2005) (Figure 1.2).

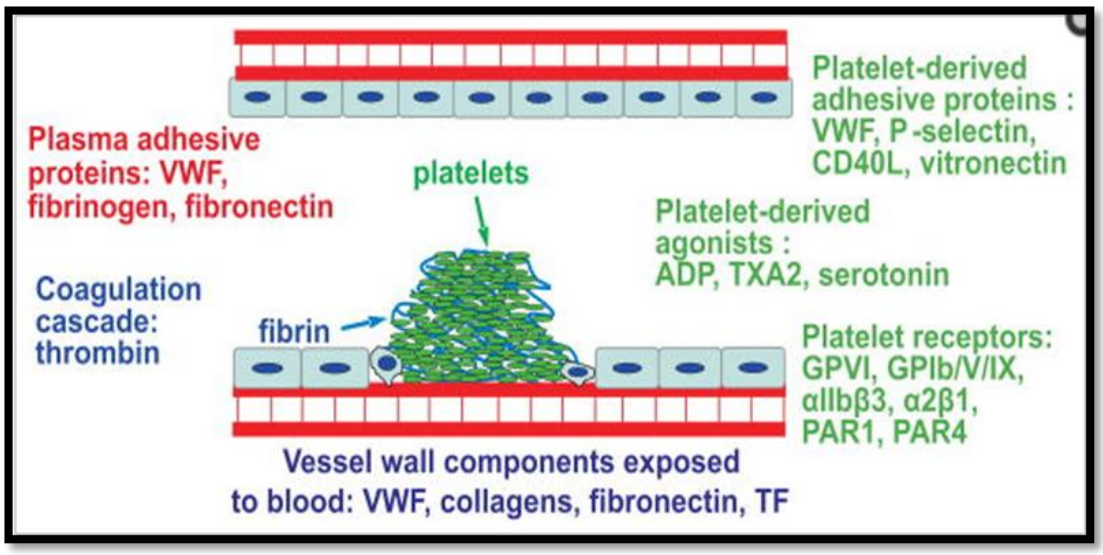

Figure 1.2: Image shows the primary haemostasis.
Platelet aggregation at the site of injury is mediated by platelet receptor agonists, platelet derived adhesive proteins and platelet-derived adhesive proteins derived from plasma. Fibrin deposition around the resulting platelet plug is generated by the coagulation cascade. ADP = adenosine diphosphate, thromboxane A2 = TXA2 and von Willebrand factor = VWF. (Gale, 2011).

1.5.3 Secondary haemostasis

At this point, secondary haemostasis is initiated. The strengthening of the initial patch occurs as a result of the soluble fibrin being changed into insoluble fibrin; this is accomplished through the cascade of coagulation serine proteases that culminates in cleavage of soluble fibrinogen by thrombin, creating a crosslinked fibrin mesh at the injury site (Gale, 2011; Monagle & Massicotte, 2011).

The creation of the insoluble fibrin occurs at the same time as aggregation of the platelets which contributes to clotting (Periayah et al, 2017). In non-injured and healthy vessels, the cascade is not activated; several anticoagulant mechanisms control the activation of the cascade including thrombomodulin and heparan sulfate proteoglycans on vascular endothelium (Gale, 2011). The significance of thrombomodulin is its role in converting thrombin from a procoagulant phase to an anticoagulant phase via stimulating activation of the anticoagulant serine protease protein C (Fuentes-Prior et al, 2000). Activated protein C (APC) is accelerated by binding to endothelial protein C receptor (EPCR) on the surface of endothelial cells. Then, APC becomes detached from EPCR and binds to its cofactor protein S and inactivates further thrombin generation by inactivating the cofactors FVa and FVIIIa (Hoffman, 2003). Thrombin is also able to activate platelets as a result of cleaving PAR1 and PAR4, and is responsible for the positive feedback activation of coagulation that is critical for clot propagation, whilst also activating factor XI which in turn activates factor IX (Gale, 2011). Thrombin is also capable of activating cofactors VIII and V; together all these interactions are

known as the intrinsic pathway of coagulation since they occur within the blood cells, though some researchers suggest that the dynamic is more like a feedback loop (Gale, 2011) (Figure1.3).

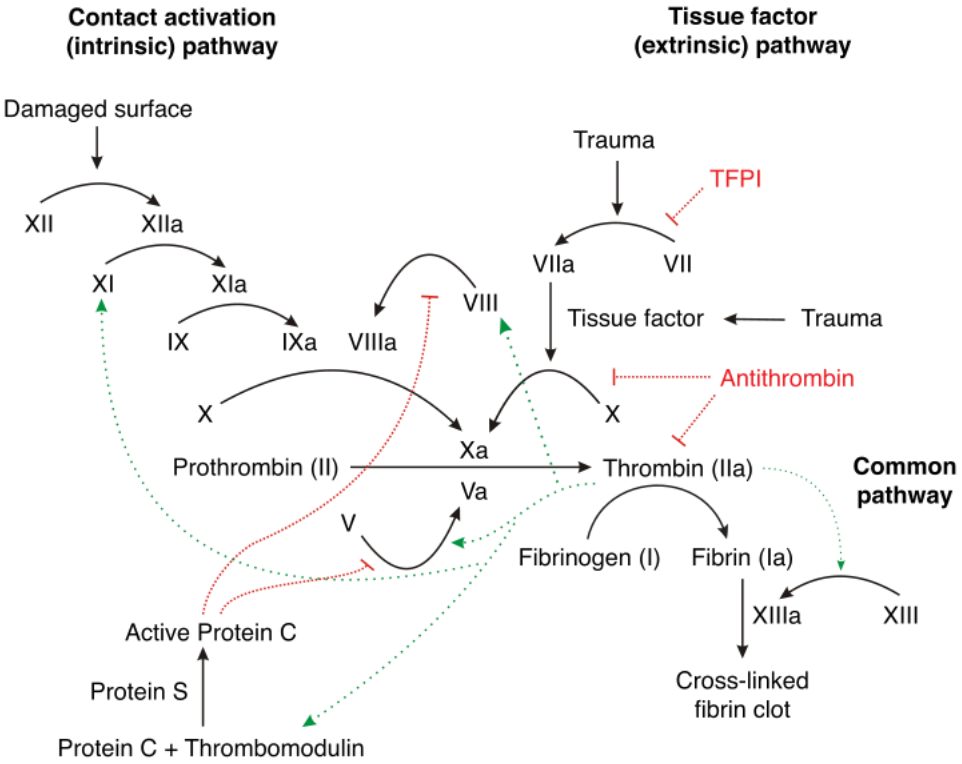

Figure 1.3: image shows secondary haemostasis.
TF initiates the extrinsic coagulation cascade that results in the formation of the serine protease thrombin. Thrombin carries out multiple functions, including the generation of fibrin, platelet activation, positive feedback activation of the intrinsic pathway (green arrows), and activation of negative feedback path (red arrows) of activated protein APC = activated protein C, FV = factor V, PS = protein S and TM = thrombomodulin. Adapted from (Gale, 2011).

Coagulation or clotting occurs after primary and secondary haemostasis. In essence, the purpose of haemostasis is to control bleeding. In the intrinsic pathway of coagulation, the effects and reactions occur to and within the platelets. But the platelets are not the only elements involved in the haemostatic process. Not only does injury expose the platelets to subendothelial matrix, blood is exposed to extravascular tissues which are rich in TF (Gale, 2011). TF is the key initiator for haemostasis (Rao & Pendurthi, 2005). It is a cofactor for serine protease factor VIIa; in order for factor X and factor IX to be activated, TF and factor VIIa must interact. This interaction of TF and VIIa to activate factors X and IX is known as the extrinsic pathway of coagulation (Butenas et al, 2005). Activations which follow the TF/VIIa interaction also produce thrombin (Chu, 2005; Gale, 2011). TF will be addressed more in-depth later in this chapter. What should be borne in mind is that the proteases and cofactors which facilitate pro- and anti-coagulation create complexes on negatively charged membrane surfaces that are

principally provided by activated platelets creating a localization of the effect; this is necessary to limit coagulation to the site of injury (Periayah et al, 2017). Without the localization and restriction of the effects of haemostasis, continuous activation of the coagulation cascade leads to consumption and depletion of coagulation proteins and platelets which induce bleeding (Ho et al, 2005).

1.6 Tissue factor (TF) and cancer

1.6.1 Background

TF is the key activator for the haemostatic process, serving as the protein component of tissue thromboplastin(Bach, 2006). TF, encoded by the F3 gene (Han et al, 2014), is a transmembrane 47-KDa-glycoprotein containing 263 amino acids known as full-length TF (flTF), factor III and CD142 (Han et al, 2014). It has an alternatively spliced isoform, referred to as soluble (asTF).

Apart from its role in haemostasis, TF is a key element in several other cellular processes such as intracellular signalling, cellular proliferation, and blood vessel development. TF occurs in normal blood and can be induced by mitogens, inflammatory cytokines, hormones, and hypoxia (Abdulkadir et al, 2000; Chu, 2011). With the considerable role that TF plays in the haemostatic system, its relevance to VTE, regardless of malignancy, is readily apparent. TF can readily travel through the circulatory system by way of vesicles (exosomes and MP) (Kleinjan et al, 2012). These MP offer TF a surface on which coagulant activity can occur (Kleinjan et al, 2012; Langer et al, 2008).

1.6.2 TF in cancer progression and angiogenesis

TF plays a role in cell signalling which can facilitate tumour growth as well as angiogenesis via the TF cytoplasmic domain coupled to proteolytic activation of the protease activated receptor (PAR) 2 or non-proteolytic integrin ligation (Ruf, 2012). The isoform of TF, asTF, has been implicated in angiogenesis; researchers have demonstrated that asTF can induce migration and capillary formation by endothelial cells, mediated by way of ligation with αvβ3 and α6β1 (Leppert & Eisenreich, 2015).

Leppert and Eisenreich (2015) demonstrated that asTF could also stimulate the proangiogenic potential and proliferation of immortalized cardiomyocytes, in addition to certain cancerous cells. Furthermore, additional research has determined that flTF and asTF both possessed the ability to influence proangiogenic processes but through different signalling pathways in both cancer and other pathophysiologic-relevant settings, such as vascular inflammation (Van Dreden et al, 2017).

1.6.3 Mechanisms of TF upregulation in cancer

Welsh et al. (2012) report around 100-150 pg/mL of TF circulates within the blood, most of which is thought to be associated with cellular microparticles in healthy individuals (Welsh et al, 2012). However, these levels have been found to be significantly elevated in a number of malignancies (Thaler et al, 2013). It should be noted at the outset that the upregulation of TF and its effects differ across malignancies, with some cancers engendering more TF production than others (Abdulkadir et al, 2000; Han et al, 2014; Thaler et al, 2013; Welsh et al, 2012).

TF upregulation can be attributed to the fact that both the body and the tumour can and will produce TF. This is somewhat the result of an increase in MP which is associated with tumour development, particularly tumour-derived MP (Welsh et al, 2012). The tumour-derived MP will necessarily be aberrant, given their origin, which in turn engenders abnormal behaviour. Furthermore, research – both *in vivo* and clinical data – has determined that the activation of the proto-oncogene K-ras and mutation of the tumour suppression gene p53, are primarily responsible for the upregulation of TF, where either the loss of function of p53 or activation of K-ras results in the activation of mitogen-activated protein kinase (MAPK) /phosphoinositide-3 kinase (PI3K) signalling pathway and subsequent induction of flTF expression (Han et al, 2014; Unruh et al, 2014). While gene suppression and silencing can sometimes result in downregulation of proteins such as tissue factor pathway inhibitor-2 (TFPI) which can engender malignancy (Sierko et al, 2007), in the case of TF the gene interference and K-ras activation prompts upregulation which can in turn promote tumour growth (van den Berg et al, 2012; Versteeg et al, 2004).

1.7 Microparticles (MP)

1.7.1 Background, function, and formation

Extracellular vehicles (EVs) that are either released by cells through multivesicular bodies, broken off from the cell surface, or both (Gold et al, 2015). composed of both larger (100-1000 nm) microvesicles (MV) also known as microparticles and nano-sized exosomes (<100nm) into the blood circulation. Initially, MP were believed to be little more than inert cellular debris or dust (Aleman et al, 2011; Campello et al, 2011; Shai & Varon, 2011), sometimes called “platelet dust” (Brodsky et al, 2004). However, the reality is that MP play many roles depending on their parent cells and the antigens the MP retain from the parent cells (Barteneva et al, 2013; Nomura & Shimizu, 2015).

MP can range in size from 0.1 to 1.0 µm (Aleman et al, 2011; Nomura & Shimizu, 2015), averaging ~200nm (Owens & Mackman, 2011), though some researchers insist this range is not

representative as a result of research protocols which may not be conducive to accurate sizing of the particles (Barteneva et al, 2013). MP are generally derived from cellular plasma membranes following structural changes involving local cytoskeletal rearrangements and membrane budding (Burnouf et al, 2015). Once the asymmetrical distribution of lipids between the inner and outer leaflets of a plasma membrane is lost the conditions are right for MP to form (Morel et al, 2011). When the cell is at rest phosphatidylserine (PS) is contained almost entirely in the inner monolayer; however, once stimulated by activation or apoptosis, the PS is externalized (such as through blebbing) or translocated, initializing the MP-creation process (Aupeix et al, 1997; Burnouf et al, 2015; Date et al, 2013; Morel et al, 2011). The cytoskeleton becomes less and less rigid as more and more externalization occurs; once this process has achieved completion, the MP are shed and enter circulation (Burnouf et al, 2015). Cellular activation or apoptosis leads to an increased release of calcium ions (Ca^{2+}) that activates proteases, including calpain. Such triggered proteases contribute to degradation of the cytoskeleton. The activation of apoptosis also stimulates apoptotic proteins, or caspases. Caspase-3 will break ROCK 1 into a constitutive truncated shape that then enhances phosphorylation and thereby activation of myosin light-chain (MLC) kinases which leads to cell membrane blebbing of the cell membrane(Muhsin-Sharafaldine & McLellan, 2018)(Figure 1.4).

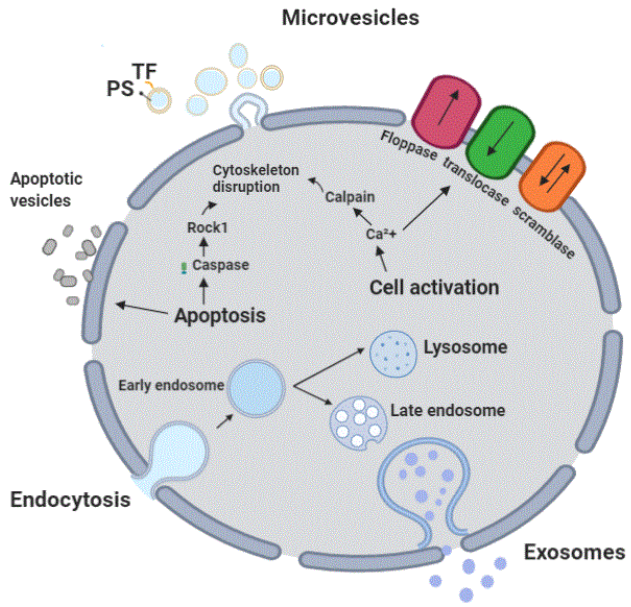

Figure 1.4: Schematic shows the extracellular vesicles release mechanism.
Microvesicles (MV) and apoptotic vesicles (ApoV) are secreted by direct outward budding of the cell membrane. Cytoskeleton disruption due to cell activation increases intracellular calcium which inhibits flippase, whereas activating floppase and scramblase. These three proteins are vital to maintain cell membrane phospholipid symmetry. Upon cellular activation or apoptosis leads to an increased influx of calcium ions (Ca^{2+}), which triggers proteases like calpain. These activated proteases cause a cytoskeletal breakdown too. During apoptosis Caspase 3 cleavage causes ROCK 1 to become activated and leads to cytoskeleton alterations and membrane blebbing.

Platelet-derived MP are composed of platelet-activating factor, β-amyloid precursor protein, Ca^{2+}-dependent protease calpain, arachidonic acid, many phospholipids and mRNA derived from their parent cells (Nomura & Shimizu, 2015). Bucciarelli et al. (2012) noted that close examination of MP' protein composition is indicative of its parent cell. MP can emerge from leukocytes, erythrocytes, endothelial cells, red blood cells (RBC), white blood cells, smooth muscle cells (SMC), platelets (where most MP come from, representing roughly 70-90% of MP), megakaryocytes, and cancer cells (Bucciarelli et al, 2012; Marco et al, 2014). The blood of healthy people will contain MPs, while the blood of individuals with certain diseases including cardiovascular disease, diabetes, sepsis, and cancer will show increased levels (Owens & Mackman, 2011).

MP have the potential to regulate inflammation, stimulate coagulation, affect vascular functions and apoptosis, and can play a role in cell proliferation and differentiation (Morel et al, 2011). Other research has suggested that MP play a role in cell interactions, immune modulation, angiogenesis, and tissue regeneration (Shai & Varon, 2011). There is suggestive research that MP shedding is a highly regulated process that occurs in a spectrum of cell types, so it is unsurprising to find them in blood or urine (Shai & Varon, 2011). However, this suggests that this regulation likely lapses in malignancies.

MP have emerged as instruments that cells use to communicate with one another on the tissue level during development and disease (Beer & Wehman, 2017). Importantly, MP are significantly involved in mediating the invasiveness of cancer cells. They can promote the remodelling of the extracellular matrix (ECM), form and stabilize cellular protrusion and therefore support cell migration and the infiltration of target tissue during the spread of metastases (Tkach & Thery, 2016). Other MP can impact lung structure and function through their ECM remodelling activities (Genschmer et al, 2019). Other microvesicles are derived from platelets and have a significant impact on inflammation and cardiac disease (Melki et al, 2017). Thus, MP can serve as important biomarkers for a multitude of conditions. Furthermore, MP can serve as important vehicles for the delivery of drugs to their specific target tissue and are thus of therapeutically significance (Agrahari et al, 2019).

1.7.2 Procoagulant potential of TF bearing MP

Over a decade ago, the work of Geisen et al. revealed that human blood contained circulating TF, which is actually in the form of MP (Giesen et al, 1999; Manly et al, 2011). MPs derived from activated, necrotic, and apoptotic cells provide a catalytic phospholipid surface for the assembly of factors for blood clotting, thus promoting the production of coagulation cascade

and thrombin. As the synergistic function of PS and TF is known to trigger blood coagulation, TF bearing MPs are suggested to represent the so-called blood borne of TF (Morel et al, 2011).

In their study of sepsis and procoagulant TF activity relative to MP, Woei-A-Jin et al. (2014) revealed that when markers of inflammation and coagulation are released in response to infection, MP bearing functional procoagulant TF (MPTF activity) are concurrently released. This echoes the findings of Caine et al. (2002) who reported that immune responses such as inflammation have the potential to disrupt normal coagulant activity (particularly in cancer patients). Demetz and Ott (2012) also point to the ways in which inflammation can stimulate procoagulant activities in the body (Demetz & Ott, 2012; Foley & Conway, 2016).

The actual mechanisms of the procoagulant potential of TFMP rely mainly on the expression of anionic phospholipid, especially PS, which is express at the surface of MP, and the basic clotting function of TF (Lacroix & Dignat-George, 2012a). Lacroix and Dignat-George (2012) observe that MP containing both TF and PS are particularly procoagulant, given the nature of TF in coagulation and the aforementioned procoagulant capability. It should also be observed that this combination of TF and PS is quite common, given that PS is required for the creation of MP and therefore appears frequently in the composition of MP (Key et al, 2010).

Biró et al. (2003) acknowledge that MP can provide the anionic phospholipid surface required to promote coagulation, as later affirmed by Lacroix and Dignat-George (2012). However, Biró et al. (2003) also pointed out that MP have the potential to expose TF which itself has the capacity to promote coagulation. It seems that the combination of providing a place for coagulation plus revealing the very factor most critical for coagulation creates what might be called a perfect storm of procoagulation (Biro et al, 2003).

It should be acknowledged that TF+ MPs also sometimes have *anticoagulant* properties as well. As noted earlier, the properties of MP are dependent upon their parent cells. Since there exist cells whose function is to prevent inappropriate activation of the coagulation it follows that some MP, even those that are TF+ will, despite the coagulant properties of PS, not facilitate coagulation. MP containing TFPI would not be likely to facilitate coagulation; this suggests that the relative concentrations of TF and TFPI on MP affects their thrombogenicity (Lacroix & Dignat-George, 2012b; Nomura et al, 2015; Pérez-Casal et al, 2005; Steppich et al, 2005).

1.7.3 Procoagulant properties of membrane surfaces

As noted in the previous section (1.7.2 and figure1.5), when the PS begins to escape the inner monolayer and is externalized, the negative charge of PS enables it to assemble calcium

dependent coagulation factors on the surfaces of MP (Lacroix & Dignat-George, 2012b). Tenase and prothrombinase complexes are able to form, leading to thrombin formation (Lacroix & Dignat-George, 2012b). Thrombin formation is critical for clotting and for stabilizing a thrombus through modulating fibrin properties, including its network structure and resistance to fibrinolysis, which suggests that the procoagulant activity of MP is also responsible for fibrin formation and stability as well (Aleman et al, 2011). Phospholipids have the capacity to serve as catalytic sites for factor Xa and thrombin generation (Marco et al, 2014). However, negatively charged phospholipids (like PS) are more likely to engender such catalytic sites (Nomura & Shimizu, 2015). Barteneva et al. (2013) emphasizes the many procoagulant properties of PS as a major prothrombotic and procoagulation signal, enhancing activation of coagulation proteins, TF and platelet aggregation (Barteneva et al, 2013; Lin et al, 2015). This suggests that membrane surfaces which contain negatively-charged phospholipids and/or facilitate thrombin formation, like cells which are externalizing PS, would be potentially procoagulant (Owens & Mackman, 2011).

1.7.4 Methods and measurement of MP in cancer patients

There are several ways of measuring MP in the human body. Key et al. (2010) assert that accurate detection regarding MP is critical, especially in the context of MP in VTE and cancer, which are accurate and precise and ideally determine the MP' cellular origins. Given the complex features of MP, ranging from origin to function, it is not surprising that many researchers combine different methods (Key et al, 2010).

A variety of assays have been employed including clot-based assays, which are usually one-stage assays (Haubold et al, 2009; Langer et al, 2008; Marco et al, 2014); the thrombin generation assay (TGA) (Marco et al, 2014); the chromogenic assay (CHA) which also looks at thrombin (Marco et al, 2014; Thaler et al, 2013); PS-dependent MP assay (Owens & Mackman, 2011); TF-dependent MP assay (Owens & Mackman, 2011); and prothrombin time assay (Yates et al, 2011). Often times multiple assays are used together in the course of research and have been used *in vivo* and *in vitro*.

Flow cytometry (FC) is considered the preferred method of MP measurement (Marco et al, 2014; Poncelet et al, 2015). The challenge with FC is that it measures neither procoagulant activity nor sized-extreme MP (Marco et al, 2014). It employs a flow cytometer (like the fluorescence-activated cell sorting FACScan flow cytometer) and attendant software for analysis (Berckmans et al, 2001; Hron et al, 2007). Flow cytometry is an attractive methodology for the detection, quantification and sorting of MP, as it is a well-established technique for cell sorting over several decades, and a plethora of reagents and protocols are available. Yet, the

analysis of MP via flow cytometry is hampered mostly by their small size and a dearth of reliable enumeration and standardization methods (Cointe et al, 2017b). Their submicron size makes it difficult to detect MP. Conventional flow cytometers are built to detect particles sizes down to ca. 300 nm diameter, and MP often measure below 200 nm. Yet even more sensitive procedures suffer from an absence of suitable reference materials (Gorgens et al, 2019).Accordingly, Gorgens et al, reported that they were able to define and optimise imaging flow cytometry (IFCM) acquisition and analysis parameters on an Amnis ImageStreamX MkII instrument for the detection of single sEVs by using enhanced green fluorescent protein (eGFP)-labelled EVs as a biological reference material(Gorgens et al, 2019).

Western blotting is also frequently used in the measurement and assessment of MP. It is particularly useful in assessing TF which has been demonstrated to be highly relevant to MP. It is sometimes used in conjunction with ELISA (Hussein et al, 2008). It is also used with assays. Western blotting can identify specific proteins in a sample (Barteneva et al, 2013).

1.8 Chemotherapy increases risk of VTE

1.8.1 Background

There is evidence that chemotherapy also increases the risk of VTE in cancer patients, with most cases occurring in the outpatient setting (Date et al, 2013; Geddings & Mackman, 2013; Khorana, 2009). One way in which chemotherapy can influence the risk of VTE bears some similarities to the ways in which cancer does, namely that it has the potential to foster increased PS expression or PS+ MP (Geddings & Mackman, 2013). As noted earlier, PS possesses significant procoagulant potential which implicates it in the development of thrombi (Barteneva et al, 2013; Burnouf et al, 2015).

Khorana (2009) notes that many anti-cancer treatments increase the likelihood of thrombosis. He points to evidence derived from two different studies – one a population-based study, the other a sizable retrospective cohort of cancer patients. In the population-based study, there was significantly increased risk of VTE in those who were receiving chemotherapy, with a reported odds ratio of 6.5 and confidence interval of 2.11-20 (Khorana, 2009). In the retrospective cohort, the findings revealed that patients receiving chemotherapy were at significantly higher risk for VTE than those patients who were not undergoing chemotherapy (Bar-Joseph et al, 2011; Blom et al, 2006; Walker et al, 2016).

It should also be noted that when chemotherapy is combined with other therapies, this can affect the way in which the chemotherapy influences VTE development. Khorana (2009) observes that when lenalidomide and the immunomodulator thalidomide are used alone,

there is not a significant increase to the risk of VTE in the patient; however, when these agents combined with steroids, melphalan, doxorubicin, or other chemotherapeutic agents, rates of VTE increase, ranging from 8% to 27%. Khorana (2009) observes that many of these kinds of therapies induce vascular damage, either directly or indirectly, thereby promoting local activation of the coagulation process. There is also some evidence that certain biomarkers could be used to assess VTE risk in cancer patients (Table 1.2).

Table1.2: biomarkers to assess the VTE risk in cancer patients.

Patient characteristics	Odds ratio (9S% CI)	VTE risk score
Site of cancer		
Very high risk (stomach, pancreas)	4.3 (1.2-5.6)	2
High risk (lung. lymphoma, gynaecologic, genitourinary excluding prostate)	1.5 (0.9-2.7)	1
Low risk (breast, colorectal, head and neck	1.0	1
Prechemotherapy platelet count ≥350 000/mm³	1.8 (1.1-3.2)	1
Haemoglobin level <10 g/dl or use of Red cell growth factors	2.4(1.3-4.2)	1
Prechemotherapy leukocyte count>11 000/mm³	2.2(1.2-4)	1
BMI ≥ 35kg/m²	2.5 (1.3-4.7)	1

That is prechemotherapy elevated platelet counts, elevated leukocyte counts, and low haemoglobin levels, all of which are commonly associated chemotherapy-induced VTE (Khorana, 2012).

1.8.2 Mechanisms of chemotherapeutic agents increasing VTE in cancer

With regard to the possible mechanisms of chemotherapeutic agents and their ability to increase VTE in cancer, Date et al. (2013) report that precise mechanisms are largely uncharacterised, though several known mechanisms have been postulated. Several of these mechanisms bear similarities to the mechanisms described earlier in this chapter. One

mechanism is the ability of chemotherapy to induce the release of cytokines and procoagulant molecules, such as TF, during chemotherapy-induced cell damage and associated tumour lysis (Date et al, 2013; Haddad & Greeno, 2006; Swystun et al, 2009). This process causes damage to the vascular endothelium, prompting the coagulation cascade. Chemotherapy is also capable of causing reductions in the production of endogenous anticoagulant proteins such as protein C and protein S (Falanga & Russo, 2012; Furie & Furie, 2006). In other words, without these critical anticoagulant proteins, the cellular environment becomes more procoagulant which promotes the development of thrombi.

All of this, according to Date et al. (2013), can be reduced to the fact that the inherent cytotoxic nature of chemotherapy regimens inevitably leads to significant cellular apoptosis (Lee et al, 2015a; Wahba et al, 2018). The way in which apoptosis occurs in the chemotherapeutic context will vary according to the chemotherapeutic agent employed which also affects the way in which that agent effects VTE risk (Date et al, 2013). In other words, some agents are less likely to foster VTE while others are more likely. Some of this may be attributed to the kinds of MP that treatment prompts and their abilities with regard to procoagulant or anticoagulant activity (Date et al, 2013). Incidentally, this suggests that tumours which are more sensitive to chemotherapy would be more likely to cause VTE, given that such tumours are more likely to shed greater numbers of MP via apoptosis, particularly TFMP, which have already been demonstrated to be a significant aspect of VTE.

1.9 Lab on a Chip (LOC)

1.9.1 Background

Studying the micro-components and micro-processes involved in the haemostatic system, MP, tumour development, and the mechanisms involved in cancer induced VTE can be difficult, given their exceedingly minuscule size (100-1000 nm). Though methods and measurements exist to study these tiny microvesicles, they are not ideal. For example, flow cytometry – which is considered the preferred method of measurement for MP – is not as precise as it could be, especially since it cannot assess procoagulant activity or particularly small MP (Marco et al, 2014). In the case of MP, precise and accurate detection is critical in identifying MP' cellular origins, which is critical in the study of cancer and VTE. Fortunately, more precise tools exist. One of these tools is lab-on-chip/lab-on-a-chip systems. LOC systems capitalize on advances in microfluidics for nanotechnology-based sensing methods (Dutse & Yusof, 2011). Microfluidics emerged from the microelectronics industry where researchers attempted to improve silicon-based micromachining processes using photolithography, etching, and bonding techniques (Dutse & Yusof, 2011). LOC systems are able to function, assess, and provide data for

nanoenvironments through their ability to mimic *in vivo* biological systems onto closely resembling *in vitro* microfluidic environments (Choudhury et al, 2012). This technology has been in use as a biological tool since the early 1990s and can be recognized in common tests like polymerase chain reaction and DNA microarrays (Zhang & Nagrath, 2013). Early LOC systems were created from silicon and glass; as the industry has evolved, more advanced materials such as elastomers have yielded LOC systems which both more biocompatible and more affordable (Whitesides, 2006).

1.9.2 LOC and cancer research

Given the ability of LOC systems to handle microliter volumes in microchannels of 1 µm to 1000 µm and where fluid flow is strictly laminar and concentrations of molecules can be well-controlled, LOC systems appear to be an ideal tool for the study of many biological systems (Zhang & Nagrath, 2013). Additionally, advances in these systems have yielded systems which are capable of many tasks including RNA manipulation, manipulation of proteins and mammalian cells through the use of biosensors, and disease diagnosis and prognosis through single cell assays, all of which definitely point to the aptness of using LOC systems in cancer research (Mitchell et al, 2008; Schrauder et al, 2012).

The ability of LOC systems to work in nanoenvironments with nanoparticles mean that LOC systems may be able to perform a critical assessment which traditional MP-measurement methods cannot do, and do it in a cost-effective manner: effectively identify critical biomarkers which can help support early detection and diagnosis (Yu et al., 2013). These biomarkers include mutated DNAs and RNAs, secreted proteins, and tumour cells which include circulating tumour cells and MP; measuring these particles should be done at high accuracy with automation and cheaply at point-of-care to reduce costs (Viator et al, 2010). However, traditional bench-top laboratories and their methods are not conducive to the high-throughput screening necessary for large-scale -omics studies (Yu et al., 2013). Not only are these methods and approaches not conducive, they are also not cost-effective, and the field of health care would greatly benefit from faster, more accurate and more highly precise diagnostic devices which reduce costs (Iliescu et al, 2019).

LOC systems solve the high-throughput problem in a cost-effective way which enables personalized diagnostic strategies (Yu et al, 2013). Given the complex of risk factors involved in VTE development – that is, patient, cancer, and treatment (Khorana, 2012). LOC systems, which are highly sensitive, can identify those biomarkers with a high degree of accuracy. They can generate better epidemiological data that can be used for infectious-disease modelling as well as cancer (Nelson et al, 2006). This means that patients can be diagnosed earlier, which is

usually associated with better rates of survival, as well as more personalized treatment which can also anticipate the risk of VTE.

A specific LOC system used in cancer research is the circulating tumour cells (CTCs) chip. This chip was developed in response to the idea that early detection of CTCs, which are released into circulation by primary tumours and are implicated in the metastatic cascade, can result in early tumour diagnosis as well as driving treatment decisions (Nagrath et al, 2007). Using CTCs for cancer detection has been practiced since 2004, when CellSearch, one of the first technologies used for detecting CTCs, was able to accurately separate CTCs from specially coated magnetic beads and correlate those isolated CTCs with patient prognosis in breast cancer (Kaiser, 2010). 2007 saw the creation of a microfluidic-based CTC capture device which utilized the special coating used in the CellSearch method; this coating is a surface antigen known as epithelial cell adhesion molecule (EpCAM) (Nagrath et al, 2007). The 2007 device was composed of 78,000 microposts coated in EpCAM embedded on a silicon chip. The device was able to capture cancer cells from milliliters of unprocessed whole blood with high sensitivity and purity, maintaining those captured cells in a sufficient state for analysis (Zhang & Nagrath, 2013). In one test, the chip was able to correctly detect CTC in 115 out of 116 samples from 68 patients. Advances since 2007 have produced more and more sensitive and specialized chips. More and more of the analysis of the captured cells can be conducted on the chips themselves (Nagrath et al, 2007). Furthermore, a novel, rapid and cost-effective microfluidic approach has developed to barcodes amplified genomic DNA from thousands of individual cancer cells narrowed to droplet. In this study, scientists developed two-step microfluidic droplet workflow to characterize the genetic diversity within cancer populations (Pellegrino et al, 2018).The scientists believed that this approach will be used in routine investigation of AML as an alternative of the Single-cell sequencing that has many disadvantages such as upon laborious, low-throughput technologies and expensive (Pellegrino et al, 2018). Moreover, comparison study was conducted between On-chip Sort and Cell search to enumerate CTCs in 30 metastatic lung adenocarcinoma peripheral blood. Interestingly, the On-chip Sort device was able to correctly detect CTCs using fluorescent labelled antibodies in 22 out of 30 (median 5; range, 0–18 cells/5 mL blood) more than by Cell Search that detect 9 out of 30(median, 0; range, 0–12 cells/7.5 mL) ($P < 0.01$) (Watanabe et al, 2018). Additionally, a microfluidic apparatus was developed that is capable of extracting antigen-specific microvesicles from biologically complex samples, such as serum and conditioned medium from cultured cells. Furthermore, the majority of microvesicles isolated microfluidically retained their native morphology(Chen et al, 2010a).

1.9.3 Advantages and disadvantages of LOC

At first glance, it seems that LOC systems offer a lot of solutions to a lot of problems. And that is most certainly true – LOC systems do offer several advantages over traditional bench-top laboratories. However, LOC systems also have several disadvantages which should be borne in mind when considering the use of LOC in research.

A few of the advantages of LOC have already been mentioned. LOC systems are capable of sensitivity and accuracy not available in other methods usually employed in assessing cancer cells (Yu et al, 2013). The sensitivity and accuracy of these systems enable them to assess and identify biomarkers crucial to early detection of cancer which in turn facilitates better treatment plans which can improve patient prognosis (Dutse & Yusof, 2011). Tan et al., 2014 reported that use the LOC as diagnostic test to detect Dengue virus (DENV) and Chikungunya virus (CHIKV) was equivalent to reverse transcription polymerase chain reaction (RT-PCR) in performance. The use of RT-PCR to detect DENV has showed diagnostic features with the specificity 96%, sensitivity 89%, negative predictive value 92%, and positive predictive value 94%. Correspondingly, the LOC had a detection of positive 90.0% agreement and a specificity of 100% for Chikungunya virus; and a positive 85.0% agreement and a specificity of 100% for DENV serotype 3 (Tan et al, 2014). Moreover, a novel method was developed that is capable of detect the creatinine concentration using LOC. They use chemiluminescence with hydrogen peroxide in the presence of cobalt ions. The researchers developed a chemiluminescence creatinine sensor with a limit of detection (LOD) of 0.07 μM and linear range of 0.1–30 μM, which is much more sensitive, simple and cost effective than most reported methods (Hanif et al, 2016).

Another advantage is the ability of LOC to perform high-throughput screening for pharmaceuticals. This kind of large-scale screening is not possible through traditional benchtop methods which supports drug discovery and other research efforts related to pharmacotherapies (Bhagat et al, 2011). Another benefit of LOC system is their versatility as biosensors. Clearly LOCs can be used for cancer research – as demonstrated in CTC chips – but they can also be used in infectious disease research as well (Ivnitski et al, 2003). For example, a microfluidics technology known as Microfluidic Integrated DNA Analysis System (MIDAS®) was integrated into disposable assay cartridges known as GeneXpert® where these cartridges contain all the specific reagents essential to detect disease organisms such as Chlamydia trachomatis, Bacillus anthracis, or foodborne germs (Ivnitski et al, 2003).Moreover, LOC systems can also be used to assess microbials and other biological agents in the environment and which can be transmitted via food, water, insect vectors, as aerosols or by direct contact (Dutse & Yusof, 2011).

Perhaps one of the most attractive advantages of LOC is that it is low-cost. Because they are fast, reliable, and sensitive – not to mention low-power – LOC systems represent an ideal solution for reducing health care costs, especially at point-of-care (POC) (Warsinke, 2009). There is a significant demand for mobile and affordable POC applications, especially for POC testing (POCT); in fact, according to Dutse and Yusof (2011), these POC demands are some of the main driving forces for the future of in *vitro* diagnostic market. Furthermore, despite genome technology has increased knowledge on cancer, there are some limitations such as complexity of the sequencing technologies, inability to predict the efficacy or toxicity of drug on an individual cell line or patients.

Despite all of these advantages, there are also some disadvantages to LOC systems. LOC systems have been and are composed of a wide variety of materials "including silicon, glass, soft or hard polymers and biomaterials (e.g., calcium alginate, cross-linked gelatin or hydrogels) (Dutse & Yusof, 2011). Furthermore, in terms of the polymeric materials, solvent-resistant substances must be used which limits what can be utilized (Ertl et al, 2004). Such materials usually include Teflon, photo patternable silicon elastomers, thermoset polyesters, poly (methylmethacrylate) (PMMA) and patterned poly-(dimethylsiloxane) (PDMS), polyimide and SU-8 (negative photoresist) polymers (Becker & Gärtner, 2008).

Another disadvantage of LOC system is that while there are many different available microfluidic technologies that have been shown to be successful, many of them remain untested in clinical settings (Lopez et al, 2017). In fact, many of the technologies have never been through clinical trials, a key step in making the jump from emerging technologies to real work applications. One of the reasons these technologies don't necessarily make it to clinical testing or trials is the challenge of technology development – the inevitable stop-and-go of testing and re-testing, designing and redesigning, in order to optimize performance (Zhang & Nagrath, 2013).In addition, Sample preparation also involves limitations and challenges, in which full automation is not always feasible, contamination may occur particularly in biological detection devices, and further nano-scaling may not be possible(Prakash et al, 2008). In addition, prototyping production techniques do not always lead to mass production. Casting PDMS from a micromachined master is currently the most common prototype method, but it can't be scaled up to produce many components (Convery & Gadegaard, 2019). In the light of this control of the manufacture of products, most microfluid start-ups struggle because, though their prototypes operate well, their manufacturing protocols for large scale production are difficult to adapt. In order to address this, efforts should be made to develop reliable development protocols which are both cheap and fast enough to provide efficient prototyping and also to provide an easy path to automated manufacturing(Convery & Gadegaard, 2019).

Furthermore, Flow-based microfluidic biochips, such as AutoCAD, are currently manually designed with the help of computer drawing (CAD) programmes. The lack of the CAD tools for microfluidic flow chips delays not only the development of products, but also hampers the use of the complex design that can be achieved with current manufacturing techniques (Hu et al, 2017). The use of PDMS, which, as previously reported, has the potential to adsorber small molecules that could have an impact upon culture, is currently an issue of organ-on-a-chip science. Moreover, existing microfabrication techniques involve a large array of engineering expertise and facilities that are inaccessible to many researchers (Convery & Gadegaard, 2019).

1.9.4 Isolation of extracellular vehicles (EVs) in microfluidics

EVs have a physiological function during development and disease, as they can transport signalling molecules, RNA and metabolites (Beer & Wehman, 2017). In addition, they can serve as biomarkers for the presence of cancer cells, tumours, and metastases; in this context, EVs do not only promote cell-cell signalling, they mediate coagulation of blood cells, prime endothelial cell layers for the passage of metastatic cells, and reprogram stromal cells to form a pre-metastatic niche (Becker et al, 2016). Thus, it is important to find reliable detection methods for EVs, so the presence of cancer cells can be probed as early as possible, ideally before the primary tumour forms metastases. In recent times, microfluidic devices have been emerged as a convenient way to detect a variety of biomarkers using only small amounts of urine, blood or any other bodily fluid. However, despite their relevance as diagnostic markers, microfluidic methods to detect EVs are just beginning to emerge.

Liquid biopsies afford several advantages compared to traditional biopsies; use of urine, blood or even saliva means a sample is easier to obtain compared with a biopsy. In those liquids the presence of metabolites, proteins, nucleic acids and microRNA can be determined, but also larger objects such as circulating tumour cells (CTCs) and tumour EVs can be measured. For the early and reliable detection of cancer, it is important that the corresponding technology is as simple and convenient as possible, to not discourage early cancer screening. The development of microfluidic on-chip devices is a step in that direction (Iliescu et al, 2019).

Cancer EVs can be difficult to identify, as all cell types in the human body can and will produce those vesicles, albeit malignancies tend to generate distinctly more EVs than healthy cells (Shao et al, 2012). A typical tumour can have a diameter of 1 cm after growing for ten years; it will contain ca. one billion cells that duplicate every five months (Gold et al, 2015). Interestingly, Alberter et al. found that in pancreatic cancer, the concentration of EVs in the blood was correlated with the stage of the disease, and that even during early tumour development, EVs could be reliably detected (Alberter et al, 2016). Exosomes are therefore

promising candidates for cancer biomarkers; however, due to their small size, their isolation is difficult and impractical in a clinical setting, at least as long as conventional methods like ultracentrifugation are used (Iliescu et al, 2019). Microfluidic methods may provide an alternative. "Nanofilters, nano-porous membranes, or nanoarrays" can be used to collect EVs when passing through the microfluidic chamber (Iliescu et al, 2019). Alternative methods involve size-based filtering through differential acoustic forces via ultrasonic sound impacting the vesicles. In addition, microfluidics based on immunoaffinity can filter out microvesicles that harbour a certain antigenic marker on their surface, independent of their diameter. Moreover, microfluidic devices can also use a combination of cell-size and affinity-based sorting for combined diagnostics and detection of EVs in more complex environments, that contain more than one type of EVs. Taken together, while conventional methods to isolate EVs involve ultracentrifugation or ultrafiltration, microfluidic devices offer a more convenient alternative by isolating EVs via micro-size exclusion chromatography and affinity-based purification (Jin et al, 2014; Son et al, 2016).

Acoustic separation techniques are predicated on the forces that a standing sound wave applies to microvesicles; as not all vesicles are the same size, the forces working on them are different, which allows for the size-based separation of EVs. Technologies like the one shown here are also known under the word *acoustofluidics*. The theory upon which the acoustic separation of microvesicles is built is complex; in brief, standing soundwaves with frequencies around 40 MHz produce nodes, where the energy density is low, and extrema, where energy density is high. As the transmitted force is the product between the mass of the objects and their acceleration, smaller vesicles will experience the strongest movements and be found between the nodes, while the larger vesicles will gravitate more towards the nodes. This setup therefore separates exosomes based on their size. If the applied acoustic field is tilted in a way that lets it align with a division in the flow channel, then larger vesicles can be moved into one channel, while smaller vesicles will fall into the other channel (Wu et al, 2017). The authors propose a platform that first filters red blood cells (RBCs) out of the solution, and then further selects or diagnoses the remaining vesicles based on their smaller size; this way, over 99% of RBCs can be removed from the initial sample, and the EVs with desired size can be further purified with an efficiency of over 98% (Wu et al, 2017). The platform can be used as a lab on chip device in a point-of-care context, and since the EVs are processed in a "label-free, contact-free, and biocompatible" protocol, they can serve as starting material for additional experiments that analyze their structure and function (Wu et al, 2017).

Exosomes can also be isolated in microfluidics devices based on affinity chromatography, using antibodies against cell surface proteins found on EVs. Interestingly, CD63 seems to be an

antigen that is predominantly found on microvesicles, but not on platelets, monocytes and granulocytes. Chen et al. (2009) were able to specifically detect and filter out EVs using CD63 anti-bodies, using microfluidics devices. Importantly, EVs enriched in CD63 antigens on their sur-face can be found on EVs derived from glioblastoma (GBM) patients or GBM cell cultures. It may well be that other cancers and cell lines produce EVs enriched in different antigens. This opens up the interesting possibility that the antigen presented on the surface of EVs can be used to detect the sort of cancer that can be found in a patient's body (Chen et al, 2010b). In-deed, in patients with bladder cancer, EVs are enriched in galectin-1 and -3, while colorectal cancer is reflected in EVs with galectin-4. This suggests that exosomes carry a molecular signature that is highly specific for the type of cancer the patient is suffering from (Yanez-Mo et al, 2015). Other studies have suggested that many of the core proteins in the membrane of EVs are the same, but the surface modifications of those proteins may be specific to the vesicles. If that is the case, highly specific antibodies will be needed to detect and sort the desired exosomes. Moreover, cancer-derived microvesicles may be enriched in certain proteins that are expressed in a more basic level in EVs; this suggest that we could isolate the EVs and detect the different proteins and their amounts on the EVs surface using a 2D gel. In the case of cancer patients, we would probably observe two distinct populations of microvesicles with differential quantitative presence of protein complexes on the surface (Yanez-Mo et al, 2015).

Taken together, microfluidic devices are emerging as useful tools to detect and isolate EVs from the bodily fluids of a patient, be that saliva, blood or urine. EVs can be enriched using either acoustic methods or affinity chromatography. There should be a wealth of information that can be used to identify the tissue origin of the EVs circulating within the body, as well as the type of disease a patient exhibit.

1.10 Spheroids

1.10.1 Background

Tumour spheroids are three-dimensional (3D) spherical cell aggregates, which are also called multicellular tumour spheroids (MCTS) (Osswald et al, 2015). MCTSs are composed from a wide variety of tumour cell lines when cultured under appropriate conditions. The spheroids demonstrate many characteristics associated with solid tumours; these characteristics include different zones of proliferation, apoptotic, and necrotic cells and an oxygen gradient with hypoxic areas in the core (Egeblad et al, 2010). Furthermore, spheroids are able to demonstrate global expression profiles of tumour biopsies much more accurately than 2D cell cultures (Giannattasio et al, 2015). Moreover, Tumour spheroids can be categorized into

homotypic spheroids that aggregates from only cancer cells or heterotypic that consist of cancer cells cultured with other cell types such as endothelial cells, immune cells and fibroblast (Costa et al, 2016).

Tumour spheroids are created through the association of thousands of cells; they possess an outer region of proliferating cells around a body of quiescent cells (Giannattasio et al, 2015). The spheroids feature a complex network of cell-cell contacts as well as pH, oxygen, metabolic and proliferative gradients" similar to the inadequately vascularized and avascular areas of both solid tumours and micrometastases (Chen et al, 2019). These spheroids can mimic several different types of cancers (Cui et al, 2017; Weiswald et al, 2015) (Figure 1.5).

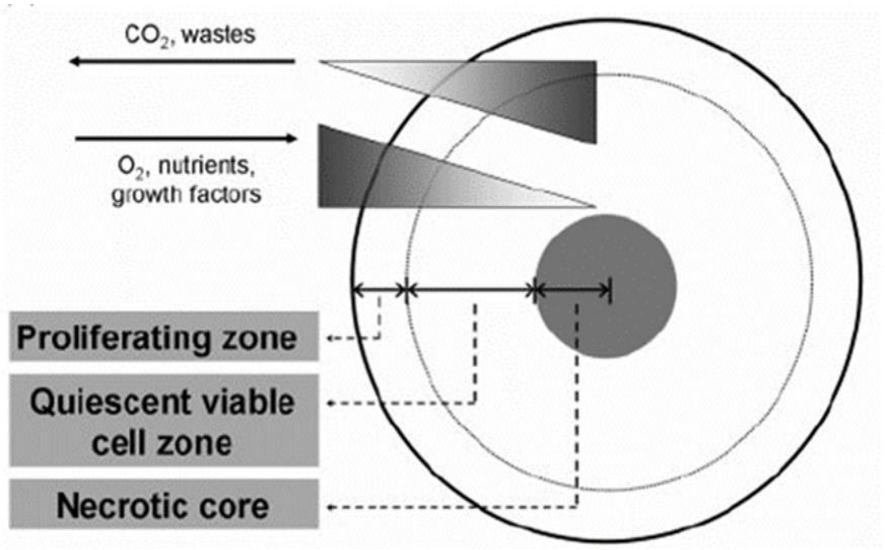

Figure 1.5: Tumour spheroid layers.
Figure shows that the proliferating zone as out layer in tumour which receive the high percentage of O_2 and nutrients. Then quiescent viable layer located in middle that receive low level of O_2 and nutrients. Low O_2 and nutrients get via to the necrotic core and inverse of CO_2 and waste products increased in necrotic core zone. Adapted from (Li et al, 2008).

There are numerous tissue culture techniques have been established to generate tumour spheroids (Figure 1.5). For example, spinner flask, spontaneous aggregation, rotary cell culture system, hanging drops, liquid overlay culture, polymeric scaffolds, low binding plates and poly-2-hydroxyethyl methacrylate (polyHEMA)-coated plates (Vinci et al, 2012). Accordingly, liquid overlay method used to generate 3D spheroid by seeds cells on different microplate's types that covered with agar (Weiswald et al, 2015). The microplate is round shape well-plates coated with ultra-low attachment materials to form cell assemblies and grow in 3D structure. On the other hand, cells in spinner flask seeds in a culture vessel with magnetic stirrer that result in inhibition of attachment to the plate and hence cells aggregate as spheroids. Another

common method that recently have developed is hanging drop method of inverted microplate. In this technique, cells suspension is grown in small droplets up to 30 µl in size are deposited on an inverted lid (Kelm et al, 2003).

Giannattasio et al. (2015) provide a concise description of the process of cultivating a MCTS. Their spheroid was – which was cultivated for a particular purpose – included seeding $5x10^3$-$1x10^4$ cells/well in a volume of 150 µl/well of culture medium in 96-well plates coated with 1.5% agarose in basal DMEM medium. 48 hours after seeding the spheroid was used for functional assays; transmission and fluorescence microscopy were used to monitor the cervical carcinoma cell lines CaSki and SiHa growth. Phase contrast pictures of independent solid spheroids were used for the spheroid's growth curves, drawn from six different experiences via Fiji software, which was also used to calculate the spheroid's volume (Giannattasio et al, 2015) (Figure 1.6).

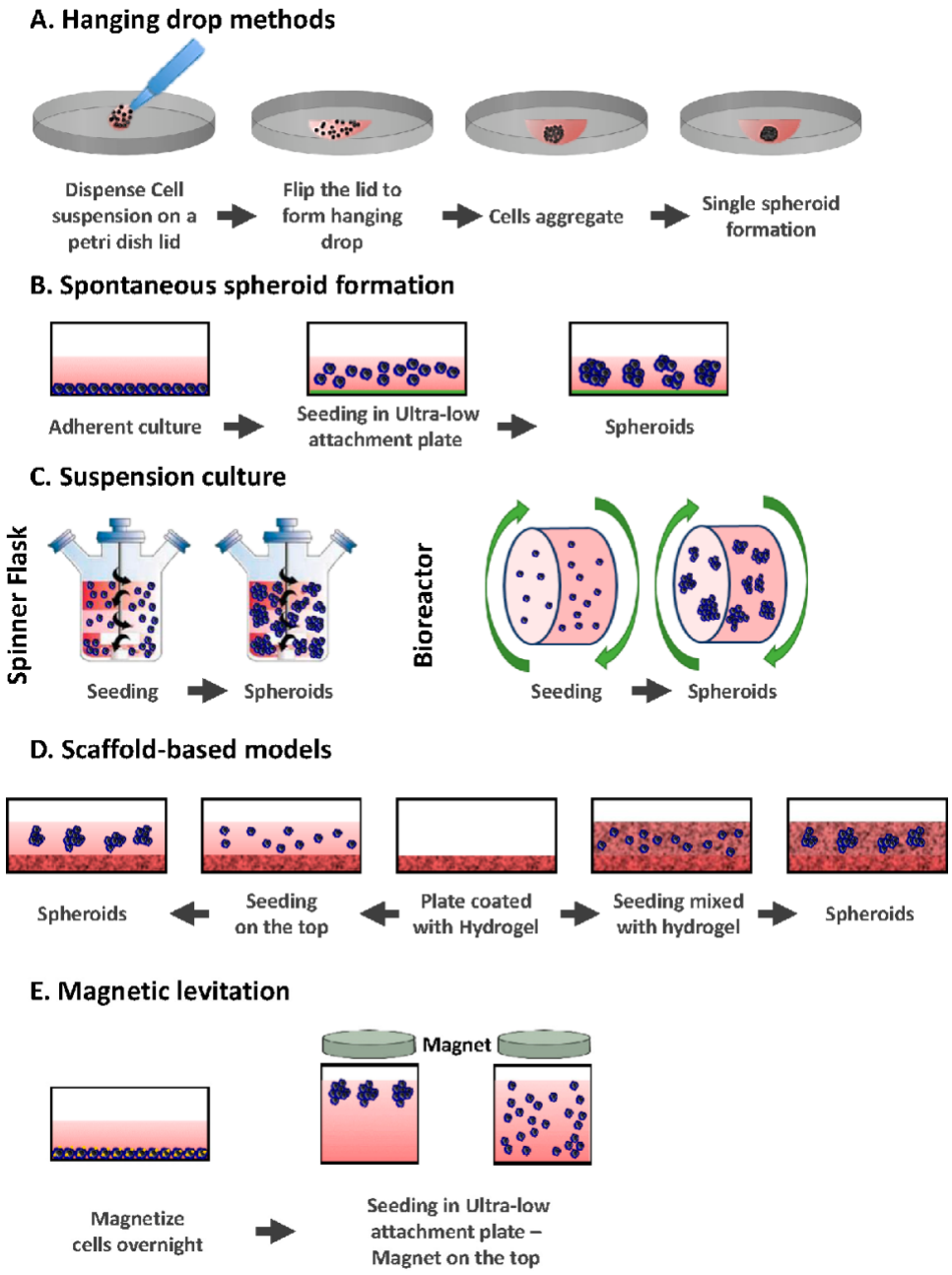

Figure 1.6: Common culture techniques to generate spheroids.
(A) Hanging drop methods. Cells suspension are grown in small droplets up to 30 µl in size are deposited on an inverted lid (B) liquid overlay method. Cells are seeded on different types of microplate that are covered with agar in order to prevent cancer cells to attaching to the plate; (C) suspension cultures. cells grown in a spinner flask are seeded in a culture vessel with magnetic stirrer that result in inhibition of attachment to the plate and hence cells aggregate as spheroids (left) or bioreactors (right) in which cells rotate and under gravitational forces to form spheroids; (D) Gel embedding. Cells are grown on a matrix (left) or grown within a matrix (right); (E) magnetic levitation. Cells are pre-loaded with magnetic nanoparticles and form spheroids via an externally applied magnetic field.(Hoarau-Vechot et al. 2018).

1.10.2 Tumour spheroids applications

Given that a variety of spheroids representing a variety of cancers can be created, spheroids have significant potential. Spheroids are able to provide a gene expression pattern that is analogous to that detected in solid tumours in *vivo* (Costa et al, 2016) One of the main

applications of these spheroids is their use in high-throughput screening for drug discovery or determining drug efficacy and toxicity (Lovitt et al, 2014). Both other applications have emerged. Giannattasio et al. (2015) used spheroids to study natural killer (NK) cell infiltration and immunosurveillance as well as NK cell cytotoxicity in the presence and absence of certain soluble mediators. Osswald et al. (2015) used spheroids for the in *vitro* analysis of bacteria as a means of gene delivery vectors in tumour therapy. In the analysis of their findings, Osswald et al. (2015) report that for their purposes, MCTSs were in fact a suitable model system to study tumour targeting strategies using anaerobic bacteria or their spores in *vitro*. Giannattasio et al. (2015) report that MCTSs can be sectioned and stained for analysis. Osswald et al. (2015) also conclude that MCTSs could be a simple or as complex as a researcher would need, depending on the tumour cell line used to create the spheroid. This hints at the opportunities available with regard to spheroids. There have not been many studies investigating therapeutic effects of substances, beyond those associated with drugs. Osswald et al. (2015) were only able to identify one study in which MCTS was used to investigate the therapeutic effect of a recombinant *S. typhimurium* strain expressing a therapeutic gene. Furthermore, according to Osswald et al. (2015), spheroids appear easier and more cost-effective to use when compared to microfluidics (like LOC systems). Giannattasio et al. (2015) report that MCTS also have the potential to play a role in personalized treatment, much like LOC.

1.10.3 Three-dimensional (3D) cell culture vs. monolayer (2D) cell culture (advantages/disadvantages)

Using In *vitro* culturing systems results in a great impact on preclinical trials cancer research. However, approaches of this kind carry with them various well-known limitations. For instance, in two-dimensional (2D) culture method or cell monolayers, biological and molecular features of cancer cells are mostly lost. In addition, 2-D tissue culture models using plastic substratum can cause major alterations in cellular phenotype and genotype (Rajcevic et al, 2014). Perhaps the most serious disadvantage of traditional 2D cell culture methods is that these techniques do not adequately mimic all of the biochemical signals and mechanical process that present in *viv* (Pampaloni et al, 2007). Moreover, another potential drawback of cell monolayer tissue culture model is lack of microenvironmental properties as in solid tumour, whereas animal models are time consuming, expensive, and usually fail to reflect human tumour biology (Hait, 2010). Therefore, because of these limitations in 2D cell culture researchers are turning to 3D cell culture models that more closely mimic the biological process in living organisms (Mazzoleni et al, 2009). According to Li et al. (2008), spheroid models may have a potential role in mechanisms of resistance to other stress stimuli. Cancer cells grown *in vitro* as spheroids represent the chemoresistance phenotype of native solid

tumours exactly and display pathways of resistance linked to hypoxia, alterated chromatin structure, impairment of apoptosis, decreased drug perfusion and cell cycle alterations (Däster et al, 2017; Sutherland, 1988).In addition, spheroids have demonstrated outstanding features more than 2-D culture method. For example, cells in spheroids are connected by membrane protein anchorage with more cell adhesion molecules for example CD44v6 and E-cadherin (Green et al, 2004). Moreover, proteins expression is increased in spheroid cells (Kumar et al, 2008a; Park & Song, 2006; Weigelt & Bissell, 2008). Green et al. 2004 has found that increased expression of cell adhesion in spheroids cells has a great impact on cell survival rate therefore inhibition of these adhesion molecules via specific antibodies may disrupt the influence of spheroid formation. Furthermore, Kumar et al. 2008 has reported that Several protein groups such as cell stress (heat shock proteins (HSPs) 90, 70, 60, and glycolytic proteins were differentially overexpressed in 3D neuroblastoma spheroid in compare to 2D monolayer (Kumar et al, 2008a). Moreover, because of their 3D structure, hypoxic core, and increased chemoresistance, MCTS are thought to be better model for the tumour microenvironment than cells grown as a monolayer (Bates et al, 2000; Weiswald et al, 2015).

However, approaches of this kind carry with them various well-known limitations. These limitations could result in decreased use of multicellular tumour spheroidal (MCTS) in different biomedical researches, such as high-throughput screening applications (Lee et al, 2009). Perhaps the common disadvantage of this method is absence of standard procedure to generate MCTS in simple and fast approach. Another limitations of this models are failure to produce spheroid or uniform geometry shape or homogenous spheroid cultures (Ivascu & Kubbies, 2006). Moreover, absence of standardization of accurate and reliable imaging tools of 3D structures, is considered also as a potential disadvantage of multicellular spheroid model. Consequently, this would result in inadequate imaging and examine the effect of anticancer agents (Ma et al, 2012). Furthermore, in order to perform flow cytometry on spheroids they must be disintegrated to a single cell suspension, but this disintegration is not always easy to accomplish (Osswald et al, 2015). Osswald et al. (2015) reported several failures in their experiment which, of course, was disruptive of the experiences they were conducting. This requirement for disintegration always represents a challenge associated with MCTS. Another challenge associated with MCTS is the lack of studies using the spheroids, but this is a challenge which time will undoubtedly address as more experiments are conducted and reported. In addition, long-term suspension cultures of spheroids, though, sometimes contribute to cell agglomeration, that contributing to necrotic centres as the nutrients and oxygen are limitedly diffused in and out of the spheroid (Edmondson et al, 2014). In static culture, agglomeration of cells can happen if cells are seeded at high rates, decreased

transmission of oxygen and nutrients and increased mortality of cells in large cell aggregates (Wilson & McDevitt, 2013). In fact, spheroids sometimes accumulate into broad agglomerates during culture, contributing to two negative effects. First, their dimension and characteristics differed considerably in the spheroids generated. Second, the movement of nutrients, oxygen and growth factors, and metabolic waste from cells in the middle of agglomerates with diameters greater than 500 μm, is well established and results in sluggish cell proliferation, apoptosis or irregular differentiation (Lin et al, 2017).

1.11 Endothelium

1.11.1 Introduction

The endothelial cells exist as a monolayer which separates the blood from the tissue. It is well-known that endothelial cells are capable of controlling blood flow and blood coagulation. The role of endothelial cells in angiogenesis, inflammation, smooth muscle cell proliferation, cellular adhesion and regulation of vascular tone has been acknowledged by a wide body of research (Galley & Webster, 2004; Yau et al, 2015). Vasodilators and vasoconstrictors are released by the endothelial cells so that blood flow and hence blood pressure is regulated. Prostacyclin and nitric oxide are important vasodilators. Endothelium and platelet-activating factor are important vasoconstrictors. In the absence of any injury, coagulation is inhibited by endothelium through generation of anti-thrombic molecules like TFPI, heparin sulfate proteoglycans and nitric oxide (Michiels, 2003). In this way, platelets are not allowed to adhere to one another or to cell surface thereby sustaining the fluid state of the blood. In case of vascular injury, protein and cellular entities gather at the point of injury to form blood clot that averts excessive loss of blood (Galley & Webster, 2004). Furthermore, the endothelium of blood vessels is essentially involved in prevention of thrombosis via offering a surface which prevents adherence of proteins and cells needed for clotting (Watson, 2009) (Figure 1.7).

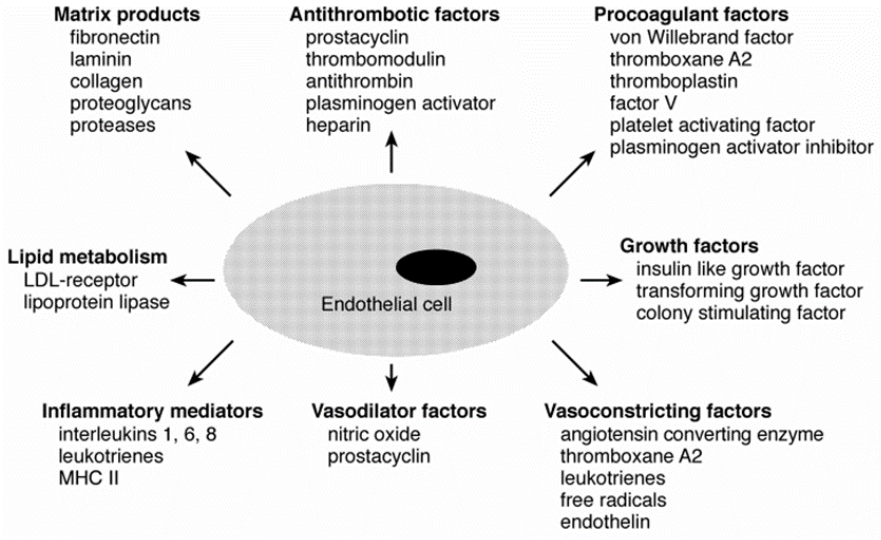

Figure 1.7: The role of endothelium in cardiovascular homeostasis and diseases. Adapted from Galley & Webster, 2004.

Several anticoagulants are expressed by a healthy undamaged endothelium. These anticoagulants include heparin-like proteoglycans, endothelial protein C receptor, thrombomodulin and TFPI (Mackman, 2012). Besides these, ectonucleotidase CD39/NTPDase1 is also expressed by endothelial cells. This enzyme mediates metabolization of the platelet agonist ADP. Lastly, platelet inhibitors like prostacyclin and nitric oxide are also released by endothelial cells (Marcus et al, 1997; Moore et al, 1987). Upon activation, the endothelial cells cause up-regulation of procoagulant protein TF expression and down-regulation of anticoagulant protein thrombomodulin expression (Yau et al, 2015). Activation of endothelial cells also results in expression of different adhesion substances over the surface like VWF, E-selectin and P-selectin which attach to platelets and leukocytes (Williams et al, 2011). It has been demonstrated that in case of hypoxia, release of VWF is promoted by Weibel-Palade bodies in ECs (Pinsky et al, 1996). In addition, the endothelium also contributes in the development of VTE through inflammation. According to Wakefield et al., mechanical or functional disturbance in endothelium results in vasoconstriction of endothelial surface. Moreover, the endothelium responds in a prothrombic manner. In particular, prothrombic factors are released by the endothelial cells. These factors include plasminogen activator inhibitor, TF, VWF, endothelin-1 (a vasoconstrictor) and platelet activating factor (Wakefield et al, 2008). Endothelium damage also causes promotion of expression of certain cell adhesion molecules on the surface such as E-selectin and P-selectin. These surface molecules support adhesion and leukocyte migration. As a consequence of these inflammatory reactions occurring after injury, development of VTE can be promote (Cote & Smith, 2016).

1.11.2 Endothelial activation mechanisms:

VWF is a multi-subunit protein that facilitates platelet adherence to subendothelial collagen at sites of vascular damage and is a carrier of circulating factor VIII (Koster et al, 1995). VWF is released by endothelial cells. This factor is crucial for adhesion of platelets to the wall of blood vessel. Researchers have found a link between increased levels of von Willebrand factor and endothelium damage (Horvath et al, 2004). In addition, research has recently shown high concentration of this factor in plasma of cancer patients who suffered thrombotic microangiopathy (Levi, 2009). Moreover, it is well established that endothelium plays crucial role in bringing about the prothrombic or hypercoagulable state. Disturbed vascular activity is indicated by altered levels of some molecules in plasma like soluble E selectin, soluble thrombomodulin and von Willebrand factor. Besides indicating damage of the endothelium, high levels of von Willebrand factor perhaps contribute in thrombosis through facilitating adhesion of platelets to one another and to sub endothelium (Blann & Yip, 1998). Likewise, high plasma levels of thrombomodulin can indicate absence of thrombomodulin at the surface of endothelium. Coagulopathy is encouraged by these two phenomena thereby offering a basic concept to explain how thrombosis could occur in cancer patients (Lindahl et al, 1993). Several different agents activate the endothelial cells such as inflammatory cytokines. In response to these agents, expression of different pro-coagulant and pro-inflammatory molecules is upregulated by the endothelial cells. Endothelial cells are triggered to synthesize TF and express it on their surface and also within derived microvesicles under pathological conditions (Combes et al, 1999). Furthermore, malignant cells generate and release several different cytokines such as pro-angiogenic factors and pro-inflammatory factors. IL-1β and TNF-α are pro-inflammatory and basic fibroblast growth factor (bFGF) and vascular endothelial growth factor (VEGF) are proangiogenic factors. Overproduction of cytokines is also demonstrated by normal inflammatory tissues when the host responds to tumour damage. The majority of these cytokines make the normal ECs and monocytes to express a procoagulant phenotype (Falanga et al, 2009). In addition, ECs are triggered by cytokines to amplify the generation of fibrinolysis inhibitor Plasminogen activator inhibitor-1 (PAI-1). Moreover, they also cause down-regulation of thrombomodulin (TM) and up-regulation of expression of TF on surface of EC. Having a strong anticoagulant activity, TM is expressed on vascular ECs as a membrane receptor. It causes activation of the natural anticoagulant protein C by binding with thrombin to generate a complex (Van de Wouwer et al, 2004). The normal anticoagulant endothelium is converted to a prothrombic one by down-regulation of the anticoagulant TM/protein C system and up-regulation of the procoagulant TF (Falanga et al, 2009).

Thrombin has proven to be an efficient activator of angiogenesis through clotting-dependent pathways that involve activation of platelet and buildup of fibrin (Falanga et al, 2009). Moreover, angiogenesis is induced by thrombin via clotting-independent pathways by activation of PAR and consequential signal transduction chain reactions. Several angiogenesis-related genes are up-regulated within endothelial cells as a result of activation of PARs by thrombin. These genes include metalloproteinase-2, basic fibroblast growth factor (bFGF), vascular endothelial growth factor receptors (VEGFR) and vascular endothelial growth factor (VEGF). Moreover, platelets are triggered by thrombin to release angiopoietin and VEGF that causes induction of tube formation with endothelial cells (Falanga et al, 2009; Wojtukiewicz et al, 2001).

It has been proposed that P-selectin is a principal endothelial cell receptor that is responsible for capturing leukocytes present in the circulation as well as the leukocyte-derived MVs that express PSGL-1(McEver & Cummings, 1997). It has been shown through a research that utilized a mouse microvascular thrombosis model that P-selectin is required for docking of leukocyte-derived MVs to the thrombus site. Moreover, mice lacking PSGL-1 or P-selectin demonstrated decreased thrombosis (Furie & Furie, 2008). In this microvascular thrombosis model, a crucial part is played by hematopoietic cell-derived TF-positive MVs. Recruitment of leukocytes has been shown to be blocked by inhibition of platelet P-selectin which also caused reduction in fibrin deposition in baboon thrombosis model (Chou et al, 2004; Palabrica et al, 1992)

1.11.3 The Effect of chemotherapy agents on EC:

The exact mechanisms by which chemotherapeutic agents increase VTE risk are largely varied. Though, several known mechanisms have been suggested. One possible mechanism is the ability of chemotherapy to induce the release of cytokines and procoagulant molecules, such as TF, during chemotherapy-induced cell damage and associated tumour lysis. This activation causes damage to the vascular endothelium and prompting the coagulation activity. Moreover, chemotherapy is also capable of causing reduction in the production of endogenous anticoagulant proteins such as protein S and protein C (Falanga & Russo, 2012; Mackman, 2012; Sousou & Khorana, 2009).

When tumour-derived products or chemotherapeutic agents damage the endothelial cells, they lose antithrombotic characteristics and this contributes in amplifying the risk of VTE (Falanga et al, 2013).Vascular endothelium can be damaged directly by chemotherapeutic agents thereby bringing about imbalance between anticoagulant and procoagulant entities, inducing death of cancerous endothelial cells, activating cytokines and amplifying activity of TF (Haddad & Greeno, 2006; Lechner & Weltermann, 2008).

Thrombosis risk can be increased by chemotherapy owing to the endothelium damage caused by it. This risk can be enhanced by anti-angiogenic agents, especially when used with conventional chemotherapeutic agents. When patients suffering from multiple myeloma or renal cell carcinoma receive thalidomide with chemotherapy (probably with steroids), rate of thrombosis is substantially increased (28% and 43% of patients respectively) (Kuenen et al, 2002). Possibly because of their damaging effect on endothelium, the new-generation anti-angiogenic agents are linked with increased VTE risk and arterial thromboembolism risk (Kuenen et al, 2002). Moreover, many studies have demonstrated that patients treated with chemotherapy have a 2 to 6 fold increased risk for VTE (Barni et al, 2011; Moore et al, 2011).Researchers have found through in *vitro* experiments that procoagulant activity of ECs and macrophages is influenced by doxorubicin (DOX) which changed the fluidity of membrane and promoted TF activation (Hoshi et al, 2011; Walsh et al, 1992). Based on previous studies demonstrating (DOX) -induced apoptosis in EC resulting in hypercoagulable state (Ben Aharon et al, 2013; Kim et al, 2009). Chemotherapy is capable of causing vascular complications, as a result of this effect, a significant overlap between signaling pathways required for normal vascular function and those required for tumour growth. Moreover, the loss of vasorelaxant effects, suppressed anti-inflammatory and vascular reparative functions all have been reported as indication of endothelial dysfunction which caused primarily by chemotherapy agents. These effects could induce and promote the development of hypertension, atherogenesis and thrombosis (Cameron et al, 2016). Furthermore, a reduction of nitric oxide release due to endothelial damage by chemotherapy agents could increase the likelihood of thrombosis (Daher & Yeh, 2008).VEGF is an important pro-angiogenic molecule. VEGF is a 45-kDa glycoprotein formed by many cell types, including renal epithelial cells, endothelial progenitor cells, endothelial cells, fibroblasts, macrophages, and certain tumours (Lee et al, 2015b). Antiangiogenic agents such as VEGF inhibitors (VEGFIs) and other cytotoxic drugs, including antimetabolites, taxanes, alkylating and anthracyclines agents could have adverse effects which include vascular toxicities and other clinical diseases such as hypertension, acute coronary syndromes, stroke and venous thrombosis (Meinardi et al, 2000; Soultati et al, 2012). A study has reported that Cisplatin-based chemotherapy is associated with a 9% risk of thromboembolic events (Nuver et al, 2004). Several known mechanisms have been postulated that might contribute to thrombus formation include endothelial cell damage and dysfunction provoking a hypercoagulable state with platelet activation, adhesion, and aggregation, and reduced nitric oxide bioavailability and increased von Willebrand factor (Rajendran et al, 2013). Moreover, -associated hypertension induced by cisplatin might result in acute cardiovascular complications (Soultati et al, 2012).Cancer chemotherapy drugs such as anthracyclines has made significant advances in the treatment of both hematological and solid

malignancies (Herrmann & Lerman, 2014). Though, these agents might cause cardiac toxicities. Cardiotoxicity caused by anthracyclines can be characterized as either irreversible type 1 which is caused by cardiomyocyte death, either through apoptosis or necrosis. Moreover, Type 2 cardiotoxicity is caused by myocardiocytes dysfunction rather than cell death and usually resolves with discontinuation of therapy (Lee et al, 2015b; Truong et al, 2014).

1.12 Aims

VTE is considered a multifactorial disease that arises from a variety of factors, including genetic, acquired, and environmental factors. This raises the question of the role of cancer in developing VTE. The answer that emerges from the literature is that cancer is considered a prothrombotic state, including thrombotic disease - that is, enables the development of thrombus. This is commonly attributed to the ability of malignancy to activate the hemostatic system and interfere with blood clotting leads to a hypercoagulable state (Seaman et al, 2014). The haematological balance between pro- and anti-coagulation factors can be tipped in favour of a more procoagulant phenotype patients with certain tumours such as pancreas and ovarian. This haematological procoagulant state is thought to be driven by tumour derived MP that are released into the blood and surgical removal of the tumour has been shown to significantly reduce MP levels in the blood of pancreatic cancer patients. Chemotherapy is an independent risk factor for venous thromboembolism (VTE) in patients and the working hypothesis is that this increased risk of VTE is due to and increased release of tumour MP into the blood via tumour apoptosis due to treatment. Furthermore, it is proposed that this increased risk of VTE is due to release of tumour MP into the blood. To further investigate this mechanism, an *ex-vitro* microfluidic model system was developed wherein tumour spheroids were transferred onto the microfluidic chip and procoagulant activity (PCA) was assessed under flow conditions. The overall purpose of this study is to investigate how tumour MP can interact *in* with endothelial cells and potentially confer procoagulant activity on the latter cell type. A more comprehensive understanding of pathways for endothelial involvement in thrombotic events will help to develop better therapeutic solutions for cancer treatment. To do this, an *ex vivo*-microfluidic device made up of two separate microfluidic biochips must be built and validated. One chip was used to maintain a traditional 2D cell culture of 3D-tumour spheroids, better mimic the microenvironment of the tumour and the release of the micro particle in vivo. A second biochip was used to grow endothelial cells under flow conditions to model in vivo blood flow and related shear stress more effectively. Finally, the two chips were connected to allow spheroid released tumour microparticles to stream directly over endothelial cells and any interactions could be evaluated.

1.12.1 Objectives

- The initial aim of this research project will be to establish a microfluidic chip for characterization and investigation of MP driven PCA in cancer. To establish this model, two chips are connected. The first chip was used to immobilise the tumour spheroid. The second chip was coated with HUVECs and the two-chip connected.
- Assess the PCA of tumour MP shed by several cancer cells using 2D and 3D cell culture methods and several cancer cell lines were screened for their ability to form tumour spheroids.
- Investigate how tumour MP are able to interact with endothelial cells *in vitro* and, potentially, confer procoagulant activity (PCA) and the effect of Doxorubicin on spheroid and HUVECs was assessed. In addition, Tumour MV were also labelled quantified by flow cytometry before and after interaction with HUVECs under static and flow condition.

Chapter 2 Material and Methods

2.1 Cell culture

2.1.1 Human cancer and normal cell line collection

The cancer cell lines that were used in this study were Human pancreatic cancer cells lines that include AsPC-1, MIA-PaCa-2 and PANC-1 which were obtained from the American Type Culture Collection (ATCC, UK). AsPC-1 is a metastatic pancreatic adenocarcinoma derived from ascites of a 62-year-old female (Chen et al, 1982). MIA-PaCa-2 is derived from tumour tissue of the pancreas taken from a 65-year-old male (Yunis et al, 1977). PANC-1 is Human epithelial cells from pancreas tissue taken from a 56-year-old Caucasian male with epithelioid carcinoma. Ovarian cancer cell lines SKOV-3 and A2780 were obtained from the European Collection of Cell Cultures (ECACC), whereas ES2 was purchased from ATCC. SKOV-3 is a metastatic ovarian adenocarcinoma taken from the ascites of a 64 year old female (Fogh et al, 1977), and ES2 was established from the tumour tissue of a 47 year old female with poorly differentiated ovarian clear cell carcinoma (Lau et al, 1991). A2780 human ovarian cancer cell line was established from the tumour tissue of an untreated patient (Behrens et al, 1987). The human glioma cell line U87 was obtained from American Type Culture Collection (ATCC, UK). U87 is epithelial cells derived from human brain tissue taken from unknown age male with glioblastoma. Primary Human Umbilical Vein Endothelial Cells (HUVECs) were isolated from the vein of the umbilical cord of single, pooled or pre-screened donors and purchased from Promo Cell.

2.1.2 Tissue culture and maintenance

In order to minimize the risk of contamination, all cell culture work was carried out within a biosafety cabinet class II sterile laminar flow that was cleaned with 70% ethanol. In addition, Virkon disinfectant (Scientific Laboratory Supplies Limited, Hessle, UK) was used frequently to sterilise and clean the water bath and waste containers. Moreover, regular testing of cell cultures to ensure absence of mycoplasma contamination in all cell lines was conducted at regular intervals by a laboratory technician (MycoProbe Assay, R&D Systems, Abingdon, UK).

2.1.3 Cryopreservation

In order to store the cells, cells were first harvested in the logarithmic growth phase and adherent cells were re-suspended. A small number of cells (10 µl) were removed and a cell count was conducted as in section 2.2. to ensure the viability of cells exceed more than 90%. Cell cultures were centrifuged at 400 x g for 3 min and resuspended in freezing medium that contains: [90% fetal bovine serum (FBS); BioSera, Ringmer, UK] and 10% dimethyl sulfoxide [DMSO; Sigma-Aldrich, Poole, UK]) to final concentration of viable cells in the range 1-3 x 10^6

cells / ml of freezing medium. To avoid damage to the cell during freezing, a cryoprotectant (DMSO) was added to the growth medium in which the cells are to be frozen. Aliquots of cells (1 ml) were transfer into 1 ml cryovials and slowly frozen in a freezer at -80°C by reducing the temperature at about 1°C per minute in a cryo-freezing container (“Mr. Frosty" Nalgene, Sigma-Aldrich) filled with isopropyl alcohol. Folowing this samples were stored in liquid nitrogen until required. To maintain consistency cells were cultured continuously for a maximum of 12 weeks.

2.1.4 Defrosting of Cryopreserved cells

A vial of frozen cells was taken from liquid nitrogen storage and directly thawed in a water bath at 37°C for 1-2 min. Once defrosted, all vials were sprayed by using 70% ethanol before being transferred into the cell culture hood. In order to remove the DMSO within the freeze media, the cells were diluted in a 9 ml of pre-warmed medium and the suspension was centrifuged at 400 x *g* for 5 mins. The supernatant was discarded then the pellet cells were re-suspended in 10 ml of fresh media and appropriate amount of cell suspension was transferred into new cell culture flask that was incubated in 5% CO_2 at 37°C for further study.

2.1.5 Maintenance of cell lines

Culture of all cell lines was conducted in a class II sterile laminar flow cabinet in 25 or 75cm² tissue culture flasks (Sarstedt, Leicestershire, UK). Flasks were maintained in a humidified incubator in 5% CO_2 at 37°C. In the log phase, all cells were subcultured at approximately 80% confluency to maintain cells in optimal condition for another passage and continued growth. All cells were detached from the surface of a flask via using a cell scraper (Sarstedt, UK) and the cell solution was centrifuged at 400 x *g* for 5 min. Then the supernatant was carefully discarded, and the cell pellet was resuspended in 1 ml of a fresh medium to determine the cell viability using the trypan blue exclusion test. Then, appropriate amount of new fresh medium was added to the pellet solution and 1 ml was transferred to a new flask contain appropriate amount of fresh prewarmed medium.

2.1.6 Pancreatic cancer cell lines

The human pancreatic cancer cells lines AsPC-1, MIA-PaCa-2 and PANC-1 were cultured in either RPMI1640 medium (AsPC-1) or Iscove’s Modified Dulbecco’s Medium (MIA-PaCa-2), while Dulbecco's Modified Eagle's Medium was used for PANC-1. AsPC-1 was seeded and maintained in RPMI 1640 medium (ATCC), supplemented with 10% (v/v) foetal bovine serum (FBS) (Bio-Sera, UK), 100 units/ml penicillin, 100 µg/ml streptomycin ,1% HEPES buffer, and 1% sodium pyruvate (all Lonza, UK) in 5% CO_2

at 37°C. MIA-PaCa-2 was seeded and maintained in Iscove's Modified Dulbecco's Medium (IMDM) (ATCC), supplemented with 1% penicillin/streptomycin, 1% L-glutamine, 10% FBS, and 2.5 %(v/v) horse serum from (Gibco®, UK).Whereas, PANC-1 was maintained in Dulbecco's Modified Eagle's Medium that supplemented with (v/v); 100 units/mL penicillin, 100 µg/mL streptomycin (Lonza, UK) and 10% FBS (Bio-Sera, UK). Serum, buffers and penicillin / streptomycin added to media were filtered through a 0.2 µm filter (Sartorius AG, Göttingen, Germany) before addition to the cancer cell lines.

2.1.7 Ovarian cancer cell lines

A2780 was seeded and maintained in RPMI 1640 medium with 10% FBS, 100 units/ml penicillin, 100 µg/mL streptomycin (all Lonza, UK). SKOV-3 and ES2 were seeded and maintained in McCoy's 5A medium (ATCC, UK) supplemented with 15% (v/v) FBS and 1% (v/v) Penicillin/Streptomycin (Lonza, UK). Culture of ovarian cancer cells was conducted in a class II sterile laminar flow cabinet in 75cm² tissue culture flasks (Sarstedt, Leicestershire, UK). Flasks maintained in a humidified incubator in 5% CO_2 at 37°C. In the log phase, all cells were subcultured at approximately 80% confluency to maintain cells in optimal condition for another passage and continued growth. All cells were detached from the surface of a flask via using a cell scraper (Sarstedt), transferred to a sterile polypropylene tube (50ml) and the cell solution was then centrifuged at 400 x *g* for 5 min. Supernatant was discarded and pellet cells were resuspended in 1 ml of a fresh medium to determine the viability percentage. Then appropriate amount of new fresh medium was added to the pellet solution and 1 ml was transferred to a new flask contain appropriate amount of fresh prewarmed medium.

2.1.8 Glioma cell lines (U87)

U87 was seeded and maintained in Eagle's Minimum Essential Medium (EMEM) supplemented with 10% (v/v) FBS and 1% penicillin/streptomycin (all Lonza, UK). Culture of glioma cells was conducted in a class II sterile laminar flow cabinet in 75cm² tissue culture flasks (Sarstedt, Leicestershire, UK). Flasks maintained in a humidified incubator in 5% CO_2 at 37°C. In the log phase, all cells were subcultured at approximately 80% confluency to maintain cells in optimal condition for another passage and continued growth. All cells were detached from the surface of a flask by washed cells with phosphate buffered saline (PBS) and subsequently incubated with 3-4 ml trypsin ethylenediaminetetraacetic acid (EDTA) (Lonza, UK) for 5-10 min at 37°C to allow the cells to dissociate. Subsequently, 3-4 ml of fresh pre-warmed medium was added to inactivate the trypsin. Cell solution was then centrifuged at 400 x *g* for 5 min. carefully, the supernatant was discarded, and pellet cells were resuspended in 1 ml of a fresh medium to determine the viability percentage. Then appropriate amount of new fresh medium was added

to the pellet solution and 1 ml was transferred to a new flask contain appropriate amount of fresh prewarmed medium.

2.1.9 Culture of the primary cells (HUVECs)

HUVECs were maintained and cultured in Endothelial Cell Basal Medium Plus Endothelial Cell Growth Medium Supplement Mix (PromoCell, UK). HUVECs were removed from flask surfaces by EDTA for 3 minutes. Then cells were washed with PBS prior to trypsinisation and subsequently with an excess of media before centrifugation at 400 x *g* for 3 min. The cell pellet was then re-suspended in medium and a cell count performed. An appropriate number of cells were then seeded into a 25cm^2 tissue culture flask with fresh media and maintained at 37° in a 5% CO_2 incubator. HUVECs were utilised at passage 3-6.

2.1.10 Three-dimensional (3D) Spheroid culture

In this study, the liquid overlay method was used to generate spheroids by seeding cells at concentration of 2x10^4 cells/well in a volume of 200 µl/well of culture medium in general tissue culture 96-well plates (Sarstedt, UK), that were pre-coated with agarose (1.5% 4% w/v in sterile water). To prepare 1.5 % agarose, an appropriate amount of agarose (BioReagent agarose, Sigma-Aldrich, UK), was added into an appropriate volume of distilled water (dH_2O) and autoclaved (121°C for 15 min). Then, the agarose was allowed to cool in a biological safety cabinet to 50 °C and 100 µl of agarose gel was added into 96 culture plate then plates were allowed to cool to room temperature. All cancer cells were harvested based on type of the cell and 200 µl of cell suspension was transferred into 40 interior wells of a 96-well plate coated with 1.5% agarose gel. Whereas, the external wells or unused wells were filled by 200 µl of phosphate buffered saline (PBS) to avoid evaporation during incubation time. Then, plate was maintained in 5% CO_2 at 37°C for 3 days. To monitor spheroid's growth, Pictures of the spheroids were taken in day 3 and day 10 by using an Oxford Optronix GelCount™ camera and spheroid size was measured using ImageJ software (National Institute of Health, US).

2.2 Cell count and trypan blue exclusion Assay

A homogenous cell suspension of adherent cells was mixed with equal amounts of 0.4% trypan blue (Sigma-Aldrich). The dye exclusion test is used to ascertain the number of viable cells present in a cell suspension. This test is based on the principle that live cells (viable cells) retain intact cell membranes that exclude certain dyes, such as trypan blue, whereas dead cells with damaged membranes allow the dye to enter and appear as blue cells. The cells and dye solution were gently mixed to attain a homogeneous cell suspension and applied to the counting improved Neubauer chamber haemocytometer improved Neubauer (depth 0.1mm

1/400mm²) (Hawksley, UK), with the area under the cover slip filling by capillary action (Figure 2.1). With the microscope, cells were counted using a 20x magnification and all cells in the central gridded square were counted and total cell count. To calculate the cell concentration, the following equation was used: cell concentration (cells/ml) = Average number of total cells x dilution factor x volume of chamber. To calculate the cell viability, following equation was used: Average counted live cells / (Average counted total cells: live and dead cell) x100.

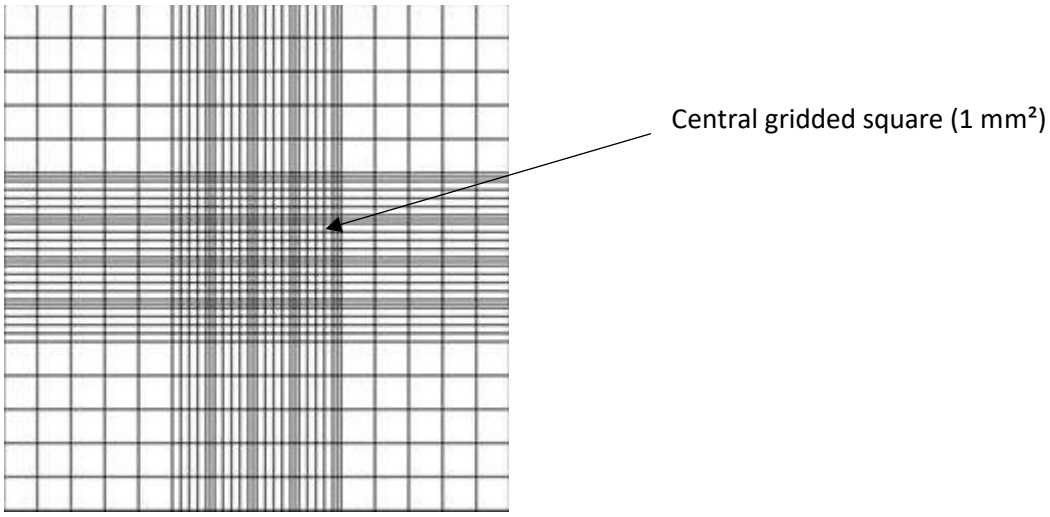

Figure 2.1: schematics showing improved Neubauer chamber haemocytometer.

2.3 Pro-thrombin Time (PT) coagulation assay of Cells and cell-free media

Procoagulant activity (PCA) of cell-free supernatant and cell suspension were measured using the semi-automated instrument Thrombotrack SOLO coagulometer. This coagulometer is based on the mechanical detection of the clotting endpoint method. The principle behind this coagulometer is based upon a beam of light detecting the magnetic rotation of a steel ball by a magnetic sensor. Once the sensor rotates, the steel ball maintains its movement when the sample is unclotted. Though, when a solid fibrin formation begins, the ball is caught in the clot and moves out of the sensor's range detection and result in stopping the timer (Figure 2.2).

Figure 2.2: Thrombotrack SOLO coagulometer.

All cells were harvested as described above. Then, cells were resuspended in blank media depend on a cell line type at cell concentration of 3 x 10^5 cells/ 100 µl. In this study, 100 µl of the sample and 100 µl normal plasma control (NormTrol, Helena Biosciences, Gateshead, UK) were dispensed into a cuvette that contains a steel ball. The normal plasma control contains all coagulation factors except TF. Then, the clotting time (CT) was initiated by the addition of 100 µL of 25 mM $CaCl_2$ solution to recalcify the sample (Glynn et al, 2015; Sørensen & Ingerslev, 2004). In order to establish standard curve, serial dilutions of cell suspension were prepared using blank medium. To determine the PCA, listed cell suspensions (100 µl) were incubated with 100 µl of control normal plasma (Helena Biosciences, Gateshead, UK) at 37 ° C for 2 min in the cuvette centre and coagulation initiated by adding 25 mM $CaCl_2$(100 µl). To determine the CT of cell-free media larger cell debris was removed via centrifugation at 1000 x g for 3 min, then 100 µl of cell free supernatant were mixed with 100 µl of control normal plasma into a cuvette containing a steel ball and incubated for two minutes. Coagulation was initiated by adding 25 mM $CaCl_2$ (100 µl).

2.4 Conductivity

The study was designed to create an in *vitro* tumour based coagulation model on a microfluidic chip so that PCA could easily be measured in a flush on the chip instead of collecting or extracting samples for off-chip processing. Conductance was investigated for this purpose as an alternative form of PCA evaluation. The ability to pass an electric current is electrical conductivity; if the cell culture media contains negatively charge MP then the conductivity should be affected in a concentrator-dependent manner.

Pancreatic cancer cell lines AsPC-1 and ovarian cancer cell lines and SKOV-3 were cultured in respective medium suggested by supplier as indicated in previous sections. The PCA and conductivity (microsiemens µS), of the cell-free supernatant were evaluated to establish a linearity relationship between conductivity and PCA. To measure a conductivity of cell-free supernatant, Jenway 4510 meter was used to measure conductivity in low volume of supernatant down to 150 µl (Figure 2.3). Essentially, conductivity is the ability of a solution to pass an electric current depends on many factors such as mobility of ions and temperature. The meter was installed and prepared as manufacturer instruction. The meter is connected with micro-volume probes that designed for the measurement of solutions in small containers. KCL solution (0.01 M) was prepared and used as standard to calibrate the meter which produced a conductivity equal to 1413 µS at 25°C. Harvested cells of AsPC-1 and SKOV-3with concentration (3 x 10^5 cell/ml) were centrifuged at 400 x *g* for 5 min to remove detached cells. The supernatant was collected, and immediately serial dilution was applied using fresh cell culture media for each cell line prior to PT clotting time assay and conductivity experiments.

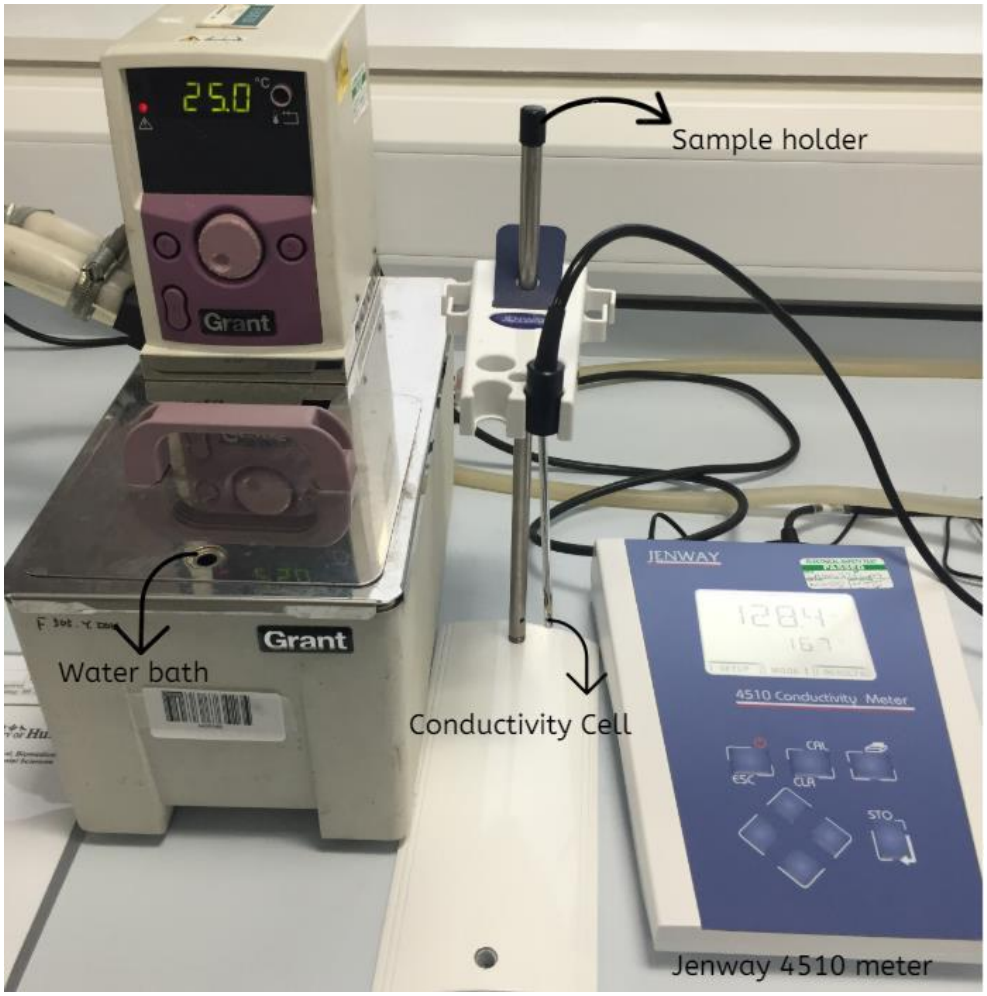

Figure 2.3: Image shows the Jenway 4510 meter and the water bath.
Temperature on meter and water bath should be at 25°C±0.5°C. All samples were tested at 25°C using 300 µl in a 1.5 ml Eppendorf vial that attached to a foam float.

2.5 Transfer of spheroids into a microfluidic chip (general approach)

After spheroids generation as described in section 2.1.10, a single spheroid with an approximate size of 500 µm-diameter was gently loaded into the tissue inlet of the microfluidic chip. In order to retrieve the spheroids, pipette tips with wide tip endings were used to handle the spheroids without disrupting them. PCA of effluents (cell- free media) was measured using a prothrombin time clotting assay. Tumour-on-a-chip system was used where tumour spheroids were maintained in a microfluidic chip and the PCA of effluent using PT clotting time assay in the thromotrack solo coagulometer was assessed. The effluent was collected over time and analysed immediately.

2.6 PCA of cell-free medium of tumour spheroids on chip

Tumour spheroids generated from cancer cell lines (AsPC-1, MIA-PaCa-2, PANC-1, A2780 SKOV-3, ES2 and U87) by using the liquid overlay method and PCA of cell-free supernatant (effluent) was measured using a prothrombin time clotting assay. Effluents were centrifuged at

400 ×g for 5 min to remove any large cell or debris. Then, PCA was assessed for all collected samples.

2.7 Determination of chemotherapeutic drug-induced cytotoxicity on HUVECs

HUVECs (1 x 10^4 cells/well) were seeded into 96-well tissue culture plates at 37°C with 5% CO_2 overnight. Then the cells were treated with different concentrations of Doxorubicin (Dox) (0.001 µM, 0.01 µM, 1.0 µM, and 10 µM and 100 µM) and incubated again for 24 and 48 hrs. Then, cell proliferation, relative to the controls (no drug), was determined by a cytotoxicity assay (CellTitre Aqueous One, Promega, UK). MTS reagent ((3-[4,5-dimethylthiazol-2-yl]-5-[3-carboxymethoxyphenyl]-2-[4-sulfophenyl]-2H-tetrazolium) uses a colorimetric method for the sensitive quantification of viable cells. It can be used to assess cell cytotoxicity or proliferation. The MTS assay protocol is based on the reduction of the MTS tetrazolium compound by viable mammalian cells to generate a coloured formazan dye that is soluble in cell culture media and can be quantified via absorbance. Briefly, cells (2x10^4) in 180 µl of cell culture media were transferred to wells in 96 well sterile tissue culture plates. Various concentration of doxorubicin was added in a volume of 20µl into the cells and incubated for 24 and 48 hours in the incubator (37°C, 5% CO_2). After incubation plates were centrifuged at 400 x *g* for 5 min and the supernatant was removed. Fresh medium (180 µl) was then added followed by MTS reagent (20 µl) and the plates incubated in (37°C, 5% CO_2) for 4 hours. The absorbance was then read at 490nm using a microplate reader (BioTek synergy HT, BioTeK, UK).

2.7.1 The effect of Doxorubicin on the procoagulant activity of MPs

PCA of effluent was assessed with or without Doxorubicin (Dox). Therefore, two chips were prepared for different tumour spheroids. In order to standardise the experiment, 40 spheroids were transferred into chip 1 to assess the Dox effect. The second chip was also contained 40 spheroids but without dox. PCA was assessed after 6 h and 24 h via PT clotting assay (section 2.3).

2.8 Flow cytometry setup

2.8.1 Background

Flow cytometry is a technology for the rapid detection and identification of cells with different physical and chemical properties; if desired, cells can also be physically sorted based on different characteristics (Davey, 2003). One of the most common ways to distinguish cells from one another is to label them with different fluorescent dyes. In flow cytometry, a population of cells in suspension is moved one by one through a laser beam that excites the cells;

photomultiplier tubes record the emitted light and send the data to software for further analysis. The procedure is usually fast - with thousands of cells analysed per second - and delivers reliable results (Finak et al, 2016).

Even size and morphology, which will result in differential scattering of the laser beam, called forward scattering (FSC) and side scattering (SSC). The variety of fluorescent probes that can bind to and visualize cellular structures and function as sensors to measure certain parameters within the cells is one of the reasons that flow cytometry has become an enormously versatile technology (Adan et al, 2017). Usually, the data that a flow cytometer produces can be recorded in a one-dimensional manner - for example, as a histogram with the intensity of the fluorescent signal at a specific wavelength on the x-axis and the frequency or cellular count on the y-axis. Another very common way is to record the data in two variables, which allows us to distinguish subpopulations in a sample. There parameters that can be measured are light scattering activity of the cells. Larger cells will scatter the laser beam more strongly than smaller cells, which enables us to distinguish cells not only based on any fluorescent signal, but also size. The number of parameters that can be used to differentiate cell populations from one another is large and covers a multitude of cell biological, biochemical and biophysical properties: cellular markers, stained with antibodies or fluorescent molecules; nucleic acid content, visualized using fluorescent probes; intracellular pH, detected using specific acid-sensitive dyes; viability and apoptosis.

2.8.2 Detection of microparticles (MP)

This study sets out to develop an efficient method to standardize the enumeration of MPs using flow cytometry.

The general formula for MPs enumeration:

MP/μl = (MP count/bead count) × (total number of beads/test volume)

2.8.3 Microbeads

To develop a method to reliably enumerate MP, fluorescent Megamix-Plus microbeads (Biocytex, France) were used that were optimized for side scatter-optimized flow cytometers based on the FACSCalibur detection characteristics as recommend from this laboratory's participation in two International Society of Thrombosis and Haemostasis workshops (Cointe et al, 2017a). Beads were of varying sizes between 0.1 and 0.5 μm (0.16 μm, 0.20 μm, 0.24 μm and 0.50 μm). A flow cytometer (BD FACSCalibur) was setup with Megamix SSC beads (Biocytex, France) that are used to define a MV gate according to side-scatter characteristics of the beads. MP gate set at approximately 0.2–0.5 μm.

2.8.4 Usage of beads in flow cytometer

Prior to use, ca. 500 µL of the bead solution was pipetted into an Eppendorf tube and thoroughly vortexed at room temperature. The time of analysis was set to 1 - 2 minutes and a suitable signal height was defined. Side-scattering (SSC) voltage was set close to 600 V, and forward-scattering (FSC) voltage was placed near 800 V. The FL-1 signal was set at 580 V. Logarithmic display for parameters was chosen, and the flow speed was selected around 10 - 15 µL/min (low flow rate).

2.8.5 FITC and SSC voltages

FITC vs. SSC signals were measured, and a rectangle was set around each singlet population (Figure 2.6). subsequently, a histogram was generated that shows the bead count in dependence of their scattering intensity, i.e. bead diameter (Figure 2.7).

2.8.6 Setting an MP gate

To provide the bead/MP analysis with upper and lower boundaries, a gate was defined to exclude lower scattering intensity and thus further reduced the noise. The lower end (LE) was defined using the medians of the 160 nm and 200 nm bead population:

LE = Median (160 nm) + 0.3 · [Median (200 nm) - Median (160 nm)],

While the upper end was set at the 99th percentile of the 500 nm bead population. The resulting gate is shown in figure 2.8.

2.8.7 Dual scatter analysis

To increase the options to further analyze bead populations, a dual scatter plot of side-scattering (SSC) to forward-scattering (FSC) signal was created. The resulting analysis with low, medium and high FSC signal is shown in figures 2.9 and 2.10, respectively.

2.8.8 Results

The preceding materials and methods described a sequence of protocols to calibrate a flow cytometer for the standardized enumeration of MPs. Subsequently, an upper and lower boundary was defined as a gate that ensured lower scattering intensities - associated with background as well as the smallest bead size - were excluded from the analysis. Figures 2.4 to 2.8 show the results of these procedures.

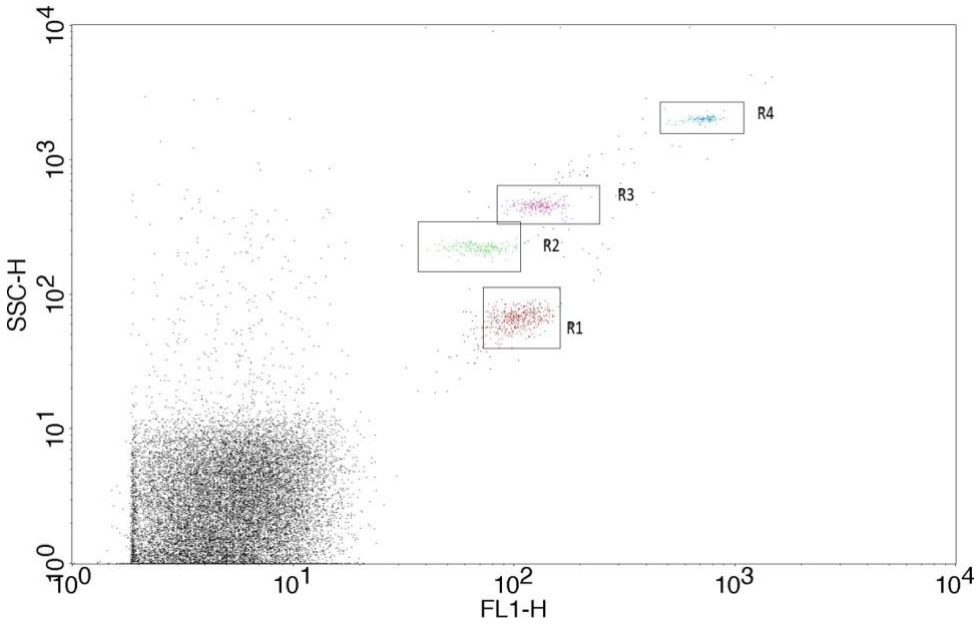

Figure 2.4: Cytogram SSC vs. FITC signal.
The figure shows four distinct bead populations, manually encased with rectangles, that scatter light differently, dependent on their sizes. The larger the SSC-H signal, the larger the bead diameter. Noise can be observed with low FL-1 and SSC.

Figure 2.4 shows the combination of side-scattering and fluorescence intensity - both on a logarithmic scale - for all four populations of beads with different diameters (160 nm, 200 nm, 240 nm and 500 nm). The light scattering signal changes with the size of the particle; here, the larger the microbead, the stronger the signal. Figure 2.5 was also used to outline the four different bead populations with rectangles and thus select the different particle signals. In future measurements, the noise in the bottom left corner of the graph - particles that elicit a combination of low fluorescent signal and low scattering intensity - should be cut off to improve the overall signal.

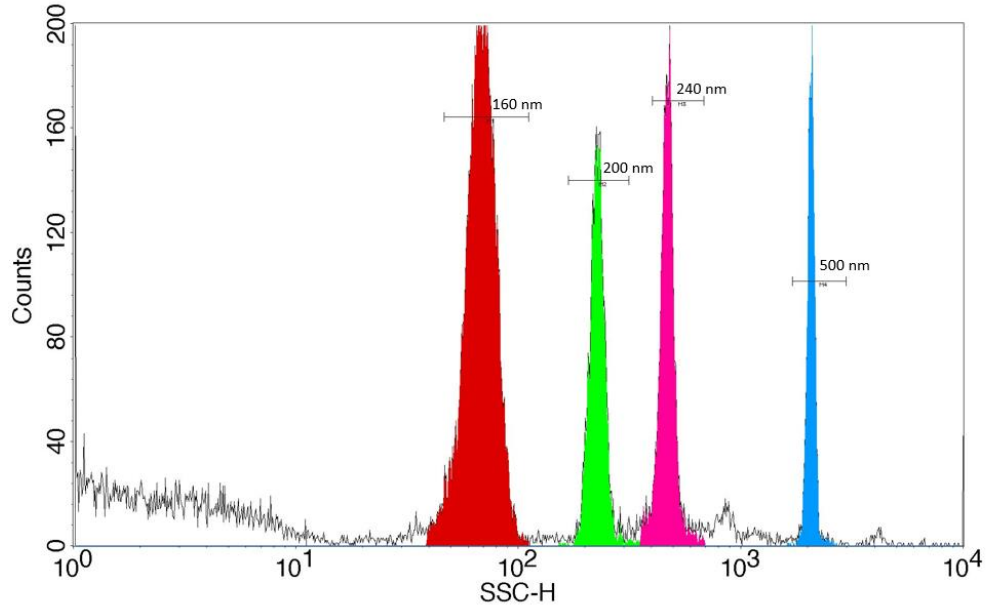

Figure 2.5. Histogram of the scattering intensity of each bead.
The colour signifies the SSC bead signals that have been selected within the four rectangles in figure 2.11.

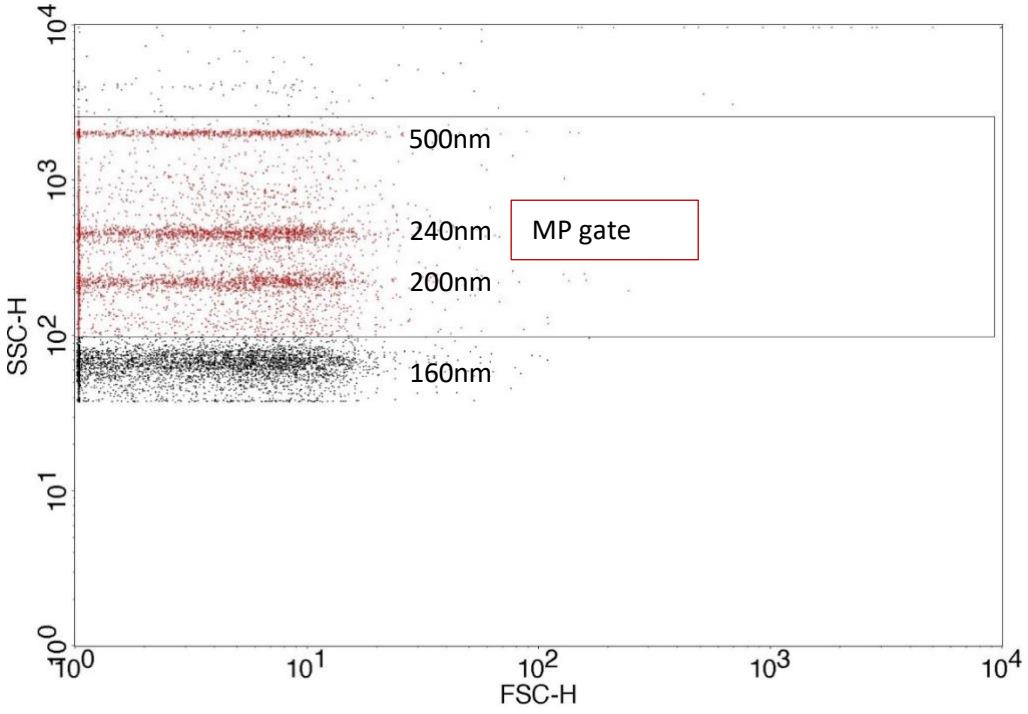

Figure 2.6: Side-scattering (SSC) intensity of MPs vs. forward-scattering (FSC) intensity.
The particles that are coloured in red are part of a user-defined MP gate that ranges from the beginning of the 200 nm particle to the end of the 500 nm particle scattering signal. The figure shows an overall low FSC signal.

Figures 2.6 to 2.8 show the side-scatter (SSC) vs. forward-scatter (FSC) signal of the beads. In addition, a size window or 'MP gate' was defined to improve the sensitivity of the analysis. The drawback is that the lowest size population of beads (160 nm) is excluded from the analysis,

yet this would still allow for a detection of the majority of MPs with a superior sensitivity. Therefore, the gating - albeit slightly wasteful - made sense in this case. It is important to be aware of the larger levels of noise and possibly the lower level of signal that biological tissue exhibits. Therefore, when calibrating the flow cytometer, it is important to optimize the procedure for sensitivity and resolution (Welsh et al, 2017).

Figures 2.7 to 2.8 also show different intensity of forward scattering. Measuring FSC in addition to SSC and fluorescence signal will allow us to further classify the MPs that we analyse.

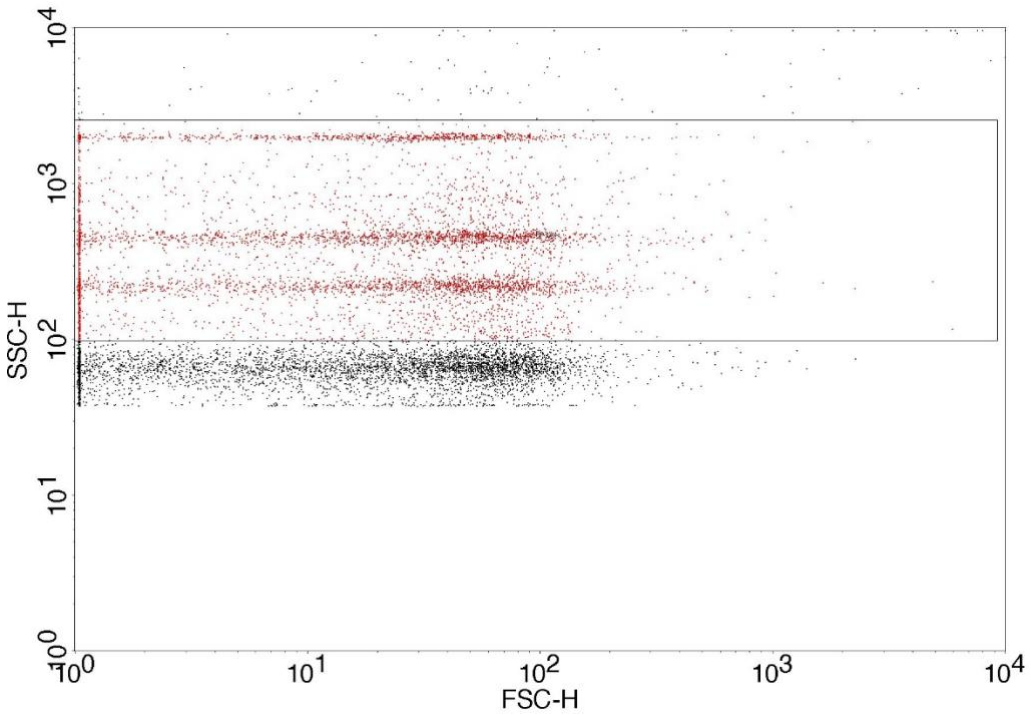

Figure 2.7: Side-scattering (SSC) intensity of MPs vs. forward-scattering (FSC) intensity.
The particles that are coloured in red are part of a user-defined MP gate that ranges from the beginning of the 200 nm particle to the end of the 500 nm particle scattering signal. The figure shows a medium FSC signal.

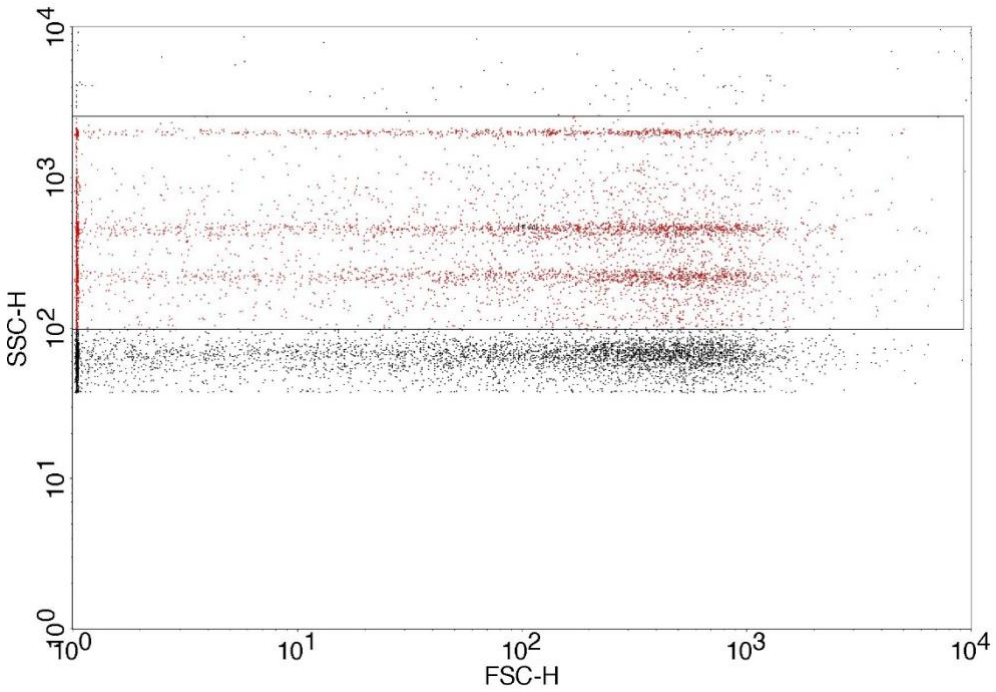

Figure 2.8: Side-scattering (SSC) intensity of MPs vs. forward-scattering (FSC) intensity.
The particles that are coloured in red are part of a user-defined MP gate that ranges from the beginning of the 200 nm particle to the end of the 500 nm particle scattering signal. The figure shows a high FSC signal.

2.9 Tumour microparticles (MP) labelling

2.9.1 CFSE staining protocol

MPs released from AsPC-1, SKOV-3, ES2 and U87 tumour cell lines were labelled with 5(6)-carboxyfluorescein diacetate N-hydroxysuccinimidyl ester (CFSE) CellTrace™CFSE dye (Invitrogen, UK) via labelling of parent cells. The Cell Trace (CFSE) Cell Proliferation reagents are all cell-permeant dyes that are cleaved by intracellular esterases to produce highly fluorescent compounds that also covalently bind to cellular amines, attaching the dye to various cellular components and providing a very stable signal. These reagents show little cytotoxicity with minimal observed effects on the proliferative ability of many cells. Initially, in order to optimise MPs labelling, AsPC-1 cells ($1x10^6$ cells/ml) were harvested via centrifugation at 400 x *g* for 5 minutes and the supernatant was discarded. Next, the cell pellet was resuspended with 1 ml PBS and incubated with CFSE at as a final working concentration. Next, the tube was incubated at 37°C for 20 minutes in the dark. Stained cells were then washed twice with PBS and seeded into six of 25 cm^2 cell culture flasks in 10 ml of the appropriate medium and incubated for 24 h at 37°C and 5% CO_2. Unlabelled cells were used as negative control. In order to count labelled MPs, a solution of 100 µl effluent and 100 µL of counting beads was mixed before flow cytometry. Having established the method to be reproducible, fluorescently labelled MP they were then flowed through a Vena8 Endothelial+™ biochip or

ibidi biochip that pre-coated with a confluent monolayer of HUVECs and imaged using a Cellix imaging system and confocal microscopy respectively.

2.9.2 CD142 staining protocol

For MP anti-TF immunostaining, 5µg of antihuman CD142: FITC antibody (Bio-rad) was added to a 4 ml flow cytometry tube (Sarstedt, UK) containing 50 µl of spheroid effluent and the solution was incubated for 30 min in room temperature in a dark place. For quantification, 50 µl of Accucheck beads were added prior to analysis (Invitrogen, UK). Then, the sample was analysed by flow cytometry for quantifying of Tissue-factor-bearing microparticles (TF+MPs).

2.10 Ibidi model Microfluidics Setup

2.10.1 µSlide I 0.8 Luer setup

A µSlide I 0.8 Luer (Ibidi, Germany) (Figure 2.9 A) was coated with gelatine SOURCE 2% (w/v) (Sitterley, 2008) and incubated overnight at 4°C. Then, HUVECs were prepared to a concentration of 1.6 x 10^6 cells/ml. Then, 150 µl of the HUVECs suspension was injected into the channel by pipetting directly into the channel's inlet. Slide was incubated at 37°C and 5% CO_2 for a minimum of 30min for cell attachment. After cell attachment, 60 µl fresh complete medium was added into each reservoir. Then, slide was further incubated for 2h to allow the cells to settle. This is important because the confluence of the layer is a crucial point in the ability of the cells to resist the shear stress.

To setup this chip for flow applications suitable tube adapter sets were required and were purchased from (Ibidi, Germany). They consist of a tubing (20 cm) with inner diameter of 1.6 mm and adapters for the connection between the ibidi µ–Slide (female Luer) and the tubing of the µ–Slide III 3D (Ibidi, Germany) (Figure 2.9 B). Microfluidic chip µSlide 0.8 Luer was set on the working surface. The first male Luer adapter was pulled from the middle connector holding it upwards to make sure there are no air bubbles remaining inside. Then, connect it to the female Luer on the slide tipping it carefully.

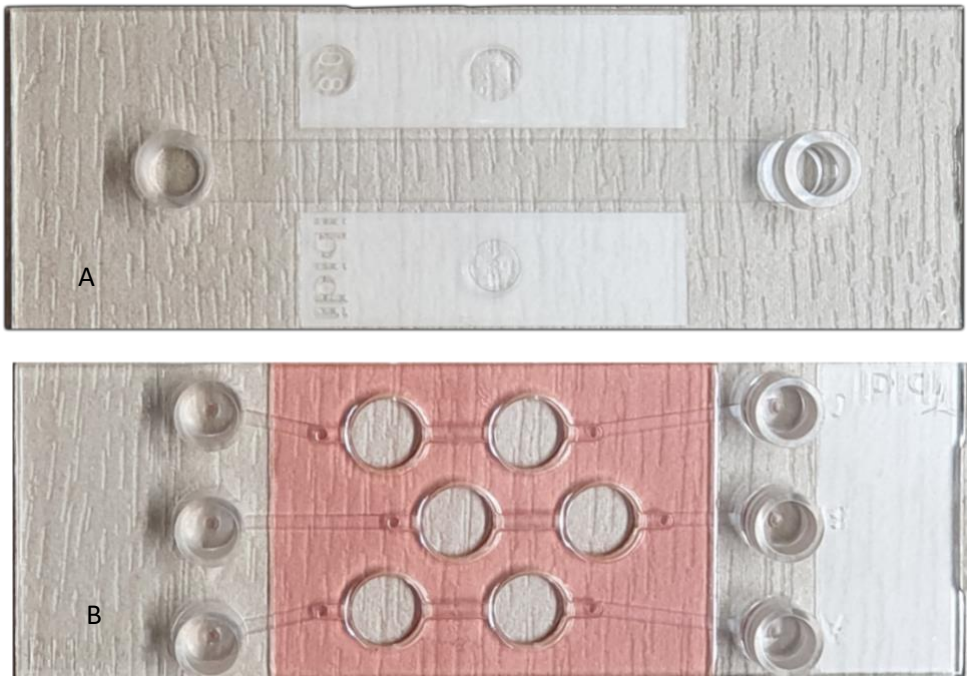

Figure 2.9: Image A shows the µ–Slide I Luer and µ–Slide III 3D.
µ–Slide I Luer which is designed for cell culture under perfusion and all flow applications (Outer dimensions (w x l)25.5 x 75.5 mm², Channel length 50 mm, Channel width 5mm). Image B shows the µ–Slide III 3D Perfusion which is an array of 6 wells where cells can be cultivated and, subsequently, investigated with microscopical methods (Outer dimensions (w x l) 25.5 x 75.5 mm², Volume of wells 30 µl, Well diameter 5.5 mm, Number of channels 3, Channel width1.0 mm). Two of the 6 wells respectively are connected by a channel. The channels can be connected to a Harvard pump for perfusing the wells in order to perform long term cell culture assays with tumour spheroids µ–Slide III 3D setup.

Preformed tumour spheroids of ES2 and U87 was loaded into each well of the uncoated µ–Slide using a pipette. Then, the µ–Slide was covered with the supplied lid and the top was sealed with the enclosed polymer coverslip. Then the protective foil was removed on the upper side of the slide and the coverslip was then placed on the adherent part of the slide. This chip was then connected to another µSlide I 0.8 Luer that contain tumour spheroids using Silicone tubing, 0.8mm ID, sterile. Then, the spheroid chip was connected with Harvard Syringe pump apparatus in a 37 °C thermostatically controlled incubator (Figure 2.10). The µ–Slide III 3D chip is made of a plastic that has the highest optical quality. The polymer coverslip on the bottom exhibits extremely low birefringence and autofluorescence, similar to that of glass. Also, it is not possible to detach the bottom from the upper part. The µ–Slides, µ–Dishes, and µ–Plates are not autoclavable, since they are only temperature–stable up to 80°C/175°F. Gas exchange between the medium and incubator's atmosphere occurs through the polymer coverslip.

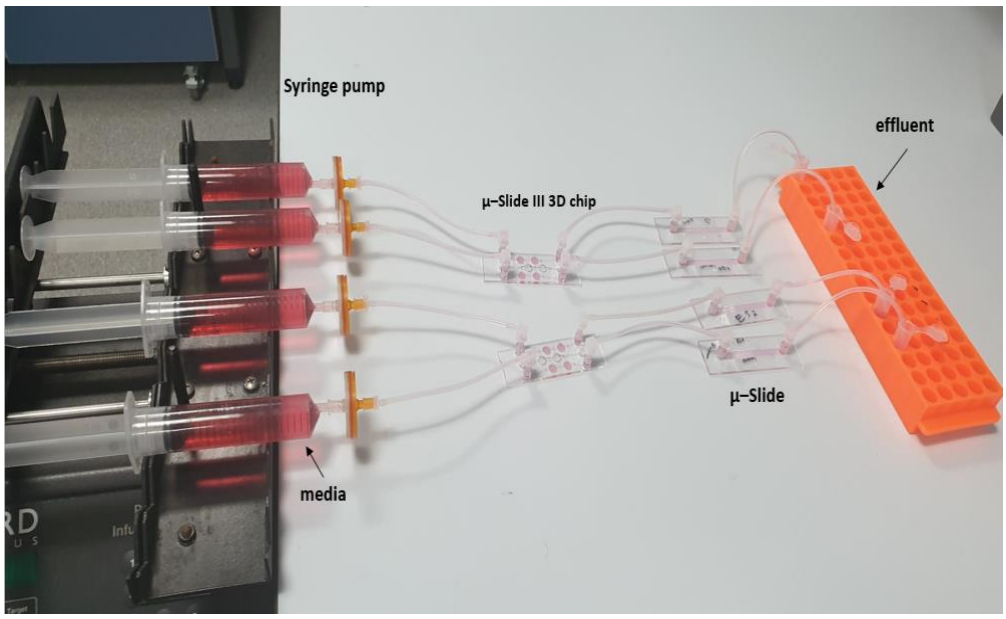

Figure 2.10: Developed experimental setup.
Image showing tumour fresh media contained in syringes connected to a multi well µ-slide III 3D biochip containing either ES2 or U87 spheroids connected through to a µ-Slide I Luer containing HUVECs and finally sample collection tubes. The experiments were carried out in a 37°C incubator.

2.11 Cellix Vena8 Endothelial+™ biochips

Cellix Vena8 Endothelial+™ biochips (Vena 8 microchannels, Cellix, Dublin, Ireland) were kept under UV for 20 minutes and coated by dispensing approximately 12 µL of type B 1% v/v gelatine (Sigma Aldrich) into the 8 microchannels. Then, the biochip was incubated for 24 hours at 4°C. 5 µl of 1.5×10^6 per 100µl of harvested HUVECs were added into each channel and all the reservoirs were then filled with 40µL of media. The biochip was incubated in the CO_2 incubator for 24 hrs at 37°C.Then, labelled/unlabelled MPs that collected from cancer cell supernatant were perfused over the Vena8 Endothelial+™ biochips coated with HUVECs, and PCA, MPs quantification and confocal images were assessed to evaluate MP's interaction with HUVECs. The Vena8 Endothelial+™ biochip is ideal for studying cell-cell study. Endothelial cells are easily seeded and cultured inside the microchannel.

2.11.1 Cellix

In order to assess interactions between tumour MPs and endothelial cells under flow culture conditions, disposable Vena8 Endothelial (Cellix), were sterilised by UV-light and coated with type B 1% v/v gelatine (Sigma Aldrich), at 4°C overnight. HUVECs were seeded into the biochips at 1.5×10^6 per 100µl per channel and allowed to adhere for 2 hours. Then the reservoirs were filled with 40µL of media the cells and were incubated for 24 h at 37°C with 5% CO_2. The biochip was connected to a Kima pump (Cellix) with shear stress at 450µl/min for 6 min, followed by 5 min of absence of flow. The flow chamber was then rinsed three times with 25µl

of media prior to each experiment, and MPs adhesion was initiated by the addition of CFSE-labelled MPs supernatant and unlabelled MPs as well. Interaction of MPs was recorded every second under a shear stress of 1 dyne/cm^2 in phase contrast and the settings were equal in all conditions (exposure time 344 ms, magnification 32×) for 5 minutes. Importantly, two types of flow were used on this biochip: pulsatile flow using Cellix system and constant flow using Harvard pump (Figure 2.11).

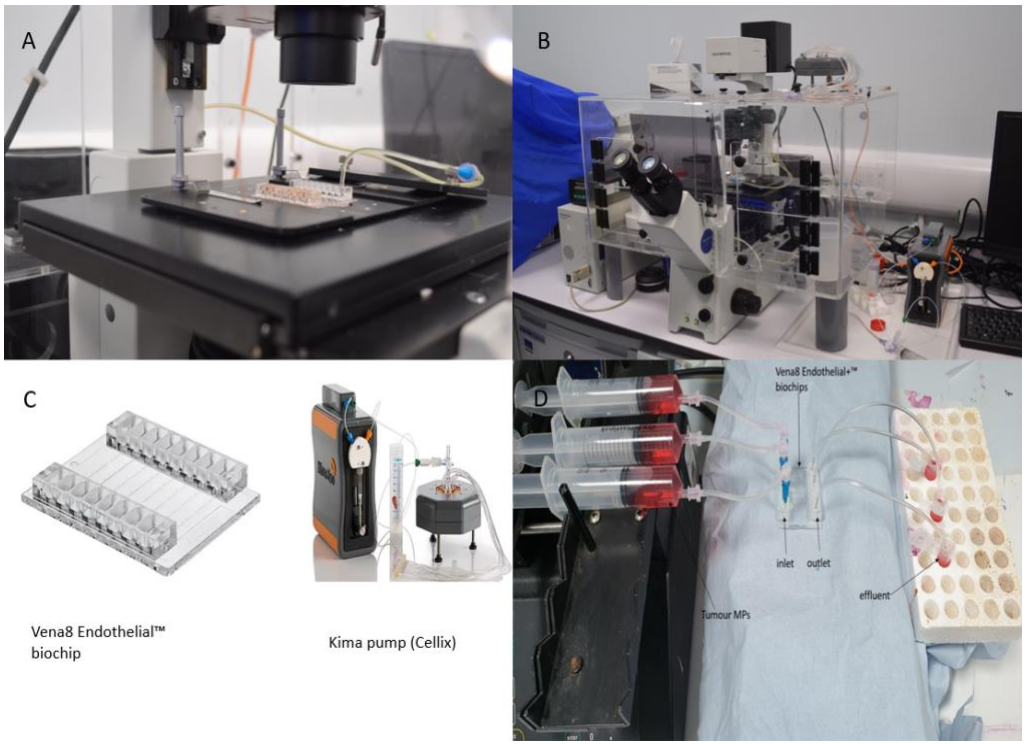

Figure 2.11: experimental setup showing the Vena8 Endothelial+™ biochip.
Image A shows the Vena 8 reedy foe flow experiment. Image B shows Vena 8 linked through to Kima pump pulsatile flow. Image C shows the Kima pump and Vena 8 (8-Channel biochip, Channel width: 0.08 cm, Channel height: 0.012 cm, Channel length: 2.8 cm, Channel volume: 2.69µL). Image D show experimental setup showing tumour fresh media contained in syringes linked to a Verna8 Endothelial+™ biochip and the experiments were carried out in a 37ºC incubator under constant flow condition.

2.12 Tissue factor quantification in cell-free supernatant using Enzyme-linked immunosorbent assay (ELISA)

The TF DuoSet ELISA development kit (R&D systems, UK) was used to determine the TF in tumour cell-free supernatants from various cancer cell lines. All samples were processed according to manufacturer's instructions and all required solutions were brought to room temperature before use. All reagents and samples were prepared at room temperature and then diluted to specified working concentrations. This kit is designed for measure natural and recombinant human TF (Coagulation Factor III).

2.12.1 Material and Solutions preparation:

Wash buffer: 0.05% Tween® 20 (Sigma-Aldrich) in PBS, pH 7.4. Reagent diluent (RD): 1% Bovine serum albumin (BSA; Sigma-Aldrich) dissolved in PBS, pH 7.4, sterilised through a 0.2 µm pore filter. Substrate solution: same volume of Colour Reagent A (stabilised H_2O_2, R&D Systems) and Colour Reagent B (tetramethylbenzidine)(R&D Systems), were mixed together in equal volumes was added and incubated for 20 min at room temperature in the dark place.

2.12.2 Standard and Antibodies:

Detection antibody: 36 µg/ml biotinylated goat anti-human TF (R&D Systems) reconstituted stocks were prepared in 1 ml reagent diluent. Capture antibody was prepared by reconstitute of 720 µg/ml mouse anti-human TF (R&D Systems) in 1 ml PBS. TF Standard: Each 90 ng/ml recombinant human TF (R&D Systems) vial was reconstituted in 500 µl reagent diluent. Then, solution was allowed to sit for 15 min with gentle agitation prior to making dilutions. A seven-point standard curve using 2-fold serial dilutions in Reagent diluent were used as following: 500, 250; 125; 62.5; 31.3; 15.6 and 7.8 pg /mL. Streptavidin- horseradish peroxidase (HRP): 1.0 mL of streptavidin conjugated to horseradish peroxidase. Dilute to the working concentration specified on the vial label using Reagent Diluent.

2.12.3 ELISA protocol

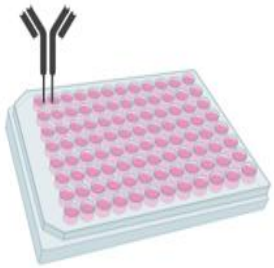

Nunc MaxiSorp® 96-well microplates were coated with 100 µL (4 µg/ml)/well with capture antibody (mouse anti-human Coagulation Factor III).

plates were sealed and incubated overnight at room temperature and subsequently washed three times with wash buffer (400 µl per well) to remove any unbound antibody

plates were blocked by adding 300 µL of Reagent Diluent to eachwell.Incubateat room temperature for a minimum of 1 hour.

100 µl of cell-free supernatants from various cancer cell lines (undiluted) and human recombinant TF standards (A seven point standard curve using 2-fold serial dilutions in Reagent diluent) were added per well. plates were covered with adhesive strip and incubated for 2 h in room temperature

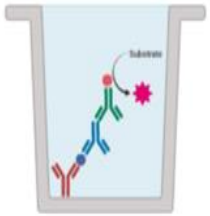

100 µl of Streptavidin-HRP was added to each well and covered and incubated for 20 min at room temperature in the dark place to allow the HRP to bind to the detection antibody.then washed as in previous step.Then, 100 µl of substrate solution was added to each well and plates were incubated for in dark place for 20 min at room temperature.

During incubation time a blue colour will develop.Then, 50 µl of stop solution was added to each well to stop the action of HRP on substrate solution(blue colur will change to yellow colour). The optical density of each well was measured using a microplate reader set at 450 nm wavelength.

Figure 2.12: Schematic showing the ELISA method.

2.13 Isolation of MPs using Vivaspin® 6 Centrifugal Concentrator (Ultrafiltration).

2.13.1 Procoagulant activity of MPs cell free media

MPs cell free media was harvested from AspC-1, PANC-1, U87, MiaPAC2, ES2 and A2780 tumour cells. The PCA of MPs cell-free supernatant was measured using a prothrombin time clotting assay. PCA was assessed under flow rate of 4.0 µL min−1 after 24 hours. Effluent was collected and MPs were isolated by using centrifugal filtration of the cell-free supernatant through Vivaspin® 6 ml concentrators (Figure 2.16). MPs cell free media was recovered from the impermeable concentrate part and PCA was assessed. Vivaspin concentrators can be used in swing bucket or fixed angle rotors accepting standard conical bottom tubes. The thin channel concentration chamber and the longitudinal membrane orientation provide optimum cross flow conditions even for particle laden solutions; the centrifugal force pulling particles and solids away from the membrane to the bottom of the device. Macromolecules accumulate in an impermeable concentrate pocket integrally moulded below the membrane surface, thereby eliminating the risk of filtration to dry. The molecular weight cut off was 100kDa and MPs were presumed not to pass through as filtrate due to their relatively vast size in comparison to the cut off value.

2.13.2 Determination of TFMP in neat, retained and filtered samples

MP cell free media was harvested from AspC-1, PANC-1, U87, MiaPAC2, and ES2 were centrifuged at 400 *g* at 4°C for 4 minutes to remove detached cells and debris. Supernatant (6ml) was collected and filtered through Vivaspin® 6 ml concentrators (Sartorius, UK) (Figure 2.13). MPs were recovered from the media concentrate and TF bearing MPs was assessed using ELIZA as described in section 2.12.3. The concentration of MPs that are positive for TF in neat, retained and filtered samples was assessed as explained in section 2.13.

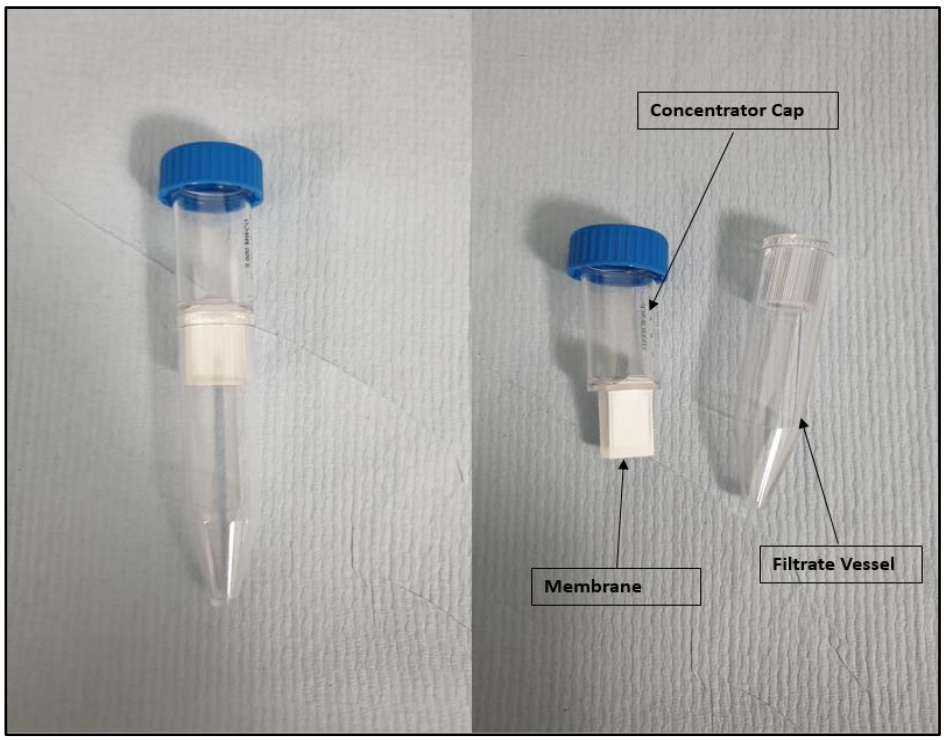

Figure 2.13: Vivaspin® 6 Centrifugal Concentrator.

2.14 Statistical analysis

The results are shown as a mean (± SD). To order to assess statistically significant differences between groups the student T-tests, Analysis of Variance (ANOVA with multiple comparisons) and Tukey's Honest Significant Difference test were used. Published P values were considered significant below 0.05. The coefficient of correlation (r) of Pearson was used to define the correlations. Any statistical analysis has been carried out using Excel software, version 16.37.

Chapter 3 Characterization of procoagulant activity of microparticles derived from various cancer cell lines.

3.1 Introduction

The dynamic between cancer and VTE has unique features which bear close examination to truly and clearly understand how one may influence the other. The association between cancer and VTE is well established, with up to 20% of patients with cancer developing VTE, which is recognized as one of the leading causes of death in these patients (Horsted et al, 2012). In addition, VTE, is the second leading cause of death in cancer patients, with the risk of VTE raised from 7-fold to 28-fold in cancer patients relative to non-cancer patients (Mitrugno et al, 2016). Furthermore, some cancers show higher incidences of VTE than others, especially those associated with haematological malignancies, such as lymphoma and multiple myeloma (MM). The risk of VTE differs among different types of cancer in which pancreatic, kidney, stomach, ovary, brain and lymphoma cancer have had the strongest correlation with venous thrombosis (Ades et al, 2017). Furthermore, cancer is a prothrombotic condition with an increased prevalence of VTE.

Circulating extracellular vehicles (EVs), are enclosed membrane structures that are released into extracellular spaces by a variety of cell types including endothelial cells, epithelial cells, platelets and tumour cells (Campello et al, 2016; Povero et al, 2014). Circulating EVs vary widely in size from tiny vesicles often referred as exosomes that are typically only 30 to 100 nanometres in diameter to larger structures that can be up to 1 micrometre across often, referred as microparticles (MP) (Barteneva et al, 2013). Exosomes are generated through invagination of the cellular membrane and release through exocytosis. Cells can also shed portions of their membrane to generate circulating MP that are typically larger and more variable in size than exosomes. Once released from the cell, circulating MP can be detected in variety of body fluids including urine and blood (Shai & Varon, 2011). Each circulating MP contains proteins and RNAs that are representative of its cell of origin including surface and cytoplasmic proteins, messenger RNAs and microRNAs (Aharon et al, 2008). It is also known that circulating MPs are capable of transferring their content to other cells, a process that is thought to be important in several biological process including the immune response, intercellular communication, angiogenesis, metastasis and cellular survival (Fatima & Nawaz, 2017). Because the molecular content of the circulating MP reflects the cell of origin, biomarkers from the cell of origin can be exploited through the circulating MP to detect the presence of a disease.

Various studies have suggested that the TF can play an important role in the pathogenesis of hypercoagulable states in cancer patients. Immunohistochemistry has confirmed TF expression in non-invasive and invasive pancreatic neoplasms tissues (Khorana et al, 2007).Tumour-derived TFMP are abundant in the plasma of advanced disease patients, and their concentration in the blood correlates significantly with VTE (Pabinger et al, 2013).Many studies have identified the presence of TFpositive microparticles in the circulation of solid cancer patients with the highest levels of microparticles-
TF activity recorded in pancreatic cancer patients (Campello et al, 2019). With TF's significant role in the haemostatic system, its relevance to VTE is readily apparent, regardless of malignancy. TF can easily travel via vesicles or MP through the circulatory system (Kleinjan et al, 2012). These MP provide TF with a surface where coagulant activity can occur, especially if the surfaces of the vesicle are derived from the tumour cells. These surfaces offer a small scaffold where a thrombus can grow (Davila et al, 2008). The actual mechanisms of the procoagulant potential of TF+ MP are mainly based on the expression of anionic phospholipids, especially Phosphatidylserine (PS), and the basic coagulation function of TF (Lacroix & Dignat-George, 2012b). This combination may independently initiate and promote coagulation via the TF/FVIIa complex (Mackman, 2012; Owens & Mackman, 2011). PS is an important negatively charged phospholipid membrane component that can be expressed by cell derived MP during cell activation or apoptosis. Moreover, Gieseler et al. (2018) reported that stimulated tumour cells with TNF- α has resulted in increased upregulation of PS on MP surfaces in breast, lung, colon, ovary and pancreas cancer cell lines (Gieseler et al, 2018). TF is incorporated into tumour-derived MVs through a complex mechanism involving its interaction with filamin- A, also known as Actin Binding Protein280, and Ser253 phosphorylation (Koizume et al, 2016). TFMP are present in both healthy individuals and cancer patients; though, cancer patients tend to show high levels of TF+ MP. This has been seen in multiple malignancies, including colorectal cancer (Hron et al, 2007), pancreatic cancer (Thaler et al, 2013), and breast cancer (Trappenburg et al, 2011). Furthermore, increased levels of circulating TFMP activity have been seen in patients with different diseases, including urinary tract infection, influenza, acute liver injury, cirrhosis, and malignancy (Hisada et al, 2018). Moreover, it is suggested that the initiation of the TF pathway through the release of cell- derived MP into the bloodstream is a pathophysiological explanation for the systemic activation of the coagulation system in patients with cancer (Thaler et al, 2012a).

3.2 Aims

In order to determine the contribution of MP to hypercoagulability among cancer patients, this chapter has focused on determining the procoagulant activity (PCA) of cell-free supernatants

collected from various cancer cell lines using a one-stage clotting assay. Cell free medium or supernatant was collected from 2D and 3D cell cultures and PCA of the MP produced was assessed.

3.2.1 Objectives

- In this chapter, one stage prothrombin assay was used to determine the PCA of seven cancer cell lines from 2D and 3D cell culture as following: AsPC-1, ES2, U87, SKOV-3, PANC-1, MIAPaCa-2 and A2780.
- conductivity cell free supernatant of AsPC-1 and SKOV-3 was investigating as an alternative method of PCA assessment.
- To further explore whether or not the procoagulant ability of supernatant cell culture is related to MP, the free cell supernatant has been ultrafiltrated by the centrifuge by filters of 100,000 Da pore size and TF bearing MPs was assessed using ELIZA.

3.3 Procoagulant activity of MP

3.3.1 Methods overview

The PCA of different cancer cell lines was investigated using the Thrombotrack SOLO coagulometer as described in section 2.3. Cancer cell lines that were used include three ovarian cancer cell lines, A2780, SK-OV-3 and ES-2; three pancreatic cancer cell lines, AsPC-1, PANC-1 and MIA PaCa-2, and one human glioma cell line, U87. The cell lines were selected because they are associated with cancers of higher risk of VTE and also were available in the laboratory. PCA for each cancer cell line and respective tumour media (or cell free supernatants) was performed four times when cells were approximately 80% confluent within the culture flask. Cell-free supernatants containing suspensions of MP were removed from tumour cells via centrifugation at 1000 x *g* for 5 min to remove cells and larger cell fragments. The cells were counted, and a cell suspension was prepared in PBS at cell concentration of 3×10^5 cells/ml. Consequently, characterizing MP activity by measuring the time for clot formation in all cancer cells and their respective cell free supernatants was assessed. To determine the PCA, 100 µL of either cell-free medium or cancer cell suspensions in blank media were mixed with 100 µL of normal human plasma for 1 min at 37°C. Then, 100 µL of (25 mM $CaCl_2$) was added, the time for the sample to clot was recorded (Thrombotrack SOLO coagulometer) in duplicate and repeated independently, four times (Figure 3.1).

3.4 Results

3.4.1 Procoagulant activity of MP in 2D cell culture

PCA of various cancer cell lines cells and media were assessed via the one stage PT assay. In brief, enumerated cancer cell suspensions in PBS were mixed with equal parts of human plasma and (25 mM $CaCl_2$) for 2 min at 37°C as described in section 2.3. For the same concentration of cells within the assay (3 x 10^5cells/ml) the PT was different between the cancer cell lines (Figure 3.1).

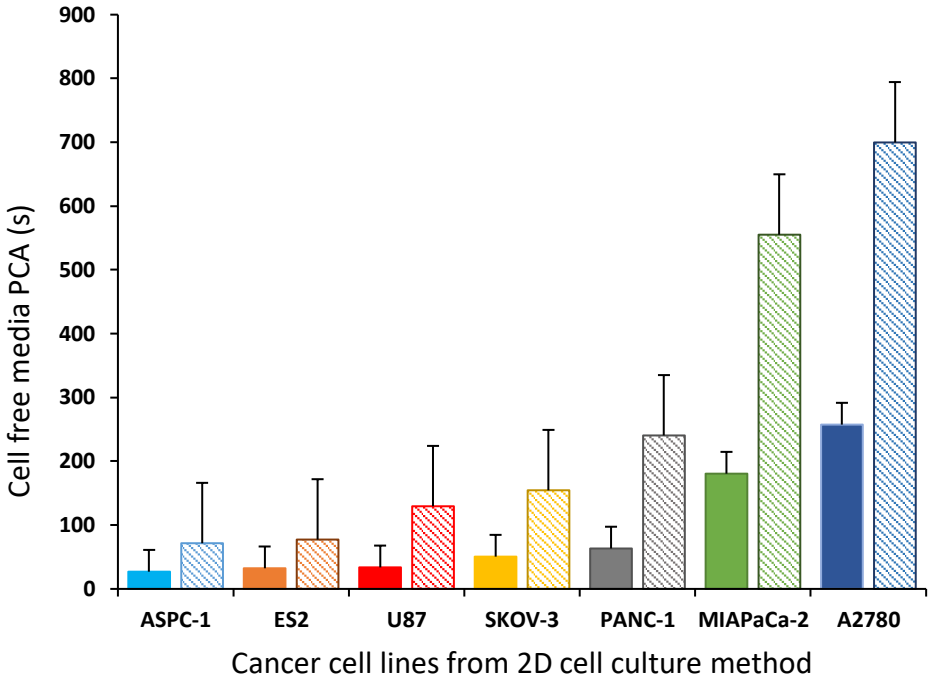

Figure 3.1: Chart showing the PCA of cancer cells and respective cell free media. pancreatic AsPC-1(n=4), panc-1(n=5), MIA-PaCa-2(n=5), ovarian ES2 (n=3), A2780 (n=5), SKOV-3 (n=5), and glioblastoma U87 (n=3) PCA was measured using a one-stage clotting assay PT. Error bars are SD. Cells (filled), cell free media (pattren fill).

It has been shown previously that both tumour cell and media concentration are linked to PCA in a power relationship (Yates, 2011), this relationship was confirmed here. All cell suspensions and their related cell-free media were found to support coagulation to a differing extent. Results also showed that the relationship between the PCA of the cancer cells and its corresponding cell free media was strongly positively correlated and significant (Pearson's correlation coefficient $r = 0.99$, $P < 0.0005$) (Figure 3.2).

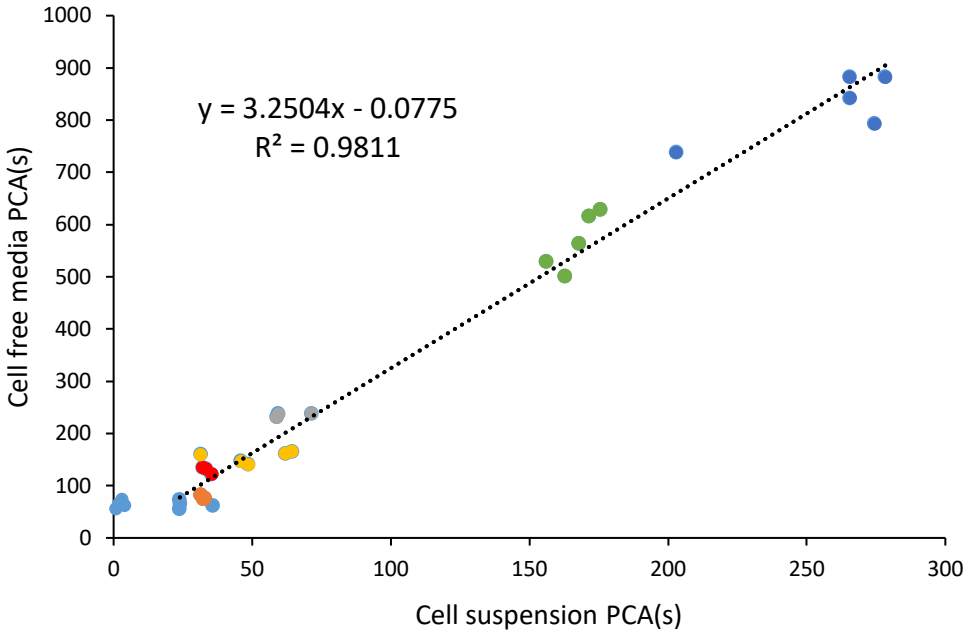

Figure 3.2: The relationship between the PCA of human cancer cells cancer cell lines versus cell free media.
Ovarian cancer cell lines, A2780, SK-OV-3 and ES-2, and 3 pancreatic cancer cell lines, AsPC-1, PANC-1 and MIA PaCa-2., and human glioma cell line, U87. Average PCA in seconds was measured using a one-stage PT clotting assay. The error bars represent ±SD of four separate experiments. AsPC-1(●), ES-2(●), U87(●), SKOV-3(●), PANC-1(●), MIAPaCa-2(●) and A2780(●).

The results show that the PCA for cancer cell suspensions correlates with the PCA of cell-free media across different cell lines. The relationship observed with tumour media and tumour cells were a proportional. Furthermore, the detected PCA across different cancer cell lines did not seem to depend on the histological types of cancer studied. For example, ovarian ES-2 and SKOV-3, pancreatic AsPC-1 and human glioma U87 showed the fastest PCA in both cell suspension of cell-free media, Whereas, pancreatic MIAPaCa-2 and ovarian A2780 showed the slowest PCA. Pancreatic PANC-1 cell line showed moderate PCA. The cell free tumour media used supported coagulation in time of 73±16s, (AsPC-1, n=4), 82±4s (ES-2, n=3), 134.5±7s (U87, n=3), 159.3±11s (SKOV-3, n=5), 253±11s (PANC-1, n=3), 563.5±101s (MIAPaCa2, n=5) and 737±175s (A2780, n=5). The differences in media are could be due to cell membrane PCA potential as shown in Figure 3.1 or numbers/rate of MV release, which may differ between cell lines. It is also important to note that the PCA in cell-free medium decreases approximately 2.6 times less than the PCA in cell suspension from cancer line to cancer line (figure 3.1). This is most likely due to the fact that cancer cells express greater amounts of cell surface procoagulant factors such as TF and PS than the cell-free medium. The observed PCA for all cancer cells is linked to cell free medium in a statistically significant power relationship (Pearson's correlation coefficient $r = 0.96$, $P < 0.0001$), (Figure 3.2). This suggests that the differences in PCA is cell surface dependent and may also suggest that the rate of MP release

between the cells is quite consistent. If for example a parent cell with low PCA shed MP at a far higher rate than a cell with moderate PCA then it would be expected that the media of the low PCA line may possess a higher PCA than the moderate PCA cell line and the observed relationship would not exist.

3.4.2 Procoagulant activity of MP released from 3D cell culture

As the aim of this study was to best mimic *in vivo* conditions, thus the release of MP from 3D cell culture was investigated. The activity of anti- cancer drugs has traditionally been assessed in two- dimensional (2D) cell culture. It is now recognized, however, that two dimensions are not always sufficient to simulate the microenvironment of the original tumours, as they grow in three- dimensions (3D) (Pampaloni et al, 2007). In addition, biological and molecular characteristics of cancer cells such as the ECM components, cell-to-cell and cell-to-matrix interaction that are important for differentiation, proliferation and cellular functions are mostly lost in the 2D culture method or cell monolayers (Mazzoleni et al, 2009; Pampaloni et al, 2007). Multicellular tumour spheroids (MCTS), also referred to simply as spheroids, are three-dimensional (3D) spherical cell aggregates (Kelm et al, 2003). Spheroids show many characteristics associated with solid tumours; these include various zones of proliferation, the presence of both apoptotic and necrotic cells, and an oxygen gradient with hypoxic areas at the core (Mehta et al, 2012).

Cell free medium was collected from tumour spheroids formed within a 96-well microplate to measure the PCA as described in sections 2.5 and 2.6. As in the two-dimensional culture, cell lines used include 3 ovarian cancer cell lines, A2780, SK-OV-3 and ES-2, and the 3 pancreatic cancer cell lines, AsPC-1, PANC-1 and MIA PaCa-2., and one human glioma cell line, U87. After incubation the plates were centrifuged and 100 μl of the supernatant was collected from each quadruplicate experiment (4 wells) and mixed together. The time for the sample to clot was recorded in duplicate as previously described and then repeated independently, four times. The data is presented in Figure 3.3. The PCA of U87 and AsPC-1 spheroid media showed the fastest collecting time whilst A2780 and MIAPaCa-2 possessed the slowest PCA.

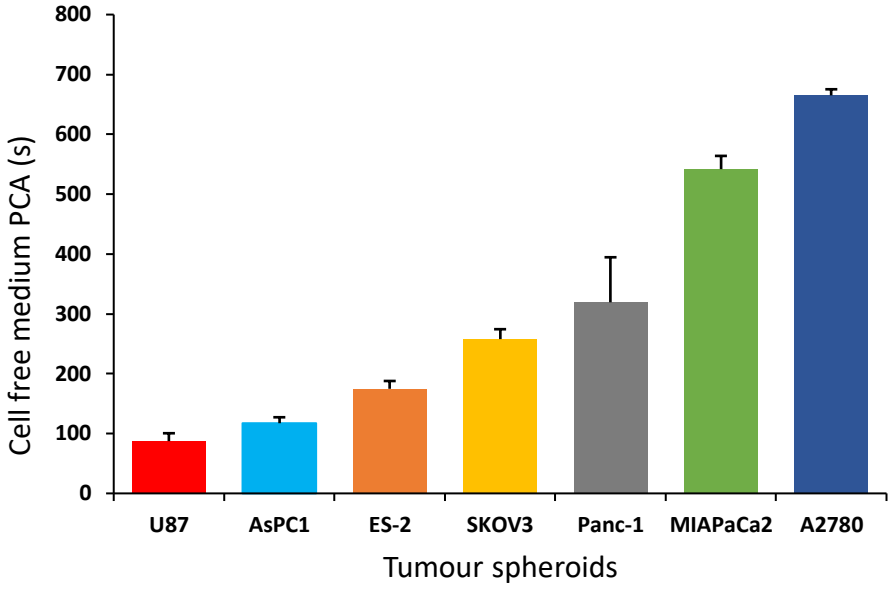

Figure 3.3: the PCA of media from Tumour spheroid culture (3D).
PCA was measured using a one-stage clotting assay. Data represent the average of four independent measurements performed in duplicate. Error bars are ±SD (n=4).

3.4.3 Comparison of procoagulant activity between 2D and 3D

To investigate whether the 3D cell culture method had a substantial difference of PCA from 2D cell culture method, the data was compared. The relationship between the PCA obtained in cell-free supernatants 2D and cell-free supernatants 3D was found to be near linear (Figure 3.4).

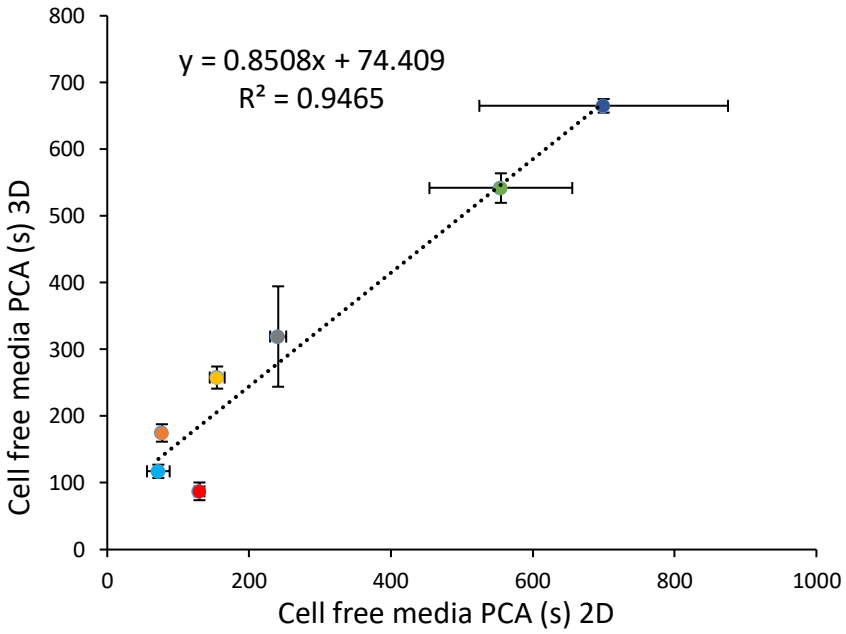

Figure 3.4: Relationship of PCA between 2D cell culture and 3D cell culture.
Lines of best fit are for a power relationship and R^2 value is 0.946. Error bars represent ±SD of 4 replicates. AsPC-1(●), ES-2(●), U87(●), SKOV-3(●), PANC-1(●), MIAPaCa-2(●) and A2780(●).

The results clearly show that PCA in cell-free supernatants from 2D and 3D cell culture is correlated in a near linear relationship with a strong positive correlation found (Pearson's correlation coefficient $r = 0.97$, $P < 0.0001$). However, the order of the cell lines was slightly different between 2D and 3D. As U87 was the fastest in 3D though it was the third fastest in 2D cell culture method. Similarly, AsPC-1 was the fastest in 2D but it was the second fastest in 3D (Figure 3.5). This is most likely due to a difference in the rate of MP release between 2D and 3D cell culture methods rather than a phenotypical difference in MP make-up.

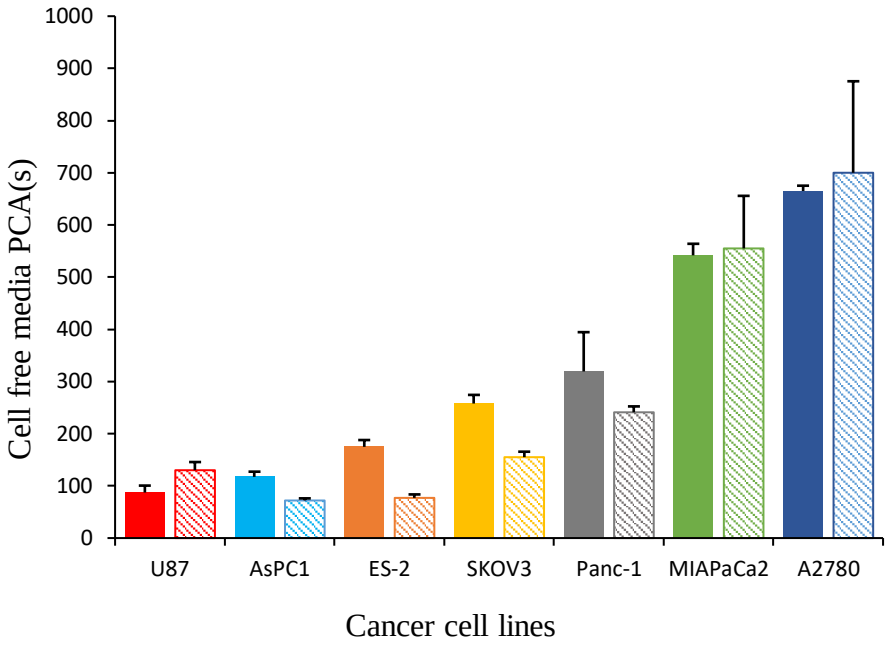

Figure 3.5: Chart showing the PCA of human cancer cells cancer cell lines versus cell free media using 2D and 3D.
Error bars represent ±SD of 4 independent replicates. 3D filled, 2D (patren filled).

3.5 Spheroid shape and procoagulant activity

As previously shown for cell free medium from 2D cell culture, cell-free medium from 3D tumour spheroids supports coagulation as well. Interestingly, cancer cell lines that formed compact spheroids had faster PCA than cancer cell lines that formed loose spheroids. In this study, U87, AsPC-1 and ES-2 produced the most compact spheroids among all cancer cell lines, and had the fastest PCA, with 87.25s, 117s and 174s, respectively (Figure 3.6). In contrast, tumour spheroids of PANC-1, MIAPaCa-2 and A2780 showed loose shape and slower PCA. However, SKOV-3 showed small compact spheroid and slower PCA (Figure 3.7). In the literature, some of the so-called 'sphere' and 'spheroids' are nothing more than loose aggregate which can easily be detached from or manipulated and transported and lack not only true spherical geometry but possible cell-cell-matrix interactions(Mayer et al, 2001;

Weiswald et al, 2015). The term "aggregate" was used mainly to describe looser packages of cells and to distinguish them from compact spherical cultures. Loose aggregate can be defined as easily be detached from or manipulated and transported and lack not only true spherical geometry but possible cell-cell-matrix interactions and easy to disperse with low mechanical forces for instance use a pipette to assess the spheroids structure. Compact spheroids, by comparison, were more stable and were resistant to mechanical disruption.

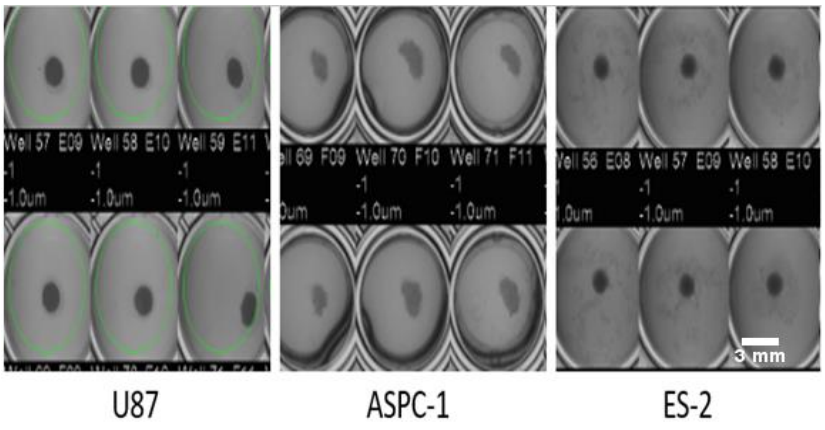

Figure 3.6: Image showing the compact tumour spheroids.
U87 shows the most compact and stable spheroid. AsPC-1 and ES-2 show compact spheroid but less strong than U87. The experiment was performed with 20 replicates.

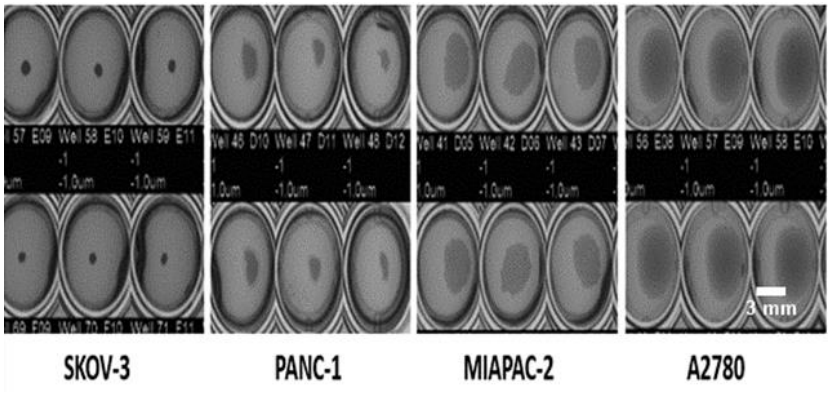

Figure 3.7: Image showing the loose tumour spheroids.
SKOV-3 shows a round spheroid but without compactness and slow PCA. PANC-1, MIAPAC-2 and A2780 show irregular aggregated spheroid cells. The experiment was performed with 20 replicates.

In contrast, tumour spheroids of SKOV-3, PANC-1, MIAPaCa-2 and A2780 showed slower PCA. When quantifying several different morphology parameters and average them over 5 - 6 spheroids for each cancer line, differences were observed. For example, the average spheroid area was lowest in SKOV-3 cells, higher for ES-2, PANC-1, AsPC-1 and U87, in that order; with MIAPaCa2 and A2780 having much larger areas (figure 3.8).

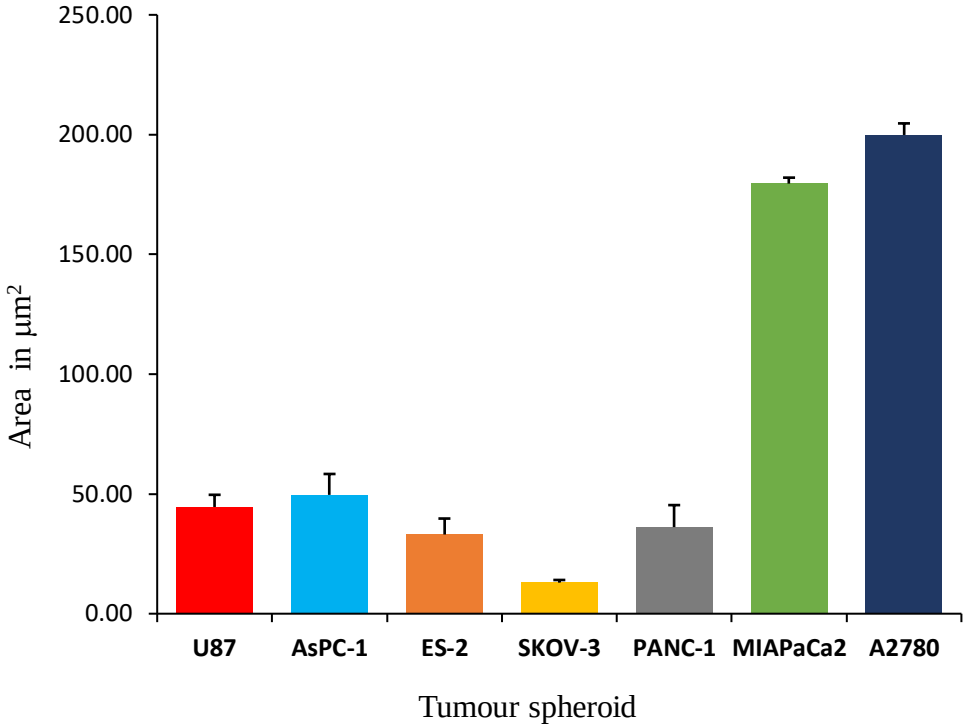

Figure 3.8: Average spheroid areas of the cell lines tested in this experiment.
Morphology was measured using ImageJ software and averaged over 5 - 6 spheroids per cell line.

Thus, SKOV-3 has the lowest average area, and that area increases incrementally to U87. A2780 and MIAPaCa2 though have much larger average areas. Interestingly, the average perimeter of the spheroids shows a very similar tendency across the cancer cell lines; as figure 3.9 shows.

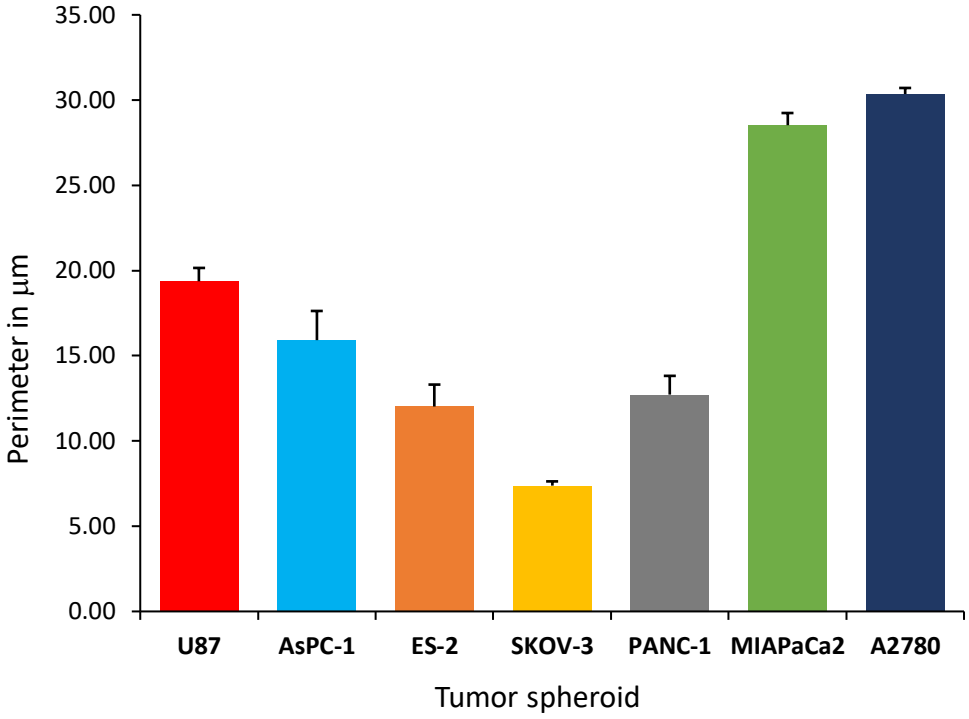

Figure 3.9: Average spheroid perimeters of the cell lines tested in this experiment. SKOV-3 perimeters are smallest, while A2780 lines show the largest perimeter. Morphology was measured using ImageJ and averaged over 5 - 6 spheroids per cell line.

As a circle has the smallest perimeter-to-area ratio, while an elongated rectangle has the largest ratio, the observation that perimeter and area behave in the same way suggests that the shape between spheroid aggregates does not show drastic differences, or at least not differences that are as drastic as seen in figure 3.8 and 3.9 between SKOV-3 and A2780. One can calculate the ratio between area and perimeter squared of any irregularly shaped object as circularity C via the relationship (Raghavan et al, 2016):

$$C = 4\pi \cdot \frac{Area}{(Perimeter)^2}$$

If our object was a perfect circle, the circularity would be C = 1.0:

$$C = 4\pi \cdot \frac{Area}{(Perimeter)^2} = 4\pi \cdot \frac{\pi r^2}{(2\pi r)^2} = \frac{4\pi^2 r^2}{4\pi^2 r^2} = 1$$

If the object under investigation was a rectangle, C tends towards zero the more the rectangle is stretched out. Thus, circularity gives a dimensionless measure of the morphology of objects. Figure 3.10 shows the average spheroid circularity across the different cell lines:

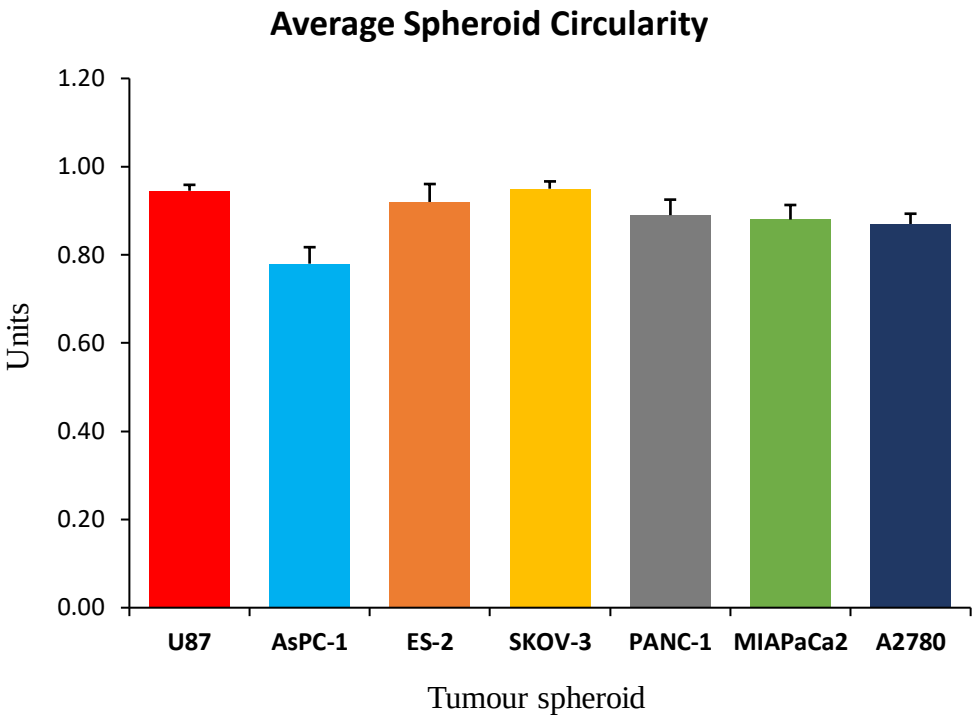

Figure 3.10: Average spheroid circularity of the cell lines tested in this experiment.
SKOV-3 circularity is largest, while AsPC-1 is least circular. Morphology was measured using ImageJ and averaged SD over 5 - 6 spheroids per cell line.

Circularities are between ca. 75% and 95%, with SKOV-3 showing the highest degree and AsPC-1 the lowest degree of circularity. These results suggest that area and perimeter correlate more with coagulation times than the shape of the aggregate; if it was assumed that the cell number is the same across all aggregates, we can appreciate that the smaller and more compact or dense the aggregate, the faster coagulation times are. In other words, the data suggests that PCA is linked to the structure of the spheroids; while the MCTS of U87, AsPC-1 and ES-2 occupy a restricted area of the wells, the MCTS formed in PANC-1, MiaPAC-2 and A2780 are more elongated and spread out; importantly, SKOV-3 did form aggregates that were round and compact, but much smaller than U87, AsPC-1 and ES-2; in turn, SKOV-3 cells showed an intermediate PCA (258 s), suggesting that the relationship between spheroid compactness and PCA may be complex (Figures 3.5-3.9); The PCA of PANC-1, MIAPAC-2 and A2780 cell lines were 319.25 s, 541.75 s and 665 s respectively. Taken together, the data suggests that cell lines that form loosely aggregated spheroids yield supernatants that require a longer time to clot than those derived from cell lines with more compact spheroids.

3.6 Conductivity of MP

3.6.1 2D cell culture

As the aim of the study was to form an *in vitro* model of tumour-based coagulation on a microfluidic chip it would be ideal to be able to measure PCA within a flow stream on-chip

rather than have to collate or extract samples to process off-chip. To this end, conductivity was investigating as an alternative method of PCA assessment. Electrical conductivity is the ability of a solution to pass an electric current and so if the cell culture media contains negatively charged MP then this should affect conductivity in a concentration dependent manner. Briefly, serial dilutions of tumour cell free supernatants (100% to 0.0048%) were used to measure conductivity which was correlated with coagulation time determined via the Thrombotrack SOLO coagulometer method used above. The supernatant was collected from the 2D cell culture after centrifugation at 400 x *g* for 5 min. After probe calibration as described in 2.2.17 section, conductivity measurements were taken for each solution in a water bath set at 25 °C ± 0.5. Specifically, 150µl was taken from each serial dilution and pipetted into 0.5 ml microcentrifuge tube; and the probe was immediately inserted into the sample tube after its temperature of sample reached to the recommended temperature. After the correct temperature was reached, the conductivity was read. The second set of the serial dilutions was used to assess the PCA and compare it to its conductivity. Figure 3.12 shows the log transformed data of PCA of AsPC-1 and SKOV-3 cell free media, depending on the conductivity of the corresponding media; the relationship is linear, and the PCA decreases with increasing conductivity, suggesting that the PCA increases with increasing conductivity (Figure 3.11). It is also important to realize that the observed linear relationship displayed in figure 3.12 involves the logarithm of the PCA; thus, the PCA increases exponentially with conductance (Pearson's correlation coefficient r = 0.85 8, P < 0.0003). This suggests that the more MP are present in the media that conduct electricity, the higher the conductivity and this is associated with a faster PCA.

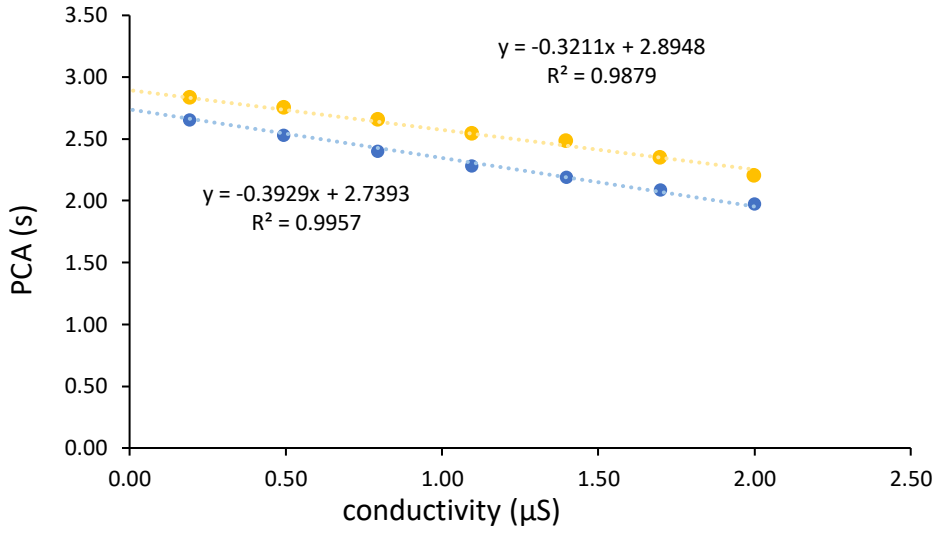

Figure 3.11: A graph showing relationship between the conductivity and the PCA.
Using a serial dilution of AsPC-1 and SKOV-3 cell culture media, conductivity was plotted aginst PCA.

3.6.2 Measuring conductivity of MP shed from 3D cell culture

Conductivity measurements in 3D cell culture were carried out in the same way as for 2D culture. Supernatants were collected from the spheroid cultures by centrifuging the 96 well microplate at 320g for 5 minutes. Supernatants were then carefully collected and pooled from repeat wells. A dilution series was generated, and conductivity and coagulation time were measured and correlated. Figure 3.12 shows the comparison of a dilution series between SKOV-3 - a cell line with a medium PCA - and AsPC-1, a cell line with a short PCA, and thus likely a higher concentration of MP. In both cell lines, one would expect the PCA to decrease with increasing conductivity.

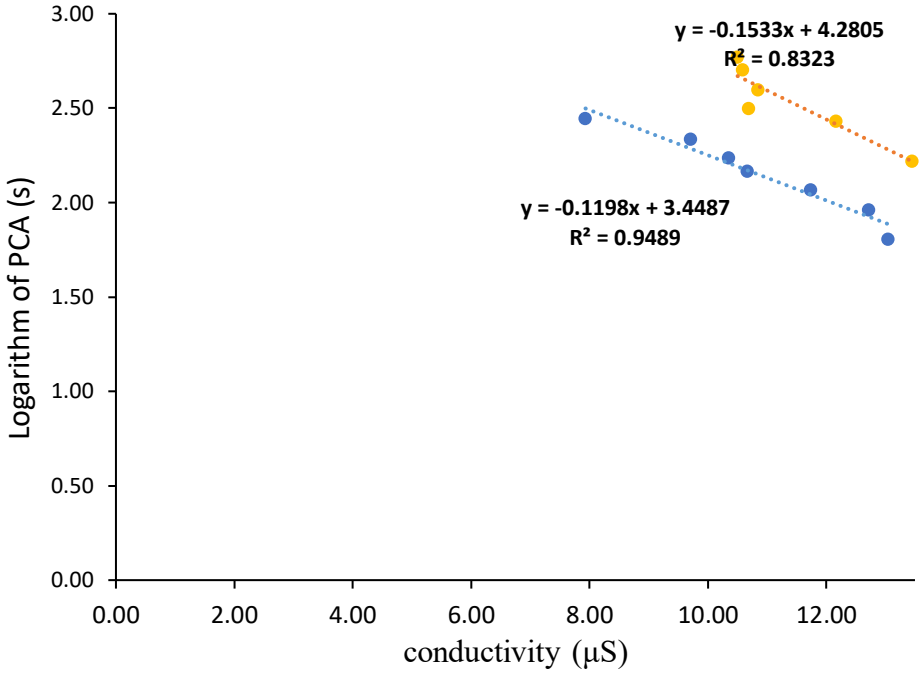

Figure 3.12: Correlation of the conductivity with the decadic logarithm of the PCA.
The supernatant (cell free media) of two different spheroid tumour media, SKOV-3 and AsPC-1. AsPC-1(●) and SKOV-3(●).

Indeed, it has been observed that the PCA was faster with increasing conductivity, suggesting that the concentration of MP was also higher as confirmed with the observed PCA. However, we also see that the AsPC-1 cell line - which has higher PCA than SKOV-3, in general - shows lower coagulation times at the same conductivity. If the concentration of MP was the only factor regulating coagulation, one would expect the same coagulation time at any conductivity value and therefore the actual MP phenotype governs conductivity. This renders conductivity problematic for measuring either PCA or MP concentration between different cell lines and so the technique was not pursued further.

3.7 Ultrafiltration

3.7.1 PCA of MP isolation

To further investigate if the procoagulant potential of cell culture supernatants is MP associated or not, the cell-free supernatant was ultrafiltrated via centrifugation through Vivaspin® 6 ml concentrators (Sartorius, UK). For this study, a molecular weight cut off of 100kDa were used, and MP were presumed not to pass through due to their relatively large size in comparison to the cut off value (Xu et al, 2017). Cell-free media from AsPC-1, PANC-1, U87, MiaPAC2, ES2 and A2780 cultures was centrifuged and isolated as described in section 2.15.1 (Figure 3.13).

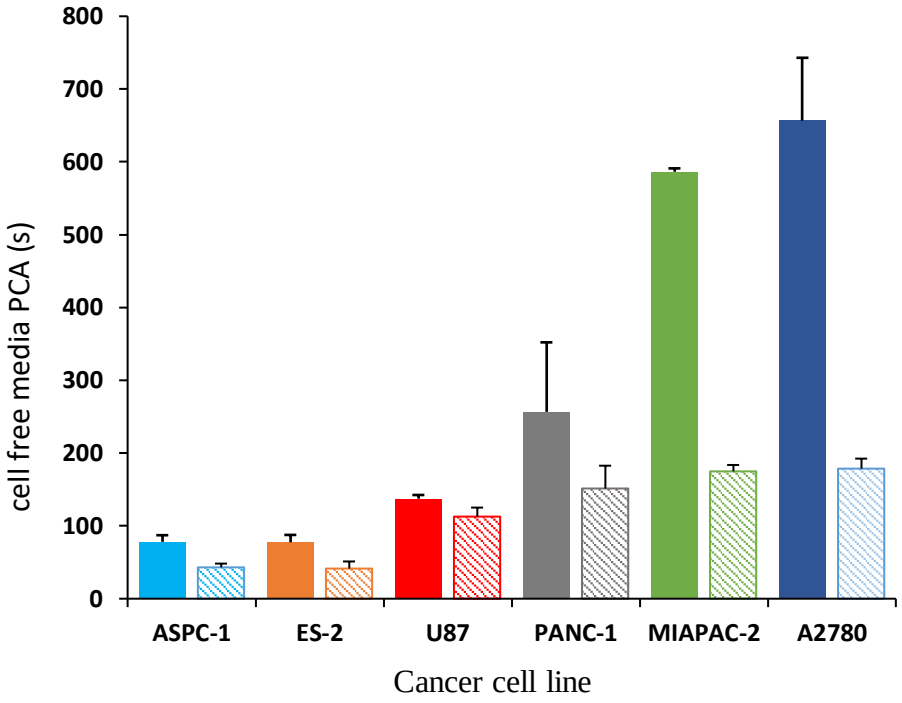

Figure 3.13:The PCA of cell free media after and before ultrafiltration.
The effect of ultrafiltration on cell-free supernatant PCA to define the contribution of tumour cell-derived MP to coagulation activity. Error bars are ± SD of four independent measurements performed in triplicate. Pre-ultrafiltration filled, post-ultrafiltration strips.

Figure 3.13 shows the results for all cancer cell lines except SKOV-3. In general, after ultrafiltration, coagulation times were significantly faster ($P < 0.001$), while the filtrate itself showed no PCA. This strongly suggests that enrichment of medium with MP increases the PCA. Moreover, the data in Fig. 3.14 suggested that that an increase of PCA from cell culture to cell culture in cell-free medium pre-ultrafiltration is accompanied by an increase in PCA in post-ultrafiltration medium. The relationship is linear, suggesting that ultrafiltration concentrated MP with a similar effectiveness between supernatants, independent of the particular cell line. This suggests a general pattern by which a corresponding retention of MP via filtration is linked with the original concentration. Thus, PCA depends on the concentration of MP, as PCA was

shortened if MP concentration was elevated. The relationship between pre-and post-ultrafiltration PCA is very close to linear, with a coefficient of determination of (Pearson's correlation coefficient *r* = 0.99). A general pattern regardless of cell line was detected.

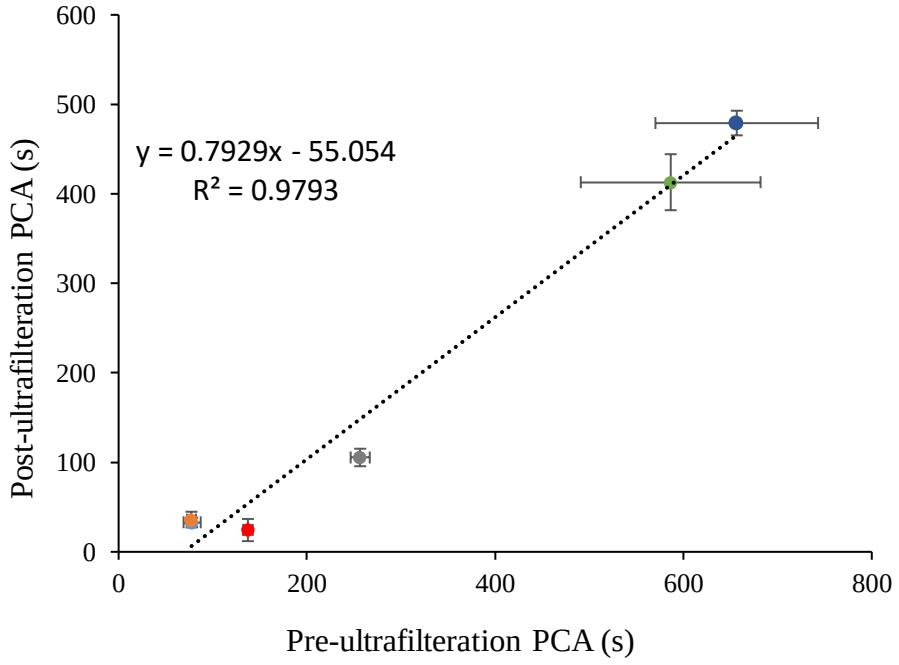

Figure 3.14: relationship between the PCA of pre and post ultrafiltration of cell-free supernatant of different cancer cell lines.
The PCA of pancreatic (PANC-1, AsPC-1, MIAPaCa2), ovarian (ES2, A2780), and human glioma cell line U87 cell-free supernatants increases following ultrafiltration. PCA was measured using a one-stage clotting assay. Error bars are the ±SD of four independent measurements performed in triplicate. AsPC-1(●), ES-2(●), U87(●), PANC-1(●), MIAPaCa-2(●) and A2780(●).

The PCA of U87, AsPC-1 and ES-2 were found to be faster, representing a higher PCA in comparison to the pre-ultrafiltration PCA, as shown in Table 3.1. If PCA was relatively slow compared to other cell lines without ultrafiltration, the increase in PCA was observed to be to be more pronounced then if PCA was faster pre-filtration. After filtration, both MIAPaCa2 and A2780 cells only had their PCA increased to 70% and 73%, respectively, of the pre-PCA time; in contrast, AsPC-1, U87 and ES-2 had post-filtration times between 18 and 46% of the pre-filtration times. PANC-1 - as an intermediate PCA cell line - had its time also reduced to 41% of the pre-filtration value, despite this line showing. These observations could be due to a higher concentration of MP in solution to begin with, in those cell lines with lower PCA; in addition, those lines could also harbour more effective MP. That the speed increase after filtration appears to MP-concentration dependent could be a sign for the exponential relationship between MPs concentration and coagulation time, similar to what we observed before.

Table 3.1: The effect of Vivaspin ultrafiltration on PCA of cell-free supernatants from various cancer cell lines. Data represents ±SD of four independent replicants.

Cancer Cell lines	**Pre ultrafiltration PCA**	**SD±**	**Post ultrafiltration PCA**	**SD±**	**Percent reduction (%)**
AsPC-1	78	11	35	6	45
ES-2	77	4	36	9	46
U87	137	4	24	13	18
PANC-1	257	11	105	11	41
MIAPaCa-2	586	104	413	34	70
A2780	657	93	479	15	73

The data obtained of (Table 3.1) shows increase in PCA of the concentrated conditioned media as using Ultracentrifugation was shown to remove all associated PCA of the filtrated media confirming that the PCA was MP associated whereas the concentrate diluted with fresh media to the original volume was shown to retain and increase PCA in all samples.

3.7.2 Determination of TF in Tumour media

Furthermore, to measure the concentration of TF in neat, retained and filtered samples, *enzyme-linked absorbant assay* (ELISA) technique was used. The total amount of TF detected in samples of media from MP generated by cancer cells was cell-type specific. Importantly, the TF concentration was significantly increased in retain samples (Figure3.15). This suggests a relationship between PCA and the concentration of TF in cell-free media; increased amounts of TFMP within the media correlated to an increase in PCA.

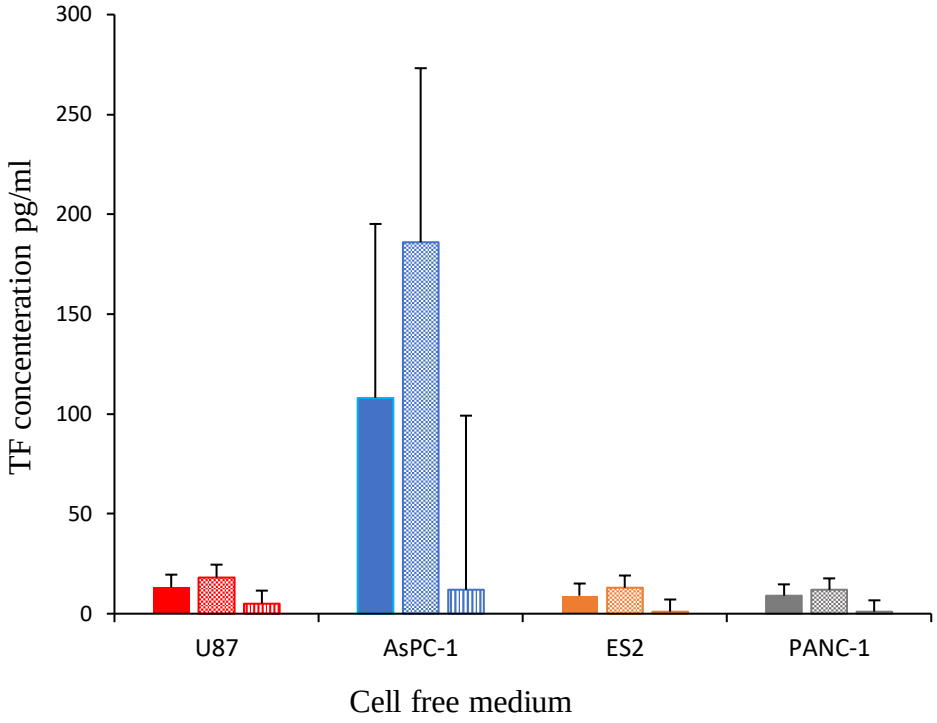

Figure 3.15: Chart showing the TF concentration.
Tumour cell free media of U87, AsPC-1, ES2 and PANC-1 was isolated using ultrafiltration (Vivaspin, 100kDa) and TF concenteration was measured by ELISA. The error bar representing ±SD of two independent experiments. Pre-treated (filled), concentrate (Dotted) and filtrate (verticle stripes).

Figure 3.16 shows a standard curve using TF controls, detected via its absorption of light at 450 nm.

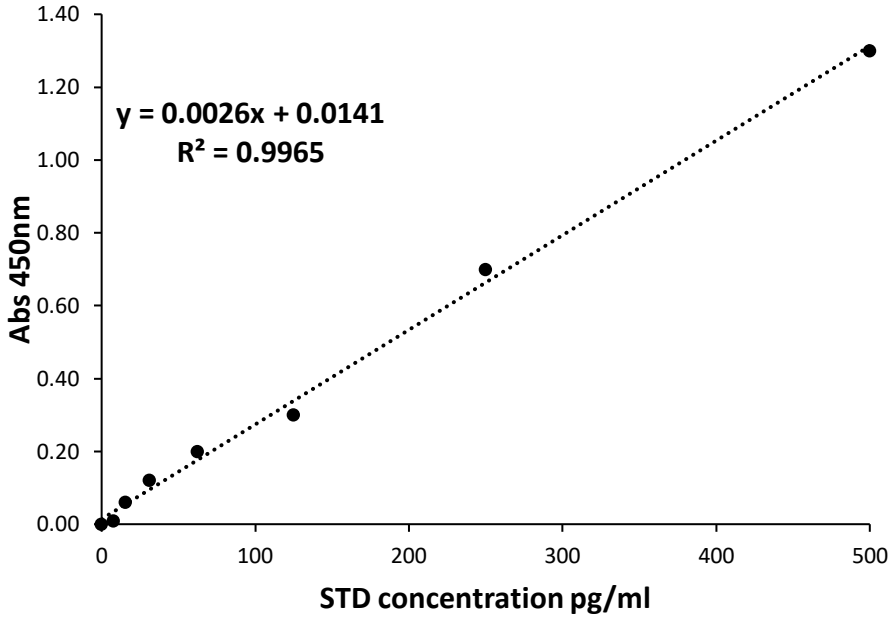

Figure 3.16: TF standard curve for known TF concentration.
Data are the mean of two independent measurements.

Table 3.2 shows the concentrations of TF in various sample types from the ultrafiltration procedure. The highest concentration of TF was detected in the AsPC-1, U87 and ES-2 retained cell-free media and this was strongly correlated with higher PCA (Table 3.1). All cell-free media showed a negligible amount of TF in filtered samples, presumably soluble TF was measured and not TFMP, this filtrate did not support coagulation. The exception was formed by AsPC-1 cells, as the TF concentration in the filtered cell-free media was 12 pg/mL; yet still, there was no coagulation and PCA was greater than 10 min. It could be that TF in those samples was either in a form soluble TF isoform (asTF) that did not support coagulation, or the concentration was not high enough to support coagulation. The data obtained from the concentration of spent tumour media via ultrafiltration suggests that the MP in tumour media are responsible for the associated PCA.

Table 3.2: Table shows the concentration of TFMP of cell free medium.

Sample type	Cancer cell lines	pg/ml
Neat	U87	13
	AsPC-1	108
	ES2	9
	PANC-1	9
Concentrate	U87	18
	AsPC-1	186
	ES2	13
	PANC-1	12
Filtrate	U87	5
	AsPC-1	12
	ES2	1
	PANC-1	1

Neat: tumour cell free media before ultrafiltration process. Concentrate: tumour cell free media diluted with fresh media to the original volume.

Samples were filtered by Vivaspin and categorised into neat, retain and filtered as sample type. Data are mean of two independent experiments. (Neat: untreated sample, concentrate retain sample accumulated in impermeable concentrate pocket, filtered: sample with soluble protein).

3.8 Impact of freezing and thawing on the procoagulant activity of MP

For ease of downstream analysis, it would be helpful if samples could be frozen and batch tested. To determine whether MP were affected by storage a series of experiments were undertaken. Proteins change their activity, depending on the sample temperature (Akazawa-Ogawa et al, 2018). If they are frozen and thawed, they may lose activity, which is important to know for the conduction of any in *vitro* studies with proteins in the lab (Cardigan & Green, 2015). To see whether freezing/thawing cycles would affect the efficiency of MP in promoting coagulant activity, PCA was determined for different cancer cell-free media (ES-2, AsPC-1, U87, MIAPaCa-2 and Panc-1), depending on the sample storage temperature. Cell-free medium was collected from ES-2, AsPC-1, MIAPaCa-2 and PANC-1 lines as previously described in section 2.1. Next, samples were categorised into three different types as following: -80 ºC, -20 ºC and live analysis (37 ºC) (Figure 3.17). PCA was taken immediately after collection, then samples were stored in -20 ºC and -80 ºC for one week, thawed, and PCA was measured again. Data obtained from these experiments show slight decreased in PCA of all cell-free media compared to the live analysis condition, suggesting that freezing and thawing cycles have no significantly change on PCA.

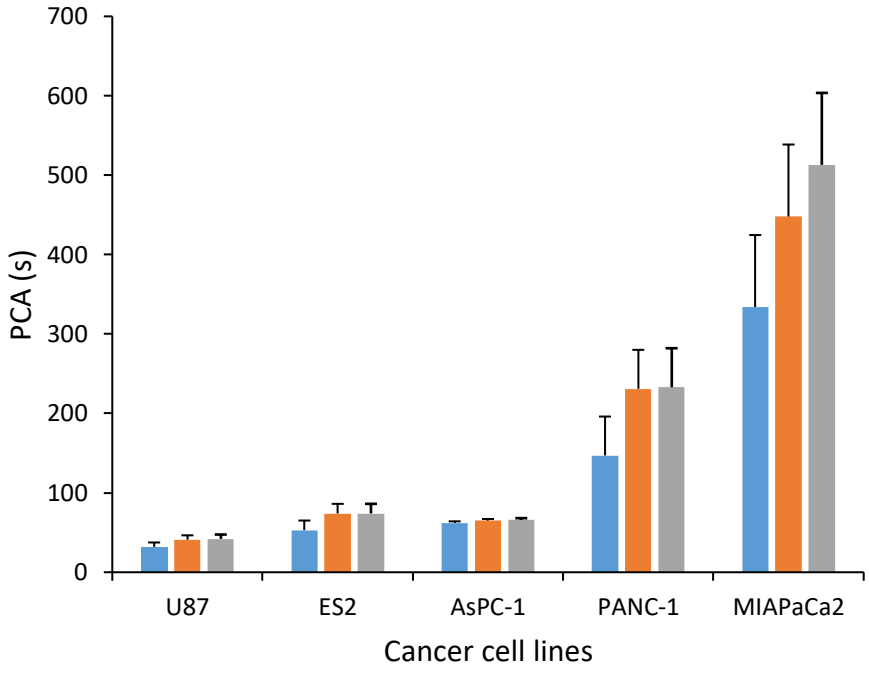

Figure 3.17 The Effect of freezing and thawing on PCA of cell-free media.
The PCA of ovarian ES-2, pancreatic (PANC-1, AsPC-1 and MIAPaCa-2), and the human glioma cell line U87 cell-free supernatants increases in 37ºC more than 80 and 20 ºC. PCA was measured using a one-stage clotting assay Data are the mean ± SD of three independent measurements performed in duplicate. Temperature live analysis (▬), -20°C (▬) and -80°C(▬).

The data suggesting that PCA of cancer cell lines has varied pattern. PCA of MIAPaCa-2 was significantly decreased due to freezing process. In particular, -80°C showed the major effect on PCA of MIAPaCa-2. In addition, moderate decrease in PCA was shown with -20°C. Conversely, similar effect of freezing on -20 and -80°C was observed on PANC-1 as PCA was not changed. On other hand, there was no effect of freezing on PCA of AsPC-1 and U87. Moreover, slight decrease in PCA of ES2 was observed. Accordingly, some of these findings previously have been reported. For example, using sequence cycles of freeze-thaw at − 20°C showed no effect on in vesicle size (Sokolova et al, 2011). However, another study reported that the EV count was lowered by 10–15% using one cycle of freeze-thaw, as detected through flow cytometry (Jayachandran et al, 2012). Together, Data from this section clearly show that freezing and thawing of cancer cell line samples inconsistently show reduction trends in some cancer cell lines suggesting that it may cause MP degradation. Though not all cancer cell lines displayed the same effect. Therefore, to avoid any inconsistency in data all samples were analysed immediately after collection through the entire study.

3.9 Discussion

The seven cancer cell lines from 2D and 3D cell culture studied varied in their PCA as determined by PT assay. The pancreatic AsPC-1, human glioma U87 ovarian ES-2 and SKOV-3, showed the fastest clotting time in both cell suspension and cell-free media, Whereas, pancreatic MIAPaCa-2 and ovarian A2780 showed the slowest clotting time. Pancreatic PANC-1 cell line has showed moderate clotting time in between the two groups (Fig 3.1). It was found that conductivity decreases with coagulation time; the faster a cell culture started to coagulate, the higher its conductivity (Figure 3.12). After removing the MV from the media via ultrafiltration (Vivaspin) the filtrate no longer supported coagulation (figure 3.13).

In this study, it was demonstrated that MP shed from various cancer cell lines and tumour spheroids *in vitro* (Li et al, 2017). The procoagulant activity (PCA) of cell-derived MP was determined using one stage prothrombin assay. Thus, PCA of tumour cell-derived MP within the cell-free supernatants of U87, AsPC-1, A2780 and MIAPACA-2, ES-2, SKOV-3 and PANC-1 was measured. In addition, PCA of tumour cell-derived MP within cell-free supernatants from tumour spheroids was also determined. TF promotes coagulation, and therefore ELISA assay was used to determine the presence of TF in cell-free supernatants - likely associated with MP -as well (Giesen & Nemerson, 2000). The correlation of PCA and TFMP concentration detected as in supernatants provides direct evidence for PCA being determined by the concentration of TFMP.

The experiments also suggest that PCA is linked to the MP concentration in an exponential relationship, as the correlation of the logarithms of the PCA between cell suspensions and cell-free supernatants is linear (figure 3.2); this is in line with previous observations where PCA across tumour sites was inversely dependent upon the cell count in an exponential relationship. This suggests that MPs in tumour media are directly responsible for PCA. Our results clearly show that PCA in cell-free supernatants from 2D and 3D cell culture is strongly associated with the concentration of TFMP in conditioned media. Interestingly, the relationship between PCA and TFMP can be correlated equally well in a linear or exponential relationship (Fig. 3.4). Importantly, CFSE labelled MP, which include both TF positive and negative MP, are able to promote the coagulation process, suggesting that some MP show PCA based on mechanisms independent of TF; it could be that phospholipids present on the MP membrane are able to support PCA as well.

Once TFMP were removed from the media via ultrafiltration (Vivaspin, 100kDa), the filtrate no longer supported coagulation. Importantly, the pore size of these filtration units would still allow soluble TF to pass through (47kDa). Therefore, these observations suggest that the PCA associated with tumour conditioned media is MP dependent.

Interestingly, the PCA in cell-free medium vs. cell suspensions revealed that for every PCA decrease in cell suspension, the cell-free medium saw a 2.6x lower PCA. Moreover, when comparing absolute PCA between cell-free media and cell suspension, the cell-free media took about three times as long; these differences were significant and suggest that either cell-free medium contains less MP, less potent MP, or loses some aspect and characteristics that are still present in cell suspension. For example, it is possible that the plasma membrane itself can act as a scaffold for clotting, and that MP may be more potent in the proximity of that membrane. It will be difficult to find out the exact mechanisms, though it may be possible if live imaging was used via green fluorescent protein (GFP) labelled cells and particles from the clotting cascade, so that we can watch a clotting process in real time. This, in and of itself, may already reveal interesting details about the clotting process and the role MP - free or cell bound, and with or without TF - may play in that procedure.

Another factor is important to note. As the PCA of cell-free supernatants and cell suspensions could be correlated in a power relationship - by plotting the logarithms of both parameters against one another, resulting in a linear relationship - it is possible that cell suspensions and cell-free media are correlated in an exponential relationship. Indeed, further analysis revealed that a linear relationship - as presented in figure 3.2 - can be fitted almost as easily through the data as an exponential curve. This suggests that the involvement of MP in the plotting process

follows a first order reaction kinetics, where the amount of clotting in a solution depends exponentially on time (Wang et al, 2018). The reason for such a relationship would be that the relative speed of the clotting process is proportional to the concentration of the factor promoting the process. A model whereby doubling the concentration of TF also doubles the clotting speed is well conceivable, and thus, the exponential relationship between coagulation time of cell -free media and cell suspensions shown figure 3.2 could be indeed explained by TF mediating the rate-limiting step of the clotting process. However, as also evidence that suggests TF negative MP can still promote clotting, the important molecule underlying the coagulation process may be different from TF, for example, the concentration of phosphatidyl serine on the surface of MP (Darabi & Kontush, 2016; Mackman, 2006).

It would be expected that the PCA from supernatants generated by 3D cell culture are following a similar exponential or logarithmic behaviour (Duval et al, 2017). 3D aggregates - spheroids – which are grown in culture are likely closer to actual tumour growth and are therefore preferable as a model. Moreover, they are slightly more convenient and easier to grow. In addition, a 3D environment has the advantage that most tissue factors can be easily supplied, thus simulating a physiological tumour environment. However, spheroids grown on agarose have the disadvantage that they are not embedded in a 3D tissue environment and rather 'float' on a layer that prevents them from making true contact to any substrate. It may be more prudent to use a three-dimensional culture matrix, which contains important ECM components such as fibronectin, collagen, but also proteins, lipids and growth factors. Though, such an environment has the disadvantage that spheroids cannot grow easily. A compromise would be to continue using spheroids as 3D cancer cell culture, and confirm the findings in a 3D matrix cell culture or even *in vivo*, using model systems (Fennema et al, 2013). Interestingly, all cell lines tested in this study formed tumour-like aggregates in 3D spheroid culture.

Moreover, the morphology of these aggregates seemed to be correlated with the cell lines' PCA, as the supernatants' PCA was high, the more compact the aggregates were. When analyzing the area, perimeter and circularity of the spheroid, area and perimeter correlated well with PCA, in that the smaller the aggregate, the higher PCA, while the circularity of the spheroids - and thus their shape - was less well correlated with coagulation time. As it would expect both the overall shape and area of the spheroids become more circular and smaller, respectively, the more compact the aggregates are, it may be that the measures like circularity or aspect ratio are not capturing differences in the morphology of the aggregates well enough. It may be necessary to take pictures with a higher resolution, so that the 'looseness' of aggregates and their morphology can be better observed. It would therefore be desirable to analyze these spheroids further. The dynamics of aggregate formation could correlate to the

cell line's PCA as well, as budding off of MP is an inherently dynamic process as well. It may be that most of the cells producing MP once they are arranged in a cluster; or, conversely, it may be that MP production only increases significantly once a certain critical aggregate mass has been formed or due to lack of oxygen and hence build-up of CO_2. Cell lines that never form any cohesive aggregates may not be able to build many MP, which would explain the slower PCA in cell lines that do not aggregate well.

As an alternative assay to measure coagulation propensity and PCA, conductivity of cell free supernatant was used. Importantly, it was found that conductivity decreases with coagulation time; the faster a cell culture started to coagulate, the higher its conductivity. As coagulation is in and of itself a process that manifests in phenotype at a specific future point in time, it is not easy to see how coagulation itself could be connected to conductivity. However, when follow the model that MP are mediating coagulation, the observations in this study can be explained by the presence of a higher concentration of MP in supernatants that mediate coagulation in a more efficient way. Indeed, it has been previously found that the impedance - i.e., the resistance and thus the ability to conduct electric currents - depends on the presence of microparticles in a phenomenon called the Coulter Effect; particles that are poor conductors can increase the impedance of a solution (Kim & Ligler, 2010). However, in this case, it is more likely that the presence of MP lowers the impedance, as we see increase in PCA with increasing conductance. It may be that MP in and of themselves can act as transporter of electrical charges.

So far, the initial measurements of conductivity suggested that within two cell line (the AsPC-1 and SKOV-3 cell lines, the higher the conductivity, the higher PCA; this relationship was linear, when using the logarithms of PCA. As we mentioned above, this logarithmic relationship suggests that the MP concentration is proportional to the coagulation time or PCA. MP could be the one central rate-limiting component that controls the coagulation process. Interestingly, when comparing the AsPC-1 cell line dilution to the dilution of SKOV-3, a cell line with slower PCA - the PCA is higher even at the same conductivity. If conductivity is a readout of MP concentration, and PCA only depended on the presence of MP, one would expect the same PCA at the same conductivity. However, the observation that PCA are still different between both cell lines suggests that additional factors beyond the MP concentration determine PCA. It could be the concentration of TFMP, or their cell surface structure, or both. More experiments are needed to elucidate the independent regulator of PCA.

It was also found that PCA of cell free media increased after ultrafiltration of cell-free supernatant; while the filtrate was mostly devoid of any coagulation activity, the MP retained

on the membrane and taken up into solution kept their activity, which suggests that ultrafiltration can be an additional assay that can be used to concentrate MP while retaining their biological activity. It is interesting to note that the filtrate - which almost certainly contained TF, as it could be measured by ELISA - did not show coagulation activity. This suggests that either most of TF is associated on MP, so that the TF concentration in the filtrate is too low to show an effect, or that TF need to be associated with MP to show an effect. It is possible that both MP and TF are needed to trigger and promote the process of coagulation (Date et al., 2017). Further research into this phenomenon will likely be of significant interest. Importantly, filtration of various cell line supernatants led to concentrated MP solutions that increased in potency by factors specific to the cell lines. In general, the more potent the cell line is as a promoter of coagulation, the more potent the concentrated post-MP solution was. Whether this reflected irregularities in the ultrafiltration process or an inherent difference in biological function remains to be further researched.

Chapter 4 Design and optimization of microfludic biochip to study tumour microparticle interaction with endothelial cells

4.1 Introduction

Traditional *in vitro* culturing systems have been widely used in preclinical cancer research (Langhans, 2018; Lazzari et al, 2017) However, methods of this kind carry with them several well-known drawbacks. For example, studying biological mechanisms such as migration, differentiation and a range of cellular functions on two-dimensional (2D) glass or plastic surfaces can result in a loss of many biological and molecular features of the original cancer cells (Yamada & Cukierman, 2007). Furthermore, 2D tissue culture models can cause major alterations in cellular phenotype and genotype (Breslin & O'Driscoll, 2013). Another disadvantage of this method is lack of cell–cell interaction and cell–ECM signalling that occurs in 3D cell culture models. This interaction is very important for cell differentiation, proliferation and another cellular functions. This interaction involves proteins such as integrins which is an important main receptor protein that cells use to both bind to and respond to the ECM (Abbott, 2003). Moreover, another potential drawback of cell monolayer tissue culture model is lack of microenvironmental properties as in solid tumours such as the lack of hypoxic and necrotic areas, while animal models are time consuming, expensive, and usually fail to reflect human tumour biology (Hait, 2010). For example, the tumour growth induced ecologically by animal models recapitulates the early stages of tumour progression, but the multifocal character of the resulting primary tumour restricts the lifespan of a mouse and, therefore, reduces metastatic growth (Francia et al, 2011; Guerin et al, 2013). Moreover, in certain experimental conditions, there are many concerns regarding the discomfort or the pain of animals and so there is an ongoing drive to utilise new models of human tumours. In addition, several experimental animals have compromised immune systems and unable to simulate the stroma-tumour microenvironment (Cekanova & Rathore, 2014). Furthermore, using animal models constitutes a major challenge as the average rate of successful translation from animal models to clinical cancer trials is less than 8% (Mak et al, 2014). Therefore, to overcome these limitations in 2D cell culture researchers are turning to 3D cell culture models that are closer to mimic the biological process in living organisms (Hoarau-Vechot et al, 2018). According to Li et al. (2008), spheroid models may have a potential role in mechanisms of resistance to other stress stimuli. Tumour spheroids comprise of multiple cells arranged in three dimensions setting. Spheroids can also be formed by spontaneous aggregation of cancer cells (Li et al, 2008). Spheroids have many advantages more than 2-D culture method. For

example, cells in spheroids are connected by membrane protein anchorage with more cell adhesion molecules for example CD44v6 and E-cadherin (Green et al, 2004; Kang et al, 2007). Moreover, proteins expression such as glycolytic proteins are increased in spheroid cells over monolayer cells due to increased glycolysis (Kumar et al, 2008b). Green et al. 2004 has found that increased expression of cell adhesion in spheroids cells has a great impact on cell survival rate therefore inhibition of these adhesion molecules via specific antibodies may disrupt the influence of spheroid formation. Consequently, using spheroids as a tumour model have provided numerous advantages in cancer research to date.

The inconsistencies in research data has led to the failure of the transfer of new discoveries to effective treatments and therefore there is a need to pursue other models than the animal models so that the gap between bench and clinical trials can be bridged (Elliott & Yuan, 2011). Microfluidics is an innovation, which started to develop during the 1950s with systems to handle microliter volumes in microchannel where fluid flow is strictly laminar and concentrations of molecules can be well controlled (Zhang & Nagrath, 2013). One of the most important advantages of these micro devices is that novel anti-cancer agents can be tested on tumours ***ex-vivo*** over a longer time and samples can be analysed throughout (Zuchowska et al, 2017). There is also needed to mimic the same environment surrounding the tumour and this can be done by using an optimised microfluidic device. Through this technology, a scenario similar to that in blood vessels surrounding the tumour can be created, where via this technology the flow and environment around tumour can be controlled (Khademhosseini et al, 2006). For instance, a microfluidic model to analyse the specificity of human breast cancer metastases to bone has been described (Bersini et al, 2014). Using human osteo-differentiated bone marrow-derived mesenchymal stem cells and endothelial cells, researchers re-formed a vascularized osteo-cell conditioned microenvironment to analyse the metastases to bone. The Authors discovered molecular pathways important for extravasation of breast cancer cells, involving bone-secreted chemokine CXCL5 and breast cancer cell surface receptor CXCR2 (Bersini et al, 2014).

4.2 Aims

The aims of this chapter were to immobilise a tumour spheroid in a microfluidic chip and use it as a model to characterize tumour MP.

4.2.1 Objectives

- Therefore, in order to achieve this goal an *ex-vitro* microfluidic device was developed to hold tumour spheroids for certain period of time to allow procoagulant activity (PCA) determination in the effluent under flow conditions.
- Consequently, several experimental parameters were tested such as flow rate, salinization effect and differing chip designs. Moreover, another aim of this chapter was to investigate how these cancer MP can interact with endothelial cells *in vitro* and potentially change PCA under flow conditions.
- Therefore, to achieve this goal an *ex-vitro* model was developed consists of two connected commercial biochips: the first biochip model was used to hold tumour spheroids and the second biochip coated with HUVECs. Therefore, once the model has established different analytical methods were performed on effluent to enumerate and characterize the tumour MP and to assess the effect of tumour MP on PCA of the endothelial cells.

4.3 Results

4.3.1 Experimental design and biochip setup

Previously, 7 cancer cell lines were screened for their ability to shed MP and form tumour spheroids as described in proceeding chapter. The PCA of tumour media associated with MP was determined by one-stage prothrombin time in 2D and 3D cell culture. In the present study, preliminary experiments were conducted to ensure tumour spheroids could be held in place in a chip device properly. Perfusion of media through captured on-chip spheroids was monitored over time ensuring the device did not leak or become blocked. Respective fresh tumour media was perfused through the device and the media effluents were sampled each hour time and stored for further analysis. The process from selecting the cell lines, assessing the PCA and spheroid formation and then the subsequently selected formed spheroids that were tested under flow conditions is shown in (Figure 4.1). Subsequently, selected tumour spheroids were subjected to flow conditions using different microfluidic chips as will be detailed in the following sections. Moreover, using a dual microfluidic chip assembly under flow conditions, the interaction of tumour MP and endothelial cells was also evaluated. Therefore, in this study four ex-vitro microfluidic device models were used throughout the study for flow applications. Two ex-vitro microfluidic device models were manufactured and fabricated in the Department of Chemistry at The University of Hull as described in section 2.7. The other two ex-vitro microfluidic devices were obtained from Ibidi and Cellix companies as commercial biochips as described in sections 2.10 and 2.11.

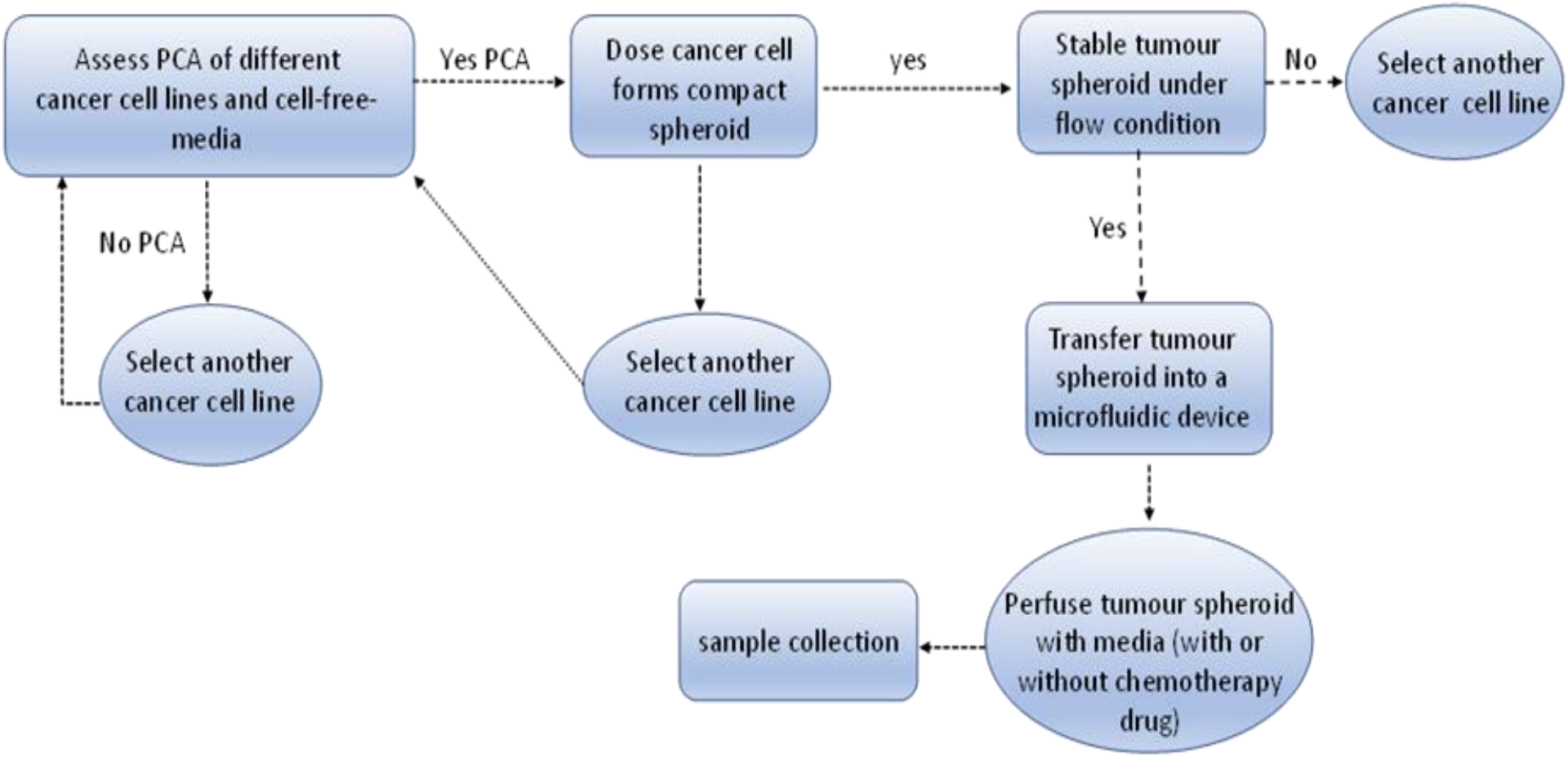

Figure 4.1: Experimental workflow shows steps of generation of spheroids to samples collection.

Pancreatic cell line ES2 and glioblastoma cell line U87 showed a relatively high PCA and ability to form stable and compact spheroids as will detailed in next section.

4.3.2 Tumour spheroids generation

The tumour spheroids show many features associated with solid tumours; these features similar to those of *in vivo* tumour tissues that include different zones of proliferation, apoptotic, and necrotic cells and an oxygen gradient with hypoxic areas in the core (Costa et al, 2016). Several tumour cells lines (A2780, SKOV3, MIA Paca2, PANC-1, AsPC1, ES2 and U87) were assessed for PCA of cell free media (MPs associated) and then subsequently assessed for spheroid formation so the general assessment process can be seen in the above flow chart (Figure 4.1). In brief, the liquid overlay method was used to generate spheroids by seeding cells at concentration of $2x10^4$ cells/well in a volume of 200 µl/well of culture medium in 96-well plates coated with 1.5% agarose as described in section 2.1.15. Consequently, a number of cancer cell lines (A2780, SKOV3, MIA Paca2, PANC-1, AsPC1, ES2 and U87), were tested for their ability to form compact and stable spheroids. Accordingly, plates were maintained in 5% CO_2 at 37°C for 10 days growth period. In addition, the spheroid growth was monitored, and images of the spheroids were taken on days 3 and 10 by using an Oxford Optronix GelCount™ camera and all spheroids were under 500 µm in average diameter until day 10. Of those cancer cell lines, observations showed that MIAPaca2 and A2780 were aggregating and generating moderate spheroids. Loose cell aggregation started on day 3 and this aggregation was stable until day 10, some cells formed a moderately compact to strong compact spheroid. In addition, SKOV3, PANC-1 and AsPC1 formed a relatively compact spheroid in comparison to those formed by MIAPaCa2 and A2780. In contrast, U87 and ES2 formed strong compact spheroids with a notable spherical shape on day 3 and this remained stable until day 10 (Figure 4.2). Subsequently, all tumour spheroids were tested on microfluidic biochip 1 (section 4.4) and some spheroids on microfluidic biochip 2 (Section 4.5). However, U87 and ES2 were ultimately selected for further studies as they formed compact and stable uniform size spheroids under flow conditions, and they were used on the commercial biochips as described section 4.6. It was the aim of this chapter to determine the optimal tumour spheroid model that can be used to evaluate and characterize cancer MPs. Moreover, another essential aim of this chapter was to develop a microfluidic device that could be used to hold tumour spheroids. Once these aims were optimised then the final aim was to assess PCA of effluent (cell free media with associated MPs) and to show the effect of cancer MPs released from spheroids under flow on HUVECs.

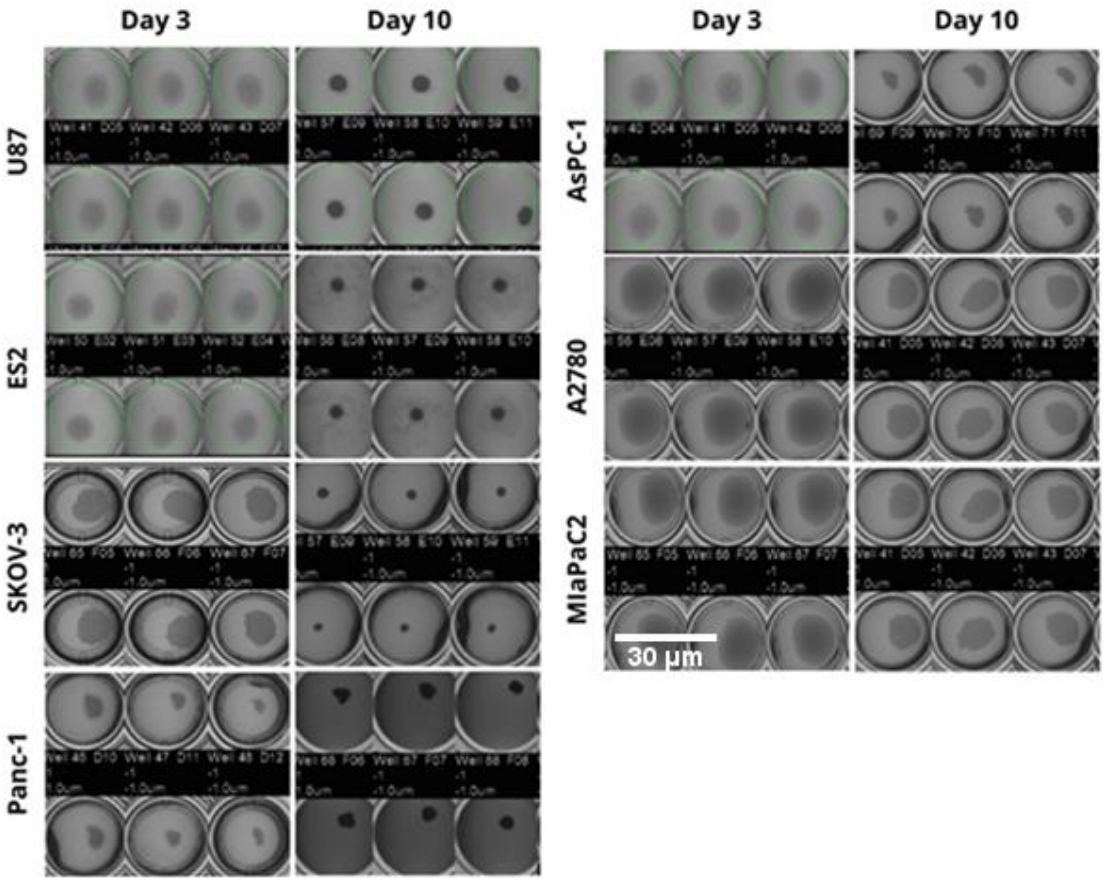

Figure 4.2: Images showing tumour spheroids from various cancer cell lines.
Several cancer cell lines grown in 3D culture for 10 days. During this growth period all cancer cell lines started to aggregate. Images shows Continuous aggregation of cancer cell lines until day 10. A slight change in Morphological appearances has been seen of A2780 and MIA PaCa-2. ASPC1, Panc-1 and SK-OV-3 generated a relatively compact spheroid. U87 and ES-2 showed the best model to form a compact spheroid. The experiment was performed with 7 replicates for each single tumour cell line with magnification 2X.

4.3.3 Transfer tumour spheroid into the microfluidic chip

Tumour spheroids were first generated using the liquid overlay method under a static condition (96-well plate) platform and then transferred to the microfluidic chip (Figure 4.3). The generation of tumour spheroids cultures with homogenous sizes was important in order to retain structure under flow condition and for reproducibility of results. Therefore, tumour spheroids were initially tested for compactness and spherical shape that was not easily disaggregated under flow conditions. Furthermore, the compactness of spheroids has several features similar to those of *in vivo* tumour tissues (Mehta et al, 2012). These features make spheroids a more suitable tool for *in vitro* drug screening assays than two-dimensional (2D)-monolayer cell cultures (Giannattasio et al, 2015). Subsequently, pre-formed spheroids were transferred from 96-well plates into a microfluidic chip using a pipette to the microfluidic chip.

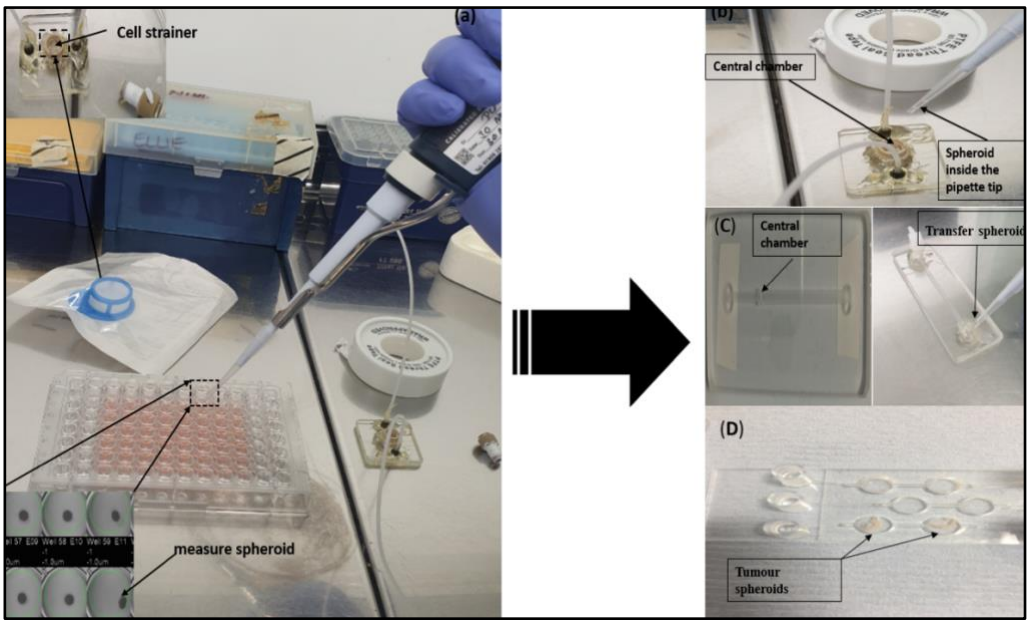

Figure 4.3: Image showing the transfer a tumour spheroid into a microfluidic chip.
(a) 96- micro plate coated with 1.5% agarose gel that contains tumour spheroids which their size was measured using an Oxford Optronix Gelcoat™ camera before transfer into a microfludic chip. In addition, a cell strainer was trapped within the central chamber of the biochip model 1 to avoid spheroid flush-out (b) Image showing a spheroid inside the pipette tip before transfer into the central chamber just above the cell strainer into chip model 1. (c) Image shows spheroid inside the pipette tip being transferred into the central chamber of biochip model 2 whereby tumour spheroid was injected into the inlet of the chip. (D) Image showing several spheroids inside the microwells of commercial a µ-Slide III 3D biochip.

4.3.4 Tumour spheroid transferring into a microfluidic biochip

Briefly, using biochip model 1, several formed tumour spheroids of A2780, MIA PaCa-2, ASPC1, Panc-1, SK-OV-3, U87 and ES-2 were transferred at day 10 into the central chamber. In addition, only SKOV-3, AsPC-1, ES-2 and U87 tumour spheroids were injected into the inlet of biochip model 2, and fresh tumour culture medium flows through the chip to push the spheroid into the trapping well. Finally, tumour spheroids of U87 and ES2 were transferred into a µ-Slide III 3D. Several tumour spheroids were added into each well and cover the slide with the supplied lid. Importantly, the µ-Slide III 3D chip was validated and hence ultimately used for further study. Further information is given in the following sections.

4.4 Microfluidic Biochip **model 1**

4.4.1 Fabrication, assembly and setup

Using the 'in-house' fabricated Hull biochip model 1 (Figure 4.4), the microfluidic device was coated by acrylate based salinizing agent reagent in order to make the inner surface of the microchannel into a hydrophobic condition (Kim & Herr, 2013). The fabricated microfluidic device contained two layers of thermally bonded glass: top (3mm) and bottom (1mm). The bottom layer of glass housed photolithographic etched channels (190µm wide and 70µm deep)

connecting to the inlet (1.5mm), the cylindrical tissue chamber (3mm, 20µL) and two outlet holes (1.5mm) drilled in the top glass layer. The pre-formed tumour spheroids from several cancer cell lines were maintained for up to 6h to demonstrate release and activity of tumour MPs under flow conditions with the aim to subsequently connect this model with another a microfluidic device lined with endothelial cells (HUVECS) so that the effect of tumour MPs on HUVECS under shear flow could be assessed. It was previously shown, using a head and neck squamous cell carcinoma line (UMSCC81B) that tumour MPs interacted with HUVECs under static conditions (Adesanya et al, 2017).

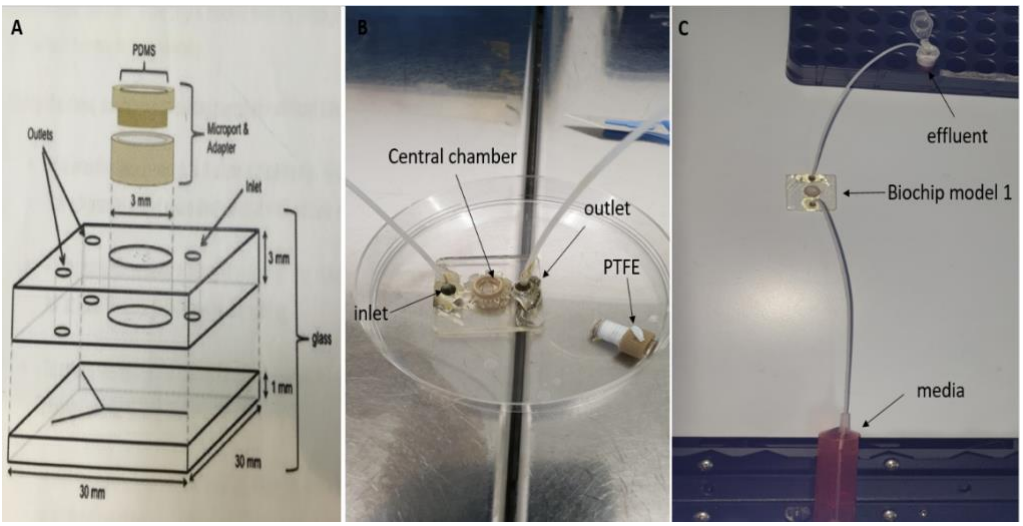

Figure 4.4: Image showing the biochip model 1 and setup method.
(a) Schematic showing the dimensions of the device. (b) Setup of the device with tubes connected to the inlet and outlet. The central chamber was sealed using a poly-dimethylsiloxane (PDMS; Dow Corning, Midland, UK)-filled adapter with polytetrafluoroethylene (PTFE) tape wrapped around the thread (c) Image shows the basic experimental showing tumour fresh media contained in syringes ready to be flowed through biochip model 1 containing spheroids.

Extensive work had to be carried to optimize and standardize this model. Briefly, for reliability and reproducibility a single spheroid of seven cancer cell lines was tested on many microfluidic chips to ensure they are stable and compact under continuous shear stress (flow conditions). The microfluidic set-up for spheroids was carried out as described in section (2.7.1). Spheroids were transferred from static (96-well) culture and placed into the central chamber and the microfluidic device was connected to a Harvard PHD 2000 syringe pump (Harvard, UK) (Figure 4.5). The microfluidics system was maintained at 37°C (via PID control) inside an incubator chamber and fresh complete medium for the relevant spheroids parent cell line was then perfused at different flow rates through the biochips to establish the optimal flow rate as described in the next section.

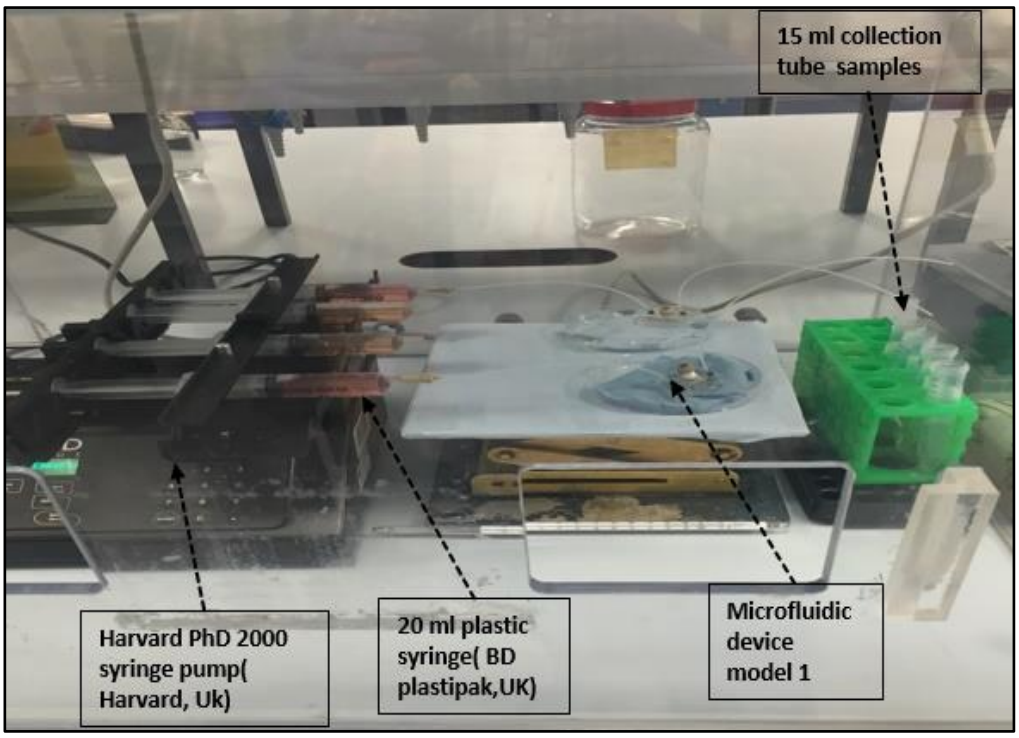

Figure 4.5: Image showing the basic experimental setup.
Image showing tumour fresh media contained in syringes linked to the microfluidic design model 1with spheroids from variuos cancer cell lines that linked to sample collection tubes. The experiments were carried out in a 37°C incubator.

4.4.2 Flow rate optimisation

The optimum flow rate was assessed by perfusing the media over a tumour spheroid to yield sufficient sample volume for analysis and to maintain the tumour spheroid structure under flow conditions for 24 hours. Initial experiments were conducted with flow rates ranging from 1-6 µl/min to examine the effect of a flow rate using total of 16 U87 tumour spheroids that was initially was selected due to its ability to form stable, compact spheroids with a typical spherical shape. Subsequently, a single U87 spheroid was transferred into the central chamber of biochip model 1 devices (n=16) as described previously in section 2.1.16. Then, the microfluidic devices were setup and run over different days with different flow rates for two hours. Failure rate of biochip performance was assessed using different parameters. Any leakage or blockage with the device during experiment was considered as a design fault. In addition, macroscopic monitoring of tumour spheroid disaggregation was considered as failure. Therefore, all experimental attempts were counted and statistically assessed. Furthermore, insufficient volume for downstream off-chip analysis was considered as disadvantage of that particular flow rate. Consequently, the main aim was obtaining sufficient volume of sample over time to enable analysis and secondary to make sure that tumour spheroids were stable throughout the experiment to enable assessment of the microfluidic device for reproducibility and reliability (Figure 4.6).

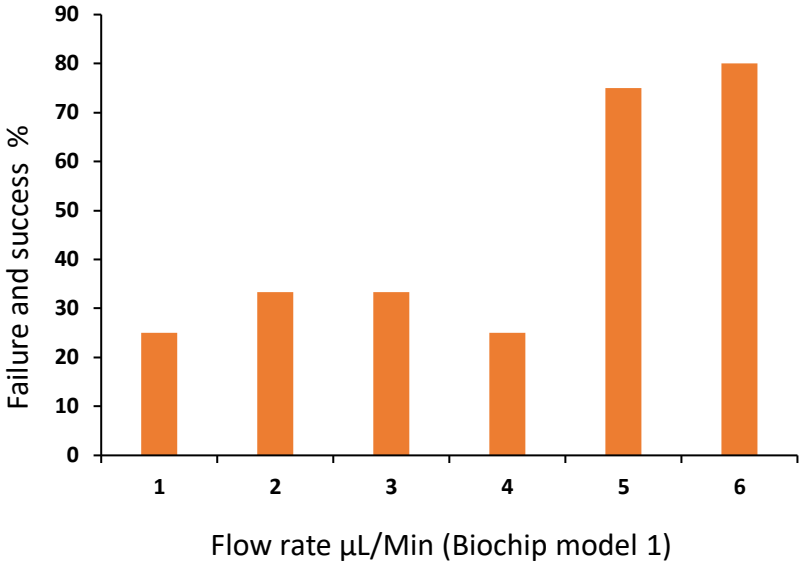

Figure 4.6: Chart showing failure rate percentages of biochip model 1.
Flow rate of 1-6 µl/min was examined for two hours using 16 U-87 tumour spheroids in 16 biochip devices (one spheroid/biochip). Low Failure rate observed when using 1 and 2 flow rates though theses flow rates were not suitable to yield sufficient volume that is > 200µl. Using flow rate of 3µl/min was also not feasible as it resulted in high failure rate and low sample volume. Flow rate 4, 5 and 6 showed high failure rate respectively but yielded the required sample volume. Failure (■).

Accordingly, after comparing the different flow rate, 4µL/min was chosen as it yields sufficient sample volume with the lowest failure rate. This flow rate had the lowest damage effect on tumour spheroid as failure rate percentage was 25% using three independent experiments. The recommended volume required was above 200 µL that will be enough to do PCA assessment and flow cytometry analysis of MPs.

4.5 Using Biochip model 1 to assess PCA of MPs (no cell strainer)

4.5.1 Operation of biochip model 1 and tumour spheroid monitoring

Previously obtained data showed that different tumour spheroids from different histological sites have expressed different pattern of PCA under static condition as described in section 3.2.2. Utilising a microchannel slide flow-based assay model, the ability of several tumour spheroids to shed MPs into the effluent samples was tested and PCA was assessed during different intervals time. Therefore, all devices were tested for any blockage or leakage before adding any spheroids. Consequently, a single tumour spheroid of A2780, MIA PaCa-2, ASPC1, Panc-1, SK-OV-3, U87 and ES-2 was transferred into the biochip model 1 as described previously in section 2.1.16 but without a cell strainer. To validate this model, different parameters were conducted such as volume of the sample, blockage, leakage and spheroid disaggregation. Having established the optimum flow rate, 4µl/min was used through the entire study. Consequently, all microfluidic devices were connected to the Harvard flow pump

and run for one hour to assess the stability of the tumour spheroids and the biochip reliability (Figure 4.7).

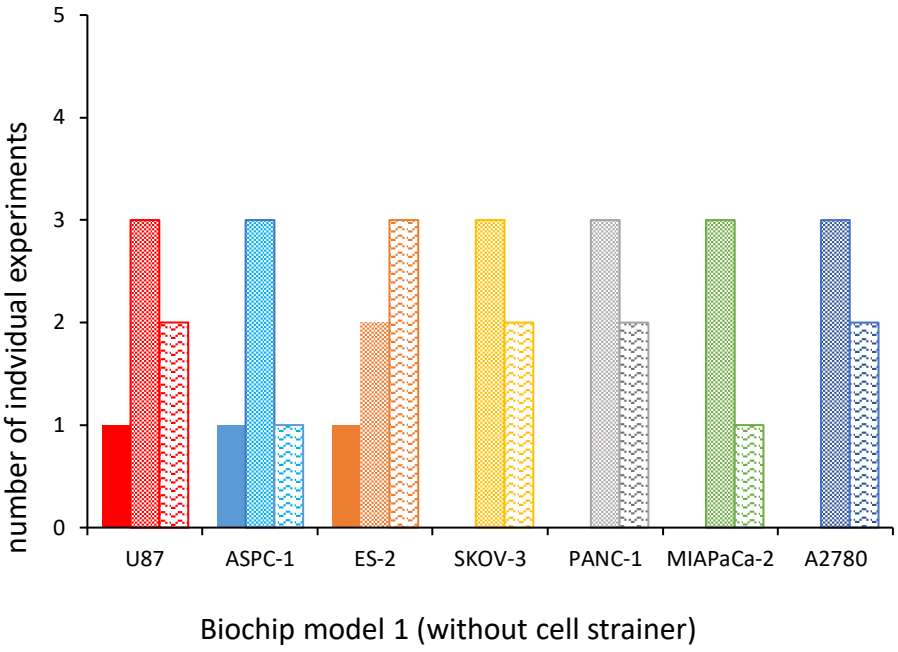

Figure 4.7: Chart showing biochip model 1 validation without cell strainer.
Several tumour spheroids were used to assess their stability under flow condition using chip model 1. Tumour spheroids U87, ES-2, AsPC-1 and PANC-1 showed the higher successful rate however this rate was only 11%. Disaggregated and blocked devices were observed to be 54%. A2780 and MIAPaCa-2 were showed the most instable and hence disaggregated easily in this model. Tumour spheroids U87 and ES-2 showed the most stable spheroids under flow condition. Data representative of total 37 independent experiments. The percentage of leaked devices was 35 %. Successful (Filled), disaggregated (hashed) and leaked (waves).

Table 4.1: table shows the statistics data evaluation of model 1.

Tumour spheroids	**U87**	**ASPC-1**	**ES-2**	**SKOV-3**	**PANC-1**	**MIAPaCa-2**	**A2780**	**Total tests**	**%**
Successful	1	1	1	0	0	0	0	3	11
Disaggregated and Blocked	3	3	2	3	3	3	3	14	52
Leaked	2	1	3	2	2	1	2	10	37
%	20	25	20	0	0	0	0	27	
failure rate	83	80	83	100	100	100	100		
mean	2	1	2	2	2	1	2		
sum	6	5	6	5	5	4	5		
SD	0.82	0.94	0.82	1.25	1.25	1.25	1.25	0.82	

The data obtained suggested that this model was not able to hold the tumour spheroids satisfactorily and therefore the percentage of blocked and leaked devices was very high. Moreover, data obtained in table 3 showed that overall failure rate across the cancer cell lines was > 80% suggesting this setup was unreliable and not reproducible.

4.5.2 PCA data that collected from successful attempts

However, despite the high failure rate using biochip model 1 without a cell strainer, a few successful experiments were achieved where a single spheroid was successfully transferred and maintained in the biochip model 1 and spent media (effluent media) was collected for 2 hours. Thus, AsPC-1, PANC-1, ES-2 and U87 tumour spheroids were stable just in one single experiment out of all attempts. Using a one-stage clotting assay, effluent media (MPs associated) were obtained and the PCA was assessed of the 4 tumour spheroids (Figure 4.8). The macroscopic observation for these tumour spheroids inside biochip was assessed however because the spheroids are normally colourless or white the images of spheroids inside the biochips were not visible.

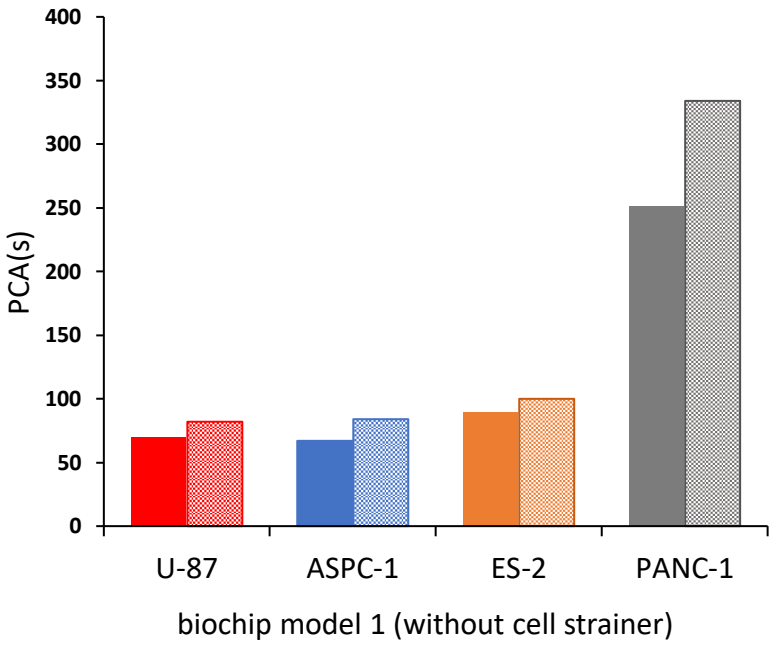

Figure 4.8: Chart showing the PCA of effluent harvested from spheroids biochip model 1. Tumour spheroids U87, AsPC-1 and ES-2 showed the fastest clotting time. Tumour spheroid PANC-1 showed the slowest clotting time. Data representative of mean 1 successful experiment. First hour (filled), second hour (hashed).

Following the experiment, all tumour spheroids where be able to be retrieved from the central chamber and upon microscopic examination were found to be both compact and intact. Tumour spheroids of AsPC1, U87 and ES-2 were shown to produce continuous PCA and this is presumably due to a continuous rate of tumour MP release. However, PANC-1 spheroids were

shown to produce continuous PCA but slower than previous spheroids and this is likely due to either MP release or less procoagulant MP being released due to the shape of the spheroid as detailed previously in section 3.3. However, although this developed model offered a way to assess tumour associated PCA under flow conditions it was ultimately too unreliable. Therefore, it was necessary to pursue an alternative microfluidic approach to improve reliability. The lack of reliability and reproducibility were the major drawbacks of the biochip 1 model as all tumour spheroids even the compact one such as U87 and ES-2 were not able to be reliably maintained inside this model mostly due to inherent design flaws for spheroid use. This was found to be due to several factors, firstly, though the size of the central chamber was ideal for holding more than one spheroid as the size of the spheroids used was up to 500 µm this design was found not to be suitable to maintain compact spheroids as they were either flushed down via outlet microchannel or disaggregated within the flow. The disaggregation of spheroids resulted in the blockage of the narrow microchannel or the tubing connected to the outlet due to cell clumping and ultimately leakage of chip device due to the increased pressure within the closed system. Based on above data, 58% of the tumour spheroids were disaggregated and led to subsequent channel clogging. A total of 33 independent experiments were conducted to validate this model however observed data suggesting that this model was not suitable to maintain tumour spheroids. Thus, Corning® cell strainers with 40-µm pore size was used to hold the tumour spheroids as follows in the next section.

4.6 Using Biochip model 1 with cell strainer

4.6.1 Cell strainer interface installation

Consequently, in order to hold the spheroids inside the central chamber and to avoid spheroid disaggregation a 40-µm cell strainer was used (Figure 4.9) which would allow MPs to pass through for analysis but retain the spheroid in position. The cell strainer was placed in the central chamber to avoid any disaggregation of spheroids. All devices were tested for any blockage or leakage before adding any spheroids. Thus, a small piece (1 mm), of the cell strainer was cut using sterile disposable scalpel inside a biosafety cabinet class II and carefully placed within the central chamber of the biochip model 1.

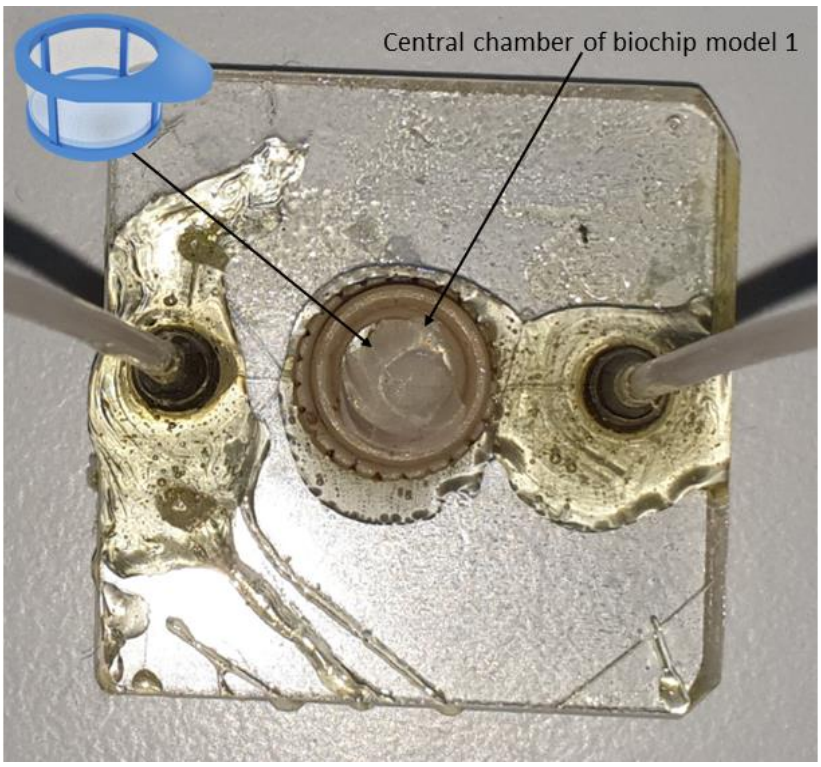

Figure 4.9: image showing the biochip model 1 with the cell strainer.
1mm of cell strainer was inserted inside the central chamber before insert tumour spheroids.

4.6.2 Operation of biochip model 1 with the cell strainer

Subsequently, one single tumour spheroid from either A2780, SKOV-3, MIAPaCa2, PANC-1, ASPC1-1, ES-2 or U87 were transferred into the biochip model 1 and placed above the cell strainer. Then, all devices were connected to the pump and macroscopic examination was conducted to sure that all devices were not blocked or leaking. Substantial work was carried out in an attempt to maintain spheroids inside the central chamber and avoid any leakage or blockages as this is essential to measure the effluent PCA reproducibly. Furthermore, another challenge of using such device is the contact adhesive (Araldite™) liquid that has been historically used within this laboratory to connect tubes to the inlet and outlet and circular tissue chamber to the top glass layer, results in difficulty obtaining a uniform thickness around the tubes and requires a long drying time. Moreover, this model was not ideal for correlative light and confocal microscopy as the devices minimal thickness was greater than 4 mm rendering it unsuitable for imaging. PCA was able to be measured in the absence of leakage or blockage on the few occasions an experiment could be completed (Table 4.2).

Table 4.2: PCA across the 2 h experimental window.

	U87	AsPC-1	ES-2	PANC-1
First hour PCA	69 ± 2s	66±2s	88±2s	253.5±4s
Second hour PCA	84.5±2s	88±2s	99±2s	338.9±2s

Data represents mean of duplicate reading (n=1).

Thus, the leakage, partial blockage, spheroid disaggregation and full blockage could lead to false positive results and inaccurate data reproducibility (Figure 4.10). Ultimately, due to these difficulties and pitfalls becoming well established a new microfluidic chip was designed and fabricated in collaboration with the University in-house fabrication unit.

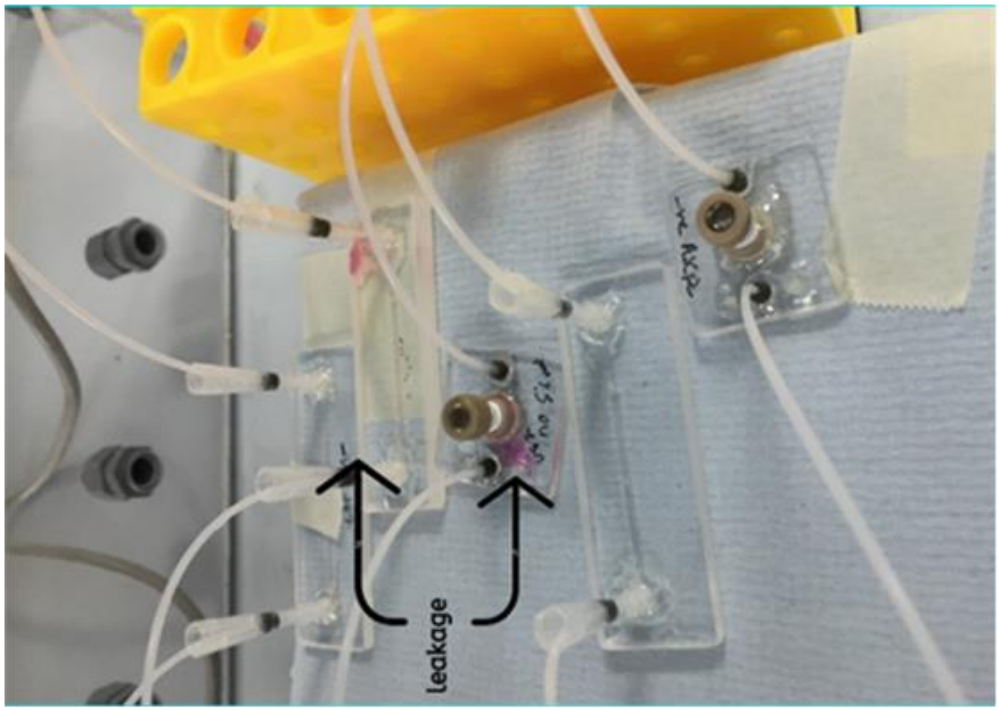

Figure 4.10: Image shows leakage and clogging of microfluidic devices of biochip model 1.

Therefore, in order to evaluate the model's reproducibility, 63 independent experiments were conducted, and numbers of leakage, blockage or spheroids disaggregation were counted as in (Figure 4.11). Despite, the encouraging results as the data observed suggesting a significant improvement in successful rate though tumour spheroids disaggregation was observed in all cancer cell lines. Moreover, the disaggregated and leaked devices were also significantly high as data showed 43% and 22% respectively. Moreover, the failure rate was obtained, and the data confirmed that there was a slight improvement (Table 4.3).

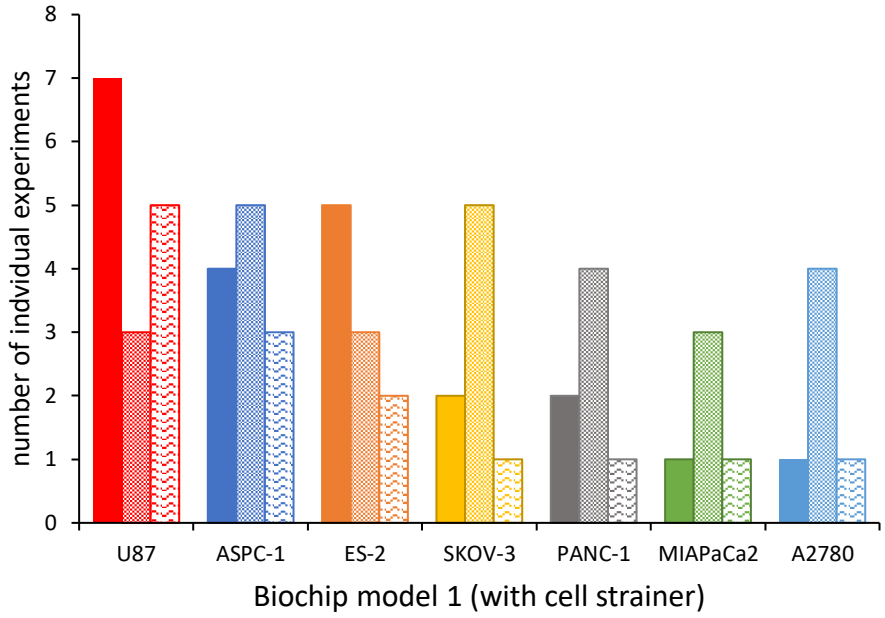

Figure 4.11: Chart showing the chip model 1 outcome.
Seven tumour spheroids were used to assess their stability under flow condition using chip model 1. Tumour spheroids A2780, SKOV-3 and MIAPaCa-2 were showed the most instable and hence disaggregated easily in this model. Tumour spheroids U87 and ES-2 showed the most stable spheroids under flow condition. (n=63). Successful (Filled), disaggregated (strips) and leaked (waves).

Table 4.3:Table shows evaluation of spheroid model 1 with cell strainer.

Tumour spheroids	U87	ASPC-1	ES-2	SKOV-3	PANC-1	MIAPaCa2	A2780	Total tests	%
Successful	7	4	5	2	2	1	1	21	37
Disaggregate and Blocked	3	5	3	5	4	3	4	23	40
Leaked	5	3	2	1	1	1	1	13	23
%	53	67	50	75	71	80	83	57	
Sum	15	12	10	8	7	5	6	63	
SD	2.0	1.0	1.5	2.1	1.5	1.2	1.7		

Despite the design drawbacks, this design proved to be successful and effective device with other types of samples such as solid tumours of Head and neck squamous cell carcinomas (HNSCC) (Bower et al, 2017).

4.6.3 Statistical comparison of biochip model 1 with and without cell strainer

An assessment of whether the use of a cell strainer had any impact on maintaining the tumour spheroids in the biochip model 1 was undertaken. Though, a slight increase in the percentage of successful rate was observed when cell strainer was used with biochip model 1 and slight decrease in disaggregated or leaked devices though this was not significant (Figure 4.12).

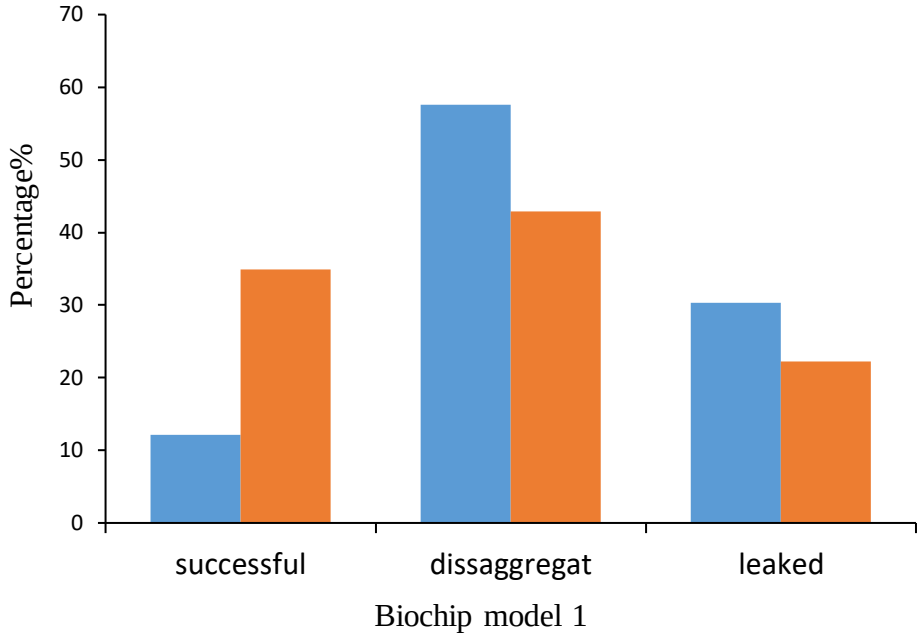

Figure 4.12: Chart showing comparison of the biochip model 1 with cell strainer vs no cell strainer. No cell strainer (■), with cell strainer (■).

Unfortunately, this also proved ineffective of the biochip model 1 to hold and maintain a tumour spheroid. It was unclear how tumour spheroids were so easily disaggregated with the use of a cell strainer although the experiments using U87 and ES-2 spheroids showed the highest success rate which may suggest the compactness of the formed spheroid is linked to the ability to maintain structure under flow. In light of high failure rates observed a new biochip model was designed with the aim to appropriately analyse spheroids MPs.

4.7 Biochip model 2

4.7.1 Fabrication, assembly and setup

Based on the data generated and problems associated with the biochip model 1 design, specifically for the aims of this work (spheroids) a new chip was designed in association with the Hull Microfluidic fabrication laboratory. The second model (Biochip model 2), was fabricated as well in in the Department of Chemistry at The University of Hull by Dr. Alex Iles Due to many drawbacks identified after using Biochip model 1 a second model was fabricated to improve the flow conditions and overcome the problems observed. Both models were designed using AutoCAD and SolidWorks software and the tool paths were generated using SolidCAM software. The parts were milled using diamond tools with a Datron 7 CNC machine (Datron Technology, Milton Keynes, UK). The type of glass used for the devices was Schott B270 (Dassault Systèmes SolidWorks Corporation). The two layers of the devices were bonded together thermally using a furnace to heat the glass to its softening temperature of approx.

590 ° C and by applying a small amount of force. After bonding, sharp edges and corners were polished using a diamond polishing wheel. This newly designed and manufactured device was specifically designed in order to hold spheroids within the flow stream to remove potential loss of the spheroids within the system and associated blockages. The final design was a microfluidic device containing a single microchannel of length 55 mm and width 1.5 mm, with a specific spheroid well 2 mm wide (Figure 4.13). Next, we assessed whether the coated or uncoated the biochip with salinizing agent a 3-(Trimethoxysilyl) propyl acrylate (Sigma Aldrich) has different PCA pattern. Salinization is known to minimize adherence of certain biological materials. Salinizing glassware increases its hydrophobicity and is used in cell culture to minimise cell adhesion. Therefore, microfluidics Hull chips model 2 were classified into silanisation, no silanisation as negative control with fresh medium. Four symmetrical chips were labelled as A, B, C and D. Chip A and B were coated with a 3-(Trimethoxysilyl) propyl acrylate (Sigma Aldrich) in order to assess the difference between coated and un-coated chips and whether this agent would affect on clotting time or not. The interior surfaces of the microfluidic chip model 2 has been silanized using 3-(Trimethoxysilyl)propyl acrylate from (Sigma Aldrich). The salinizing agent was diluted to 5% by volume in methanol. During incubation, microflow channels was rinsed with isopropyl alcohol. Chips C and D were uncoated and PCA of effluent (MP associated) was assessed. Cell free media was harvested from two 75cm² flasks with a total volume of supernatant of 40 ml that was then divided into 8 ml for each chip. The remaining volume (approx. 8 ml) was transferred into a 50 ml polypropylene tube and was incubated inside tissue microfluidics chamber in order to assess the PCA off-chip, over time. CT was taken throughout the experiments to see the effect of on-chip and off-chip on PCA during a 24-hour period. The first CT was taken prior to the start of the experiment and subsequent samples were taken at 4h intervals where possible. The last reading was taken after 24 hours. Subsequently, 40 ml of spent media of U87 obtained from a 20ml culture ($1*10^6$ cells/ml), was collected and centrifuged at 400 x *g* for 5min to discard cells and large cell debris. Next, 8 ml of the supernatant was perfused over 4 identical biochips using microfluidic system for 24 hours (Figure 4.15). In addition, 8 ml of the same spent media was dispensed into 50 ml polypropylene as off-chip static same temperature control. PCA was taken in 4 hours and 24 hours' time intervals. The initial PCA value of U87 spent media prior to perfusion was 47s (+/-5s).

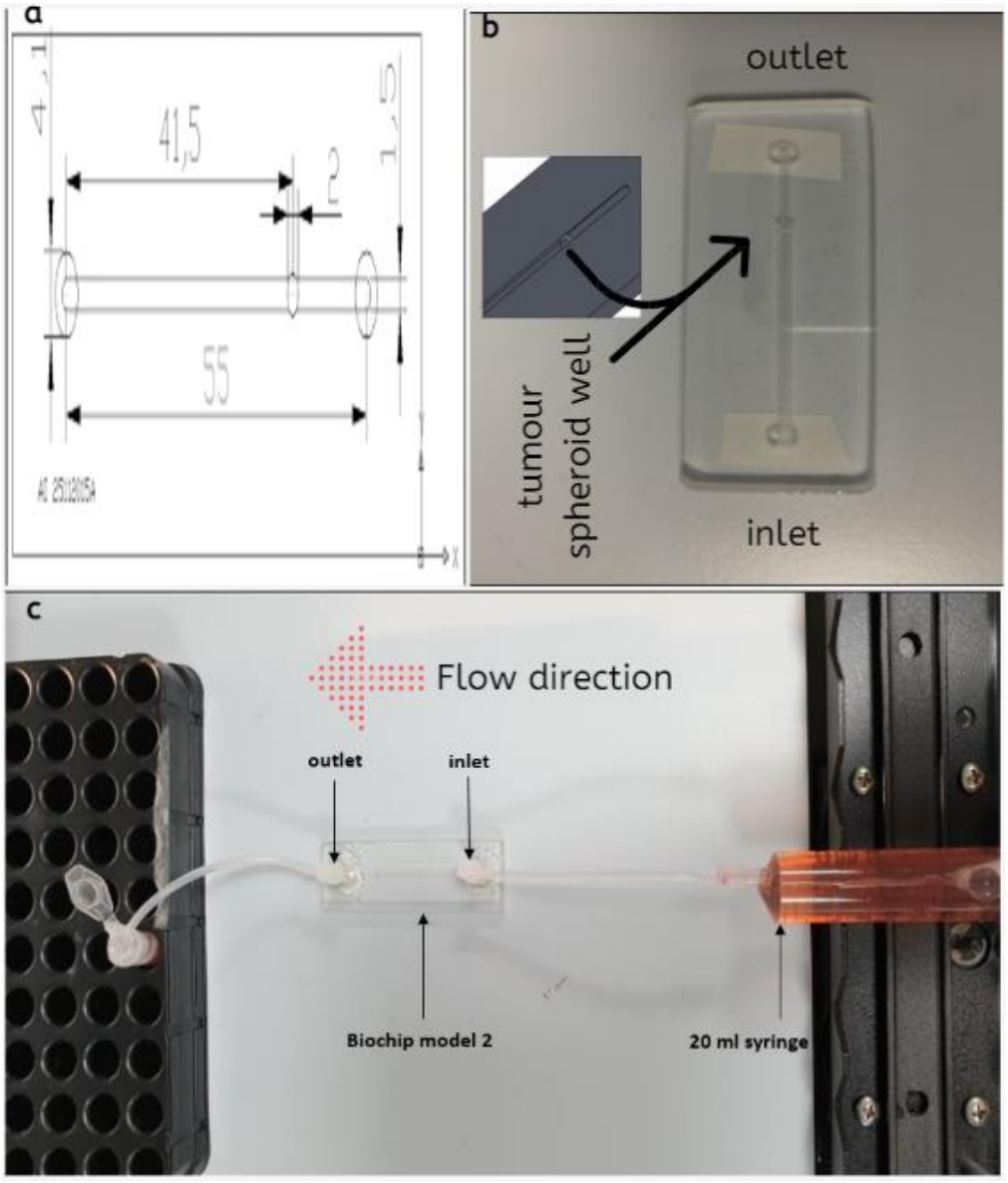

Figure 4.13: Image showing the biochip model 2 assembled.
Image (a) shows the biochip model 2 dimensions. Image (b) shows the biochip model 2 after fabrication process contains lateral well. Image (c) shows the biochip model 2 setup.

The data suggesting that silanisation treatment had no effect on biochip model 2 characteristics compared to one without treatment (Figure 4.14). Moreover, this data suggesting that MPs did not adhere to the inner surface of the microchannel as PCA values were not significantly different over the course of the experiment. Thus, biochips without silanisation reagent were used for the remainder of the study.

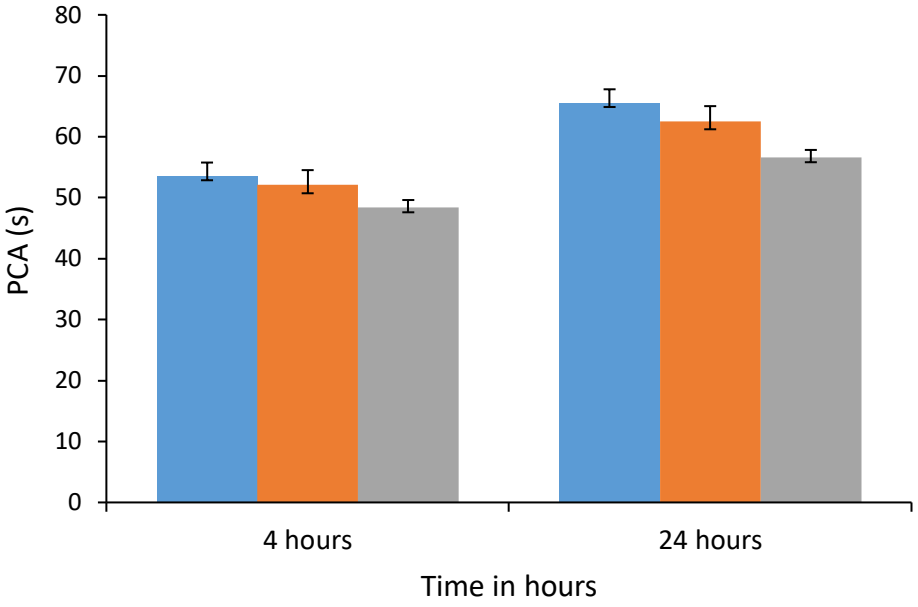

Figure 4.14: Chart showing the PCA of U87 tumour media in different conditions.
Error bars representing ±SD of two independent replicates. no salinization ( ), with salinization ( ), off-chip ( ).

The data is representative of two separate experiments. There was no significant difference in PCA. Therefore, the data suggesting that we can use the microfluidic chip without silanisation. Moreover, the data showed that there was no effect of flow condition on PCA as there was no significant difference of PCA between static controls and flow conditions suggesting some stability of the MP present within the media.

4.7.2 Cleaning and checking blockage of microfluid device (1 and 2 models)

The tubing and connectors were washed through with 70% (v/v) ethanol and sterile water and blockages were tested. To remove any blockage inside the microchannel, the device was dipped in concentrated hydrochloric acid (HCl; 11.6-12.0 M) overnight. If the device was still blocked, it was sent to the furnace in Chemistry department of chemistry and then consecutive use of ethanol and distilled water were used to clean the devices.

4.7.3 Tumour spheroid biochip model 2

To retain simplicity and reliability, this model was designed to hold several spheroids at once via an increase in the capacity of the microchannel. Briefly, collected spheroids were transferred using a small (200 µL) pipet tip from a 96-well plate into the chip channel inlet and 500 µl of the fresh media was added into the inlet reservoir that caused movement of spheroids to the centre holding well. A cell strainer (40 µm) was inserted into the outlet pore to avoid sample contamination with cells and cell aggregates lost from potential spheroid disaggregation. Then, Elbow Luer connector tubes were connected to the inlet and outlet

pores of the biochip through adapted pipettes tips glued onto the ends of the chip (Figure 4.15).

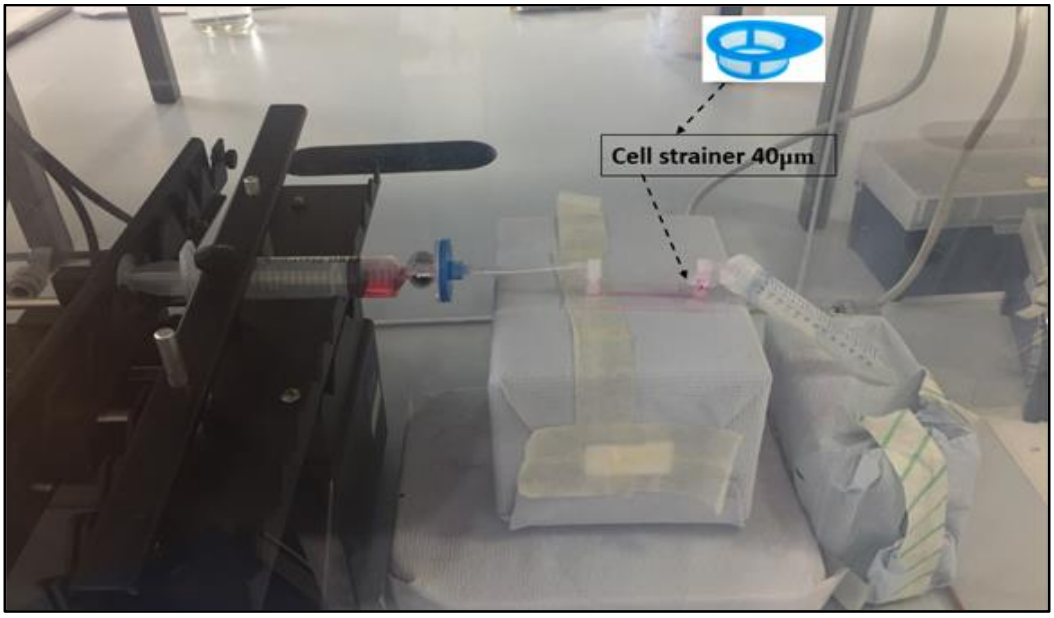

Figure 4.15: Image showing how the Biochip model 2 was assembled with a cell strainer fixed in outlet to hold spheroids.

Extensive work was done on this model as well to preserve spheroid integrity within the new device. A slight improvement over biochip model 1 design was observed in model 2 however, a large number of spheroids in this model during this study disaggregated or partially disaggregated. Leakage was almost eradicated in this device but the problem of disaggregation under flow of certain (SKOV-3 and AsPC-1) spheroids remained (Figure 4.16) again suggesting the compactness of the spheroids affects integrity under flow.

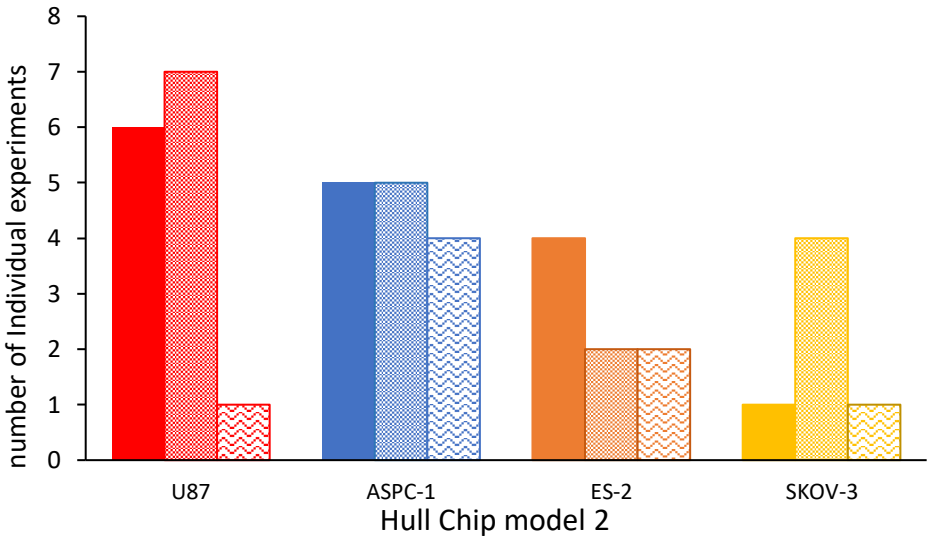

Figure 4.16: Chart shows the biochip model 2 assessment.

42 independent experiments were conducted, of which 16 were successfully maintains the spheroids in 6 hours' time intervals. 18 Chips were blocked and 8 leaked. SKOV3 spheroids size was very small so all spheroids moved from spheroid well to outlet hole and this caused chip blockage in most experiments. Successful (filled), blocked and disaggregate (hashed), pattern fill: leaked (waves).

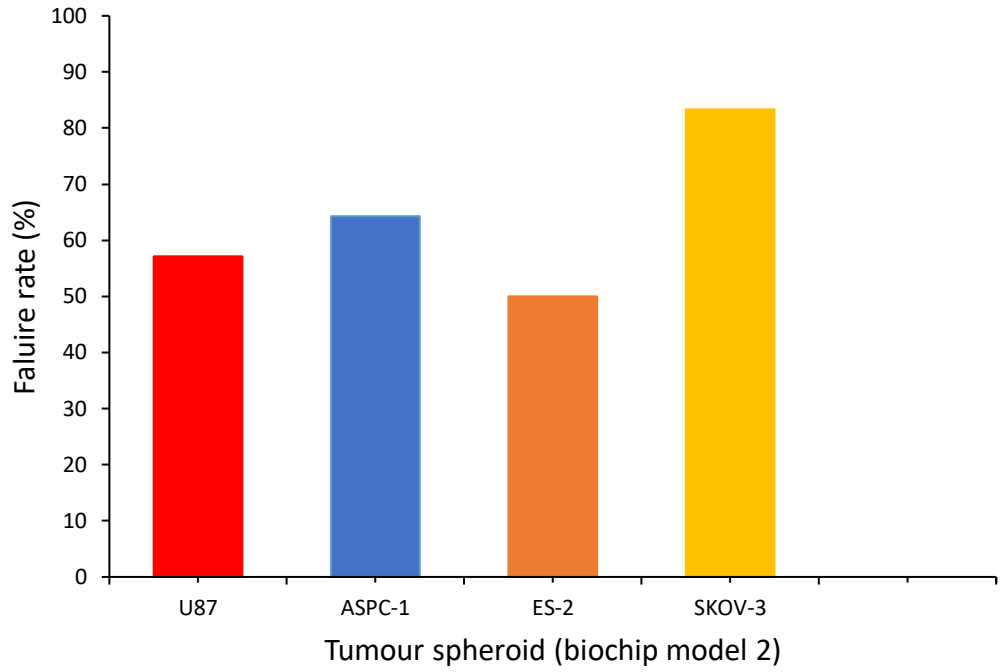

Figure 4.17: Chart showing the experimental failure rate of biochip model 2.

PCA data obtained from these experiments are shown in Figure 4.18. Over the course of 5h there was a general decline in PCA as shown by the longer times taken to form a clot. After the first hour U87 and ES-2 consistently displayed the higher PCA which was consistent with the parent cell PCA as discussed previously. However, all spheroids failed to maintain their structure beyond 5h. Moreover, only three tumours spheroids (ES-2, U87 and AsPC-1) yielded any data within the experimental window due to disaggregation. Furthermore, the gluing step that has been used in the first model had to be used again in this model to connect the inlet and the outlet tubes. Ultimately 116 individual experiments were conducted to design, develop and optimise both models in order to successfully maintain spheroids in under flow conditions. The aim was to characterise MPs released from spheroids under flow condition and eventually to evaluate the interaction between HUVECs and MPs in flow status.

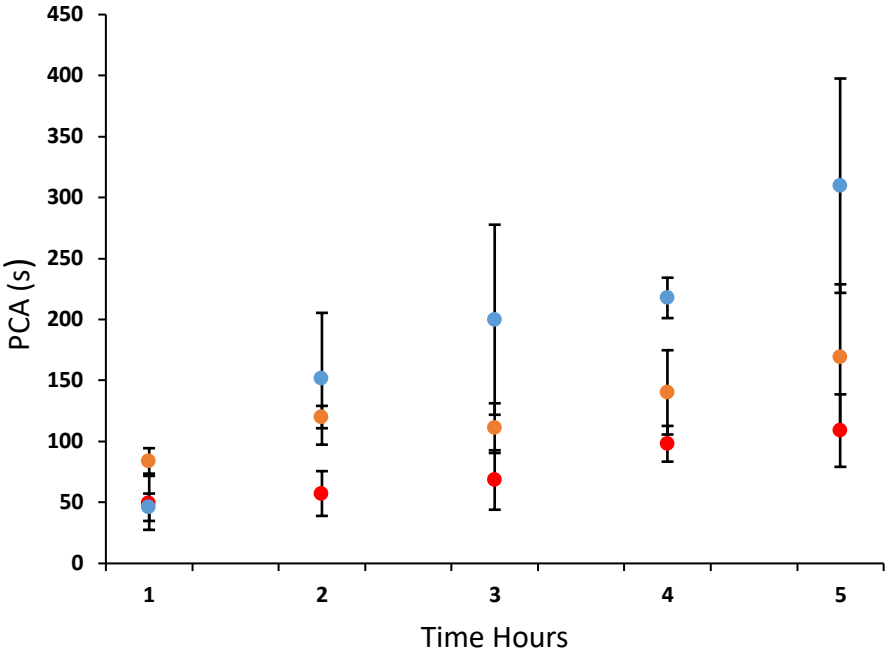

Figure 4.18: Chart showing PCA data for five hours.
Four tumour spheroids of (ES-2, U87 and AsPC-1) were used. U87 and ES-2 showed the fastest CT and formed compact spheroids. AsPC-1 showed moderate CT and weak compact spheroid. Error bars representative of ±SD of four independent experiments. AsPC-1(●), ES-2(●), U87(●).

The PCA for ES-2 and AsPC-1 on biochip model 2 in hour 3 and 4 respectively were higher than hour 2 and 3 respectively. All three-cell line derived tumour spheroids showed a decrease in PCA (slower coagulation time) over the course of the 5h experimental period. (Fig 4.18). At the first time point of 1h incubation with flow all three also showed the highest PCA which may be due to the transfer of spheroids from static culture or the application of shear stress (flow) or a combination of the two leading to increased MP shedding at the beginning of the flow period. After this time there was a general loss of PCA associated with the media which may be due to the spheroids being relatively stable within the flow and a gradual reduction in MP release. With micro size and colourless characteristics of the tumour spheroids, obtaining clear images was difficult and would require more advanced imagery to enable dimensional analysis.

In conclusion, according to the work presented above in order to determine the best model to hold and maintain spheroids, both model 1 and 2 fail to achieve the primary aim of this study during the first year. Both models possessed poor reproducibility and while some data was gathered on MP release under flow the lack of robustness led the decision to use commercially available microfluidic chips for further work. While a number of previous successful attempts have been made to develop an *ex-vitro* model so the PCA of tumour microparticles shed by cancer cells can be investigated in detail, these are limited in the number and considered insufficient.

4.8 Commercial microfluidic biochip

In accordance with the approaches used for the investigating the role of tumour MPs in hypercoagulibity status in cancer cell lines, different microfluidic devices were assessed in order to optimise a consistent, reproducible protocol for immobilisation of tumour spheroids within a microfluidic device. It was found that microfluidic chip model 1 and 2 were not appropriate for this study as discussed in sections 4.6 to 4.7. Accordingly, the commercially available Vena 8 endothelial biochip was obtained to achieve the initial aim of the study though due to lack of connect ability it was not possible to connect this biochip to another biochip that contains a tumour spheroid. Therefore, it was necessary to look for another approach so the main aim can be achieved.

Subsequently, two commercial biochips model was connected to mimic the biological process in a tumour. Briefly, a dual flow microfluidics biochip was obtained, and effluents was collected over time points. The first biochip is µ-Slide III 3D contains 6 wells where tumour spheroids can be cultivated and, subsequently, examined with different methods. A channel respectively connects two of the six wells. The female Luers allow easy connections to tubing and Harvard pump systems for perfusing the wells in order to perform long-term cell culture assays with tumour spheroid. This biochip is connected to the µ-Slide I Luer biochip which is designed for cell culture under perfusion. µ-Slide I Luer biochip was coated with HUVECs. Subsequently, the association of tumour MPs with HUVECs will be study.

4.8.1 µ–Slides I luer

The µ–Slide I Luer is designed for cell culture under perfusion and all flow applications. The female Luers allow easy connections to tubing and pump systems. Ibidi µ–Slides, is made of a plastic that has the highest optical quality similar to that of glass. The µ–Slides is not autoclavable, as it is only temperature–stable up to 80°C/175°F. The gas exchange between the medium and incubator's atmosphere occurs partially through the polymer coverslip. HUVECs were cultured on a µ-Slide I Luer for 24h prior to connection to the µ-Slide III 3D (Figure 4.19).

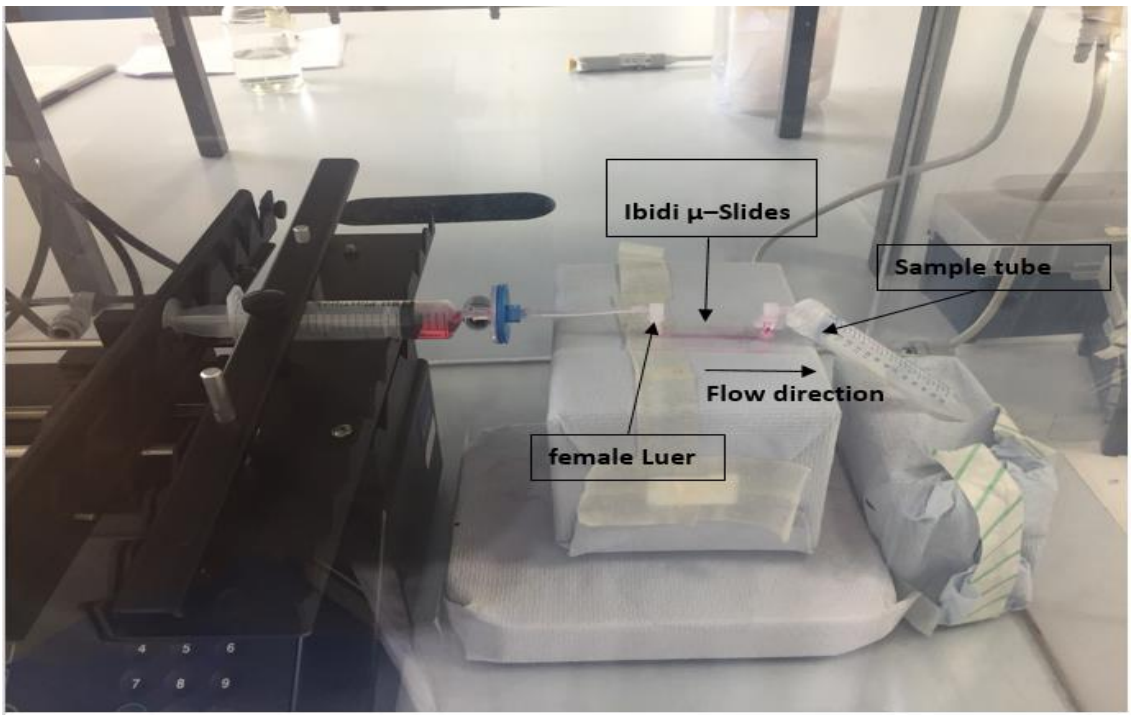

Figure 4.19: µ–Slide I Luer setup.
Image showing µ–Slide I Luer coated with HUVECs and connected to Harvard pump.

4.8.2 µ-Slide III 3D

Subsequently, the main focus in this section was to develop a dual biochip model. The first one was intended to hold a tumour spheroid that linked to a second biochip that is coated with endothelial cells so the interaction between tumour MPs and the endothelial can be examine (Figure 4.20).

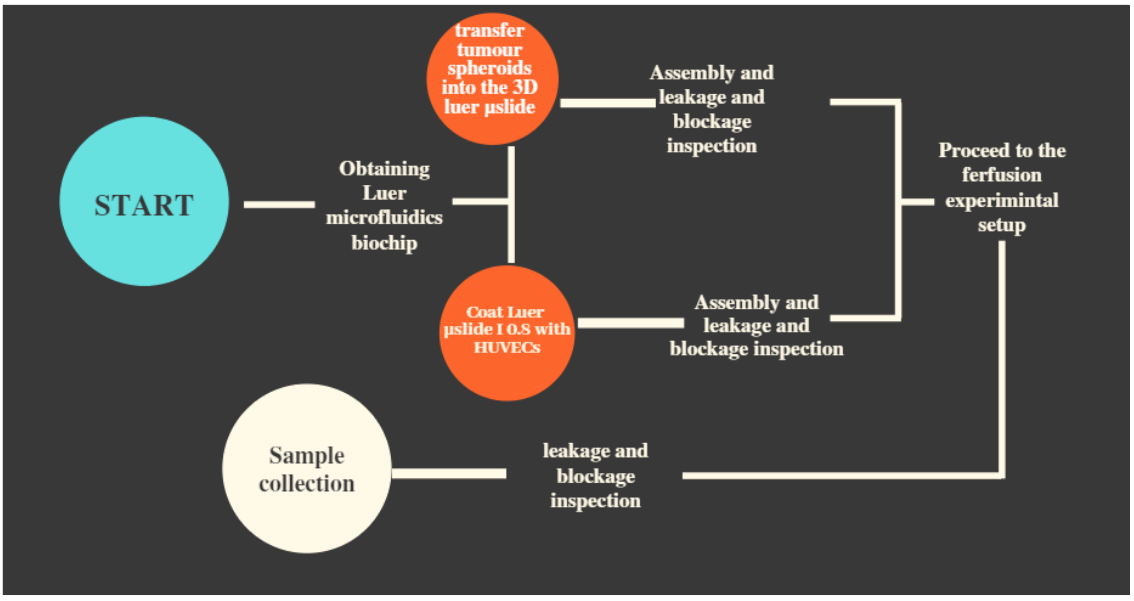

Figure 4.20: A flowchart illustrating the alternative tumour spheroids on commercial biochip design approach.

The commercial chip was purchased from ibidi Company which provide all-in-one chamber system for long-term analysis of MPs interaction with HUVEC. The flowchart illustrating two types of biochip that connected to each other.

Accordingly, second biochip model was purchased from (Ibidi, Germany). µ-Slide III 3D Perfusion and µ-Slide I Luer. Both chips are connected as described in section (2.11.1). µ-Slide III 3D Perfusion is an array of 6 wells where cells can be cultivated and, subsequently, investigated microscopically. The channels can be connected to a pump for perfusing the wells in order to perform long term cell culture assays with tumour spheroids. The µ-Slide I Luer is designed for cell culture under flow condition (Figure 4.21). The biochip µ-Slide III 3D Perfusion was used to hold spheroids and connected to µ-Slide I Luer that coated with 2% gelatine prior to culturing HUVECs. Activation of endothelial cells with TNF-α has shown an increase in expression of different surface adhesion substances like ICAM-1 and VCAM-1) in four hours (Benam et al, 2016). Consequently, to explore the effect of the tumour MPs from different spheroids on HUVECs in different time points and whether this effect could potentially damage HUVECs and results in hypercoagulibity. Interestingly, HUVECs showed two different patterns of reaction. MPs that perfused over HUVECs for 10 20 30 s has not showed any effect and HUVECs did not retain PCA. In contradict reaction, HUVECs retain prothrombotic characterization from tumour MPs after incubation for 6 hours or 24 hours. The 3D ibidi µSlide was used to hold some spheroids and directly connected into the ibidi µSlide 0.8 that pre-coated with HUVECs.

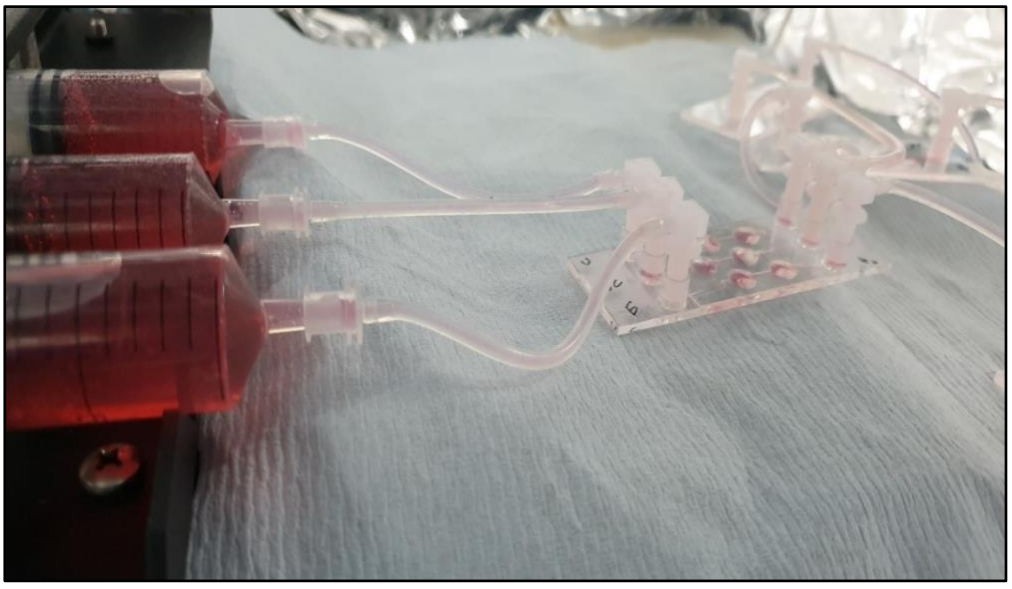

Figure 4.21: Image shows the biochip ibidi one single channel and 3D biochip which has spheroids. Both biochips connected to 20 ml a plastic syringe.

Accordingly, to evaluate the model's reproducibility, 28 independent experiments was conducted, and number of leakages, blockage or spheroids disaggregation was counted as in (Figure 4.22).

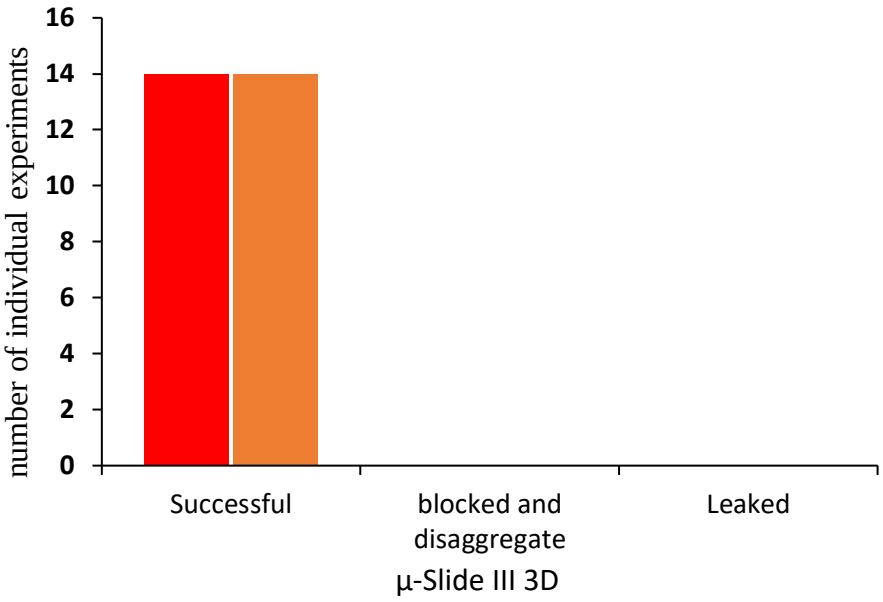

Figure 4.22: Chart showing the number of successful rates of IBIDI biochip models. U87 (■, *n* =14), ES2 (■, *n*=14).

Briefly, 40 tumour compact spheroids of ES-2 and U87 were transferred into µ-Slide III 3D (each 2 connected wells contain 20 tumour spheroids) and connected into Ibidi µ–Slides coated with HUVECs (Figure 4.23). Perfusion of media through captured on-chip spheroids was monitored over time ensuring the biochips did not leak or become blocked. Respective (2D) media was perfused through the biochips and the media effluents were sampled each hour time and stored for further analysis.

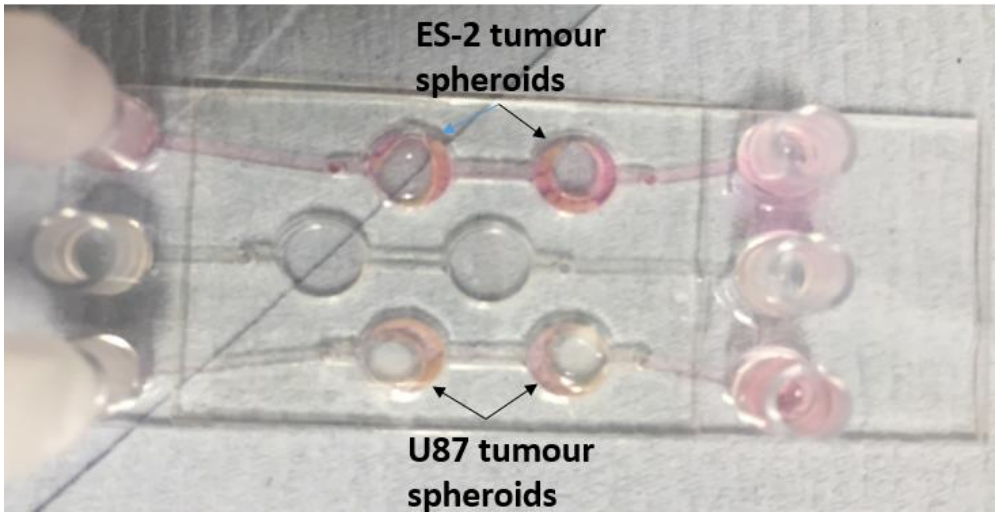

Figure 4.23: Image showing the µ-Slide III 3D. 20 tumour spheroids inside each well of ES-2 and U87.

The growth area per well is 25 mm² which was enough to introduce more than 20 tumour spheroids in each well. Moreover, each micro slide has 6 wells, and this was effective as compared to previous biochip as was not possible to load this number of the tumour spheroids. Furthermore, there was no any optimisation steps on this biochip, and this accelerated the data collection and produced accurate and consistent results as outlined in next section.

4.8.3 PCA determination using microfluidic chips

In this section initial work has conducted on U87 and ES- tumour spheroids to determine how PCA value of tumour MPs that shed from spheroid is consistent. Therefore, a number of experiments were performed to evaluate µ-Slide III 3D. Briefly, 40 tumour spheroids of either U87 or ES-2 were transferred into the µ-Slide III 3D and connected to 20 ml plastic syringe that contains blank EMEM and McCoy's 5A medium respectively as described in section 2.2.25. Using the microfluidic system, the media was perfused over the tumour spheroids for 6 hours at 4 µl/ min and effluent was sampling each hour and PCA was assessed. The µ-Slide III 3D has 6 wells per slide and each well has 20 tumour spheroids. We observed a slight reduction in PCA, but it was insignificant (Figure 4.24).

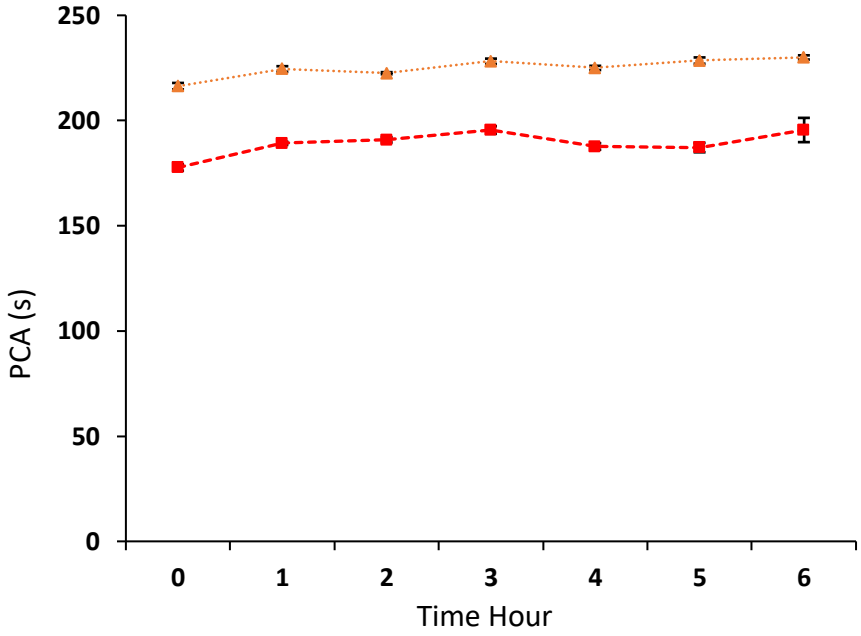

Figure 4.24: Graph showing the PCA over 6 hours using µ-Slide III 3D.
Data represents three independent experiments. Error bars are SD. U87(■, *n*=4), ES2(■, *n*=3).

The PCA is useful parameter to monitor MPs that shed by tumour spheroids. The relatively constant PCA of the trapped tumour spheroids showed that the tumour spheroids were relatively stable under flow condition in comparison to the data generated with biochip model

2, thus a relatively constant rate of MP release was observed via PCA data (Fig. 4.24). Therefore, it can be concluded from these results that µ-Slide III 3D biochip was the better model to hold tumour spheroids as there was not any leakage or blockage and all spheroids were intact and did not disaggregate under flow. Table 4.4 illustrated the main advantages and disadvantages of all microfluidics chips that have used thus far in this study. Subsequently, a general schematic that shows the steps from selecting a microfluidic chip, through to cell culture and selected spheroids to finally investigate how tumour MPs are able to interact with endothelial cells *in vitro using* imaging tools and flow cytometry, is illustrated in figure 4.25.

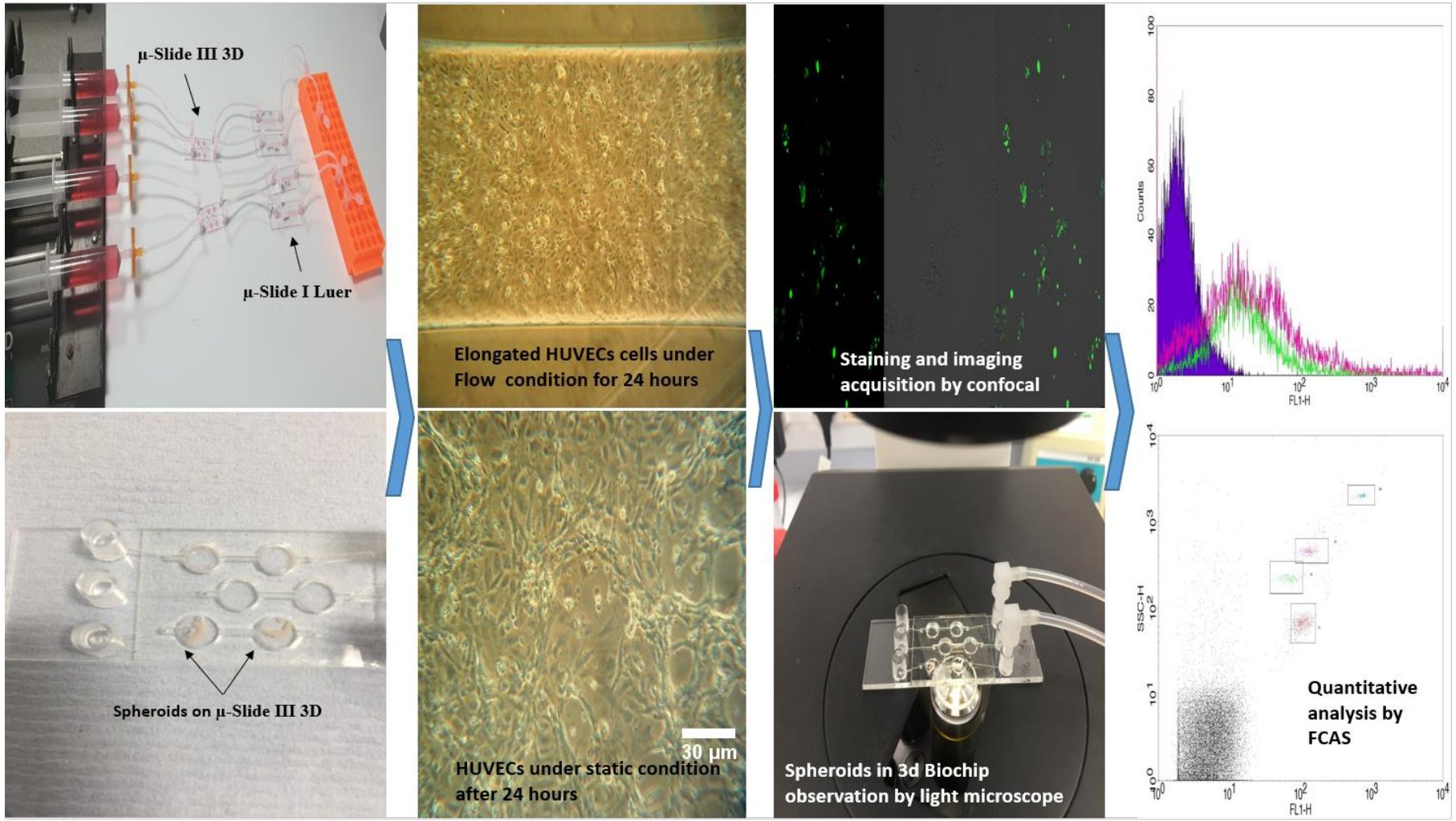

Figure 4.25: Flow chart showing the general platform of new ibidi microfluidic system and analytical tools. 40x magnification.

Table 4-4:Features and specifications of all microfluidics chips that have been used in this study.

Biochip type model	Specification and advantages	disadvantages	cost
Hull model 1	suitable for autoclave and reusable relative cheap single channel 3 inlet and 3 outlet points optically transparent non-toxic	Blockage Leakage Labour work Unproducible or inconsistent Not suitable for imagining	One chip cost: 4 pounds
Hull model 2	autoclave relative cheap reusable single channel with one inlet and one outlet optically transparent non-toxic	Blockage Leakage Labour work Unproducible or inconsistent Not suitable for imagining	One chip cost: 4 pounds
Vena8 Endothelial+TM Biochip	8 channels. So many samples can run in same time. HUVECs can be culture and media can be injects using special pump. It supports a range of shear stress/shear flow rates. Ideal for cell-cell interaction and adhesion assays on cell monolayers and cell culture under shear flow. Perfect model for use with PCR. Compatible with bright field, phase contrast imaging and fluorescence microscopy. Advanced design and high standard	disposable	One chip cost: 87.5 pounds
ibidi µ-Slide I Luer	Standard format with thin bottom for low or high magnification microscopy (up to 100x) Large observation area for microscopy Channel volumes of 50 µl, 100 µl, 150 µl, or 200 µl Defined shear stress and shear rate levels Easy connection to tubes and pumps using Luer adapters Available as Varity pack containing all heights	disposable	pk15 125.00 pounds. Single Chip cost: 8.3 pounds.

Biochip type model	Specification and advantages	disadvantages	cost
	Fully compatible with the Harvard pump Compatible with bright field, phase contrast imaging and fluorescence microscopy Advanced design and high standard		
Ibidi µ-Slide III 3D Perfusionµ	Observation of single cells in 3D matrices or tissue samples (e.g., spheroids, small organoids, or organisms) Perfusion of samples Long-term cultivation of cells in 3D matrices Compatible with bright field, phase contrast imaging and fluorescence microscopy. Advanced design and high standard	disposable	pk15 189.00 pounds. One Chip cost: 12.6 pounds

4.9 Vena8 Endothelial+™ biochip

4.9.1 Vena8 Endothelial+™ biochip setup

The aim of this section was to assess the adhesion of tumour MPs into the endothelium cells under shear stress, thus a Vena8 Endothelial™ biochip (Cellix Ltd, Dublin, Ireland) was used. The Vena8 Endothelial+™ biochip was purchased in order to link the spent MP-rich media released from spheroid chips directly to cultures endothelial cells. Vena8 Endothelial+™ biochip is designed for cell culture under shear flow conditions. This biochip has 8 identical channels (channel volume: 2.69 µl, channel width: 0.08 cm, height: 0.012 cm and length: 2.8 cm). In this model HUVECs were cultured as a monolayer cell under flow conditions as described in section 2.10. Briefly, the biochips were coated with a 12 µl of type B 1% v/v gelatine solution (Sigma Aldrich), incubated for 24 hours at 4°C. Then, 5 µl of 1.5×10^6 per 100µl of harvested HUVECs were seeded in each channel and left to adhere for 2 h with media (40µL) placed in the reservoirs of media. The biochip was incubated in the CO_2 incubator for 24 hrs at 37^{o}C. The biochips were then connected to a Harvard pump, set up on perfusion mode with a 4 µl/min within in a flow chamber incubator at 37 ◦C for 24 hours (Figure 4.26).

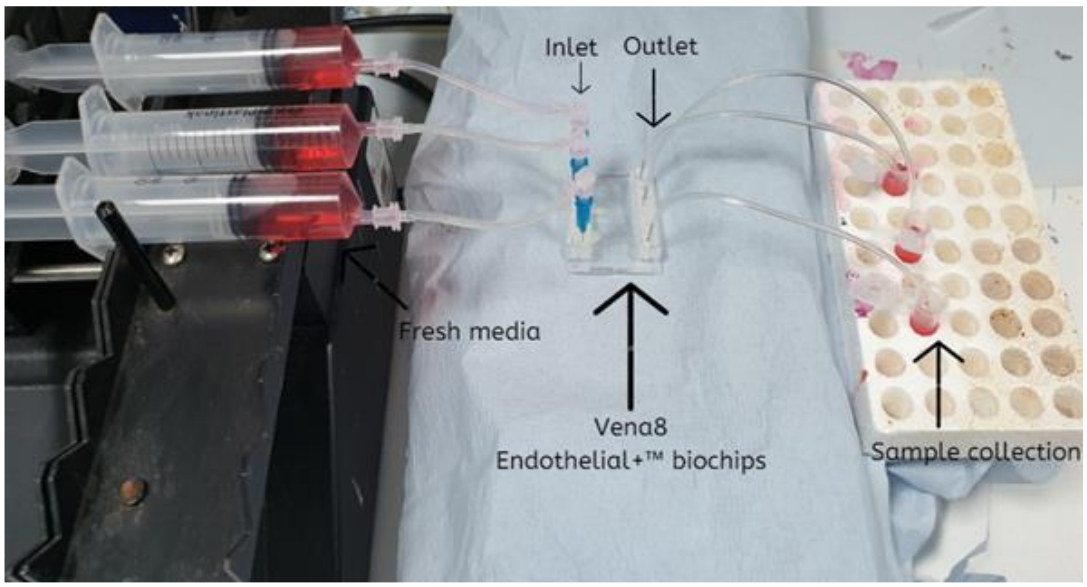

Figure 4.26: Image showing the Vena8 biochip setup.
Collected tumour (2D) spent media from ES-2 and U87 cancer cell line was perfused over Vena8 Biochip coated with HUVECs. PCA, MPs quantification and confocal imaging were used to assess the effect of MPs on HUVECs under constant flow condition. This platform was kept in 37°C in flow chamber.

Subsequently, to confirm if a synergistic effect existed between tumour MPs and HUVECs, different analytical methods were used as following:

4.9.2 PCA of tumour MPs using Vena8 Endothelial+™ biochip

HUVECs were cultured on a Vena8 chip for 24h prior to introduction of tumour media. No PCA was observed from endothelial media passed through the Vena8 biochip coated with HUVECs in 10, 20 and 30 seconds sequentially. A control series of Vena8 biochip channels coated with HUVECs (n=3) were subjected to control tumour media in the same way as the experimental (MPs containing) media. Briefly, the Vena8 biochips were coated with a 12 µL of type B 1% v/v gelatine solution (Sigma Aldrich), incubated for 24 hours at 4°C. Then, harvested HUVECs (75×10^3 cells) were seeded in each channel. Cell free media of AsPC-1, SKOV-3 and U87 was flushed into (n=6), the biochip channels in 10, 20 and 30 seconds sequentially (Figure 4.27). No significant change was observed in PCA across all cell-free media tested which suggesting that HUVECs were not affected by tumour MPs in this time interval however the interaction between tumour MPs and cultured endothelial cells on a Vena8 biochip appeared to happen for 24 hours as will be discussed in subsequent sections.

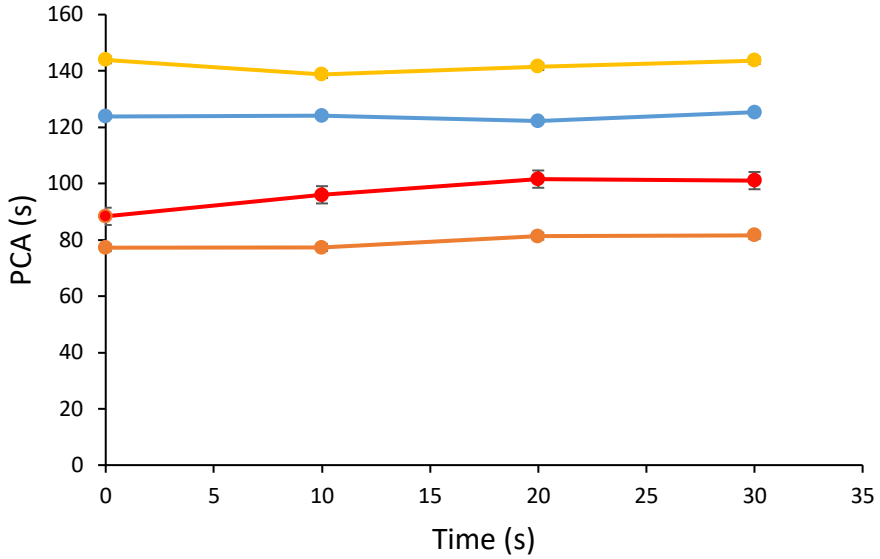

Figure 4.27: Chart showing the clotting time against tumour MPs quantification as pre and post exposure with HUVECs.
PCA was measured using a one-stage clotting assay. Data are the average of four independent measurements performed in duplicate using log10 scale. The observed data of PCA and MPs quantification suggesting that there was not a significant interaction using 10s cycles method (R^2: 0.4731). U87 (●), ES2 (●). AsPC-1 (●) and SKOV-3 (●).

4.9.3 MPs quantification using Flow cytometry

CFSE labelled PCA of tumour MPs pre and post perfusion on HUVECs after the 30 second perfusion was also assessed. Previously it was shown interactions between tumour MPs and endothelial cells in vitro under static culture conditions. To further assess this interaction MPs released from tumour cells under flow condition. U87 and ES-2 cell lines were labelled with CFSE as described in section 2.9.1. Cell free media from each tumour cell line was then removed and perfused over HUVEC adhered to a microfluidic Vena8 biochip 8-channel microfluidic device. CFSE labelling allowed for quantification of released MPs by flow cytometry before and after pass through the endothelial chip. Then, PCA and MPs quantification was determined before and after being perfused over HUVECs (Figure 4.28).

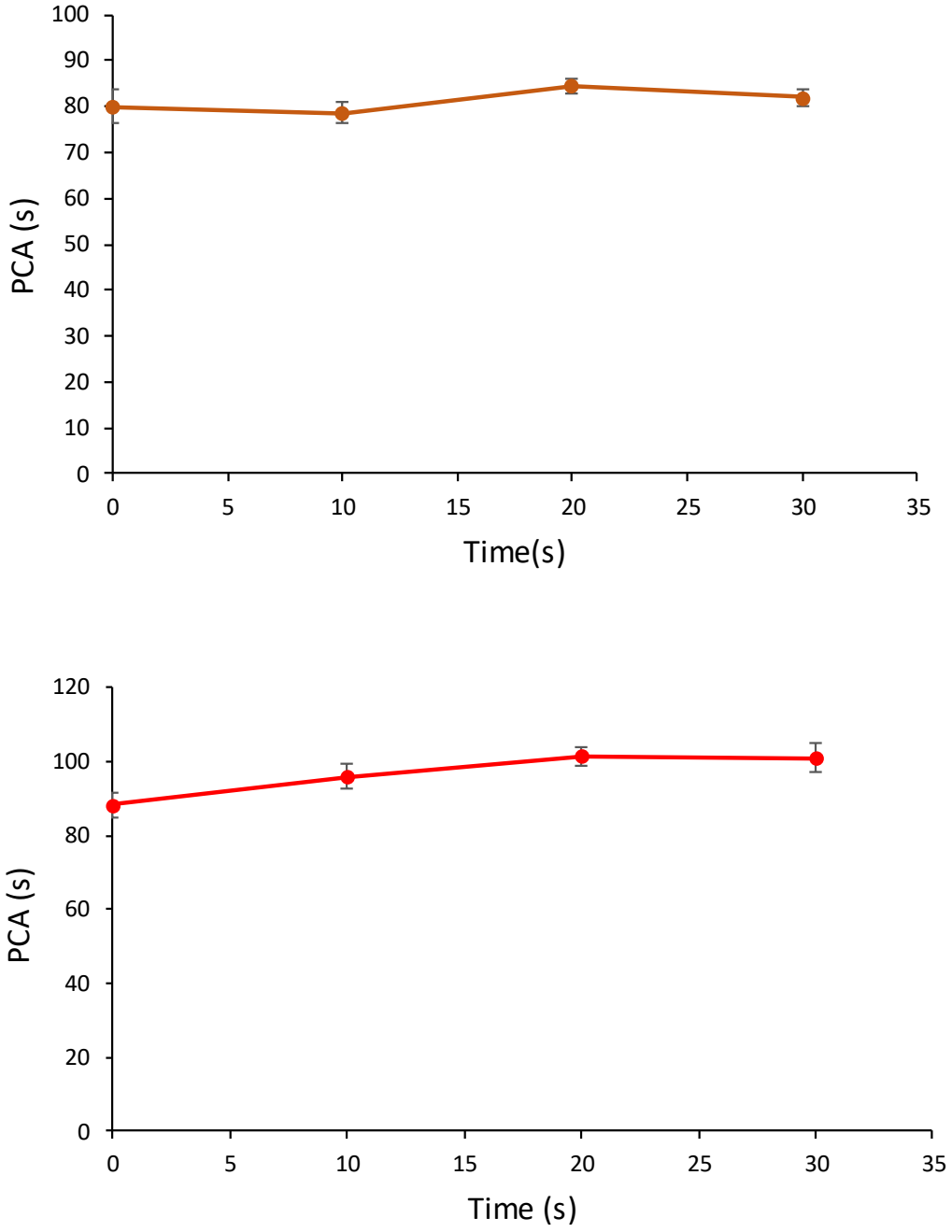

Figure 4.28: Relationship between time and PCA of ES-2 and U87 before and after perfusion cycles with HUVECs.
Error bars represent SD from 3 indepentents experiments. ES-2 (orange circle) and U87(red circle).

Data obtained showed that there was not a significant correlation between PCA and MPs quantification using 10 seconds cycles. Therefore, the data suggesting there was not interaction or adhesion as there was not lose in MPs number or change in PCA values (Figure 4.29). The flow cytometry data indicated no loss of CFSE-MPs using these 10s cycles which may indicate that the constant of PCA is MPs associated.

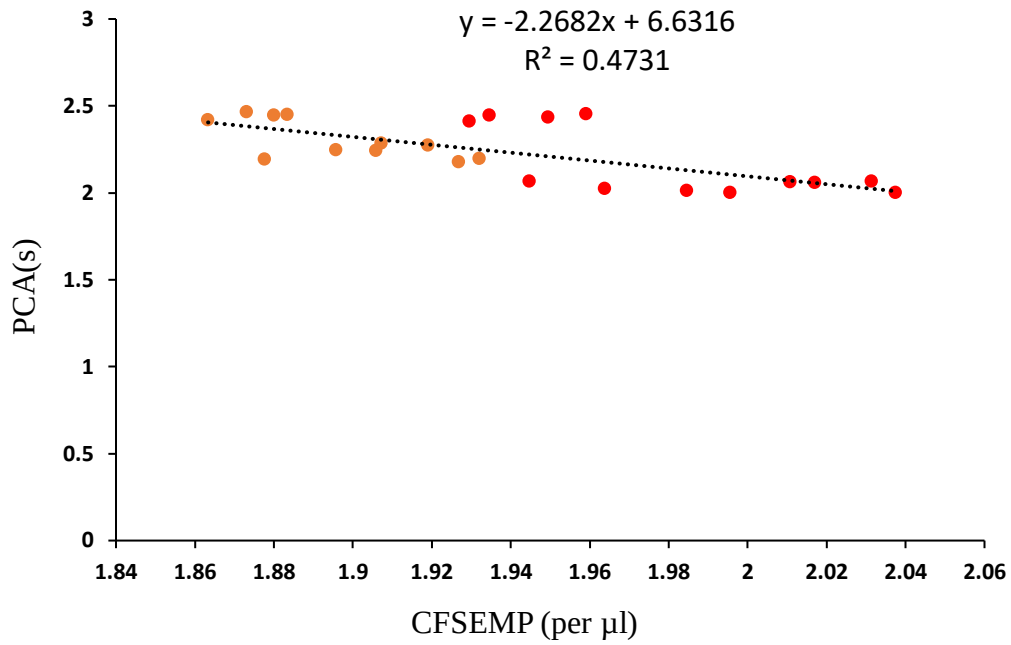

Figure 4.29: Relationship between CFSEMP and PCA.
Chart shows the correlation between CFSEMP and PCA of U87 (Red circle, n=4) and ES-2 (Orange circle, n=3) media when perfused over HUVECs for 10s cycles.

4.9.4 Microscopy

The deposition of MP on endothelial cells was studied using an automated microfluidic platform (Vena8 Endothelial+ biochips; Cellix, Dublin, Ireland) to mimic physiological flow status. The biochip was coated with HUVECs as described previously in section 2.11. The biochip connected to the Kima pump (pulsatile flow) with shear stress at 450µl/min for 6 min, followed by 5 min of absence of flow. The flow chamber was then rinsed three times with 25µl of media prior to each experiment, and MP adhesion was initiated by the addition of CFSE-labelled MPs supernatant of (ES-2 and U87) and unlabelled MP as well (Figure 4.30).

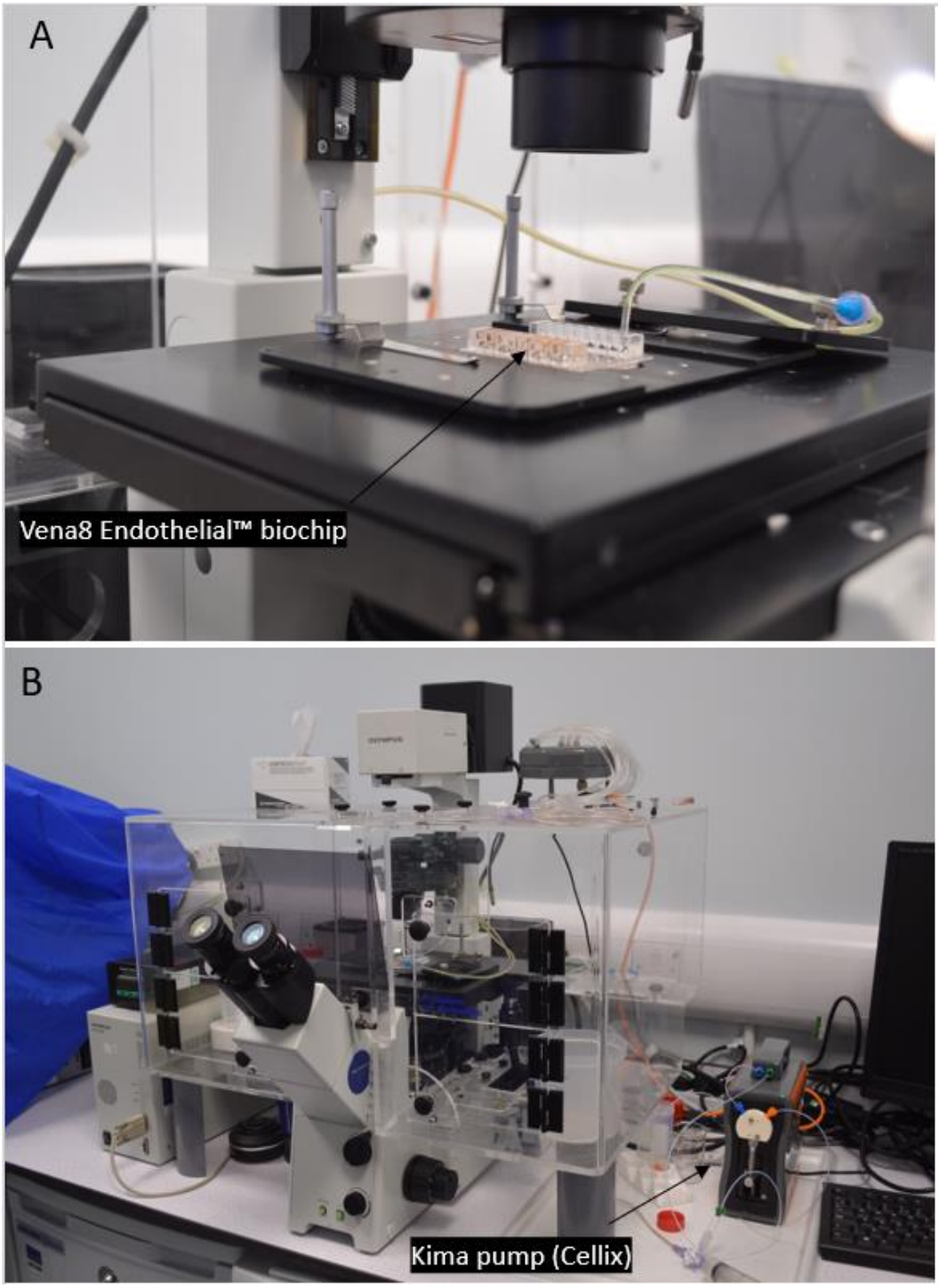

Figure 4.30: Image A showing preparation of the Vena8 Microfluidic Chip for Live Imaging. Image B showing flow Adhesion Assay and Image Acquisition.

Interaction of MP was recorded every second under a shear stress of 1 dyne/cm^2 in phase contrast and the settings were equal in all conditions (exposure time 344 ms, magnification 32×) for 5 minutes (Figure 4.31).

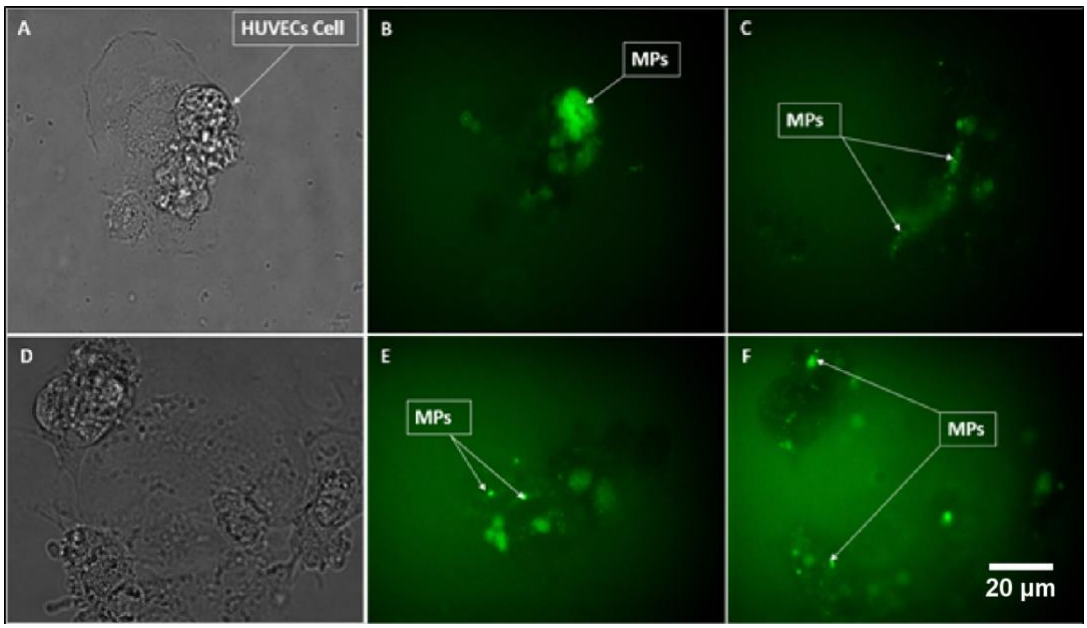

Figure 4.31: Images showing the MP deposition on HUVECs under flow condition.
The top panel (A-C), shows labelled ES-2 MP deposition. Image (A) shows HUVECs cell with unlabelled ES2-MP. Image B and C show two different MP deposition with HUVECs. The bottom panel (D-F), Image D shows U87 unlabelled-MP with HUVECs. Image E and F represents the labelled U87 MP deposition on HUVECs.

The Cellix system was used for live image capture under physiological flow conditions and hence to examine the adhesion of MP with HUVECs. CFSEMP were constantly passed over a Vena8 microfluidic chip precoated with HUVECs and images captured under pulsatile flow. Tumour MP were observed to associate with HUVECs in 6 mins time window. Interestingly, this data suggesting that the associated of tumour MP with HUVECs need more than 30 seconds.

Though, due to inability to provide The Vena8 pump which will be use in pulsatile flow. In addition, this model was found to be unsuitable to connect to a second chip which contains spheroid. In addition, this type of chip was found to be high in cost as described in (table 1). Consequently, another commercial biochip was used with considering that it should be compatible with Harvard pump and able to connect to spheroid biochip model. Moreover, it was essential to have a microfluidic chip that is cost effective and reliable.

4.10 Discussion

The pathophysiology of VTE in cancer is multifactorial and rather unclear. Recently, increasing evidence link MP to cancer associated thrombosis. Specifically, TF -bearing (TF-MPs) can be found in plasma of cancer patients and are considered as possible risk factor for the development of thrombosis (Manly et al, 2010). MP are circulating, phospholipid-rich particles of <1 µm diameter released from the membranes of platelets, endothelial cells, erythrocytes and leucocytes (Bucciarelli et al, 2012; Thaler et al, 2012b). MP exist in the body independently

of malignancies, but malignancies are capable of producing them as well. Tumours are known to release subcellular particles MP and exosomes) into the bloodstream (Freyssinet, 2003; Minciacchi et al, 2015). These particles have been putatively linked to the propensity of patients with cancer to develop venous thromboembolism (Davila et al, 2008; Donnellan et al, 2014), but further investigation of this potential mechanism is required. MP are shed from cells via a number of pathways such as apoptosis and membrane remodelling (Aupeix et al, 1997; Burnouf et al, 2015). The actual mechanisms of the PCA of TFMP rely mainly on the expression of anionic phospholipid, especially PS, and the basic clotting function of TF (Lacroix & Dignat-George, 2012b). Therefore, the aim of this chapter was to develop an *ex-vitro* model system in which a tumour spheroid will be maintained in a microfluidic device and the PCA of MP released from tumour, with and without the application of appropriate chemotherapy agents, will be assessed. In this research, it was demonstrated for the first time that MP developed in vitro from tumour spheroids interacts with endothelial cells in dual microfluid chip assembly, in flow conditions.

Accordingly, the purpose of this chapter was to develop a microfluidic *ex-vitro* model to assess PCA and numeration of MP that shed either from 2D or 3D cell culture methods. In addition, how tumour MP are able to interact with endothelial cells *in vitro* and, potentially, confer PCA. Moreover, another main aim was to develop a microfluidic chip that can hold a tumour spheroid and monitored MP shed from the tumour spheroid. In addition, another key aim was to develop a microfluidic chip that is compatible with imaging tools and high standard. Therefore, in this chapter four biochip were used as an *ex-vitro* models to assess cancer MP that shed by different tumour spheroids. It was shown that two biochips that were fabricated locally in house of Chemistry at Hull University were not a suitable device for this study as spheroid disaggregation and hence blockage of chip was a regular and dominant disadvantage. Despite its low cost and reusable, these two biochip devices suffered from several major drawbacks such as disaggregation of tumour spheroids, labour work, time consuming and other vital problem like blockage and frequent leakage. Moreover, despite the huge work that already conducted to optimise these biochips, the process of working with these biochips were not easy and had many difficulties. However, there were some successful attempts, semi-disaggregation of tumour spheroids adversely affects the results as this result was inconsistent as found in (Fig.4.18). The inconsistency in PCA data suggesting that the tumour spheroids in both 1 and 2 chip models were easily disaggregated. Therefore, to avoid these drawbacks a commercial biochip was used, and it was found that ibidi biochips had a significant advantages and data that was collected had a statistical significance. It was shown that the connect two biochip models could be used and hence tumour MP that shed by different tumour spheroids

and cancer cell lines were monitored and interaction with HUVECs under flow condition was assessed. Moreover, it was found that not all cancer cell lines can form a stable and compact tumour spheroid therefore were not suitable to use them under flow condition. For instance, Tumour spheroids of A2780, PANC-1 and MIAPaCa2 were easily disaggregated under sheer stress. Moreover, SKOV3 cancer cell line formed compact spheroid though its size was very small to use it in this study as it was easy to flow via the microfluidic chips and hence flushed out into the effluent. On other hand, tumour spheroids of ES-2 and U87 cancer cell lines were formed stable and compact spheroid thus were selected as *ex-vitro* model in this study. The µ-Slide I Luer and µ-Slide III 3D microfluidic chips showed a consistent results and significant advantages (Figures 4.22 and 4.24). For instance, these biochips do not need gluing material and it was easy to assemble and setup. Statistically, there wasn't any leakage or blockage in the µ-Slide I Luer and µ-Slide III 3D biochips and this indicated the consistency and reproducibility. Furthermore, they are compatible with bright field, phase contrast imaging and fluorescence microscopy. Also, µ-Slide I Luer and µ-Slide III 3D biochips have advanced design and high standard. With the ability of the immobilised a tumour spheroid to produce continuous procoagulant MP established, the next aspect was to determine the interaction of the tumour MP over time with endothelial cells under flow condition.

Chapter 5 Capacity of tumour MP of different cancer cell lines to interact with HUVEC cells

5.1 Introduction

MP are small membrane fragments, often in vesicular form, that bud off from the plasma membrane and are released into extracellular space. While their significance has not been completely clear upon their initial discovery, MP have emerged as instruments that cells use to communicate with one another on the tissue level during development and disease (Beer & Wehman, 2017). Metastasis is a cross-step process that leads to primary tumour cells being disseminated to remote organs. Almost all stages of tumour invasion and metastasis have been affected by tumour derived EVs. Studies have shown that tumour related EVs play a significant role by invadopodia development in invasion and metastasis. Invadopodia are dynamic, high-actin membranes, which degrade and invade tumour cell cells through extracellular matrix. Recently invadopodia was proposed to be docking sites for EVs to help degrade the extracellular matrix by locating the metalloproteinase MT-1-MMP secretion and thus to promote cell invasion. Tumour-associated EVs proteomic analyses have found that EVs releases certain proteins such as SERPINA1, SERFINF2 and MMP9 that play a major role in ECM restructuring, vascular leakage and invasion (Maacha et al, 2019).

It has been reported that direct co-culture of MP shed by cells of the Squamous Cell Carcinoma-81B (UM-SCC-81B) line and HUVECs at a ratio of 25, 50, and 100% v/v in endothelial cell growth medium (ECGM) under static-based adhesion assay induced increased PCA of HUVECs via cell membrane surface expression of TF (Adesanya et al, 2017). In the present study, two distinct models of Microchannel Slide Flow-Based Adhesion assay (MSFBAA) (vena-8 and ibidi model) were used to investigate how tumour MP are able to interact with endothelial cells *in vitro* and confer PCA. Utilising developed microchannel slide flow-based adhesion assay, Tumour MP shed by ES2, U87 (2D and 3D cell culture) and SKOV-3 and AsPC-1 (2D) were perfused over HUVECs under flow condition in the absence of any *ex vivo* manipulation. It was observed that MP adhered to the HUVECs and the media showed a reduction in PCA concurrent with a loss of MP from the media post-perfusion. In addition, HUVECs exhibited increased PCA after perfusion with tumour MP. Furthermore, HUVECs only gained increased PCA though incubation for longer time intervals as exposure for less than 60s showed no effect. The integrity of the HUVECs monolayer was not compromised by the association with MP as there were no gaps on HUVECs monolayer inside the microchannel where the MP had attached. In addition, more MP shed by U87 tumour spheroids adhered to the HUVECs than MP shed from ES2 spheroids as observed as PCA of HUVECs exposed to U87

showed increased PCA than ES2. Furthermore, the effect of doxorubicin on tumour spheroids and HUVECs was assessed as described in section 2.7.

5.2 Aims

The overall aim of this chapter was to form a model to allow for characterization and investigation of the interaction of tumour MP with the endothelium. To establish this model, primarily the effect of conditioned tumour media (MP associated) on endothelial cells under flow condition was investigated. In order to do that firstly, fluorescently labelled tumour MP were isolated from 2D culture then flowed through a Vena8 Endothelial+™ biochip pre-coated with a confluent monolayer of endothelial cells and imaged using a CELLIX fluorescent imaging system. Subsequently the PCA of cell free tumour media was assessed before and after flowing through the VENA8 Chip by a one stage PT assay and endothelial cells were then visualised by confocal microscopy (Zeiss LSM710) in order to confirm the CELLIX observations. The second aim of this study was to investigate the effect of tumour MP shed by tumour spheroids (3D) on endothelial cells under continuous flow conditions where media was passed over the tumour spheroids and then directly onto endothelial cells. Therefore, two channels chips were connected into a single system where one contained tumour spheroids and the other was pre-coated with HUVECs.

5.2.1 Objectives:

- In this chapter, flow cytometry was used to quantify CFSE labelling of MP from media of 2D cell cultures: AsPC-1, ES2, U87 and SKOV-3.
- Flow cytometry was used for the determination of TF labelling (anti-human TF: FITC) of MP from media of U87 and ES-2 tumour spheroids.
- The procoagulant potential of tumour-derived MP shed by various cancer cells was determined.
- The interaction of tumour MP on HUVECs was studied using microchannels Vena8 Endothelial, μ-Slide I 0.8 Luer and μ–Slide III 3D microfluidic biochips.
- Investigate how tumour MP are able to interact with endothelial cells *in vitro* and, potentially, confer PCA was also studied via different imaging systems.

5.3 Material and methods

MP released from various tumour cells labelled CFSE were initially analyzed by flow cytometry for degree of CFSE labelling as described in section 2.9.1. Having established reproducible, fluorescently labelled MP they were flowed through a Vena8 Endothelial+™ biochip pre-coated

with a confluent monolayer of HUVECs and imaged using a CELLIX imaging system as described in section 2.11. HUVECs were then visualised by confocal microscopy to confirm the CELLIX observations. CFSE Labelled MP released from ES2 and U87 tumour cells were quantified by flow cytometry before and after being passed through the µ–Slide I Luer biochip as described in section 2.10. MP released from ES2 and U87 tumour spheroids in ibidi µ–Slide III 3D microfluidic biochip were labelled with anti-TF: FITC (Bio-rad)) and unlabelled samples were immediately analyzed by flow cytometry as described in section 2.8 and 2.9.2. Procoagulant activity of cell free tumour media was assessed before and after flowing through the both microfluidic chips by a one stage prothrombin time (PT) assay as described in section 2.3. HUVECs were then visualised by confocal microscopy.

5.4 Results

5.4.1 Cell labelling by CFSE

Initially, to label tumour MP, AsPC-1 cells were labelled with 5(6) -carboxyfluorescein diacetate N-hydroxysuccinimidyl ester (CFSE) and analysed by flow cytometry for degree of fluorescent labelling (Figure 5-1). Harvested cells (1×10^6 cells/ml) of AsPC-1 was labelled with CFSE and split into six of 25 cm^2 cell culture flasks in 10 ml of the appropriate medium and incubated for 24 h at 37°C as described in section 2.11.1. Unlabelled cells were used as negative control. Then flow cytometry was used to detect the percentage of labelled MP shed into the media over a period of 5 days as detailed in section 2.10 (Figure 5.1).

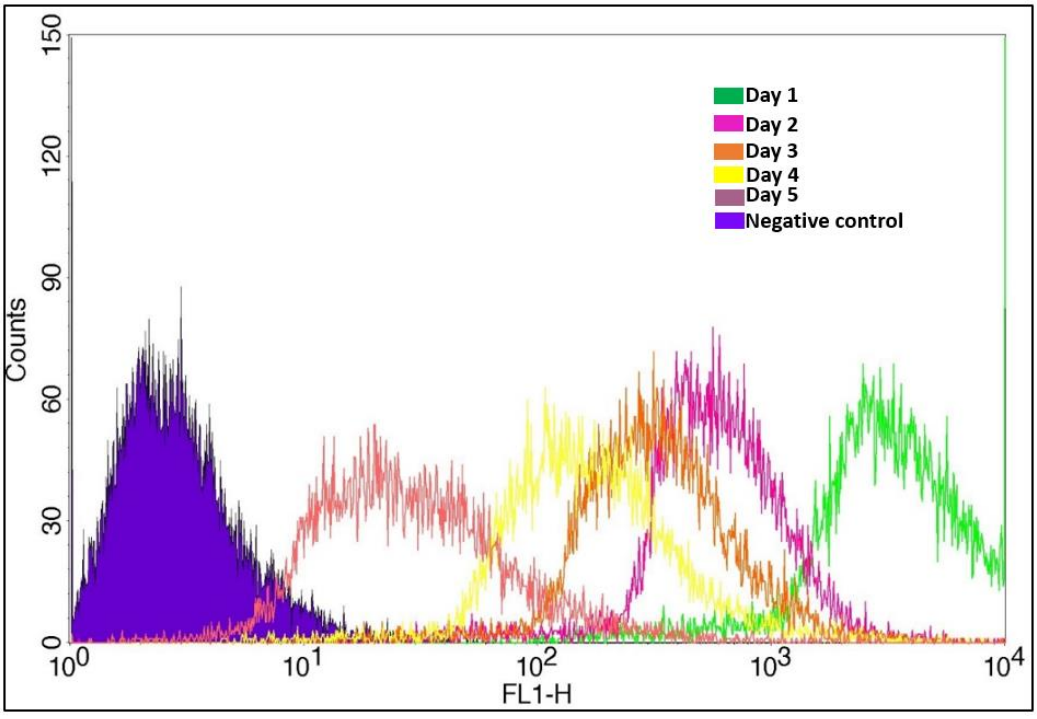

Figure 5.1: Fluorescence of AsPC-1 cells untreated and stained with CFSE then cultured for 5 days.

AsPC-1 cells were labelled 2µM of CFSE solution and mean fluorescence intensity was measured. Data represents two independent experiments.

Figure 5.1 shows histogram of MFI for each day for 5 days. The MFI in day 2 (indicated as pink colour) has showed the highest signal among other. Having established reproducible, fluorescently labelled MP were collected in day 2 for further study. Accordingly, CSFE staining of tumour cells was shown to be an effective method of labelling shed MP for a period of up to 48h (Figure 5.2). The degree of labelling to background was shown to decrease from (29.91%) to (9.38%) over the course of 5 days. MP released from AsPC-1 tumour cells incubated with CFSE were initially analysed by flow cytometry to confirm CFSE labelling. Unlabelled cells were used as the negative control.

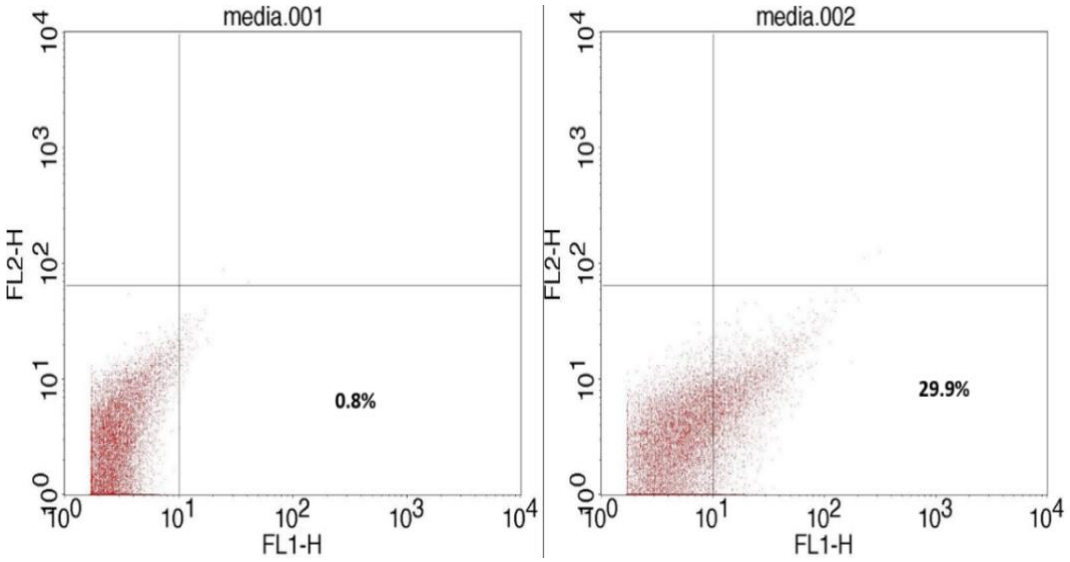

Figure 5.2: MP unlabelled and labelled with CFSE.
Flow cytometry detection of fluorescence intensity of tumour MP. Right panel shows MP derived from AsPC-1 cells labelled with 2 µM CFSE where the percentage of positive MP was 29.9%. Left panel shows unlabelled MP derived from AsPC-1 cells without CFSE stain.

MP released from AsPC-1 tumour cells labelled with CFSE were compared to CD142 antibody (Anti-TF) for degree of fluorescent labelling and analysed by flow cytometry over 6 days (Figure 5.3).

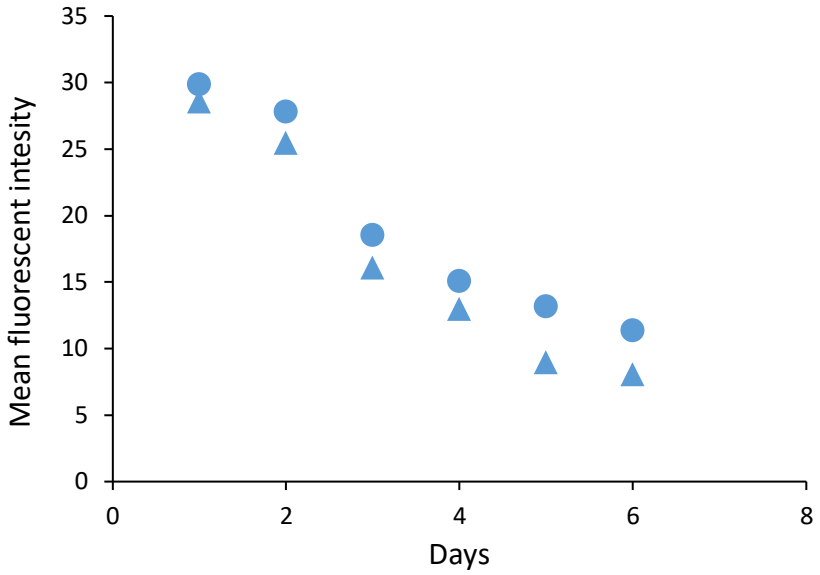

Figure 5.3: Chart showing CFSE labelled MP released from AsPC-1 over 6 days in culture in comparison to TFMP labelled with CD142 antibody.
(The data is representative of two separate experiments). ▲%TFMP, ●% CFSEMP.

Data obtained suggests that there was no difference in mean fluorescent intensity percentage between the two dyes.

5.4.2 Quantifying CFSE label decay

Initially, CFSE labelling of MP from media of AsPC-1 and SKOV-3 cell culture was used to quantify the CFSEMP and assess the relationship between TFMP with PCA. Thus, Cell free tumour media was with CFSE as described in section 2.11.1. PCA was assessed by a one stage prothrombin time (PT) assay. Cell free medium was harvested daily for six days and labelled MP were determined by flow cytometry. The highest labelling percentage was shown to be in day 2 so all labelled MP were collected in that day from both SKOV-3 and AsPC-1through entire study (Figure 5.4).

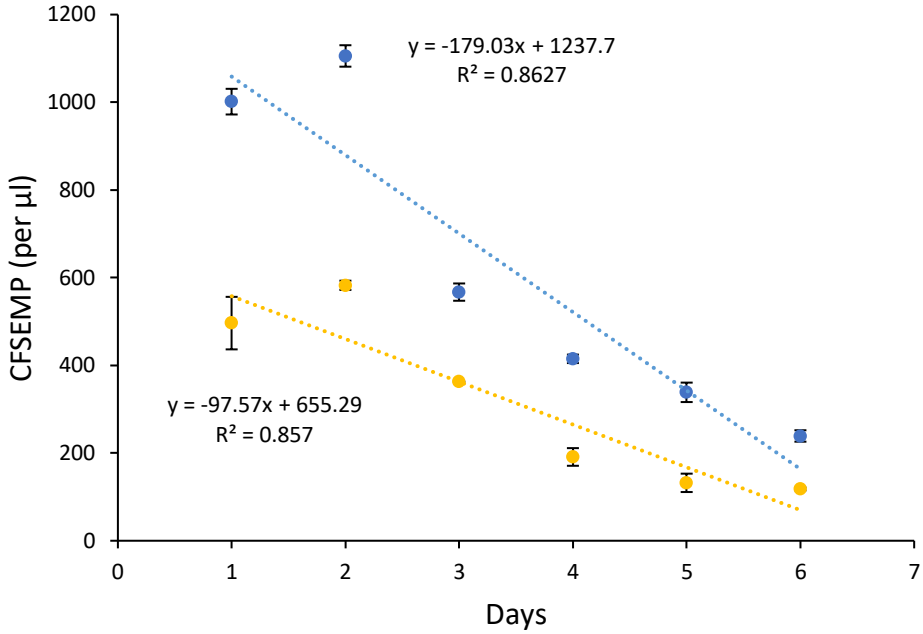

Figure 5.4: Chart shows labelling intensity of MP released by AsPC-1 and SKOV-3 tumour cells over the course of 6 days.
AsPC-1 and SKOV-3 cells labelled with CFSE and MP count was measured during 6 days. AsPC-1(●), SKOV3 (●). Error bars represent SD (n=3).

5.4.3 Correlation between the CFSEMP number and procoagulant activity

Initially, CFSEMP released from AsPC-1 and SKOV-3 tumour cells was used to quantify CFSEMP and assess PCA. Thus, MP was labelled as described in section 2.12.2 and quantify by FCAS. PCA of cell free tumour media was assessed by a one stage prothrombin time (PT) assay and the relationship between CFSEMP and PCA was then analysed. Labelled MP of SKOV-3 and AsPC-1 was correlated with PCA obtained showed a significant relationship between the tumour MP and PCA. A relationship between PCA and number of CFSEMP in the media was observed whereby increased amounts of MP within the media correlated to an increase in PCA and thus a faster PT (Figure 5.5).

(a)

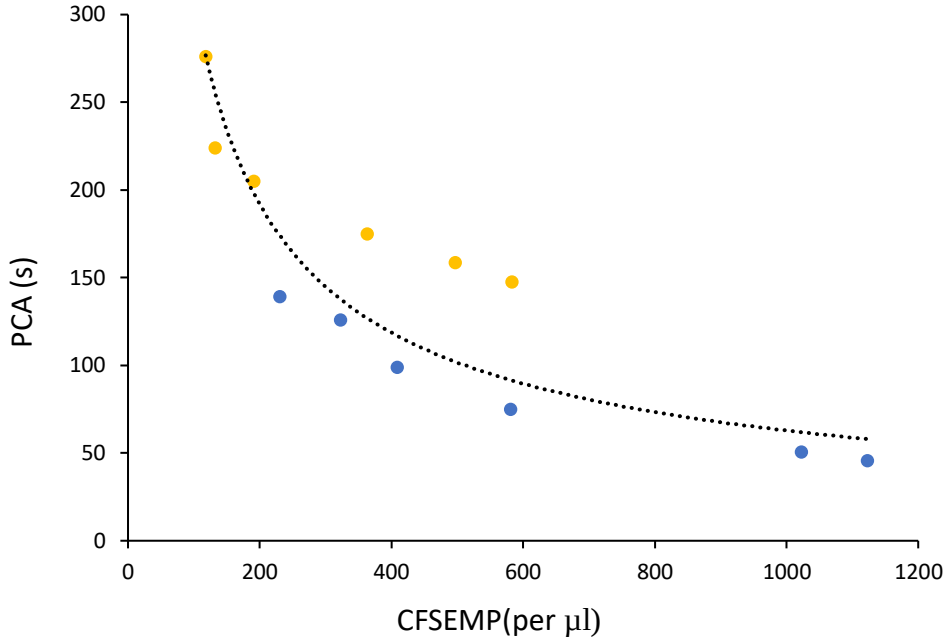

(b)

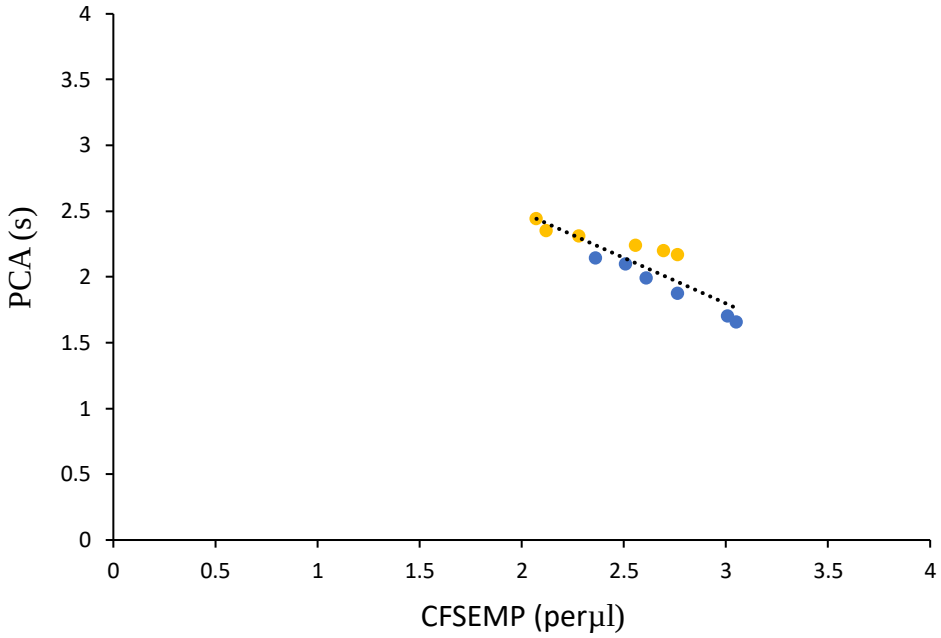

Figure 5.5: Relationship between CFSEMP and PCA of AsPC-1 and SKOV-3.
Data representative of n=3 experiments. Pearson's correlation coefficient r = -0.91 (SKOV-3) to -0.95 (AsPC-1). (b) Chart showing the correlation between CFSEMP and PCA using Log10 scale. Overall a consistent negative correlation was observed between CFSEMP and PCA with an average Pearson's rank correlation of with an average Pearson's rank correlation of r= -0.83 ± 0.05. AsPC-1(●) and SKOV-3(●)

5.4.4 Introduction

Tumours shed MP into the circulation that can then interact at sites remote to the tumour source, particularly those MP that express TF, which are thought to possibly play a role VTE in cancer patients (Aharon et al, 2008; Aleman et al, 2011). The pathophysiology relating to cancer-induced VTE are not yet fully understood but we have previously shown that tumour MP appear to bind to endothelial cells in static conditions and confer PCA via TF (Morel et al, 2005). This suggests that there may be a role of the endothelium in cancer related VTE in patients. To further assess this interaction MP released from tumour cells under static and flow culture conditions (through a microfluidic chip) were subsequently passed through a second microfluidic chip coated with human endothelial cells (HUVECs). Cancer patients have an increased risk VTE, as is suggested by PCA of supernatants from various tumour cell lines discussed so far in this study. Our experiments performed so far suggest that MP that are shed from cancer cells, and that are often positive for TF, may mediate PCA. Interestingly, several studies suggest that chemotherapy can contribute to the promotion of PCA, yet it is not well understood how this therapy can be a risk factor for the development of VTE. For example, tamoxifen can increase VTE risk by a factor two to seven; other drugs, such as immunomodulators such lenalidomide and thalidomide increase the risk for VTE in individuals with multiple myelomas by 10 - 40%, if applied in combination with glucocorticoids. The cytotoxic drugs fluorouracil and cisplatin can also lead to VTE, as does asparaginase as treatment of lymphoblastic leukaemia (Jiang et al, 2019). There are multiple mechanism in which chemotherapy can contribute to VTE, though "cancer type, stage, various biologic markers, and the use of central venous catheters" may contribute as well and confound or modify the effects of chemotherapy in this respect (Jiang et al, 2019). As the mechanisms by which a specific form of chemotherapy functions is diverse, the ways in which VTE risk is elevated are likely variable as well. Applying cytotoxic chemotherapy - for example, by using cisplatin or fluorouracil, kills cancer cells and may release pro-thrombotic elements like MP. L-asparaginase functions by depleting the cells of asparagine, which leads to a block in protein anabolism, and an induction of apoptosis. Thus, VTE risk could be elevated by the possible release of MP as well, although L-asparaginase could also function by reducing protein levels that function as inhibitors of platelet coagulation. Other drugs like tamoxifen or aromatase inhibitors may interfere with the thrombin/thrombinogen cascade as well, without the direct involvement of MP. A large group of chemotherapeutical drugs function by preventing tumour angiogenesis; often, they do this by inhibiting vascular endothelial growth factor (VEGF) or downstream components like specific tyrosine kinases. In addition, or because of this effect, they can also have a destructive effect on the endothelial lining of existing blood vessels, which triggers thrombosis. Immunomodulatory agents like thalidomide may interfere with platelet

aggregation and thrombosis formation via their influence on immune cells and their negative effects on vascularization. It is conceivable that any drug that modulates blood vessel growth may also affect platelet coagulation (Oppelt et al, 2015). Taken together, chemotherapy may interfere with the normal mechanisms for angiogenesis and vascular homeostasis, damaging blood vessels and thus precipitating coagulation; they may directly interfere with the pathways governing thrombosis; they may enable the release of MP from apoptotic cells, which subsequently promote blood clotting; or they may enact any combination of these mechanisms (Oppelt et al, 2015). Thus, the exact mechanism by which chemotherapy increases the risk for VTE is not precisely known, and as study conducted here addresses the effects of MP on coagulation, it can be used to shed more light on the effects of chemotherapy drugs on PCA of cancer cell lines. Doxorubicin (DOX) is a chemotherapeutical drug that is in widespread use. It interacts with DNA and blocks topoisomerase-2, which leads to the formation of double strand breaks; these breaks induce apoptosis. Thus, a potential mechanism by which DOX could increase VTE risk in cancer is by destroying cells and releasing MP, which will in turn increase tumour cell based PCA (Zhu et al, 2016).

Previously, two model biochips were designed that can immobilise a spheroid and assess the PCA under flow condition. However, the big pitfalls of these designs are that spheroids can easily disaggregate and block the flow micro channel and hence block the model system. Also, it wasn't easy to retrieve spheroids after running. Moreover, the fabrication and delivery for these chips had a huge impact on my project as I have to wait for months to get these chips and yet large number of them have not worked properly due to variation in inlet and outlet size. Therefore, it was used a model that only commercially available to increase the chances of standardization and to find a new model that circumvents the previous drawbacks of the old biochip. Consequently, the interaction of tumour MP (that shed from different cancer cell lines using 2D cell culture method) when incubated with HUVECs was examined. Moreover, the effect of tumour MP that shed from tumour spheroids (using 3D cell culture method) on HUVECs was also assessed. The behaviour of adherent MP from both 2D and 3D cell culture method on HUVECs was significantly important.

5.4.5 The effect of coculture of (2D) MP with IBIDI HUVECs biochip on PCA

5.4.5.1 HUVECs growth on ibid µSlide I 0.8 lure I biochip

MP released from AsPC-1, U87 and SKOV-3 tumour cells labelled with CFSE were initially analysed by flow cytometry for quantification. Having established reproducible, fluorescently labelled MP they were flowed through an ibid µSlide I 0.8 lure that pre-coated with a confluent monolayer of HUVECs and imaged using confocal microscopy (Zeiss LSM710) (Figure 5.6). PCA

of cell free tumour media was assessed before and after flowing through the ibid µSlide I 0.8 lure biochip by a one stage prothrombin time (PT) assay.

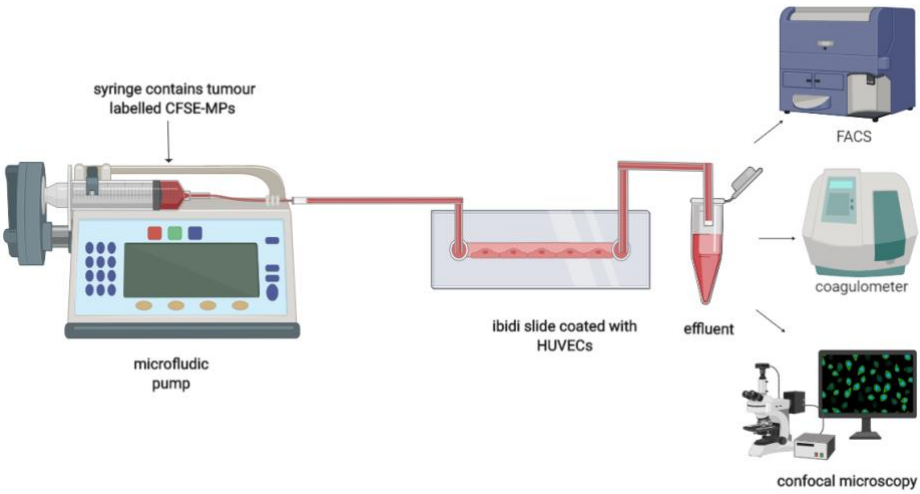

Figure 5.6: Schematic showing the basic model setup.
Labelled tumour media were flowed via either a syringe pump (constant flow) or a Kima pump (pulsatile flow) through a microfluidic chip containing HUVECs to study their interaction.

Therefore, initial experiments were conducted using labelled CFSEMP that collected from different cancer cell lines. Then, the tumour media was perfused over the ibid µSlide I 0.8 lure that coated with HUVECs. Next, PCA and MP quantification was assessed using different methods (Figure 5.7).

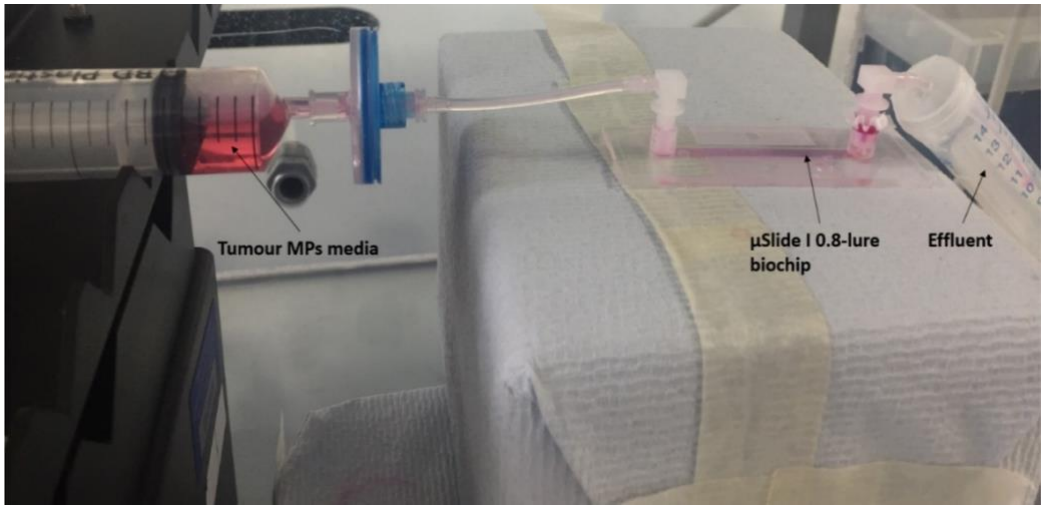

Figure 5.7: Image showing the basic experimental setup of ibid µSlide I 0.8 lure.
Tumour CFSEMP of AsPC-1 or U87 or SKOV-3 in syringe linked through to a µ-Slide I Luer containing HUVECs and finally sample collection tubes. The experiments were carried out in a 37 °C incubator. Media were flowed via either a syringe pump (constant flow) through a microfluidic chip containing HUVECs.

Accordingly, ibid µSlide I 0.8 Luer was coated with B 2% v/v gelatine and keep it overnight at 4°C. Then, HUVECs concentration of 1.6 x 10^6 cells/ml was prepared. Then, 150 µl of the cell suspension was inject into the channel by putting the pipet tip directly onto the channel's inlet. Slide was incubated at 37°C and 5% CO_2 for half an hour for cell attachment. After cell attachment, 60 µl fresh complete medium was added into each reservoir. Then, slide was further incubated for two hours. Then, the slide was observed under microscope to assess the attachment of HUVECs and incubated overnight in CO_2 at 37°C. HUVECs are exposed to 4 µl/min flow rate that mimics their physiological condition. Thus, cultivating cells under flow condition will correlate more closely to their usual physiological environment than cells in a static cell culture method (Figure 5.8).

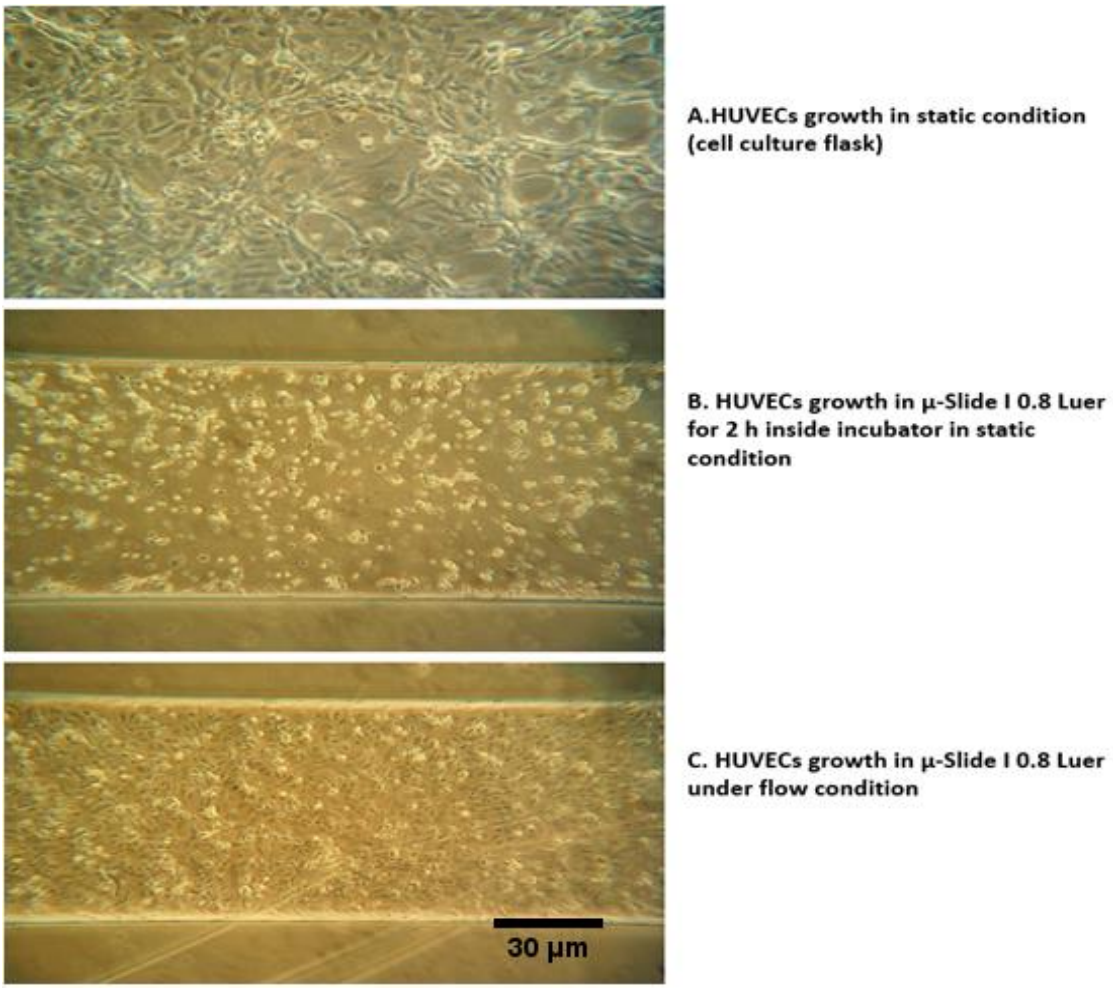

Figure 5.8: comparison of the morphology of HUVECs cultivated in different condition.
Image (A) showing HUVECs growth under static condition after 24 hours. Image (B) showing the HUVECs in µ-Slide I 0.8 Luer cultivated for 2 hours under static conditions (HUVECs concentration of 1.6 x 10^6 cells/ml). Image (C) showing HUVECs in µ-Slide I 0.8 Luer cultivated for one day. The cells show a good orientation in the direction of the flow.

5.4.5.2 The effect of CFSEMP on HUVECs using ibid µSlide I 0.8 lure

Labelled tumour media was harvested from (AsPC-1, SKOV3 and U87) and then flowed across a µ-Slide I 0.8 Luer culture biochip pre-coated with HUVECs for 24h at a flow rate of 4uL/min to assess any interaction between the release CFSEMP and the HUVECs. Effluent was collected in a single tube for the duration of the 24 experiment then re-analysed for CFSEMP and their relationship with PCA as assessed by PT (Figure 5-9). Therefore, tumour media was collected from AsPC-1, SKOV3, and U87 and perfused over HUVECs for 24 hours. The PCA before and after perfusion was assessed. Data representative of n=4 independent experiments. For all flow through experiments on the HUVECs chip the data was collated and an overall trend was observed whereby the number of quantified CFSEMP was correlated with PCA. Overall a consistent negative correlation was observed between CFSEMP and PCA with an average Pearson's rank correlation of r = -0.76 ± 0.05 (Fig 5.9).

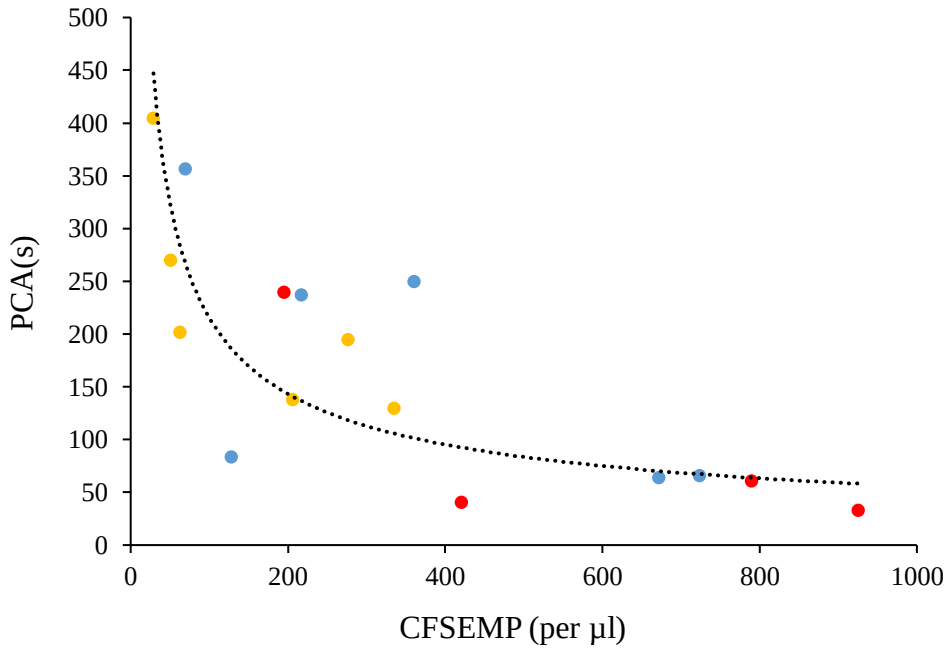

Figure 5.9: The Relationship between CFSEMP and PCA.
Chart showing the Relationship between CFSEMP and PCA of U87(red square, n = 2) andSkov-3 (Yellow circle, n = 3) and AsPC-1 (blue circle, n=3) media when perfused over HUVECs for 24 h. Lines of best fit are for a power relationship. AsPC-1(●), U87 (●), SKOV-3(●).

The relationship observed was similar to that observed previously with tumour media and tumour cells where a proportional decrease in either conditioned media or cell number resulted in a decrease in associated PCA in a power relationship. As such the data obtained for conditioned media flowed through a HUVECs coated biochip was log transformed independent of tumour cell line origin and this showed a linear relationship around the scatterplot (Fig

5.10). Again, a negative correlation was observed between CFSEMP and PCA with an average Pearson's rank correlation of r = -0.79 ± 0.05.

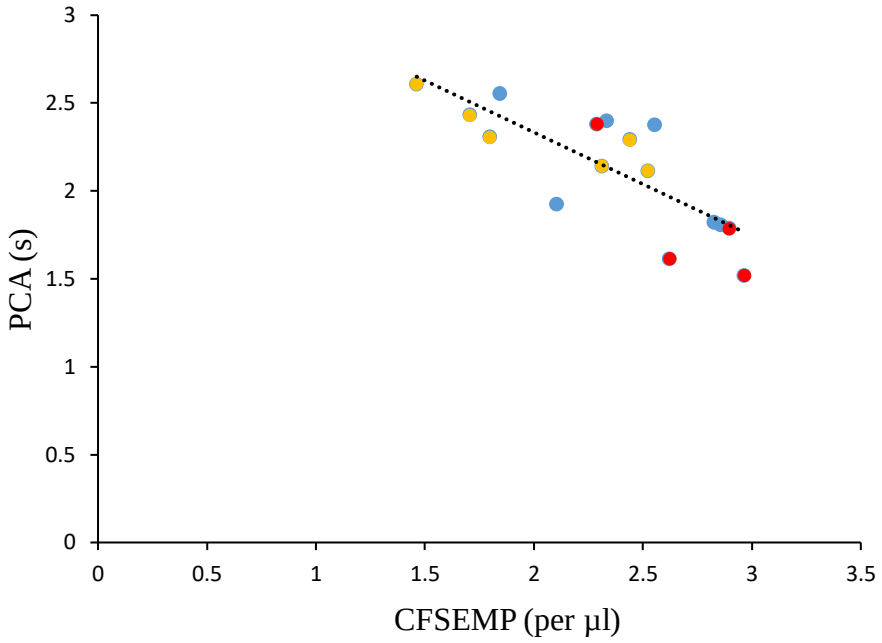

Figure 5.10: Chart showing Chart showing the Relationship between CFSEMP and PCA using log10/log10 plot.
AsPC-1(●), U87 (●), SKOV-3(●).

Here, a near-linear relationship existed between PCA and CFSEMP on a log10/log10 plot such that high enumerated MP tends to result in short clotting time, R^2= 0.6236. (The data is representative of four separate experiments). A general pattern regardless of cell line was detected by which a corresponding reduction of MP was linked with the original concentration. The relationship observed was generally strong.

5.4.5.3 The effect of circulating MP on HUVECs

labelled CFSEMP was taken from culture flasks of CFSE labelled confluent cells, centrifuged to remove any whole cells and subsequently passed through a confluent chip of HUVECs. HUVECs were cultured on a µ-Slide I Luer for 24h prior to introduction of tumour media. Then, prior to exposure to the ex-ovarian supernatant, the HUVEC media was removed and cells were washed with PBS. The tumour media used supported coagulation in a time of 138±19.62s (SKOV3), 75±32.33s (AsPC-1) and 41±6.92s (U87). After the 24 hours exposure the media was removed and tested again for PCA After long exposures the loss of PCA was observed. HUVECs acquire PCA from the media (MP) and PCA was assessed after 24 hours in a time of 338±122.2s (SKOV3 media over HUVECs), 293±52.65s (AsPC-1) 266±67.82s (U87 media over HUVECs) (Figure 5.10). Furthermore, HUVECs acquire PCA from the media associated MP and PCA was

assessed after 24 hours in a time of 166±24.0s (ES2 media over HUVECs) and 149±29.7s (U87 media over HUVECs) and 921±15.5s (HUVECs without tumour media). A control channel coated with gelatine without HUVECs was used as control to see the effect of chip or coating protein on MP or PCA so CFSE labelled tumour media of AsPC-1, U87 and SKOV-3was passed over the chip showed no effect (Figure 5.11).

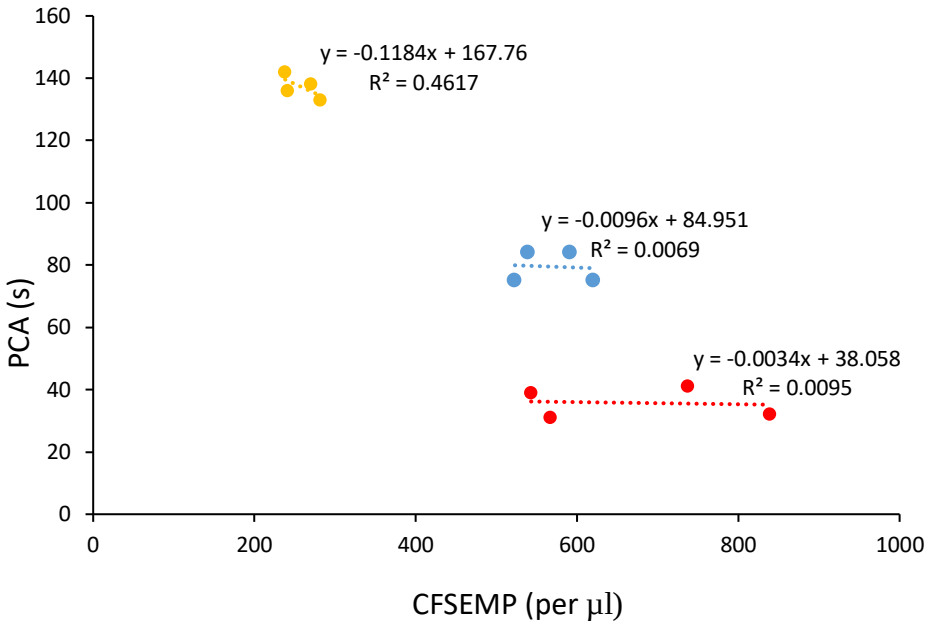

Figure 5.11: Chart showing the relationship between CFSEMP and PCA using control chips (without HUVECs).
Data represents 3 experiments. AsPC-1(●), U87 (●), SKOV-3(●). Data representative mean of 3 independent experiments.

5.4.5.4 The effect of 10 cycles on HUVECs

CFSEMP from media of ES-2 and U87 cancer cell lines was used to quantify the interaction with HUVECs using 10s cycles and the relationship between CFSEMP with PCA. ES2, U87 $1*10^6$ cells/ml seeded into 25 cm² flask labelled with 2 µm CFSE incubate 24 hrs. Then labelled CFSEMP ES2 and U87 was collected and incubated with HUVECs for 10 sec, 20 sec, 30 sec. PCA and CFSEMP quantification was taken before HUVECs and after. Therefore, HUVECs were cultured on a µ-Slide I 0.8 Luer culture biochip for 24h prior to introduction of tumour media. No PCA was observed from endothelial media passed through the µ-Slide I 0.8 Luer culture biochip coated with HUVECs. A control of µ-Slide I 0.8 Luer culture biochip microchannel coated with gelatine without HUVECs were subjected to control tumour media in the same way as the experimental (MP containing) media. Thus, tumour CFSEMP was passed into a series of biochips of confluent HUVECs. Conditioned tumour media (500µL) was pipetted into a confluent Slide I 0.8 Luer culture biochip of HUVECs and gently rocked for 10s before being entirely removed for analysis. Next, the same tumour volume was passed into a second Slide I

0.8 Luer culture biochip for 20s and then a third in sequence for 30s. The CFSEMP was then assessed and HUVECs were analysed by flow cytometry for CFSE expression postperfusion (Figure 5.12).

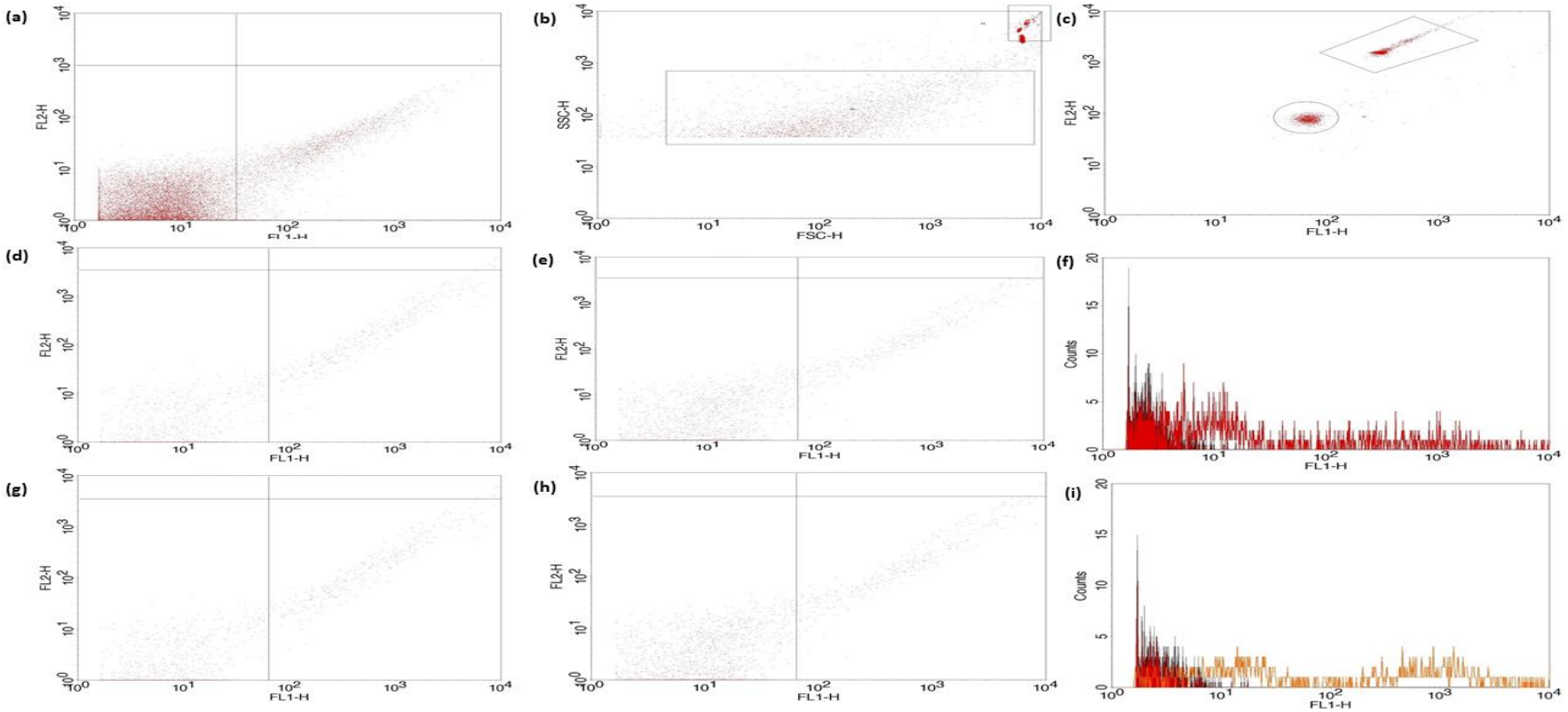

Figure 5.12: CFSE fluorescently labelled MP of ES2 and U87.
(a) The individual MP events in the lower right quadrant correspond to CFSE-labeled MP. (b) Side-scattering (SSC) intensity of MPs vs. forward-scattering (FSC) intensity. (c) Image shows two distinct bead populations. (d) The individual MP events in the lower right quadrant correspond to CFSE-labeled MP of U87 before perfused over HUVECs biochip. (e) The individual MP events in the lower right quadrant correspond to CFSE-labeled MP of U87 after perfused over HUVECs biochip. (f) Representative histogram plots low signal of fluorescence of HUVECs perfused with U87 MP rich media for 30 seconds, compared to HUVECs perfused with control media (left peak). (g) The individual MP events in the lower right quadrant correspond to CFSE-labeled MP of ES2 before perfused over HUVECs biochip. (h) The individual MP events in the lower right quadrant correspond to CFSE-labeled MP of ES2 after perfused over HUVECs biochip. (i) Representative (n = 3) histogram plot low signal of fluorescence of HUVECs perfused with ES-2 MP rich media for 30 seconds, compared to HUVECs perfused with control media (left peak).

Accordingly, unchanged of CFSEMP after perfusion across HUVEC coated slides was further investigated through analysis of the PCA associated with the media following perfusion across the 10 seconds cycles. The data suggests that no relationship was observed between CFSEMP and PCA for both cell lines, and the subsequent unchanged number of CFSEMP over time with HUVECs perfusion resulted in constant PCA. the flow cytometry data indicated no loss of CFSEMP through these cycles which associated with PCA. The data obtained (Table 5.1) shows no reduction in PCA of the conditioned media from 73s (ES2) and 85s (U87) to 75s (ES2) and 91s (U87) after 30s incubation with HUVECs. However, incubation of conditioned media with HUVECs resulted in a loss of PCA as found in longer incubation time. Conditioned media added to µ-Slide I 0.8 Luer culture biochip coated with gelatine in the same way showed no loss of PCA. The quantified CFSEMP data obtained via flow cytometry showed no significant change in the number of detected MP through these 10s cycles. This suggesting that the coat protein has not any effect on MP characteristics.

Table 5.1: The effect of 10 cycles on MP and PCA characteristics.

Data representative of four experiments.

	MP	PCA
ES2 pre-test	196±8	77±2
ES2 post-test		
10s	204±6	77±2
20s	207±30	81±5
30s	215±39	80±6
U87 pre-test	160±6	88±6
U87 post-test		
10s	161±8	94±5
20s	163±6	101±6
30s	172±6	100±4

Subsequently, the relationship between PCA and CFSEMP number was plotted as in figure 5.13. Overall unchanged correlation was observed between CFSEMP and PCA where no loss of PCA or TFMP when 10s cycles was used. Overall, the data suggests that the interaction between tumour CFSEMP and cultured HUVECs on a µ-Slide I 0.8 Luer culture biochip appeared to not happen quickly as it as it has proven to happen after long incubation period.

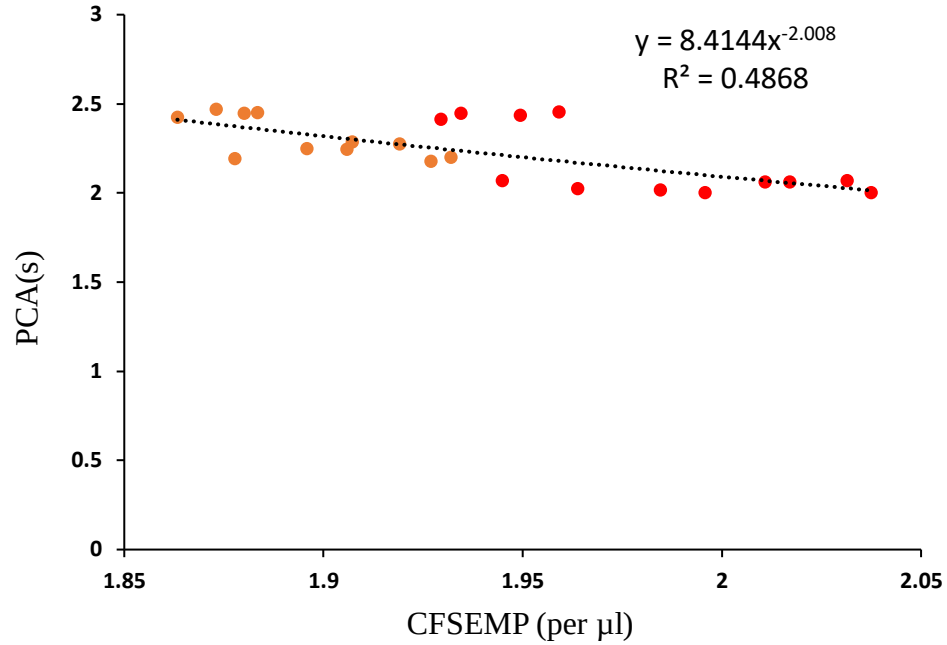

Figure 5.13: relationship between CFSEMP and PCA.
Chart showing the realtionship between CFSEMP and PCA of U87 (red circle, n = 3) and ES-2 (orange circle, n = 3) media when perfused over HUVECs using 10 seconds cycles. Lines of best fit are for a power relationship. Data representative of 3 independent experiments.

Furthermore, control chips containing HUVECs were subjected to flow of MP rich tumour media from ES2 and U-87 passed through blank µ-slide luer chips and the data showed no change in PCA across the 10s cycles experimental window (Figure. 5.14).

(a)

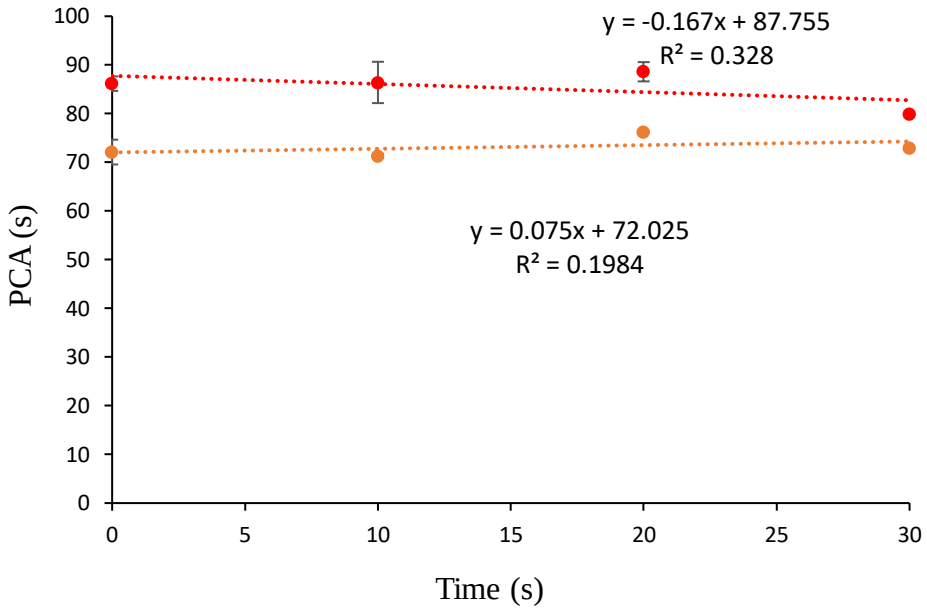

(b)

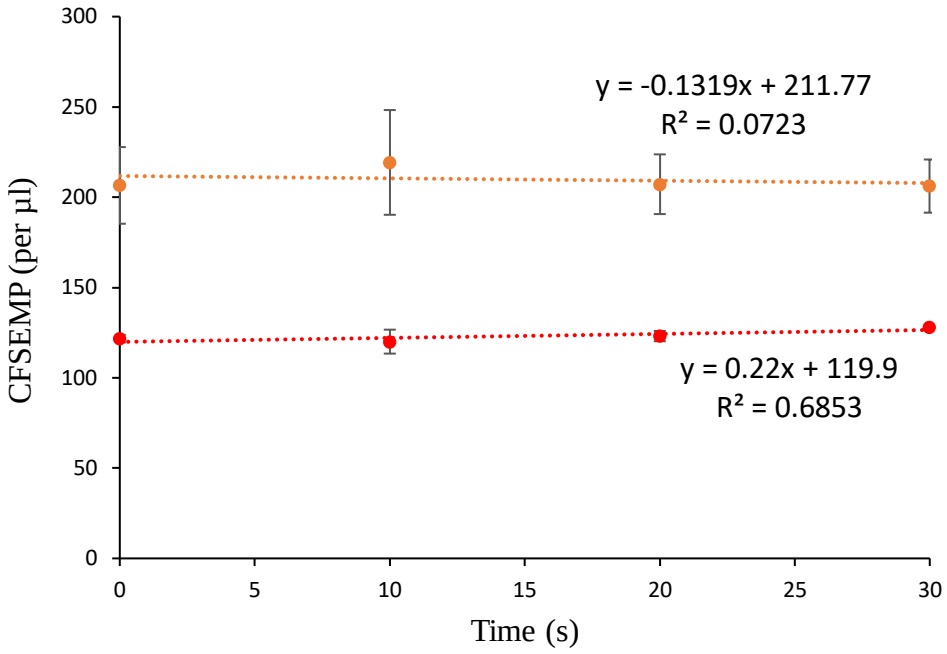

Figure 5.14: CFSEMP of ES2 and U87 as a percentage of baseline values (n=3) when perfused across a µ-Slide I Luer blank control chip with no HUVECs present (n=4) for 10s cycles.
(a) chart shows the relationship between PCA and time. (b) Chart shows the relationship between CFSEMP and time. Error bars are SD.

5.4.5.5 The effect of incubation of tumour MP on cancer cell lines

In order to investigate the effect of tumour MP on cancer cells and to explore if the tumour MP react differently on abnormal cells, tumour CFSEMP of ES2 and U87 was collected as described in section 2.11.2. Thus, 10 ml of ES2 tumour media (1×10^6 cell / ml), was incubated with (1×10^5 cells/ml) of U87 in 25 cm^2 cell culture flasks after media was removed for different time points. In the same way, tumour media of U87 (1×10^6 cell / ml), was incubated with ES2 cells for the same frame time (Figure5-15). PCA was obtained at 0 (h) which is the control. PCA at 1 (h) and 24 (h) was measured. The PCA observed in the collected media was unaltered.

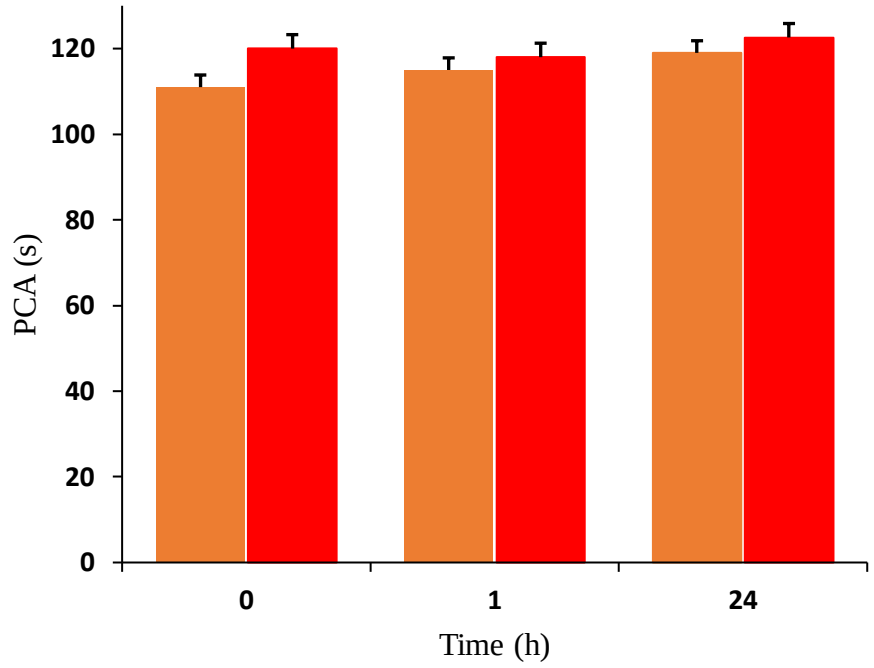

Figure 5.15: Chart showing the effect of tumour MP on cancer cell line.
Error bars representing of ±SD three independent experiments. ES2 (■), U87 (■).

The data indicate that, incubation of tumour MP that collected from ES2 and incubated on U87 cancer cell has shown no effect. Similarly, U87 tumour media was incubated with ES2 cancer cell lines and there was no effect on PCA. Therefore, tumour media associated MP when cultured with non-endothelial cell lines did not show any interaction as it didn't change PCA significantly.

5.4.6 The effect of circulating MP shed from tumour spheroids (3D) on HUVECs

5.4.6.1 Using tumour spheroids on microfluidic chip

A three-dimensional (3D) spheroid model demonstrate many characteristics associated with solid tumours over 2D cell cultures. These characteristics include different zones of proliferation, apoptotic, and necrotic cells and an oxygen gradient with hypoxic areas in the core (Osswald et al, 2015). Moreover, spheroid model can mimic the relevant in-vivo physiological conditions and can be a suitable model to use in drug discovery, the investigation of disease pathology, and tissue engineering (Vadivelu et al, 2017). Therefore, in this study we use tumour spheroid model to characterize MP that shed from different tumour. Previously we explained that not all cancer cell lines can form a compact spheroid that can be a suitable model to use in microfluidic chip system. Consequently, in this study we use ES2 and U87 as suitable model as these two cell lines exhibit compact and stable spheroid under flow condition.

5.4.6.2 The effect of MP that perfused from the Spheroids biochip model on HUVECS biochip model

In order to form spheroid, the liquid overlay method was used to generate spheroids by seeding cells at concentration of $2x10^4$ cells/well "in a volume of 200 µl/well of culture medium in 96-well plates (Sarstedt, UK) that coated with 1.5% agarose as described in in section 2.2.15. To monitor spheroid's growth, Pictures of the spheroids were taken each 5 days by using an Oxford Optronix GelCount™ camera and spheroid size was measured using ImageJ software (National Institute of Health, US). After spheroids generation, 40 spheroids by size of 500 µm-diameter was gently loaded into the ibidi µ–Slide III 3D microfluidic biochip as described in section 2.2.25. We used tumour-on-a-chip system where tumour spheroids maintain in a microfluidics chip system under flow rate of 4.0 µL/ min for different time (depend on experiment) (Figure 5.16).

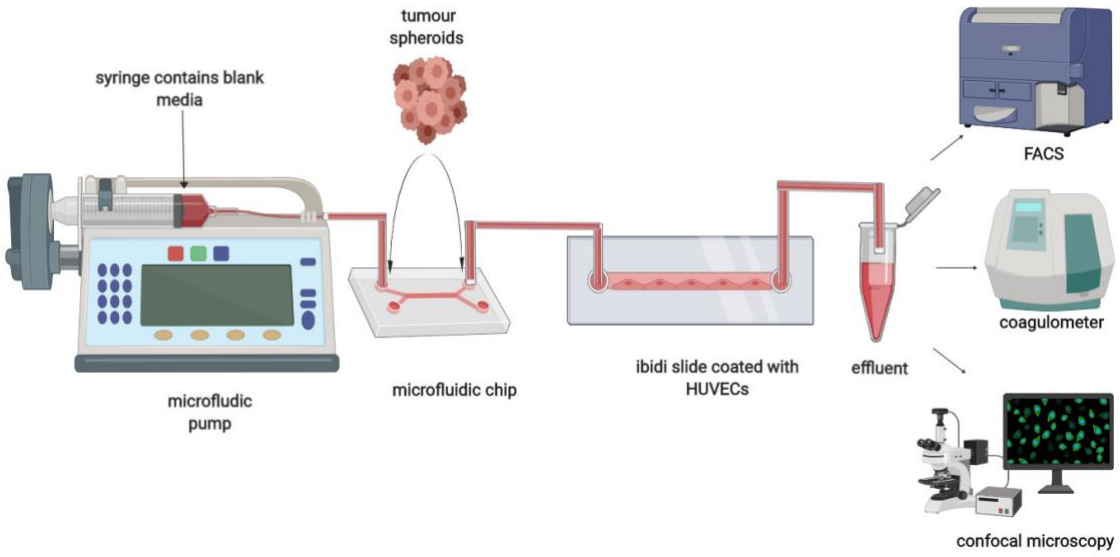

Figure 5.16: Schematic showing the tumour spheroids - HUVECs model setup.
Tumour fresh media contained in syringes linked to a multiwell µ-slide III 3D chip containing either ES-2 or U87 spheroids linked through to a µ-Slide I Luer containing HUVECs that linked to sample collection tubes. Next, all effluent samples and analysed using different experiments.

Consequently, as previously described, ibid µSlide I 0.8 lure was coated with gelatine and keep it overnight at 4°C. For a final cell number of 1 x 10^5 cells/cm² (2.5 x 10^5 cells/µSlide) a concentration of 1.6 x 10^6 cells/ml was prepared. Then, 150 µl of the cell suspension was pipetted into the channel by putting the pipet tip directly onto the channel's inlet. Slide was incubated at 37°C in 5% CO_2 for half an hour for cell attachment. After cell attachment, 60 µl fresh complete medium was added into each reservoir. Then, slide was further incubated for 2 h. Subsequently, the cells should have formed a confluent cell layer. This is important because the confluence of the HUVEC cells is a crucial point in the ability of the cells to resist the shear

stress and to produce a uniform monolayer. The chips were then incubated at 37 °C for 24 h. Cells proliferation was monitored, and images were taken after 24 hours (Figure 5.17).

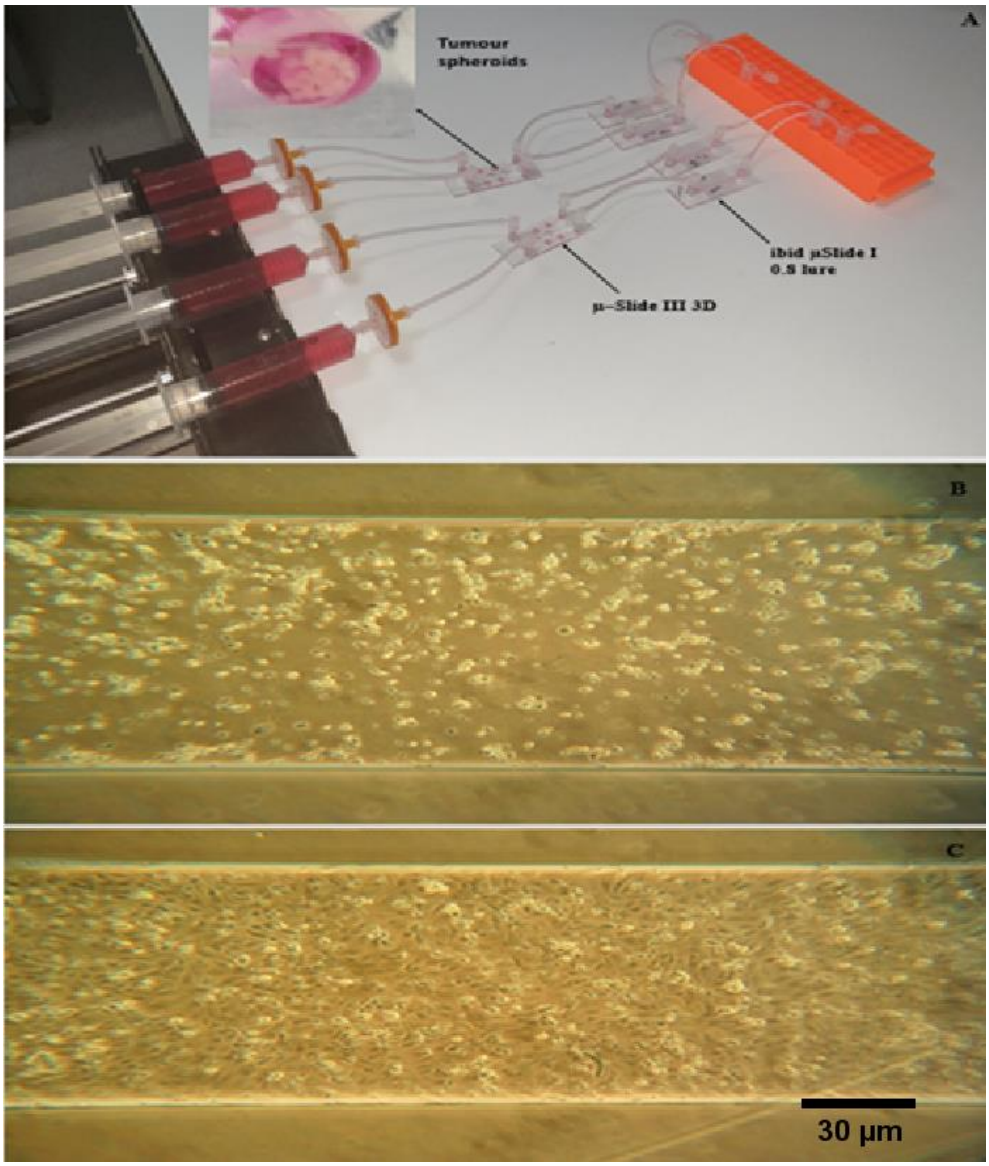

Figure 5.17**:** Images of the basic experiment showing the perfusion system and HUVECs culture on ibid µSlide I 0.8-lure biochip.
(A) Image showing tumour fresh media contained in syringes linked to a multiwell µ-slide III3D chip containing either ES-2 or U87 spheroids linked through to a µ-Slide I Luer containing HUVECs and effleunt finally collected in tubes (B) Adherence of HUVECs in the microchannel after incubation for 2 h inside the incubator. (C) HUVECs monolayer adherence after 24 hours and the cells started to elongate. HUVECs cells evenly distributed in the chip as shown in image C, leading to the elongating HUVECs structure.

subsequently, Tumour spheroids of U87 and ES2 were transferred into the µSlide 3D as described in section 2.2.25. Breifly, 40 tumour spheroids from ES2 nad U87 were transferred into the ibidi µ–Slide III 3D and connected to a plastic syringe contains 20ml of respective fresh tumour media. Next, the spheroid biochip was connected to the µSlide I 0.8 lure that coated with monolayer HUVECs. Using microfludics pump, the blank media was perfused over

the spheroids for 12 hours. Cell free media from each tumour spheroid biochips was perfused over HUVECs that coated the µ-Slide I Luer 12 hours. The PCA and FACS was taken before and after perfused over HUVECs . Both biochips were subjected to flow at a flow rate of 4µl/min for 12 hours (Depend on experiment). To label MP, anti-TF immunostaining, with 5µg of antihuman CD142: FITC antibody was added to the 1.5 ml tube contain 50 µl effluent and 50 µl of Accucheck beads (Invitrogen, UK) and 150µl of 0.2µm-filtered sterile PBS. Then, the solution was incubated for 30 mins in room temp in a dark place. Next, the sample was analysed by flow cytometry for quantifying of TFMP.

5.4.6.3 Procoagulant activity of cell-free media containing MP

As shown in the previous section, HUVECs acquire PCA in the presence of tumour CFSEMP. Here, Tumour MP that shed from ES2 and U87 spheroids were perfused over HUVECs under flow condition. HUVECs were cultured on a µSlide I 0.8 lure for 24h prior to introduction of tumour media that shed from spheroids ibidi µ–Slide III 3D biochip. A control µSlide I 0.8 lure channels coated with gelatine (without HUVECs) were subjected to control tumour media directly perfused out of spheroid µ–Slide III 3D in the same way as the experimental (MP containing) media. For all flow through experiments on the HUVECs chip the data was collated (Figure 5.18) and an overall trend was observed whereby the number of quantified CFSEMP was positively correlated with PCA.

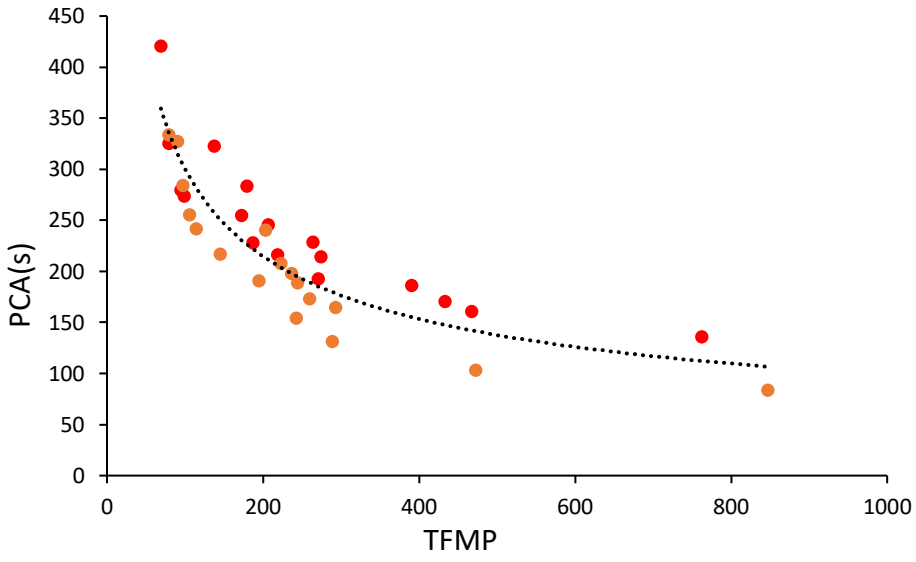

Figure 5.18: Relationship between TFMP and PCA of U87 and ES-2 media when perfused over HUVECs for 12 h.
Lines of best fit are for a power relationship and R2 value is 0.7993. Overall a consistent negative correlation was observed between TFMP and PCA with an average Pearson's rank correlation of -0.77 ± 0.05. U87(red square, n = 17) and ES-2 (orange circle, n = 17).

The relationship observed was similar to that observed previously with tumour media (2D) where a proportional decrease in conditioned media resulted in a decrease in associated PCA in a power relationship. As such the data obtained for conditioned media flowed through a HUVECs coated biochip was log transformed (Figure 5.19) independent of tumour cell line origin and this showed a linear relationship around the scatterplot.

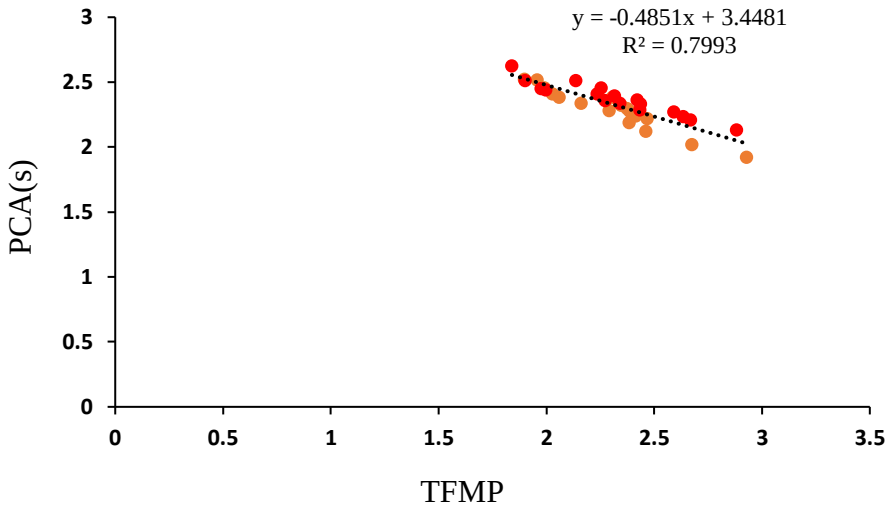

Figure 5.19: Chart showing the relationship between TFMP of U87 and ES-2 using log10/log10 plot. Overall a consistent negative correlation was observed between TFMP and PCA with an average Pearson's rank correlation of -0.89 ± 0.05. U87(red square, n = 17) and ES-2 (orange circle, n = 17).

The loss of tumour MP released by ES2 and U87 spheroids when media was flowed through the HUVECs biochip and associated loss of PCA was found related to the initial concentration of MP measured. An overall trend irrespective of cell line was observed whereby a proportional decrease of MP was related to the original concentration. Furthermore, the PCA prior to and after flow through the HUVECs biochip was determined and a decrease was observed across all cell lines (Figure 5.20, Figure 5.21). The PCA of each cell line media followed the same pattern pre to post with U87 media supporting the highest PCA both before and after passing the HUVECs biochip and ES2 having the least PCA both before and after.

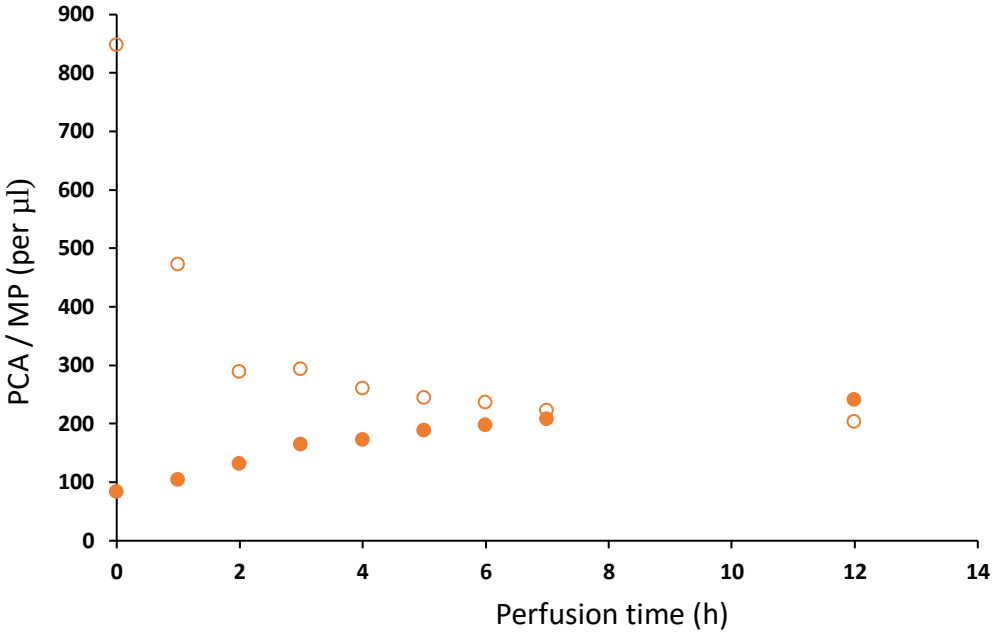

Figure 5.20: Relationship between TFMP and PCA of ES2 (Filled circle:PCA, n = 12) and (unfilled circle: TFMP, n = 12) media when perfused over HUVECs for 12h.
Overall a consistent negative correlation was observed between TFMP and PCA with an average Pearson's rank correlation of -0.81 ± 0.05.

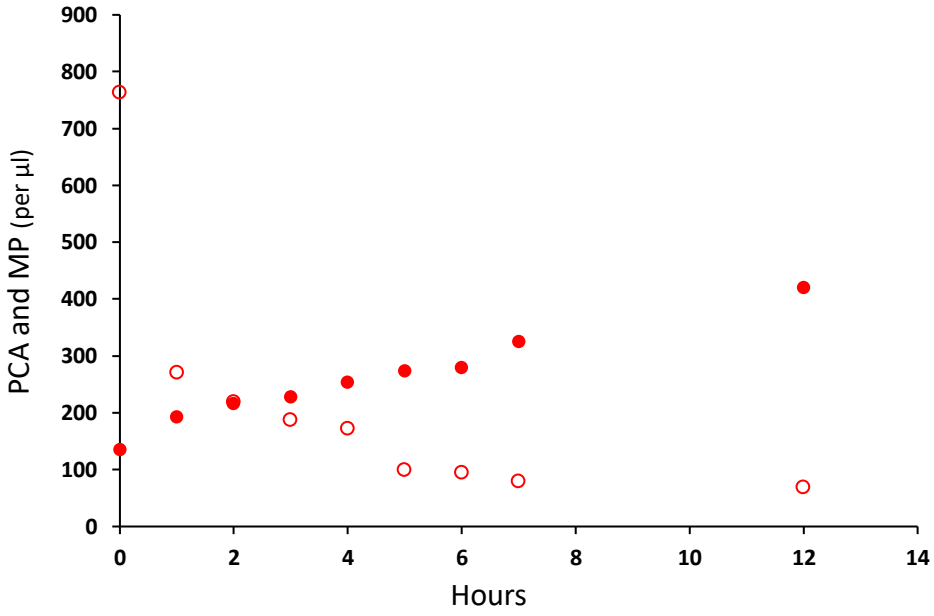

Figure 5.21: Relationship between TFMP and PCA of U87 (Filled circle:PCA) and (unfilled circle:TFMP) media when perfused over HUVECs for 12h.
Overall a consistent negative correlation was observed between TFMP and PCA with an average Pearson's rank correlation of -0.82± 0.05.

Furthermore, PCA prior to and after flow through a control biochip without HUVECs was determined. There was no change in PCA and TFMP across both cell lines and no relationship was observed. Though, there was an associated loss of PCA relative to loss of TFMP in biochips coated with HUVECs, and the relationship between loss of PCA and loss of TFMP was again consistent with TFMP being responsible for PCA. Thus, over a 6-hour duration, TFMP of both cell lines declined linearly after perfusion on a µ-slide Luer biochip with HUVECs compared with the control biochip without any HUVECs. (Figure 5.22-23).

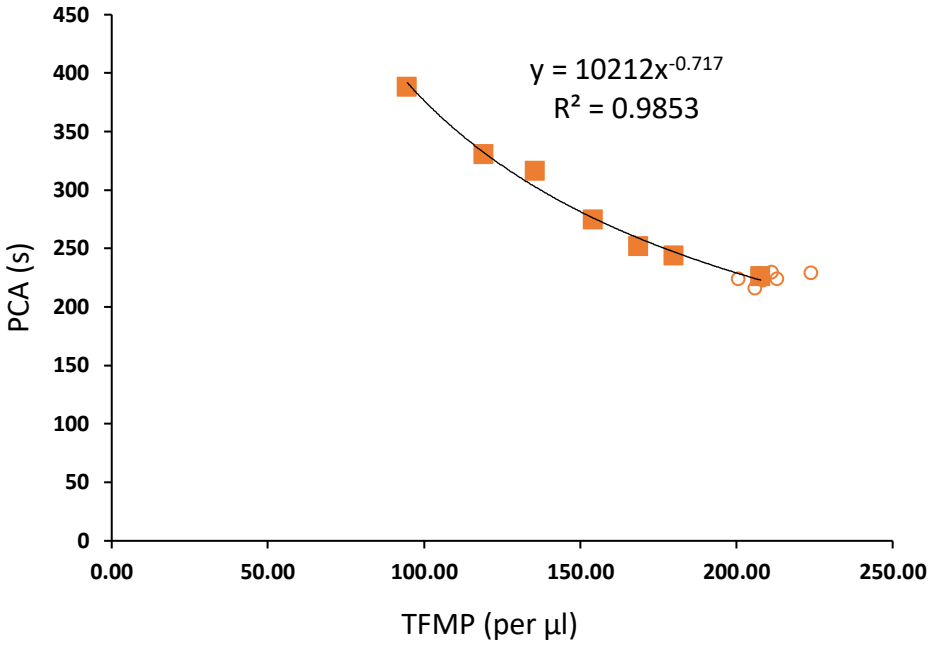

Figure 5.22: relationship between the TFMP and PCA.
Chart showing the relationship between the TFMP and PCA of ES2 spheroids as a percentage of baseline values (r=-0.98, n=8)when perfused across a µ-Slide I Luer containing cultured HUVECs (orange square) or a gelatine control chip (unfilled orange circle) with no HUVECs present (r= 0.49, n = 4) for 6 h.

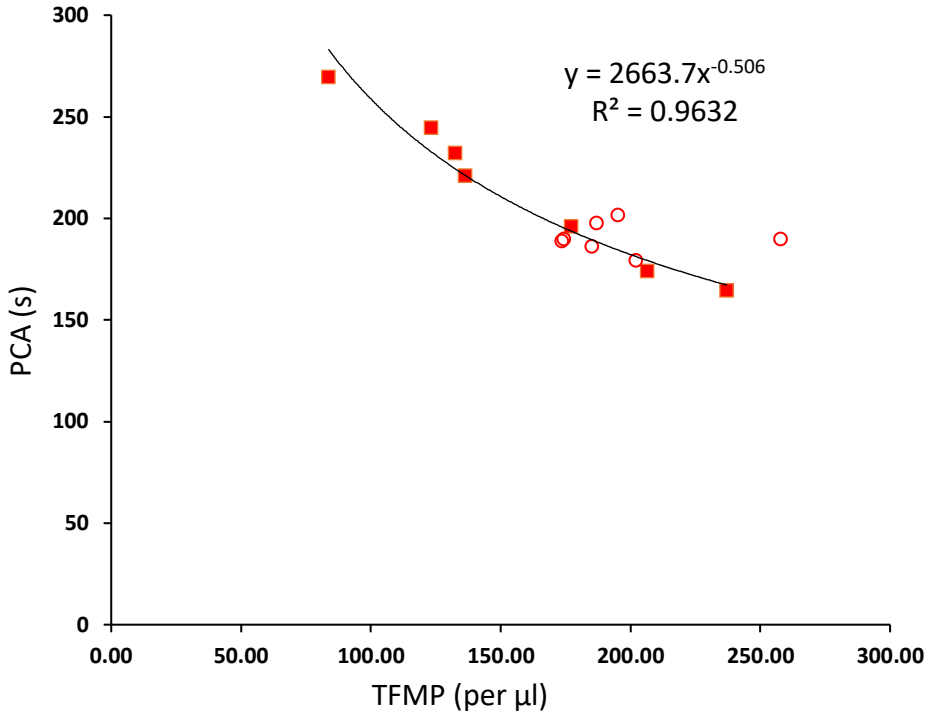

Figure 5.23: the relationship between the TFMP and PCA.
Chart showing the relationship between the TFMP and PCA of U87 spheroids as a percentage of baseline values (r=-0.99, n=8) when perfused across a µ-Slide I Luer containing cultured HUVECs (orange square) or a gelatine control chip (unfilled orange circle) with no HUVECs present (r=- 0.07, n = 4) for 6 h.

5.4.6.4 Procoagulant activity of HUVECs cells on a microfluidic chip

We tested the effect of adhesion of MP to EC on HUVECs PCA using a one stage prothrombin time (PT) assay. HUVECs were cultured on a µSlide I 0.8 lure for 24h prior to introduction of tumour spheroid media. No PCA was observed from endothelial media passed through the µSlide I 0.8 lure coated with HUVECs. Subsequently, cells were washed with PBS prior to trypsinisation and subsequently with an excess of media before remove the HUVECs cells using yellow tip. Then, cells were centrifuged at 400 x *g* for 3 minutes. The cell pellet was then re-suspended in PBS. The PCA and TFMP was then assessed. The data obtained (Table 3) shows increase in PCA of the HUVECs cells that co-cultured spheroid media from NC s (ES2) and NC s (U87) to 163s (ES2) and 137s (U87). Furthermore, for the detection of TF cell surface expression on HUVECs 50µl of pellet cells was incubated with 5µg of fluorescein isothiocyanate (FITC)-conjugated mouse anti-human CD142/TF antibody as described in section 2.2.31. The quantified TFMP data obtained via flow cytometry showed a distinct subpopulation of HUVECs that had acquired TF expression (Figure 5.24).

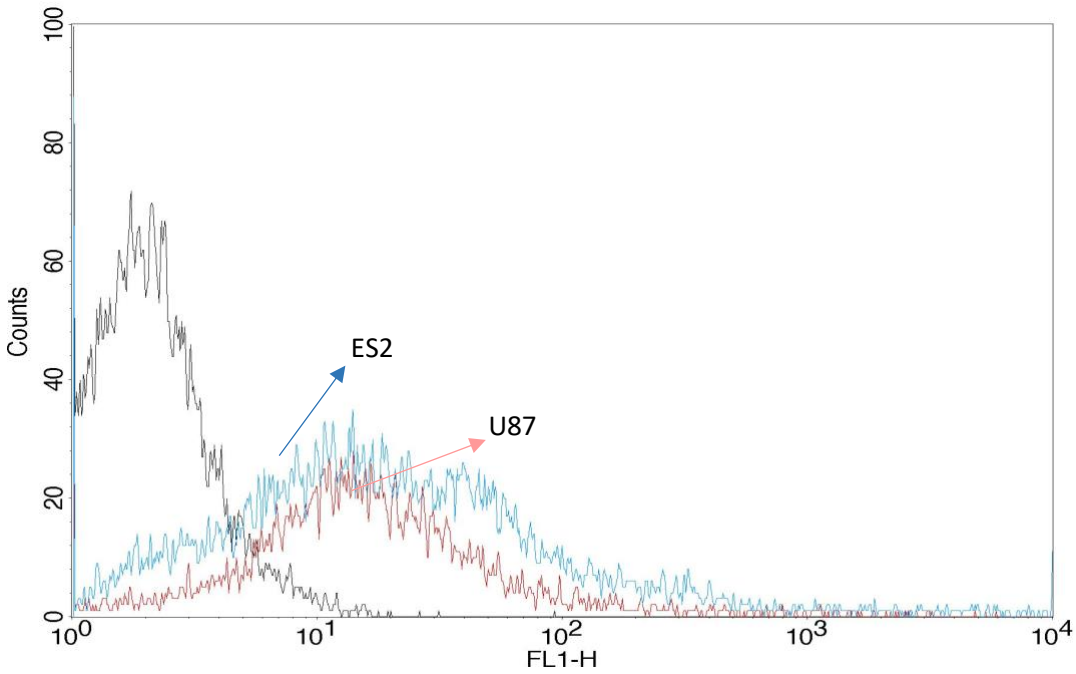

Figure 5.24: Analysis of adhesion of tumour TFMP into HUVECs surface.
Representative histogram plots of TFMP perfused with U87 or ES2 MP rich media for 6h on HUVECS surface compared to HUVECs control. MP were labelled with CD142: FITC antibody from the parent cell.

The flow cytometry data indicated that HUVECs are able to express TFMP after perfused with spheroid media. Furthermore, this indicate that PCA is associated with tumour TFMP as HUVECs exhibit increase in PCA compare to control HUVECs.

5.4.6.5 Adhesion of TFMP on HUVECs endothelial cell surface after under flow condition

Subsequently, HUVECs were then visualised by confocal microscopy (Zeiss LSM710) to confirm the MP adhesion to HUVECs surface (Figure 5.25).

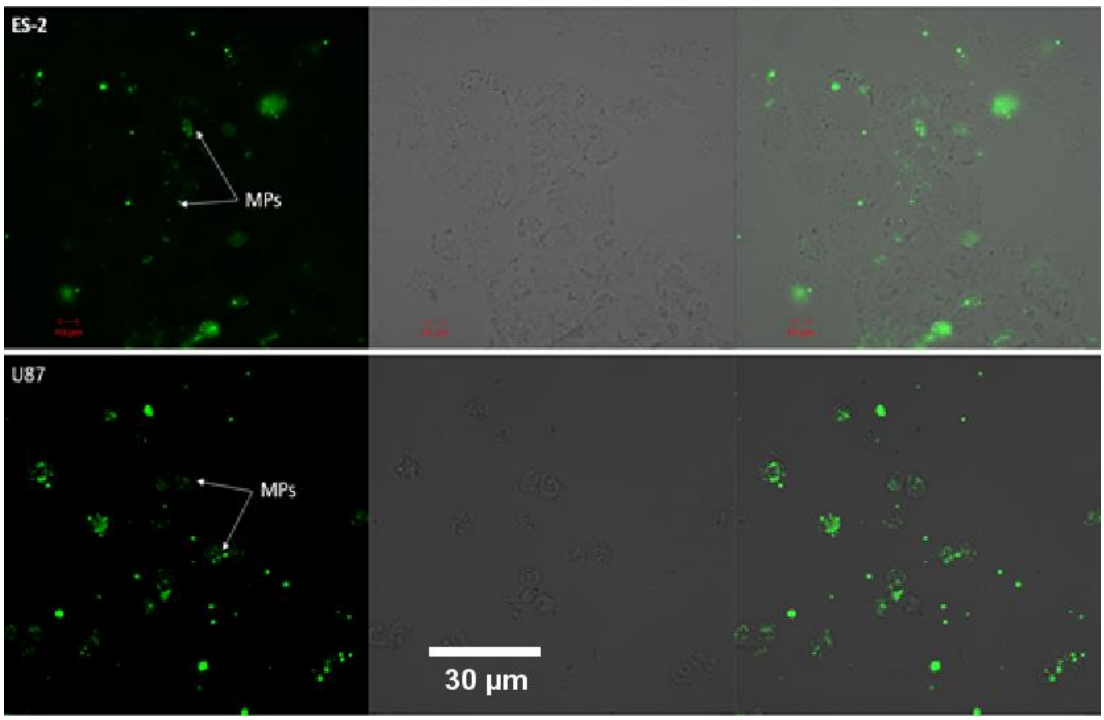

Figure 5.25: Localization of TFMP on HUVECs cell surface after 12hr of continuous perfusion with MP from ES2 and U87 spheroids.
Left and right panels showing the HUVECs acquiring CFSEMP of ES2 and U87 tumour media. Middle panel showing the control HUVECs cultured without MP presence.

5.4.7 Vena 8 model (2D)

Briefly, in order to immobilize the MP, Cellix Vena8 Endothelial+™ biochips were kept under UV for 20 minutes and coated using a standard yellow tip pipette, by dispensing approximately 12 µL of type B 2% v/v gelatine (Sigma Aldrich) into 8 microchannel as described in section 2.2.26 (Figure5.26).

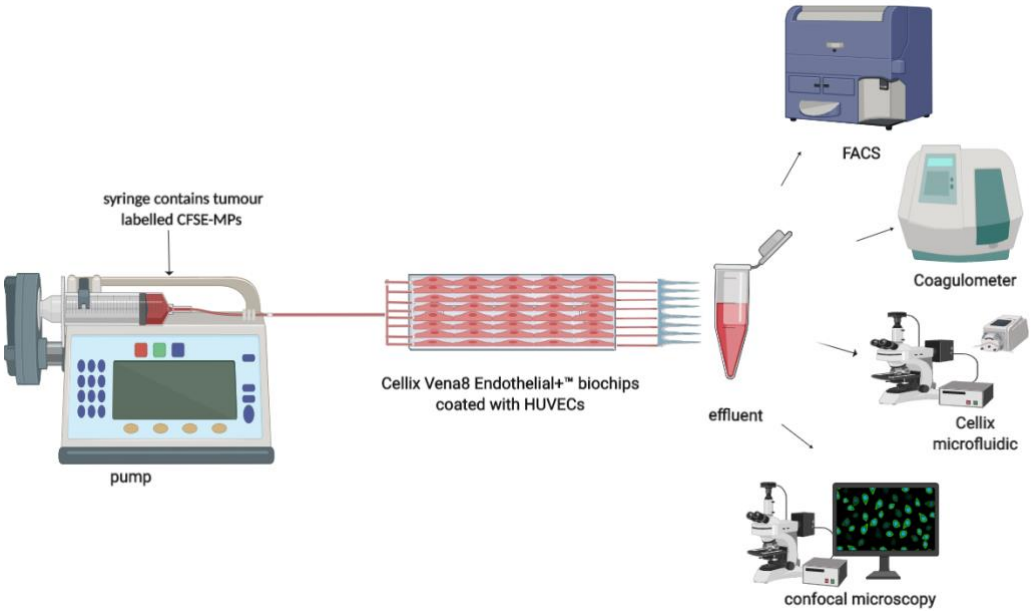

Figure 5.26: Schematic showing the Cellix Vena-8 model.
Schematic showing syringe containing fresh tumour media linked to Cellix vena 8 Endothelial biochip precoated with HUVECs and samples collection tubes. Finally, FACS, coagulometer and confocal microscopy were used to analyse the samples.

Then, the biochip was incubated for 24 hours at 4°C. 5 µl of 1.5×10^6 per 100µl of harvested HUVECs were added into each channel and top up all the reservoirs with 40µL of media. The biochip was incubated in the CO^2 incubator for 24 hrs at 37°C.Then, labelled MP from (AsPC-1, SKOV-3, ES2 and U87) were perfused over the HUVECs for different times (Figure 5.27). Then, PCA, MP quantification and confocal images were assessed to evaluate MP's interaction with HUVECs.

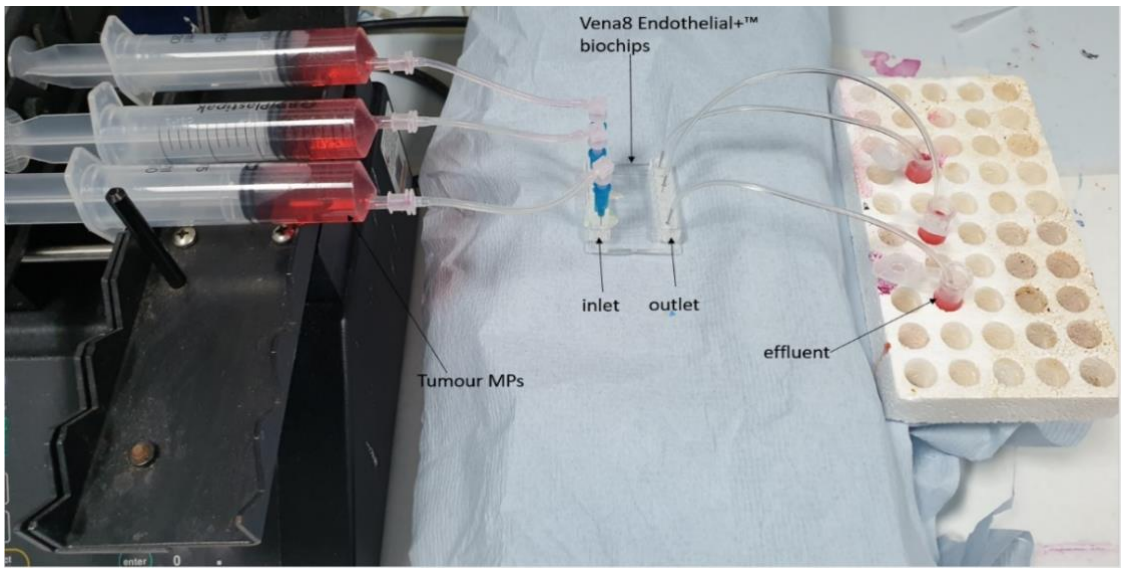

Figure 5.27: Image showing the microfluidic Vena8 Endothelial+™ biochip.
10 ml of conditional tumour MP media was perfused over Cellix Vena8 Endothelial+™ biochip for 24 hours using either constant flow (4µl/min) or a Kima pump (pulsatile flow).

5.4.7.1 Effects of MP perfusion from different cancer cell lines in direct contact with HUVECs on PCA

Labelled MP of AsPC-1, SKOV-3, ES2 and U87 were perfused over Vena8 HUVECs biochip. Briefly, Conditioned tumour media (10 mL) was pipetted into a confluent vena8-biochip of HUVECs and perfused over for 24 Hours. The PCA and CFSEMP was then assessed. AsPC-1, SKOV-3, ES2 and U87 CFSEMP were found to reduce after flow through the HUVECs coated chip. This was accompanied by a reduction in measured PCA. Tumour media was collected from AsPC-1, SKOV3, ES2 and U87 and perfused over HUVECs for 24 hours. The PCA before and after perfusion was assessed. For all flow through experiments on the HUVECs chip the data was collated and an overall trend was observed whereby the number of quantified CFSEMP Overall a consistent negative correlation was observed between CFSEMP and PCA with an average Pearson's rank correlation of -0.79 ± 0.05 (Figure 5.28).

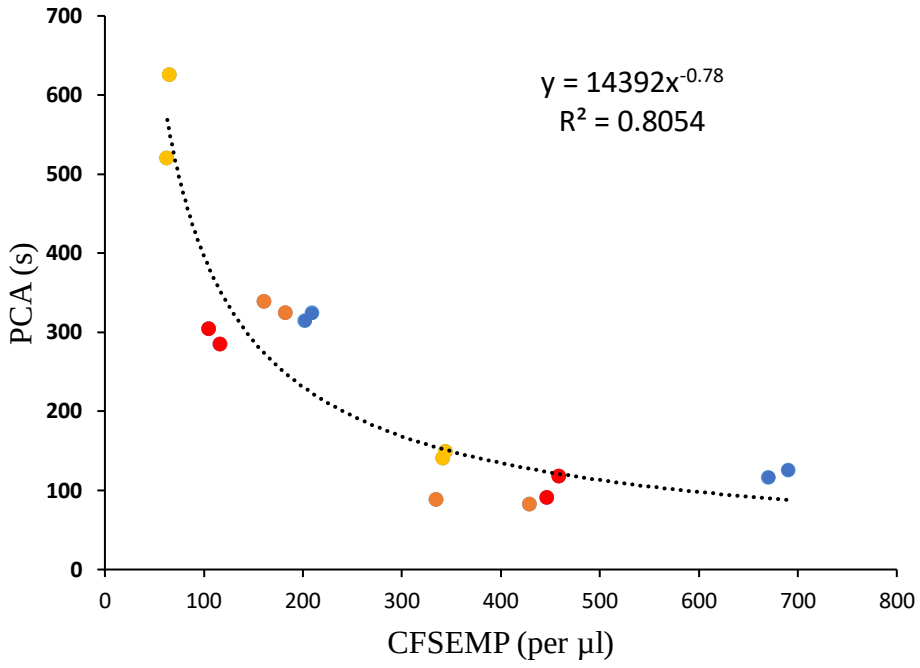

Figure 5.28: Relationship between CFSEMP and PCA.
Chart shows the relationship between CFSEMP and PCA of AsPC-1, ES-2, U87 and SKOV-3 (n=4 for each cell line) media when perfused over HUVECs for 24hrs. AsPC-1(●) (r=-1.0), ES2 (●) (r=-0.96), U87 (●) (r=-0.99), SKOV-3(●) (r=-0.98).

The relationship observed was similar to that observed previously with tumour media and tumour cells where a proportional decrease in either conditioned media or cell number resulted in a decrease in associated PCA in a power relationship. As such the data obtained for conditioned media flowed through a HUVECs coated biochip was log transformed independent

of tumour cell line origin and this showed a linear relationship around the scatterplot. Overall a consistent negative correlation was observed between CFSEMP and PCA with an average Pearson's rank correlation of -0.90 ± 0.05 (Fig 5.29).

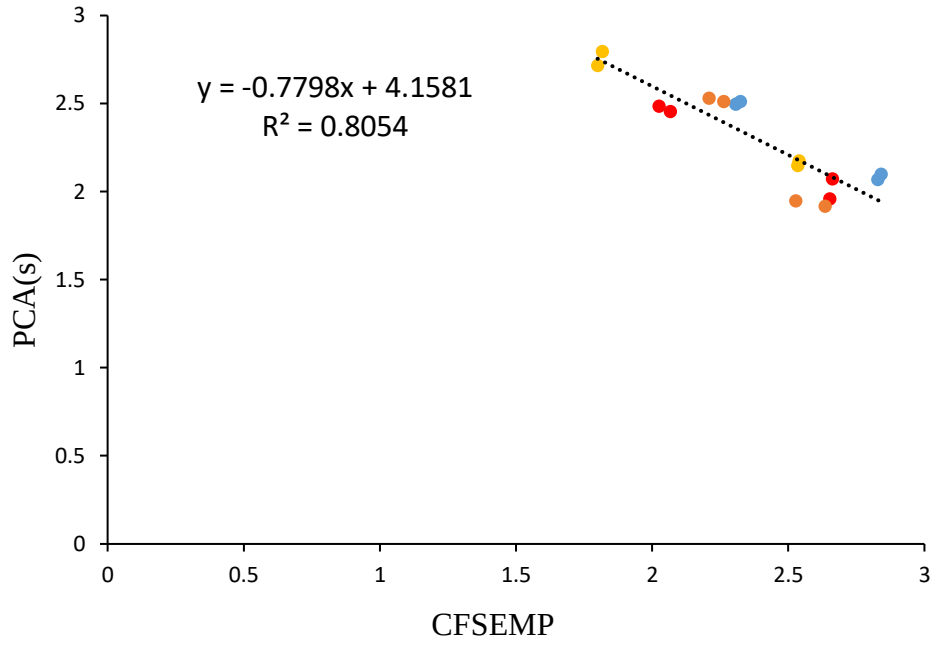

Figure 5.29: Chart showing the relationship between CFSEMP and PCA of AsPC-1, ES2 , U87, SKOV-3. AsPC-1(●), ES2 (●), U87 (●), SKOV-3(●).

Here, a near-linear relationship existed between PCA and CFSEMP on a log10/log10 plot such that high enumerated MP tends to result in short clotting time, R^2= 0.8. (The data is representative of three separate experiments). A general pattern regardless of cell line was detected by which a corresponding reduction of MP was linked with the original concentration. The relationship observed was generally significant.

5.4.7.2 Ability of tumour MP from different cancer cells to incorporate to HUVECs

5.4.7.2.1 Assess the interaction of tumour MP with HUVECs by Cellix

Next, in order to assess interactions between tumour MP and endothelial cells (HUVECs) under flow culture conditions, disposable Vena8 Endothelial (Cellix), were coated with HUVECs as described in section 2.2.27. The biochip connected to the Kima pump (Cellix) with shear stress at 450µl/min for 6 min, followed by 5 min of absence of flow. The flow chamber was then connected to the Mirus Evo Nanopump (Cellix) and the channels were rinsed three times with 25µl of media prior to each experiment, and MP adhesion was initiated by the addition of

CFSEMP supernatant and unlabelled MP as well. Interaction of MP was recorded every second under a shear stress of 1 dyne/cm2 in phase contrast and the settings were equal in all conditions (exposure time 344 ms, magnification 32×) for 5 minutes (Figure 5.30).

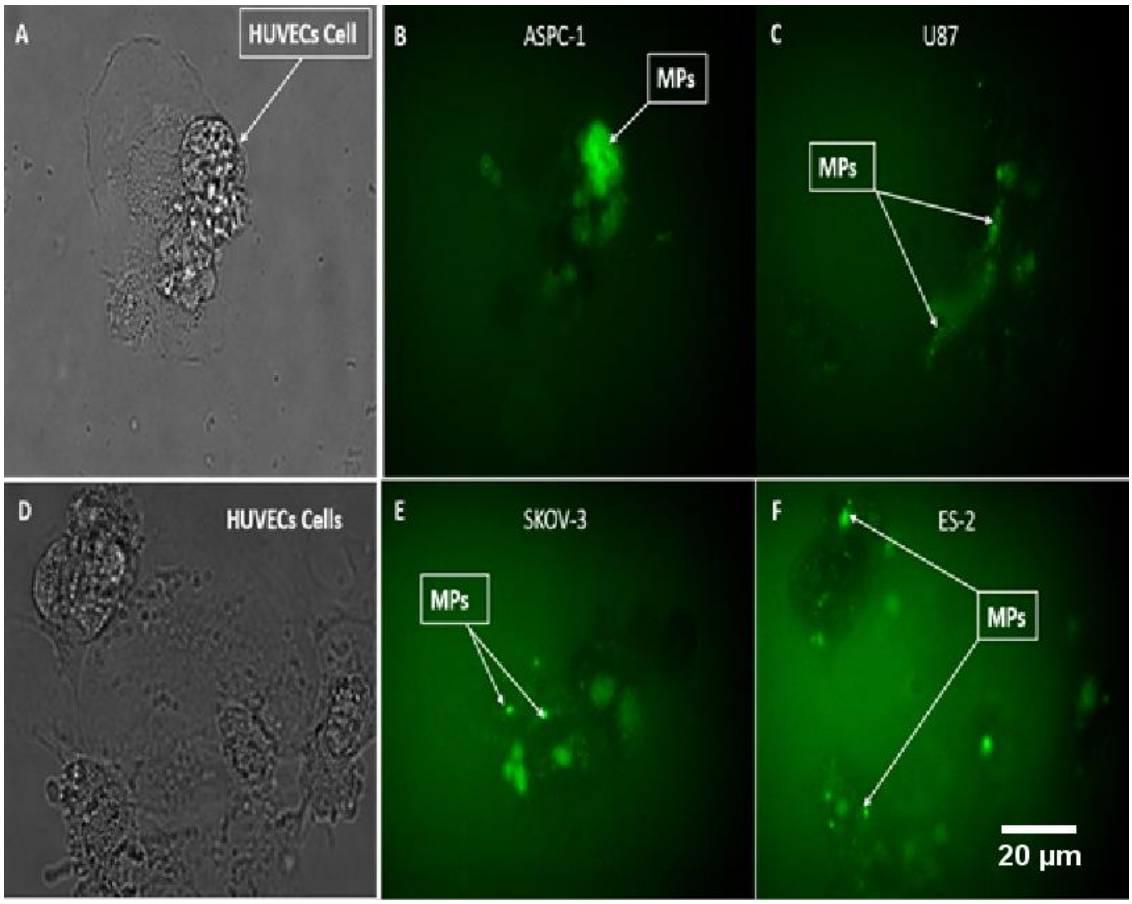

Figure 5.30: Accumulations of fluorescently labelled MP on HUVECs cells.
(a) HUVECs cells cultured on the Vena8 Endothelial+™ biochip without labelled MP. (b) AsPC-1 MP labelled with CFSE were flowed through a Vena8 Endothelial+™ biochip pre-coated with a confluent monolayer of HUVECs and imaged using a CELLIX imaging system. (c) Deposition of U87 MP on HUVECs. (D) HUVECs cells perfused with unlabelled MP. (E-F) Deposition of (SKOV-3 and ES2 respectively) tumour MP on HUVECS. Images representative of n=2 experiments. Media was flowed via Kima pump (pulsatile flow) and the experiments were carried out in a 37°C incubator.

5.4.7.2.2 Confocal

Then, labelled/unlabelled MP were perfused over the HUVECs for 24 hours and PCA, MP quantification and confocal images were assessed to evaluate MP's interaction with HUVECs. Briefly, 10 ml of conditional tumour media of (ASPC-, SKOV-3, ES2 and U87), were perfused over vena-8 HUVECs biochip for 24 hours using HARVARD pump. Then, all biochips were disconnected from the microfluidic system and washed with PBS twice. Then, the MP's interaction with HUVECs were then visualised by confocal microscopy (Zeiss LSM710) to confirm the CELLIX observations (Figure 5.31).

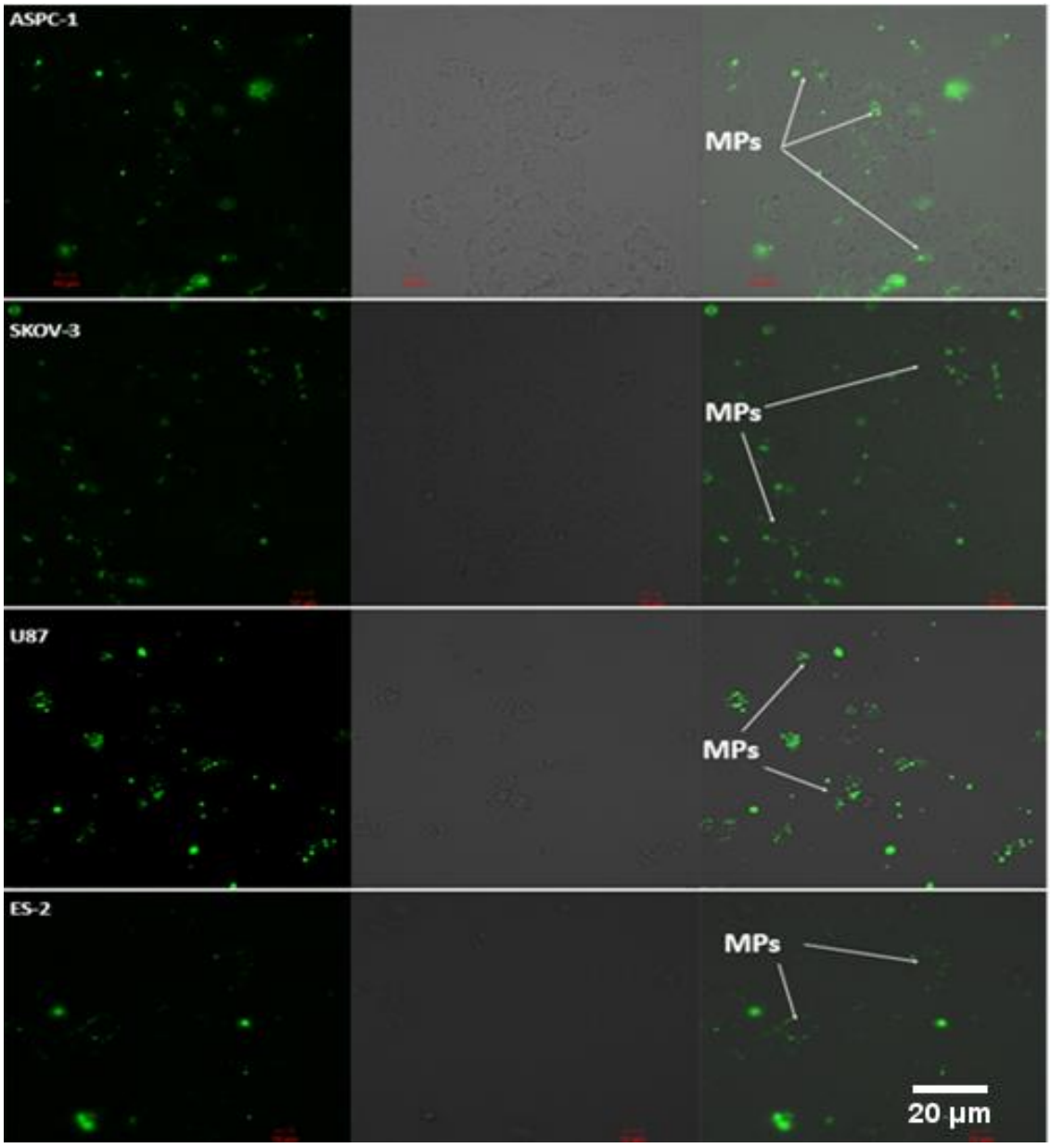

Figure 5.31: Images showing the MP deposition on HUVECs using vena-8 biochip.
Tumour media of AsPC-1, SKOV-3, U87 and ES2 were perfused over HUVECs for 24 hours under flow condition then the interaction was imaged using confocal microscopy. The panel in middle represents the HUVECs cells with unlabelled MP. Media was flowed Harvard syringe pump (constant flow) and the experiments were carried out in a 37°C incubator.

As the interaction between tumour MP and cultured endothelial cells on a vena-8 biochip appeared to happen for 24 hours tumour MP were labelled with CFSE and passed into vena8 microchannel. Conditioned tumour media (10 mL) was pipetted into a confluent chip of HUVECs and perfused over for 24 Hours. The PCA and CFSEMP was then assessed. The data obtained (Table 5.1) shows a reduction in PCA of the conditioned media from 126s (AsPC-1) to 325s 149s (SKOV-3) to 521s and 113s (U87) to 305s and 89s (ES2) to 339s (Figure 5.32).

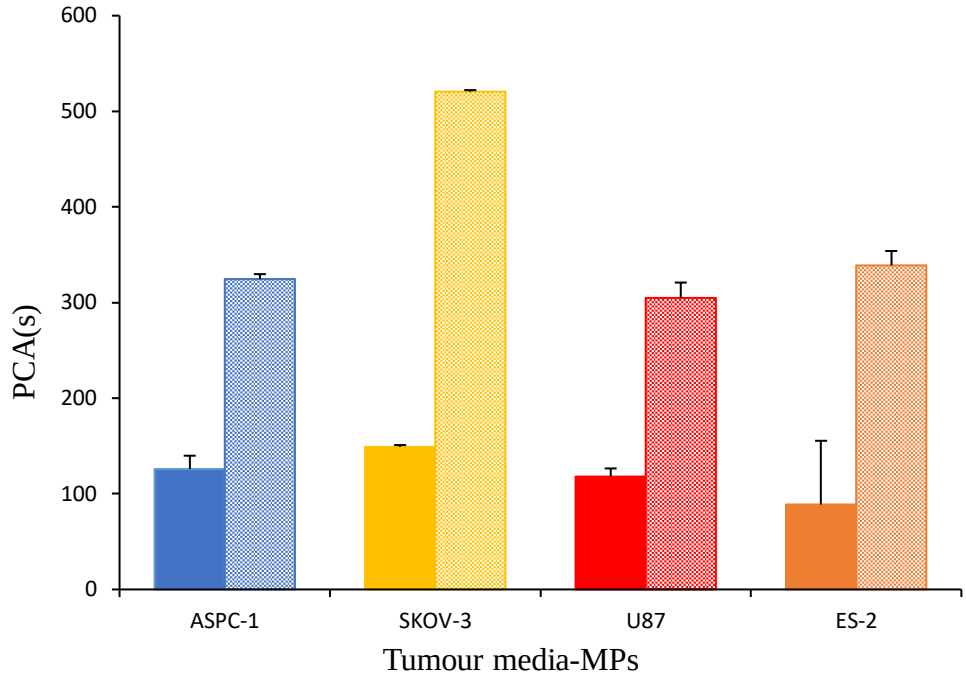

Figure 5.32: Chart showing the PCA of tumour MP pre and post perfusion HUVECs vena-8 biochip. Data representative of three independent experiments. Pre-test filled, post-test non-filled. Error bars representing ±SD of two independent experiments.

Table 5.2: Table showing the MP count versus the PCA before and after incubation with HUVECs biochip.

Pre-test	MP (per µl)	PCA (s)
AsPC-1	691±14	126±7
SKOV-3	345±2	149±6
U87	459±9	118±20
ES2	335±66	89±5
Post-test	MP	PCA (s)
AsPC-1	210±5	325±7
SKOV-3	63±2	521±74
U87	106±8	305±14
ES2	161±15	339±10

Conditioned media added to an empty tissue culture flask in the same way showed no loss of PCA. The quantified CFSEMP data obtained via flow cytometry showed a significant reduction in the number of detected MP. The loss of PCA through 24 hours of incubation of MP rich conditioned media suggests attraction of tumour MP to HUVECs. The flow cytometry data indicated significant loss of CFSEMP through this time which may indicate that the loss of PCA

is MP associated. Moreover, the data obtained from Cellix and confocal indicated that MP could interact and deposit on HUVECs via flow condition.

To investigate the effects of a cytotoxic agent on the interaction between tumour MP and HUVECs DOX was used. Initially the minimum concentration of DOX that would have an effect on cell viability was determined using a cell proliferation assay (MTS). Various concentration of DOX were used on U87, ES-2 and HUVECs in order to determine the optimal concentration (Figures 5.33 to 5.35). A concentration of 0.75mM was selected as an effect (decrease) of cell viability was observed at this concentration on all cell lines, lower concentrations had no effect whereas higher concentrations resulted in an increased loss of viability of all cell lines.

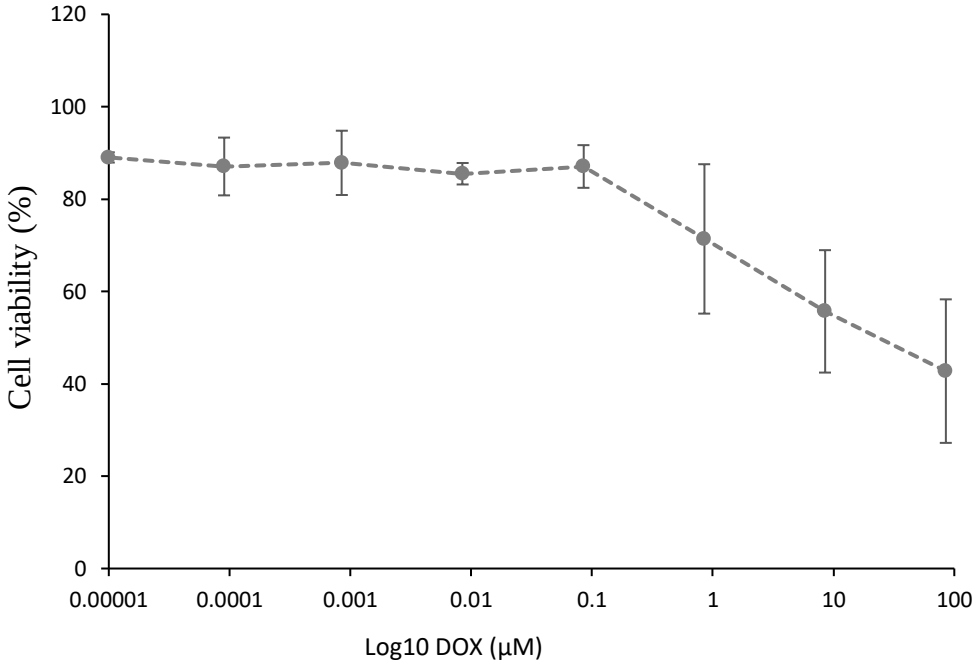

Figure 5.33: The effect of DOX treatment on the cell proliferation of HUVECs for 24 h.

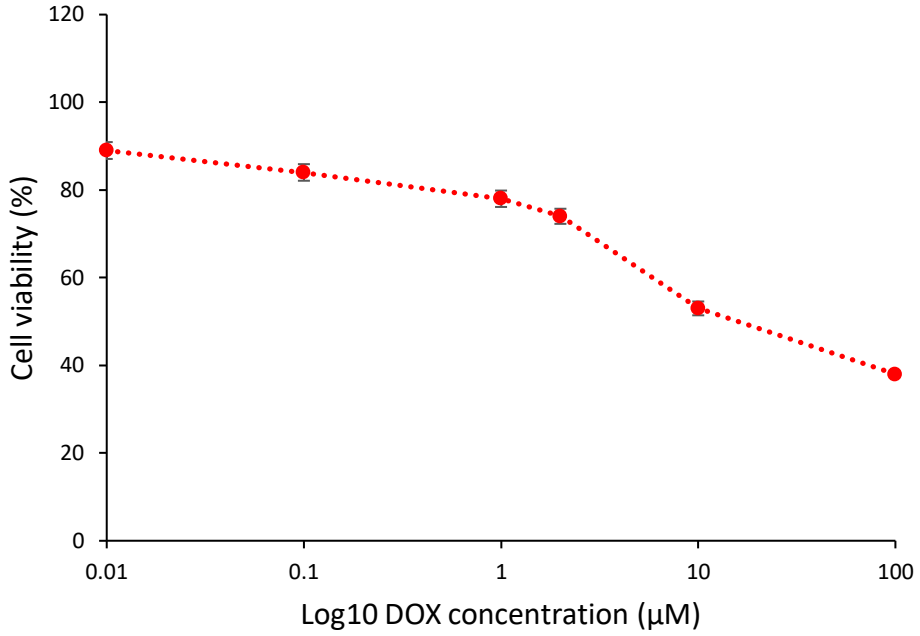

Figure 5.34 The effect of DOX treatment on the cell proliferation of U87 cancer cell line for 24 h.

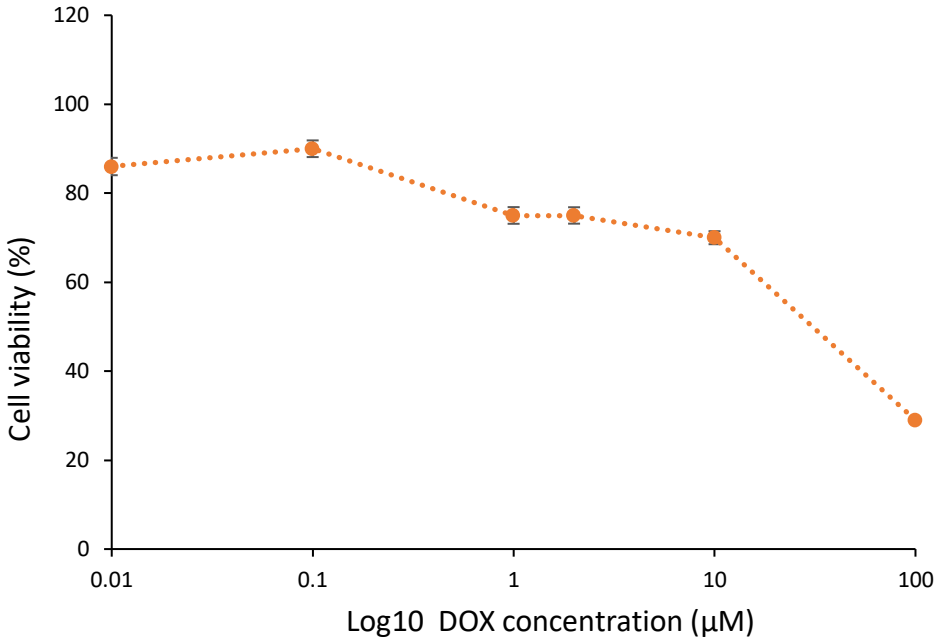

Figure 5.35: The effect of DOX treatment on the cell proliferation of ES2 cancer cell line for 24 h.

Further experiments were carried using the methods detailed previously (Chapter 4). Briefly, U87 and ES-2 tumour spheroids were formed and then transferred into 3D Ibidi chips which was then linked to a µ-slide leuer containing a monolayer of HUVECs. Media with or without the addition of DOX (0.75µM) was then flowed across the spheroids and linked HUVECs and

then collected and analysed (PCA and TFMP) every hour for 6h and HUVECs were then harvested from the ibidi µ–Slide III 3D following overnight flow and analysed for PCA and TF expression.

A continual loss of TFMP and PCA was observed in the collected media over the 6h window for both U87 and ES-2 (Figs 5.36 and 5.37) and the presence of DOX in the media had no effect on either loss of TFMP or loss of PCA.

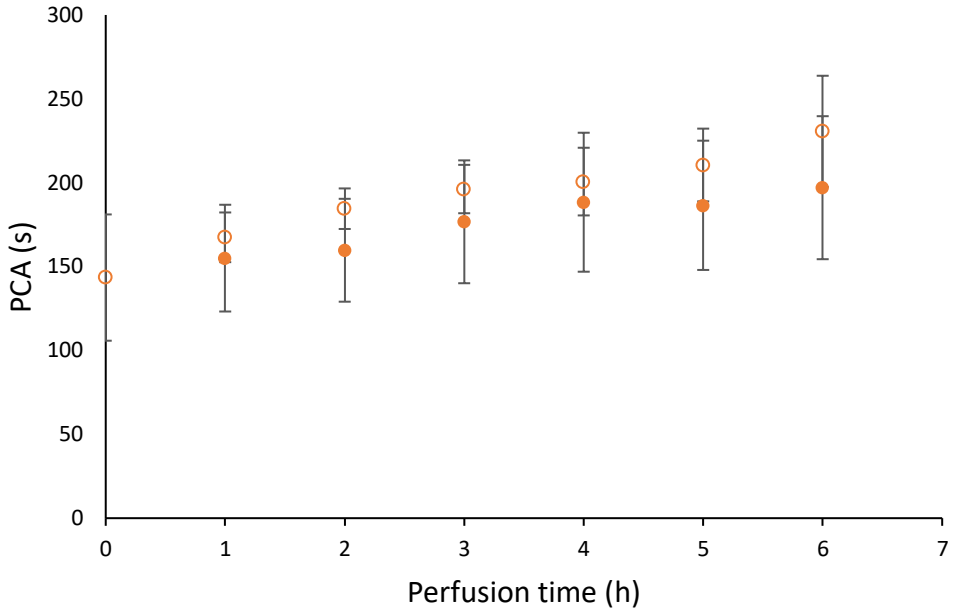

Figure 5.36: PCA of media samples of ES2 spheroids collected through the dual chip model. no DOX filled, DOX unfilled. N=6.Error bars are SD.

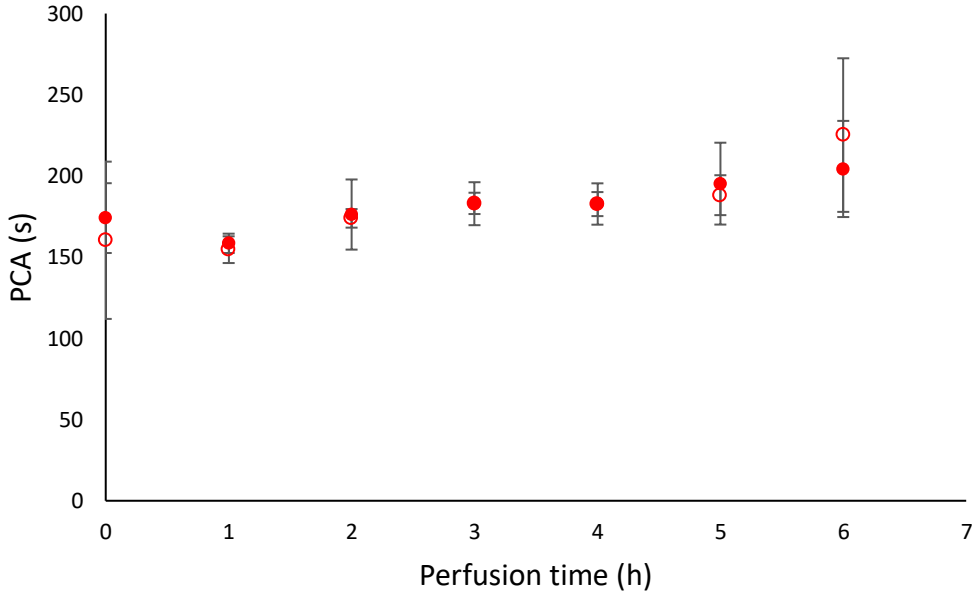

Figure 5.37: PCA of media samples of U87 spheroids collected through the dual chip model.

no DOX filled, DOX unfilled. N=6.Error bars are SD.

The relationship between PCA and concentration of TFMP observed in the collected media showed a correlation which was unaltered by the presence of DOX (Figure 5.38). Overall a consistent negative correlation was observed between TFMP and PCA with an average Pearson's rank correlation of -0.85 ± 0.05.

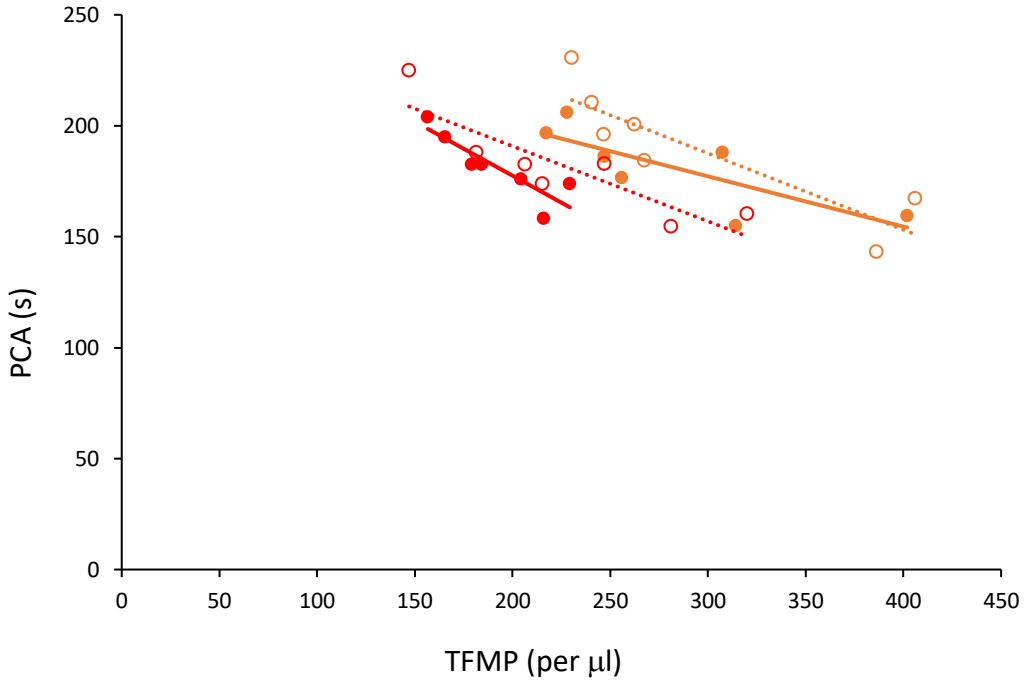

Figure 5.38: average TFMP and associated average PCA of media.
ES2 no DOX (orange circle filled, r=-0.78) ES-2 DOX (orange circle unfilled, r=-0.88), U87 no DOX (red circle filled, r=-0.88) and U87 DOX (red circle unfilled, r=-0.87).

To further confirm this relationship the loss of PCA and loss of TFMP was calculated as a percentage of the initial values prior to the start of the experiments. Again, a negative correlation was observed (Figure. 5.39, r=-0.70) for all data, independent of time.

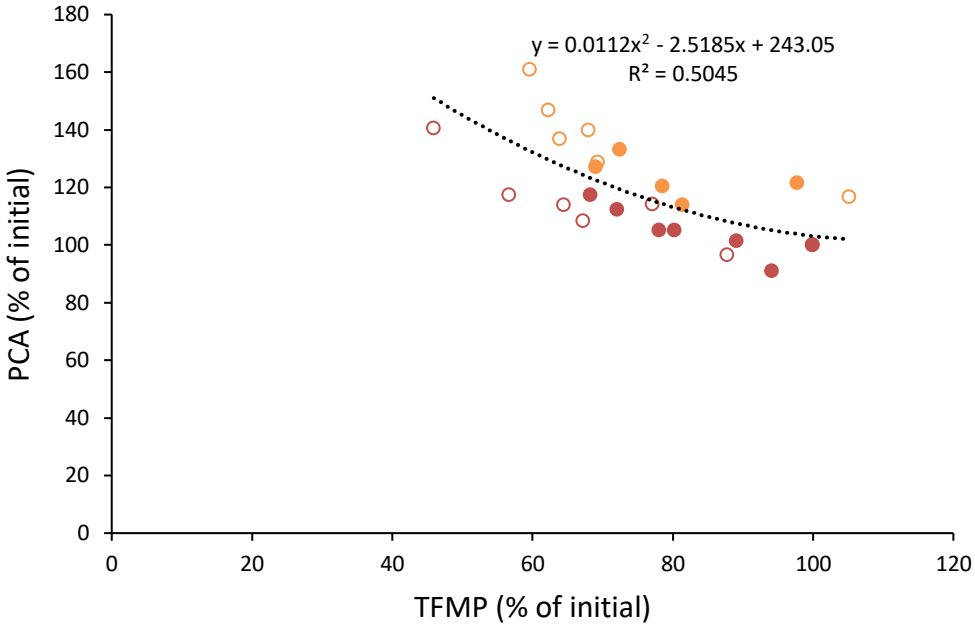

Figure 5.39: data as a % of initial values, independent of time.
ES2 no DOX (Orange circle filled), ES2 DOX (Orange circle unfilled), U87 no DOX (red circle filled), U87 DOX (red circle unfilled).

Having observed no effect on loss of PCA or TFMP in the presence of DOX a further series of experiments were undertaken in which the HUVECs could be harvested at the completion of each experiment and analyzed. Firstly, TFMP and PCA was assessed and again a gradual loss of TFMP and PCA was observed across a series of independent experiments. The largest reduction in TFMP concentration was generally observed within the first 3h where an approximate loss of 50% of TFMP was observed, following this a plateau was seen from 4-6h where less TFMP per hour were lost suggesting a saturation of binding sites on HUVECs may have occurred (Figure 5.40). This is most pronounced for ES-2 where there is practically no further loss of MP from 3-6h, whereas the U87 TFMP continue to slowly decline. There are two possible mechanisms for MP interaction with HUVECs, one being a direct incorporation within the cell membrane (fusion) and the other being a receptor-mediated interaction. The plateau of ES-2 TFMP from 3-6 suggests the latter is true and a saturation of binding sites has occurred.

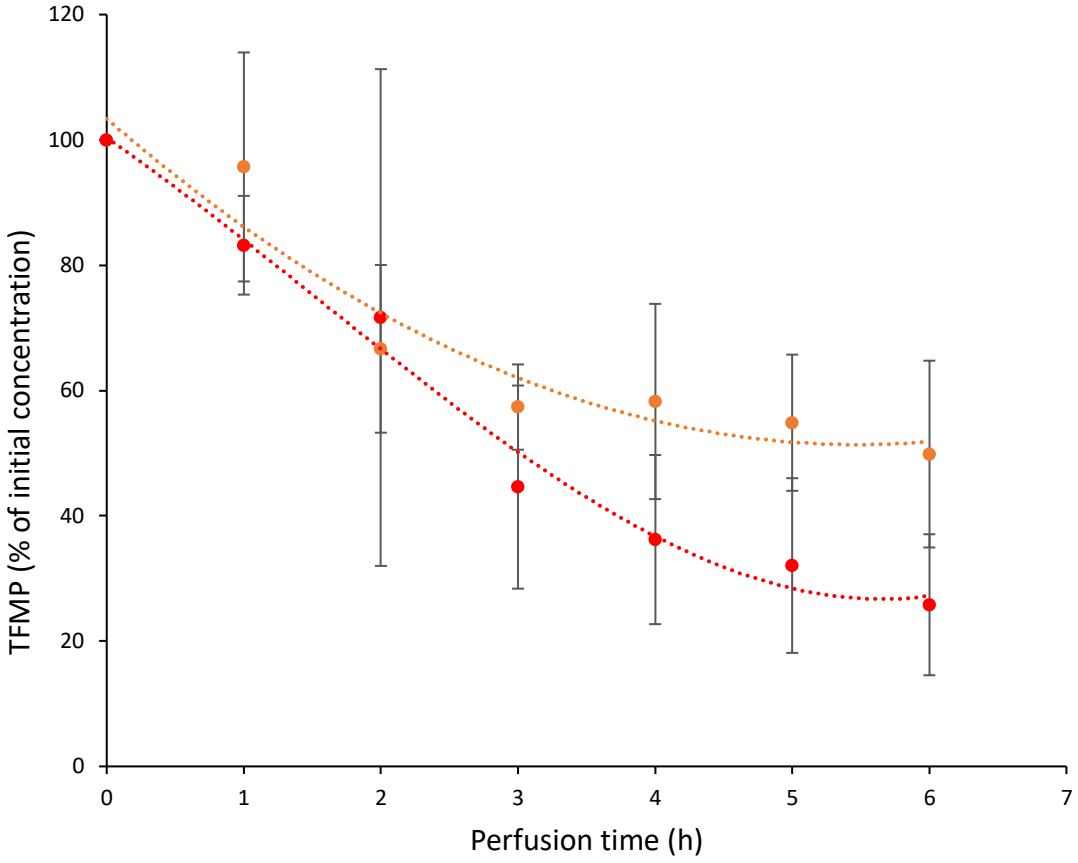

Figure 5.40: Loss of TFMP (expressed as % of initial concentration and averaged) from ES2 (orange circle) or U87 (red circle) spheroid media perfused with HUVECs for 6h in the presence of DOX (0,75mM, n=5 independent experiments).

A concurrent loss of PCA associated with the loss of TFMP was also observed (Figure 5.41) and the relationship between loss of PCA and loss of TFMP was again consistent with TFMP being responsible for PCA (r=-0.87, Figure 5.42).

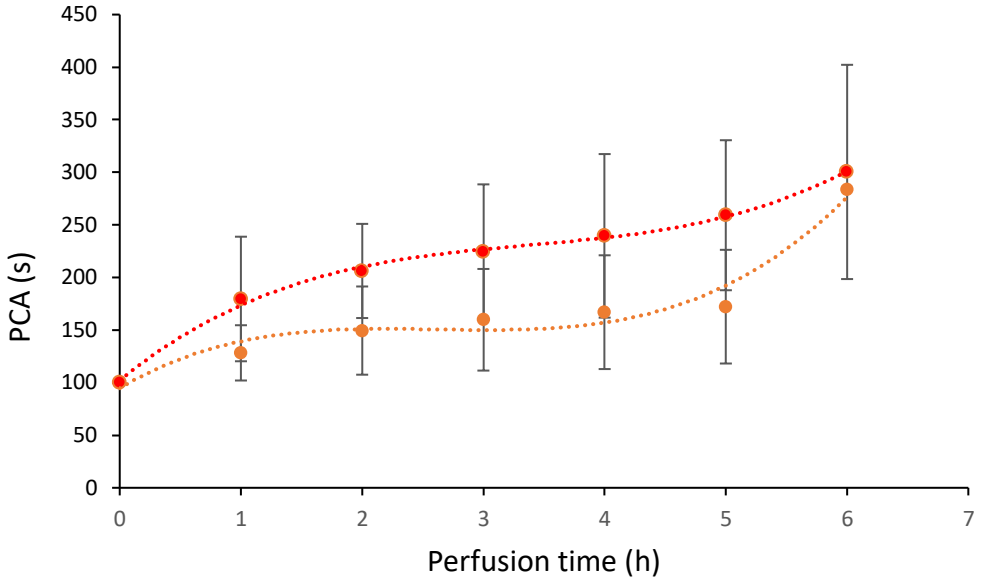

Figure 5.41: PCA (as determined by PT assay) of effluent media after flow over HUVECs in the presence of 0.75mM DOX.
ES2 (orange circle), U87(red circle), average (SD) of 5 independent experiments.

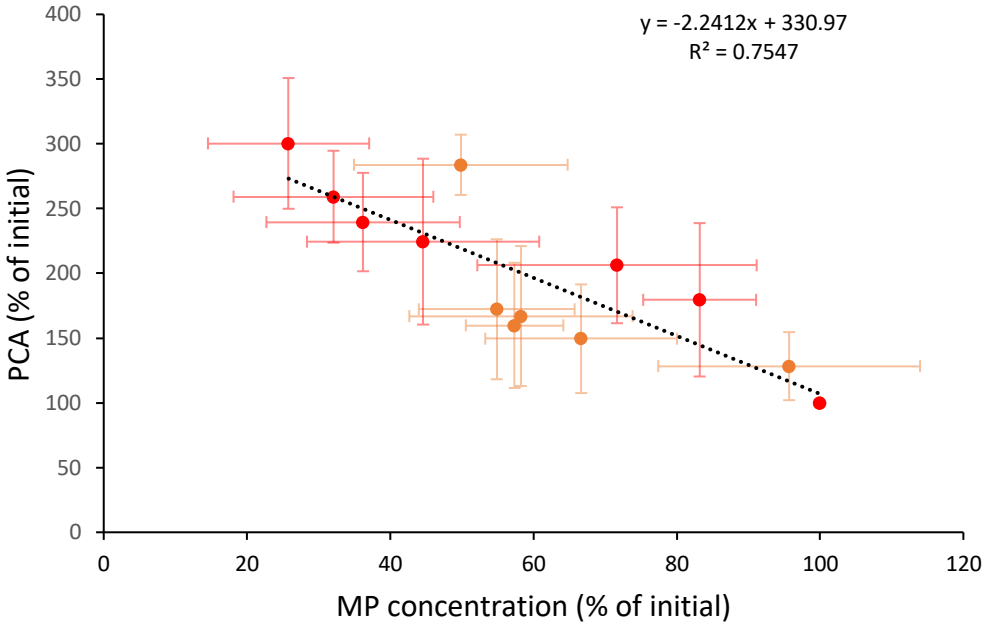

Figure 5.42: The relationship between loss of PCA and loss of TFMP from media collected after perfusion with HUVECs from tumour spheroid 3D culture in the presence of DOX (0.75mM).

Finally, HUVECs from these experiments were then harvested and analysed for PCA via the PT assay. Control chips containing HUVECs were subjected to flow without the presence of tumour spheroids in the proceeding 3D Ibidi chip. DOX controls are described as no DOX within the dual chip setup and finally the same experiments in the presence of DOX were all run in parallel on five separate occasions. The PCA of HUVECs was shown to be significantly higher than HUVECs controls when tumour media from the spheroids was flowed for 24h

(Figure 5.43). Furthermore, in the presence of DOX the HUVECs were shown to have a significantly increased PCA over both the control HUVECs and the no DOX (but tumour media) conditions.

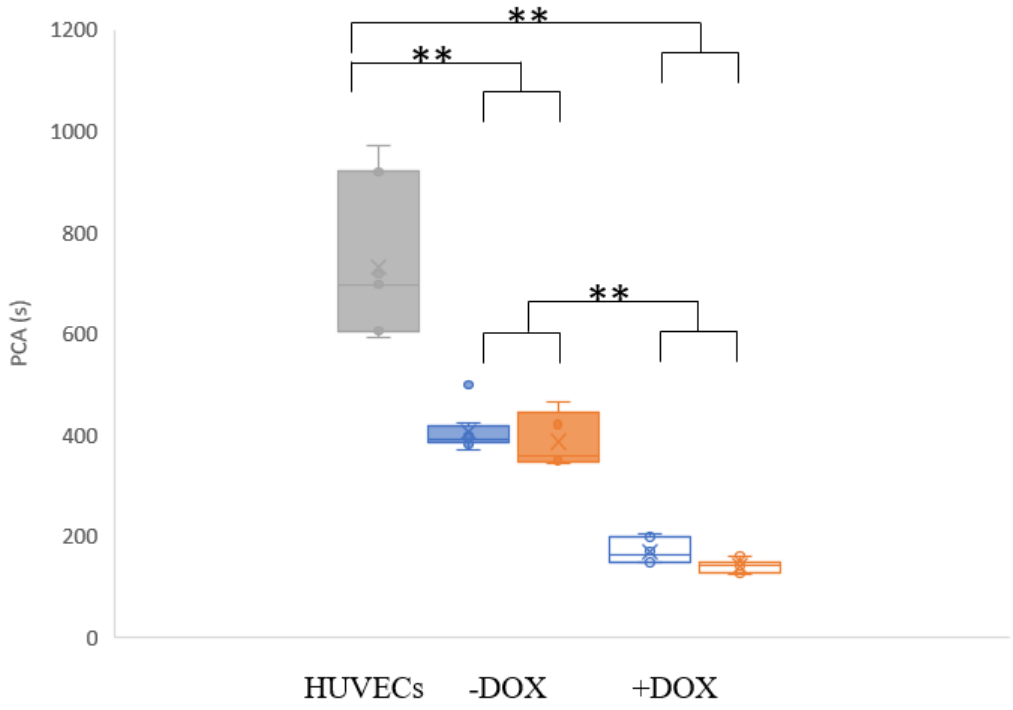

Figure 5.43: PCA of HUVECs harvested after 24 h of flow from (grey) blank, coated 3D chips, ES-2 or U87 spheroid 3D chip without DOX (filled) and ES-2 or U87 in the presence of DOX (0.75 µM, unfilled).** $p < 0.01$.

The viability of HUVECs after 24h flow with tumour spheroid MP with or without DOX was assessed by trypan blue exclusion. The viability of HUVECs in the absence of DOX was 88.5±3.4% whereas in the presence of DOX the viability was decreased to 69.3±4.0%. In static conditions the viability of HUVECs in the presence of DOX was found to be 77.6±6.0%. This increased loss of viability under flow conditions could be due to the fact the DOX is perfused over the HUVECs at a constant concentration rather than being added at a single time and thus is constantly replenished. Another factor to consider is the concentration of DOX that comes into contact with the HUVECs is unknown as the tumour spheroids are exposed first in the dual chip model.

5.5 Discussion

MP are suspected to mediate a comorbidity of various forms of cancer and may underlay a major problem in clinical practice - the tendency to induce VTE in patients. MP are shed from tumours, reach the blood stream and induce the coagulation of platelets and the generation of thromboses(Meikle et al, 2017). As it was found in previous chapters, MP are often associated

with TF, a protein that facilitates the interaction of MP with components of the thrombin/factor VII pathway that leads to clotting (Repetto & De Re, 2017). Of course, such clots can close up flow in certain blood vessels, so that the associated tissues are cut off from oxygen and nutrient supply and will die off (Kalaria et al, 2018). If a thrombosis detaches from its place of formation and reaches the lung or the heart, potentially lethal complications can result. Thus, understanding how MP interact with blood vessels, specifically, with the endothelial cells that constitute the lining of the vessel, is of significant importance. The goal of this chapter was therefore to further elucidate how MP from various cancer cell lines interact with endothelial cells in culture; the interaction of MP from various tumour cell lines with HUVECs was analysed, using in vitro flow chambers and microscopy assays, in addition to flow cytometry and coagulation assays introduced in previous chapters.

It has been reported in previous studies that MP from the UMSCC81B cells induced PCA, in co-cultivated HUVEC cells when TF was also expressed (Adesanya et al, 2017). This assay was performed in a static environment within a culture flask. In other words, MP were given ample time to interact with HUVECs; importantly, MP mediated PCA in this assay may have induced TF expression within the HUVEC cells. However, the human body is a very different environment, and especially within blood vessels, which are the sites of VTE formation, blood is in constant flow. Therefore, in this study, HUVEC cells seeded in flow chambers was used as a proxy for the lining of human blood vessels. Cell cultures used for the generation of MP were ES2, U87, SKOV-3 and AsPC-1; these cell lines were used in two dimensions, while ES2 and U87 were also used to generate MP from spheroid cultures in three dimensions. The experiments were repeated with setups from different manufacturers. The cancer cell lines were fluorescently labelled with CFSE, so that any MP shed from those cells would also be fluorescent. That way, adhesion process of MP on non-labelled HUVECs could be followed by fluorescent and confocal microscopy. Importantly, it was found that the supernatant medium that contained the MP showed less particles and required longer CT after it was used to perfuse HUVECs, which suggests that the MP interact with and adhere to those cells. Importantly, adhesion of MP to HUVEC cells did not compromise the integrity of the cellular monolayer, suggesting that adhesion of those MP does not lead to mechanical damages or adverse cellular reactions. Interestingly, several recent studies suggest that the interaction of TFMP with a cell layer can induce the phosphorylation of downstream targets, such as p42/p44 MAPK and Akt in HUVECs (Van den Berg et al, 2009); moreover, A549 MP also stimulate the expression of IL-8, VCAM and ICAM *m*RNA (Rautou et al, 2011; Wysoczynski & Ratajczak, 2009). Also, MP from the human cancer lines A549, A431, DLD-1 display an ectopically activated EGFR; upon uptake by endothelial cells, EGFR-dependent responses - MAPK and Akt

activation, for example - become enhanced (Al-Nedawi et al, 2009). Moreover, VEGF is expressed and VEGFR-2 is activated. In addition, MP from glioblastoma trigger PCA in hypoxic HUVECs via Par-2 signalling (Svensson et al, 2011). These findings suggest that MP do not simply passively adhere to the target cells, but indeed induce several cellular and biochemical reactions. Such a mechanism might also explain how HUVECs can themselves produce MP and TF and secrete them into the medium after interacting with MP from cancer cell lines. This would, subsequently, aid the formation of thrombosis and blood clots even without the presence of a significant number of MP from tumour cells. It would be interesting to assess whether perfusion of HUVECs with MP-containing supernatant from 2D or 3D cancer cells activates downstream EGFR targets, such as components of the Akt/MAPK or PI3K pathway. This could be combined with analysis using confocal microscopy whether MP interact with endocytic markers in HUVEC cells, which would suggest MP become endocytosed, as this cellular mechanism is part of the EGFR pathway in several different contexts (Barbieri et al, 2016). Interestingly, MP derived from red blood cells have been shown to be endocytosed by pulmonary endothelial cells, suggesting that MP do not just bind to the cell surface, but that they can become internalized (Kim et al, 2018); importantly, activation of vascular endothelial cells by MP requires caveolin, which points at the possibility that endocytosis is required for MP to activate downstream signalling responses (Andrews & Rizzo, 2016).

The first important step was to see whether the cell surface labelling with CFSE left MP functional. It was found that cells incubated with CFSE can give fluorescent particles into the medium for several days and possibly longer; however, when counting the fluorescent particles using flow cytometry or FACS, day two saw the largest number of MP in the medium. Moreover, the MP number decreased towards day 5 (Figure 5.1). This could suggest that cells have a certain time window in which they release MP into the medium. Still, it is less clear whether the MP found in the supernatant are functional, or whether they are artefacts, for example, fragments of apoptotic cells. In addition, the cells may display a significant amount of autofluorescence, and therefore not measure MP, but normal cell surface fluorescence without any labelling *per se*. Importantly, however, when testing unlabelled MP from AsPC-1 cells in flow cytometry, only 0.8% of cells showed up as fluorescent vs. 29.9% after CFSE labelling (Figure 5.2). That is a ca. 37 - 38 times higher amount of fluorescence, or in other words, approximately 2.7% of MP fluorescence from AsPC-1 cells come from auto fluorescence. Furthermore, a figure 5.3 shows, when using TF antibodies on MP, the antibody signals behaved similar to the CFSE signal, suggesting that the MP carry TFs and are functional. Importantly, CFSE labelled MP can indeed elicit biological reactions, as the CFSE labelling intensity correlated with the PCA of MP. The higher the amount of fluorescent signal, the

shorter the coagulation time. This suggests that the CFSE label does not interfere with the functionality and activity of MP. The observed fluorescence intensity in particles from cancer cell culture supernatants is not due to artefacts.

Moreover, the labelled CFSEMP seem functional, as the PCA increased with increasing CFSEMP number. Data obtained from (Figure 5.5 a) appears as if the PCA increases towards higher CFSEMP numbers in an exponential manner; yet, since lower and higher MP concentrations are constituted by different cell lines, we could also be looking at two different linear decreases. More datapoints would be needed to figure out the exact shape of the line. As the same graph shows a completely linear shape when using double logarithmic scales (Figure 5.5 b) - suggesting that a 10x larger MP number means a ten-time increased in PCA - we could be looking at a truly linear decrease. What it does show is that clotting speed depends on the concentration of MP, suggesting the exponential curve for a first order reaction. However, even though having more precision would be commendable, it may not be needed for the purpose of this study, as our hypothesis is that higher MP concentrations lead to faster clotting time thus increase the PCA. No matter whether we have an exponential curve or a linear curve, both versions point at the same observation: the more MP there are, the faster the clotting. In addition, the CFSE labelling does not reduce the MP functionality. Taken together, CFSE does seem to be a good way of measuring MP, as autofluorescence is low, the MP numbers correlate with the presence of TF, and the MP are able to induce clotting in a PT assay.

Do tumour MP that carry TF play a role in VTE? We know from previous experiments that tumour MP interact with endothelial cells in static culture, where they can act at the surface of blood vessels. Importantly, we found out that the interaction is specific to endothelial cells as MP cultured with non-endothelial cell lines didn't show any interaction (Figure 5.15).

In this study, it was demonstrated that MP released from tumour spheroids interact with endothelial cells under flow conditions in a dual microfluidic chip setup. Labelled MP were shown to associate with HUVECs under hemodynamic flow conditions
in a time dependent manner after first adherence to HUVEC surfaces in a static state. The correlation of loss of PCA and reduction in detected labelled MP when tumour media was perfused over HUVECs under flow suggests direct evidence for PCA being determined by MP concentration and also that MP are lost due to their adhesion with the HUVECs. When conditioned media was perfused into control chips coated with gelatin but without HUVECs showed no loss of MP or PCA through the experiments; consequently, the observed loss can be attributed to the interaction with HUVECs.

Accordingly, HUVECs grown under flow show orientation along that flow. This is more closely related to the situation in blood vessels, compared to static adhesion conditions. It was found that MP number correlated to PCA after passing the biochip coated with HUVECs. Overall a consistent negative correlation was observed between CFSEMP and PCA with an average Pearson's rank correlation of r = -0.76 ± 0.05 (Figure 5.9). Similarly, negative correlation was observed between CFSEMP and PCA with an average Pearson's rank correlation of r = -0.79 ± 0.05 using log10 scale (Figure 5.10). The presence of CFSEMP on HUVECs within the microfluidic chip after tumour MP were perfused over the cells was clearly demonstrated in figures 5.25,5.30 and 5.31 using fluorescence and confocal microscopy.

Interestingly, HUVECs acquire PCA from tumour media, as the clotting time of a solution passed over HUVEC cells is increased when the endothelial cells were previously incubated with tumour media, compared to incubation with media without MP. Does this mean HUVECs now actively produce MP, or are we just regaining the MP stuck on the cell surface from the previous incubation with cancer cell supernatant? The biochemical EGFR studies mentioned above would suggest that HUVEC cells themselves indeed acquire coagulant activities. Importantly, when flooding blank medium (without MP) over HUVECs, no PCA is observed in the effluent. However, if the same HUVEC cells are then perfused with tumour MP, washed in PBS and resuspended, the resulting medium after resuspension of the HUVEC cells shows enhanced PCA, and TF antibody show positive staining in cell flow cytometry.

MP need a minimum of time to interact with HUVECs in a functionally significant manner. If cancer cell supernatants are perfused over HUVEC cells for 10 seconds, the effluent shows no loss in PCA. This remains true even when using multiple 10 second perfusion pulses, after which the cells are flooded with empty medium again. Even though 100 second perfusion would lead to a reduction in PCA potential when kept on the HUVECs continuously, 10 cycles of 10 seconds do not show any effect (Figures 5.12 to 5.14). This suggests the MP require a minimum time of more than 10 seconds to interact with their target cells.

Importantly, our observations essentially do not change if we derive the MP from spheroids instead of two-dimensional culture. The longer the medium has been incubated over the HUVECs, the slower the clotting time and the lower the TFMP number in the effluent, as measured by TF antibodies in flow cytometry.

Moreover, to confirm above results, another flow chamber was used to perfuse an MP containing supernatant across HUVEC cells. MP were either harvested under static conditions from the cancer cell lines, before using them to perfuse HUVEC cells, or MP were harvested

under flow as well. The latter setup is an even closer simulation of the in vivo situation in the human body. A commercial system was used where a pump delivers statically derived MP over HUVECs and then into 8 different channels, so the tumour MP medium can be analysed with FACS, coagulation assay, other microfluidics chambers, confocal microscopy etc. After HUVECs have been perfused with CFSEMP from AsPC-1, SKOV-3, ES2 and U87, the number of MP was reduced and the PCA was decreased in the medium that came out after perfusion - which we would expect (Figures 5.28 and 5.29). As flooding the conditioned MP-medium through an empty biochip (not coated with HUVECs) did not show a reduction, these results suggest that the HUVECs modify the number and potency of the MP, presumably via adherence on their surface. Figure 5.11 confirm the observation. The clotting time appears to be decreasing exponentially with a larger MP number (figures 5.28 and 5.29). The number of data points is large enough to trust the observed shape. As expected, when taking the decadic logarithm of PCA vs. CFSEMP number, there is a linear relationship, although this relationship was significant with an average Pearson's rank correlation of -0.90 ± 0.05 (Figure 5.29).

The data obtained shows the interaction of tumour MP from different cell lines with HUVEC cells in a direct manner using phase contrast and fluorescent microscopy (see figures 5.30 and 5.31). MP definitely adhere to HUVECs. Moreover, the interaction seems to be a stronger adherence to actual cell clusters vs. the sparse cells at the periphery of the HUVEC clusters (Figure 5.31). It would be interesting to label MP from different cell lines in different colours and see whether they all adhere in the same way, or whether there are differences. The advantage of such an assay would be that it is done in the same HUVEC culture, and thus, the adhesive behaviours of different MP could be directly compared. It would also be interesting to see whether there are adhesive differences based on the clustering or confluences of the HUVEC cells in the clusters. Using confocal microscopy, MP from ES2, U87, SKOV-3 and AsPC-1 adhering to HUVEC cells as well was clearly observed. The observed MP tended to precipitate in different ways; some formed larger clusters, others were more evenly distributed throughout the cell surface. Some MP also bind more readily to the surface of HUVECs than others. As mentioned above, different colour labels with the same HUVEC cells would be interesting to observe.

These data suggesting that MP actively modulate the behaviour of HUVECs. Wysoczynsk et al. (2009) report that murine LL-2 and human A549 derived MP induced phosphorylation of MAPKp42/44 and AKT in HUVECs and they observed that stimulation of HUVECs with A549 - derived MP upregulated expression of mRNA for IL-8, VCAM, and ICAM (Wysoczynski & Ratajczak, 2009). Moreover, Khalid Al-Nedawi et al. (2009) report that MP produced by human

cancer cells (A431, A549, DLD-1) harbouring activated epidermal growth factor receptor (EGFR) can be taken up by cultured endothelial cells, in which they cause EGFR-dependent responses, including activation of MAPK and Akt pathways and triggers endogenous expression of VEGF, followed by the activation of VEGFR-2 (Al-Nedawi et al, 2009). Furthermore, TFMP derived from glioblastoma cells were found to trigger TF/VIIa–dependent via activation of PAR-2 signalling on hypoxic HUVEC cells (Svensson et al, 2011).

Chemotherapy has been known to significantly increase the risk for VTE in cancer patients. Based on the literature and the results from this study, there are several mechanisms by which the application of chemotherapy drugs leads to an increased tendency for the factorVII/platelet-based coagulation cascade to be activated is via cytotoxicity of the drug. Drugs can either interfere with intra- and intercellular biochemical signalling pathways involved in blood clotting, stimulate the release of MP and TF, or lead to the apoptosis of cells that subsequently release MP into the blood. As thrombosis form inside the blood vessels, and as we have seen previously in our study that HUVEC cells can be stimulated to produce MP on their own and release them into the bloodstream, we first tested the effects of Dox on HUVEC cells *in vitro*. Dox interferes with the DNA replication process by blocking topoisomerases, which leads to the inhibition of cell division. As cancer cells proliferate more strongly than other cells, blocking the process of DNA replication will inhibit tumour cells from spreading. Moreover, blocking cell division can be toxic to the cell, and Dox therefore destroys cancer cells. The drug's interference with the DNA replication process, however, can also affect non-dividing cells by interfering with mitochondria which are actively dividing in non-mitotic cells; Dox leads to the accumulation of double strand breaks in those organelles, which induces the cells to undergo apoptosis, releasing MP in the process. As Dox has been described to attack non-cancer cells like cardiomyocytes, it is entirely conceivable that Dox may affect endothelial cells, in this case, HUVEC cells (Mitry & Edwards, 2016). Indeed, Dox has been known not only for its cardiac, but also vascular toxicity (Wojcik et al, 2015).

Chemotherapy is an independent risk factor for VTE in cancer patients. Here we showed that TFMP, released from 3D tumour spheroids under flow are lost from the media and this effect is associated with a transfer to endothelial cells whose PCA increased in the presence of tumour MP and then increased further in the presence of doxorubicin. We have previously shown that tumour MP are able to bind to endothelial cells and transfer or enhance the PCA of endothelial cells in static and flow conditions (Adesanya et al, 2017; Algarni et al, 2019) and here we demonstrate that the presence of a cytotoxic agent increased further the PCA of endothelial cells when exposed to tumour MP. The average loss of MP over the HUVEC layer was similar but slightly enhanced in the presence of dox compared to no dox. As the dox concentration

used was selected as low as possible to cause an effect of the tumour spheroids and HUVECs the increased PCA of HUVECs harvested after 24 perfusions can be attributed to a loss of viability rather than changes in MP binding.

Doxorubicin treatment of tumour spheroids resulted in an enhanced PCA of an endothelial cell layer under flow. This increased PCA was not MP associated but due to the presence of doxorubicin within the media which reduced HUVECs viability by 20% and could have relevance to the mechanism by which cancer patients undergoing chemotherapy have an increased risk of VTE.

Since Dox reduces cell survival in a similar manner between HUVEC and cancer cell lines (Figures 5.33 to 5.35), it implies that chemotherapy with Dox has side effects that limits its use in cancer patients. Indeed, this is what people have observed; however, there are several compounds that can be used to protect vascular cells, for example, Gingerol or Nicorandil (Al-Abbasi et al, 2016; Chen et al, 2019). Interestingly, Gingerol appears to protect the vasculature by counteracting Dox mediated vascular relaxation (Al-Abbasi et al, 2016). This underscores another important point: even though higher concentrations of Dox led to a lower rate of both HUVEC and cancer cell survival, it does not mean that Dox employs its vascular toxicity by the same mechanisms by which it destroys cancer cells. Sometimes, drugs have additional effects that are not obvious from cell culture alone. It would therefore add to the quality of the study if the findings from cell culture would be tested *in vivo* in a model organism such as mice; this would also open the door to genetic tools with which genes can be mutated and MP can be labelled. Moreover, the tumour environment can be targeted in three dimensions, and there are more cell types that can show a reaction to Dox (Cappetta et al, 2018). Taken together, the best way to proceed is likely to first characterize the formation of MP in culture with or without Dox, analysing potential cellular and biological mechanisms, and subsequently expand the studies into a 3D tumour model *in vivo*.

There is one important caveat to the whole microfluidics experimental setup; in *vivo*, endothelial cells have a glycocalyx on their surface that protects the cells from mechanic stress but may also play a role in coagulation and platelet and MP adhesion. HUVEC cells in *vitro* form a much thinner calyx; this is significant, as the calyx is likely important for the uptake of microparticles by the cell surface (Möckl et al, 2017). In addition, Limitations would be the use of *in vitro* systems to mimic *in vivo*. The use of HUVECS as an endothelial model is not without limitations (Medina-Leyte et al, 2020). Using media rather the more complex blood simplifies the model, but blood would no doubt clot without heparin which wouldn't work.

Chapter 6 General Discussion

MP have emerged as key players that mediate the invasiveness of tumour cells, as they can facilitate communication between cancer cells and the stroma, i.e. the tissue environment that can host primary and secondary tumours (Gopal et al, 2017). Thus, MP often accompany the development of cancer in the body, and they are often released into the blood stream. Besides their oncogenic function, they constitute an additional problem for the body, as a high concentration of MP in the blood vessels can lead to the development of VTE, likely via triggering the platelet derived coagulation cascade, which leads to the formation of blood clots (Falange et al, 2017). Moreover, cancer treatment via cytotoxic chemotherapy often increases the risk for the generation of VTE, presumably due to apoptotic cells releasing a high concentration of MP into the blood (Chaari et al, 2014). However, the development of VTE is difficult to study in cancer patients, as the heterogenous nature of tumours and the varying stages patients may all influence the effect of MP on cancer developments. This study therefore set out to systematically study the formation of MP in cancer cell lines and the effect of chemotherapeutic drugs in that process. Specifically, the aim was to establish a model for the PCA of MP in cancer, based on the investigation and characterization of MP derived from media conditioned by various cancer cell lines and their effect on HUVECs under static and flow conditions. This study also included experiments to show whether TF was present on the measured microparticles. TF is one of the main factors involved in the induction of the coagulation cascade and could thus play an instrumental role in the promotion and formation of VTEs (Date et al, 2017). Studies have shown that once endothelial cells are activated, the expression of coagulation inhibitors like thrombomodulin is downregulated, while cell surface expression of TF is increased, priming the blood vessels for coagulation by transforming endothelial cells into a hypercoagulable state (Moore et al, 1987). Importantly, the presence of TFMP in cancer patients does not always correlate with an enhanced risk for VTE. It is possible that there is a connection between inflammation, TFMP and VTE, as enhanced inflammation increases the risk for VTE in pancreatic cancer, and inflammation leads to the generation of mononuclear phagocytes that may contribute to coagulation as well. In addition to TF, the presentation of phospholipids like phosphatidylserine on the surface of MP or that of activated endothelium may be required for coagulation to occur as well (Date et al, 2017). In the experiments conducted in this study, the clotting time (CT) was used as a proxy for PCA. Cell suspensions or supernatants from cell culture were incubated with a thrombin containing solution, and the time until clots could be observed was measured. The higher the PCA, the smaller the CT.

It was found that PCA of cancer-cell suspensions and cell-free media exposed to the same cell line strongly correlate in a positive manner (Figure 3.1). These observations suggest that cells mediate clotting via secreted components, which could be proteins or other biomolecules with coagulant activity or entire MP; importantly, the PCA of cell-free medium are smaller than the PCA within the cell cultures, suggesting that the cell membrane provides additional factors that aid in the coagulation process. Interestingly, there is still a strong linear relationship when comparing the decadic logarithms of both PCA (figure 3.2). The linear correlation when comparing $\log_{10}$of PCA between cell suspensions and cell-free media, suggests that there is an exponential or power-relationship. It is interesting to note that in a murine model, the clotting time increases exponentially as well with increasing concentrations of the clotting inhibitor lactadherin; this suggests that differences in clotting activity can indeed affect clotting time in a logarithmic manner (Tian et al., 2015). More studies are likely required for the exact characterization of the mechanism that is responsible for differences in PCA across various cell cultures. As clotting time depends on the clotting rate, and since first order reactions - where the reaction speed depends in a logarithmic manner on the concentration of one reactant, the linear logarithmic relationship in this case suggests that the PCA depends on the concentration of a common factor - for example, the presence of tissue factor in the medium, or an enhanced phosphatidyl serine (PS) concentration within the membrane of MP (Orfeo et al, 2005). There is one potential caveat to these observations: the observation that $\log_{10}$(Meikle et al) values are correlated in a linear manner suggests that absolute CTs would be correlated in an exponential or logarithmic manner, yet we find a strong linear dependence of the absolute values. It is possible that the absolute values can also be correlated via an exponential relationship, though it is difficult to distinguish between both linear and exponential relationship, as in figure 3.1 and figure 3.2, the majority of values are clustered at the low and high end of the PCA range. More specifically, there are no values between 100s and 150s for the cell culture PCA and 300s and 400s for the cell-free medium PCA. It was confirmed that the presence of cell bodies is not required for clotting to occur *per se*. We can also appreciate that different cell cultures yield different PCA (see figure 3.1), suggesting that the generation of MP - their concentration, their association with TF, the presence of any other pro-coagulant molecules like PS on its membrane, or any other structural or biochemical factor, depends on the type of cancer cell. Indeed, Papageorgiou et al. (2019) found that Myeloma plasma cells promote coagulation via the release of TFMP, and phosphatidylserine (PS) in the cell membrane has been implicated as an enabler of platelet-mediated coagulation, suggesting that PS can contribute to the clotting process (Katelowitz et al. 2017). Moreover, the presence of systemic inflammation may enhance clotting activity of TFMP via neutrophil-mediated processes (Date et al, 2017; Hisada et al, 2020).

Interestingly, if we compare the clotting time from 2D cell cultures - a confluent monolayer - with 3D cell cultures - so-called tumour spheroids, it was found that the PCA are related (compare figure 3.1 and figure 3.5). This suggests that differences in PCA are intrinsic to the cell line and not necessarily the organization of the cells in space and within coherent aggregates of cells. However, when observing the shape of spheroids, it appeared that a higher PCA was correlated with a more compact spheroid. This is slightly surprising, as one might hypothesize that the less compact a cell aggregate is, its 'looseness' would also lead to MP being more easily severed from the cell membrane. Another possibility is that biomolecules, such as TF, which are expressed at the cell surface and facilitate coagulation, are simply more concentrated in more adherent spheroids. Moreover, secretion of MP may be a highly regulated process that functions better in a well-structured cell. Alternatively, one might expect the two cell lines with the strongest PCA - X and Y - to form the most compact spheroids.

As the PCA in the supernatant from 2D cultures are related to those in 3D cultures - and different across different cell lines - the PCA may not depend on the 3D shape of the spheroids, but on the type of the cell that forms it. Thus, the nature of the cells may influence PCA by influencing the number of MP released, the speed of release, or the concentration of TF and other molecules associated with them. However, it could still be that the shape and size of the 3D spheroids enhance or diminish the PCA potential of any cell line. Thus, it would be interesting to see whether there is a connection between spheroid compaction and the release of MP, which could be observed via time-lapse fluorescence or confocal microscopy (Hisada et al, 2017).

Furthermore, we also find that ultrafiltration and resuspension of the filtrate increase the speed of coagulation. This suggests that TF is physically linked with MP surfaces, because if it was more loosely associated, TF would likely be found in the eluate, not the filtrate, leading to shorter clotting times (Figure 3.14).

Importantly, as we observe in chapter 5, we can label MP with fluorescent dies and retain their functionality; there is a time dependence for the labelling intensity, as two days after labelling, the largest amount of fluorescence intensity could be counted. This is true for AspC-1 cells; similarly, SKOV-3 cancer cell lines were shown same results (Figure 5.4). It is possible that one of the differences between cell lines that leads to differential clotting times is the speed with which MP are released. Whether this is due to different expression levels of those factors important for MP release, or the intracellular organization the cells display. One could use techniques such as *in vivo* confocal time-lapse microscopy of fluorescently marked MP and

differentially labelled cell organelles to get insight into the cell biological mechanism by which MP are budding off, if possible, combined with genetic knockdown studies (Agbani & Poole, 2017; Cocucci & Meldolesi, 2015).

Importantly, when comparing the PCA of AspC-1 and SKOV-3 cells, we can recognize a clear relationship between the CFSEMP and PCA; the higher the CFSEMP concentration, the higher PCA (see figure 5.5). Especially for SKOV-3 cells, this relationship appears to be logarithmic; this suggests, as mentioned above, that a factor like TF or any other molecule associated with MP directs the coagulation speed similar to a first order reaction - the higher the TFMP concentration, the faster the clotting speed; see Mackman (2012) and Date et al. (2017) for a closer discussion of the function of TFMPs in coagulation. Thus, we can indeed take the PCA as a proxy for the MP concentration.

Interestingly, when perfusing a biochip seeded with HUVEC with MP rich media, it was found that the PCA decreased after perfused over HUVECs (Figures 5.9,5.18 and 5.28). This suggests the MP interact with HUVEC cells, but stay attached with them, as their removal from the medium is likely connected to the decrease in PCA within the medium itself. This confirms what has been previously observed - that MP interact with endothelial cells (Myers et al., 2003; Date *et al.*, 2017). It is possible that this interaction leads to endothelial activation, which facilitates the formation of VTEs (Hijmans et al, 2019). Indeed, our confocal microscope showed that fluorescent vesicles adhere to the surface of the HUVEC cells (Figures 5.25 and 5.31).

We also treated both cancer cell lines and HUVEC cells with Dox as an example of a cytotoxic chemotherapy drug with well-known vascular toxicity (Zhang, 2015); Dox inhibits the function of topoisomerases, which interferes with DNA multiplication so much so that DNA becomes fragmented in the process, which is then followed by apoptosis (Zhu et al, 2016). We found that increasing the dose of Dox leads to a reduction of clotting time in almost all cell lines studied. One explanation for this observation is that the destruction of cells leads to an increased release of MP into the medium, which then enhances PCA.

To sum up, in this study two *ex-vitro* chip Microfluidic system was developed, showing that tumour MP released in a complex and appropriate flow state from spheroids bind to endothelial cells. The procoagulant of MP derivative from tumour spheroid was shown to be attached to endothelial cells under flow conditions using dual microfluid setup. The cause of the procoagulant activity in *vitro* was demonstrated by tumour MP.

Future work:

The use of 3D cultures in recent decades has been a major advantage of cancer research. In order to achieve a correct recapitulation of the high complexity of human tumours, better 3D tumour models still are required. In terms of a correct recapitulation of human tumour microscopic environments, the so-called tumour-on-chip devices are among 3D culture systems. MP function and study are unambiguously of scientific importance for diagnostic and prognostic researches. But their usage in therapeutic sites is still far from daily use, owing to their high identification and characteristically difficulties utilising traditional research techniques**.** In this study, the progress made in microfluidic co-culture systems to examine the interaction of MP and HUVECs was described. As powerful tools to research cell to cell interactions, microfluidic modelling is evolving. The advantages of this model are low cost, reproducibility, accessibility and ease of operation. The 3D microfluidic platform allows natural cell environment simulation. In addition, most of these efforts are focused not on developing a universal scheme that replaces existing models with the theoretical proof. In future, efforts should be made to select and combine standard components and the application of them to be more like biological microenvironments within microfluidic chips. The commercially available microfluidic chips can be optimized for generating a wide variety of applications readily available for testing and also for the clinical diagnosis and screening of a personalized medication prescription for patients with cancer. One of the objectives that must be met to bring technology closer to clinical practise and thus to be used at industry level and to approach clinical practice and the market are also the incorporation of single modules to analyze MP into complex lab on chip. In addition, future research will concentrate on the exact mechanism of how tumour MP binding to endothelial cells and the response of endothelial cells to the stimuli in terms of activation, apoptosis, or altered cells surface marker expression. Furthermore, the future study will assess the effects of MP on endothelium inflammation cell and oxidative stress under flow condition. Moreover, A key underlying factor in the cellular effects of MP is the ability to transport, bind and transfer their content into the cells. Therefore, further research is required to establish RNA and protein cargo of MP and their function and their effect on endothelial cell function. Also, additional studies performed on a larger number of cancer cells and using more parameters reflecting hemostasis and activation of endothelial are necessary.

Reference list / Bibliography

Abbott, A. (2003) Cell culture: Biology's new dimension. *Nature*, 424(6951), 870-872.

Abdulkadir, S. A., Carvalhal, G. F., Kaleem, Z., Kisiel, W., Humphrey, P. A., Catalona, W. J. & Milbrandt, J. (2000) Tissue factor expression and angiogenesisin human prostate carcinoma. *Human pathology*, 31(4), 443-447.

Adan, A., Alizada, G., Kiraz, Y., Baran, Y. & Nalbant, A. (2017) Flow cytometry: basic principles and applications. *Critical Reviews in Biotechnology*, 37(2), 163-176.

Ades, S., Gilchrist, S., Holm, A., Libby, K., Cushman, M., Douce, D. & Holmes, C. E. (2017) Venous Thromboembolism Prevention in the Ambulatory Cancer Clinic (VTE-PACC): a Systems-Based, Personalized, Multidisciplinary Program to Increase Venous Thromboembolism (VTE) Risk Assessment, Education and Anticoagulant Prophylaxis in Cancer Outpatients Initiating Therapy. *Blood*, 130.

Adesanya, M. A., Maraveyas, A. & Madden, L. A. (2017) Cancer microvesicles induce tissue factor-related procoagulant activity in endothelial cells in vitro. *Blood Coagulation & Fibrinolysis*, 28(5), 365-372.

Agbani, E. O. & Poole, A. W. (2017) Procoagulant platelets: generation, function, and therapeutic targeting in thrombosis. *Blood, The Journal of the American Society of Hematology*, 130(20), 2171-2179.

Agrahari, V., Agrahari, V., Burnouf, P. A., Chew, C. H. & Burnouf, T. (2019) Extracellular Microvesicles as New Industrial Therapeutic Frontiers. *Trends in Biotechnology*, 37(7), 707-729.

Aharon, A., Tamari, T. & Brenner, B. (2008) Monocyte-derived microparticles and exosomes induce procoagulant and apoptotic effects on endothelial cells. *Thrombosis and Haemostasis*, 100(5), 878-885.

Akazawa-Ogawa, Y., Nagai, H. & Hagihara, Y. (2018) Heat denaturation of the antibody, a multi-domain protein. *Biophysical reviews*, 10(2), 255-258.

Al-Abbasi, F., Alghamdi, E., Baghdadi, M., Alamoudi, A., El-Halawany, A., El-Bassossy, H., Aseeri, A. & Al-Abd, A. (2016) Gingerol synergizes the cytotoxic effects of doxorubicin against liver cancer cells and protects from its vascular toxicity. *Molecules*, 21(7), 886.

Al-Nedawi, K., Meehan, B., Kerbel, R. S., Allison, A. C. & Rak, J. (2009) Endothelial expression of autocrine VEGF upon the uptake of tumor-derived microvesicles containing oncogenic EGFR. *Proceedings of the National Academy of Sciences of the United States of America*, 106(10), 3794-3799.

Alberter, B., Klein, C. A. & Polzer, B. (2016) Single-cell analysis of CTCs with diagnostic precision: opportunities and challenges for personalized medicine. *Expert review of molecular diagnostics*, 16(1), 25-38.

Alcalay, A., Wun, T., Khatri, V., Chew, H. K., Harvey, D., Zhou, H. & White, R. H. (2006) Venous thromboembolism in patients with colorectal cancer: Incidence and effect on survival. *Journal of Clinical Oncology*, 24(7), 1112-1118.

Aleman, M. M., Gardiner, C., Harrison, P. & Wolberg, A. S. (2011) Differential contributions of monocyte- and platelet-derived microparticles towards thrombin generation and fibrin formation and stability. *Journal of Thrombosis and Haemostasis*, 9(11), 2251-2261.

Algarni, A., Greenman, J. & Madden, L. A. (2019) Procoagulant tumor microvesicles attach to endothelial cells on biochips under microfluidic flow. *Biomicrofluidics*, 13(6), 064124.

Andrews, A. M. & Rizzo, V. (2016) Microparticle-induced activation of the vascular endothelium requires caveolin-1/caveolae. *PloS one*, 11(2), e0149272.

Aupeix, K., Hugel, B., Martin, T., Bischoff, P., Lill, H., Pasquali, J.-L. & Freyssinet, J.-M. (1997) The significance of shed membrane particles during programmed cell death in vitro, and in vivo, in HIV-1 infection. *The Journal of clinical investigation*, 99(7), 1546-1554.

Bach, R. R. (2006) Tissue factor encryption. *Arteriosclerosis, thrombosis, and vascular biology*, 26(3), 456-461.

Bar-Joseph, H., Ben-Aharon, I., Tzabari, M., Tsarfaty, G., Stemmer, S. M. & Shalgi, R. (2011) In vivo bioimaging as a novel strategy to detect doxorubicin-induced damage to gonadal blood vessels. *PloS one*, 6(9), e23492.

Barbieri, E., Di Fiore, P. P. & Sigismund, S. (2016) Endocytic control of signaling at the plasma membrane. *Current opinion in cell biology*, 39, 21-27.

Barni, S., Labianca, R., Agnelli, G., Bonizzoni, E., Verso, M., Mandalà, M., Brighenti, M., Petrelli, F., Bianchini, C. & Perrone, T. (2011) Chemotherapy-associated thromboembolic risk in cancer outpatients and effect of nadroparin thromboprophylaxis: results of a retrospective analysis of the PROTECHT study. *Journal of translational medicine*, 9(1), 179.

Barteneva, N. S., Fasler-Kan, E., Bernimoulin, M., Stern, J. N. H., Ponomarev, E. D., Duckett, L. & Vorobjev, I. A. (2013) Circulating microparticles: square the circle. *Bmc Cell Biology*, 14.

Bates, R. C., Edwards, N. S. & Yates, J. D. (2000) Spheroids and cell survival. *Critical Reviews in Oncology Hematology*, 36(2-3), 61-74.

Becker, A., Thakur, B. K., Weiss, J. M., Kim, H. S., Peinado, H. & Lyden, D. (2016) Extracellular Vesicles in Cancer: Cell-to-Cell Mediators of Metastasis. *Cancer Cell*, 30(6), 836-848.

Becker, H. & Gärtner, C. (2008) Polymer microfabrication technologies for microfluidic systems. *Analytical and Bioanalytical Chemistry*, 390(1), 89-111.

Beer, K. B. & Wehman, A. M. (2017) Mechanisms and functions of extracellular vesicle release in vivo-What we can learn from flies and worms. *Cell Adhesion & Migration*, 11(2), 135-150.

Behrens, B. C., Hamilton, T. C., Masuda, H., Grotzinger, K. R., Whangpeng, J., Louie, K. G., Knutsen, T., McKoy, W. M., Young, R. C. & Ozols, R. F. (1987) CHARACTERIZATION OF A CIS-DIAMMINEDICHLOROPLATINUM(II)-RESISTANT HUMAN OVARIAN-CANCER CELL-LINE AND ITS USE IN EVALUATION OF PLATINUM ANALOGS. *Cancer Research*, 47(2), 414-418.

Ben Aharon, I., Bar Joseph, H., Tzabari, M., Shenkman, B., Farzam, N., Levi, M., Shalgi, R., Stemmer, S. M. & Savion, N. (2013) Doxorubicin-Induced Vascular Toxicity - Targeting Potential Pathways May Reduce Procoagulant Activity. *Plos One*, 8(9).

Benam, K. H., Villenave, R., Lucchesi, C., Varone, A., Hubeau, C., Lee, H. H., Alves, S. E., Salmon, M., Ferrante, T. C., Weaver, J. C., Bahinski, A., Hamilton, G. A. & Ingber, D. E. (2016) Small airway-

on-a-chip enables analysis of human lung inflammation and drug responses in vitro. *Nature Methods*, 13(2), 151-+.

Berckmans, R. J., Nieuwland, R., Boing, A. N., Romijn, F., Hack, C. E. & Sturk, A. (2001) Cell-derived microparticles circulate in healthy humans and support low grade thrombin generation. *Thrombosis and Haemostasis*, 85(4), 639-646.

Bersini, S., Jeon, J. S., Dubini, G., Arrigoni, C., Chung, S., Charest, J. L., Moretti, M. & Kamm, R. D. (2014) A microfluidic 3D in vitro model for specificity of breast cancer metastasis to bone. *Biomaterials*, 35(8), 2454-2461.

Bhagat, A. A. S., Hou, H. W., Li, L. D., Lim, C. T. & Han, J. (2011) Pinched flow coupled shear-modulated inertial microfluidics for high-throughput rare blood cell separation. *Lab on a Chip*, 11(11), 1870-1878.

Biro, E., Sturk-Maquelin, K. N., Vogel, G. M. T., Meuleman, D. G., Smit, M. J., Hack, C. E., Sturk, A. & Nieuwland, R. (2003) Human cell-derived microparticles promote thrombus formation in vivo in a tissue factor-dependent manner. *Journal of Thrombosis and Haemostasis*, 1(12), 2561-2568.

Blann, A. D. & Dunmore, S. (2011) Arterial and venous thrombosis in cancer patients. *Cardiology Research and Practice*, 1(1), 394740-11.

Blann, A. D. & Yip, G. Y. H. (1998) The endothelium in atherothrombotic disease: assessment of function, mechanisms and clinical implications. *Blood Coagulation & Fibrinolysis*, 9(4), 297-306.

Blom, J. W., Vanderschoot, J. P. M., Oostindier, M. J., Osanto, S., van der Meer, F. J. M. & Rosendaal, F. R. (2006) Incidence of venous thrombosis in a large cohort of 66 329 cancer patients: results of a record linkage study. *Journal of Thrombosis and Haemostasis*, 4(3), 529-535.

Bower, R., Green, V. L., Kuvshinova, E., Kuvshinov, D., Karsai, L., Crank, S. T., Stafford, N. D. & Greenman, J. (2017) Maintenance of head and neck tumor on-chip: gateway to personalized treatment? *Future Science Oa*, 3(2).

Brandes, A. A., Scelzi, E., Salmistraro, G., Ermani, M., Carollo, C., Berti, F., Zampieri, P., Baiocchi, C. & Fiorentino, M. V. (1997) Incidence and risk of thromboembolism during treatment of high-grade gliomas: a prospective study. *European Journal of Cancer*, 33(10), 1592-1596.

Breslin, S. & O'Driscoll, L. (2013) Three-dimensional cell culture: the missing link in drug discovery. *Drug Discovery Today*, 18(5-6), 240-249.

Brodsky, S. V., Zhang, F., Nasjletti, A. & Goligorsky, M. S. (2004) Endothelium-derived microparticles impair endothelial function in vitro. *American Journal of Physiology-Heart and Circulatory Physiology*, 286(5), H1910-H1915.

Broos, K., Feys, H. B., De Meyer, S. F., Vanhoorelbeke, K. & Deckmyn, H. (2011) Platelets at work in primary hemostasis. *Blood Reviews*, 25(4), 155-167.

Brose, K. & Lee, A. (2008) Cancer-associated thrombosis: prevention and treatment. *Current Oncology*, 15(Suppl 1), S58.

Bucciarelli, P., Martinelli, I., Artoni, A., Passamonti, S. M., Previtali, E., Merati, G., Tripodi, A. & Mannucci, P. M. (2012) Circulating microparticles and risk of venous thromboembolism. *Thrombosis Research*, 129(5), 591-597.

Burnouf, T., Chou, M.-L., Goubran, H., Cognasse, F., Garraud, O. & Seghatchian, J. (2015) An overview of the role of microparticles/microvesicles in blood components: are they clinically beneficial or harmful? *Transfusion and Apheresis Science*, 53(2), 137-145.

Butenas, S., Bouchard, B. A., Brummel-Ziedins, K. E., Parhami-Seren, B. & Mann, K. G. (2005) Tissue factor activity in whole blood. *Blood*, 105(7), 2764-2770.

Caine, G. J., Stonelake, P. S., Lip, G. Y. H. & Kehoe, S. T. (2002) The hypercoagulable state of malignancy: Pathogenesis and current debate. *Neoplasia*, 4(6), 465-473.

Cameron, A. C., Touyz, R. M. & Lang, N. (2016) Vascular Complications of Cancer Chemotherapy. *Canadian Journal of Cardiology*, 32(7), 852-862.

Campello, E., Ilich, A., Simioni, P. & Key, N. S. (2019) The relationship between pancreatic cancer and hypercoagulability: a comprehensive review on epidemiological and biological issues. *British Journal of Cancer*, 121(5), 359-371.

Campello, E., Spiezia, L., Radu, C. M., Bulato, C., Castelli, M., Gavasso, S. & Simioni, P. (2011) Endothelial, platelet, and tissue factor-bearing microparticles in cancer patients with and without venous thromboembolism. *Thrombosis Research*, 127(5), 473-477.

Campello, E., Spiezia, L., Radu, C. M., Bulato, C., Gavasso, S., Tormene, D., Woodhams, B., Dalla Valle, F. & Simioni, P. (2016) Circulating microparticles and the risk of thrombosis in inherited deficiencies of antithrombin, protein C and protein S. *Thrombosis and Haemostasis*, 115(1), 81-88.

Cappetta, D., Urbanek, K., Rossi, F. & De Angelis, A. (2018) Anthracycline cardiotoxicity: new actors on the stage. *Translational Cancer Research*, 7(5), S580-S583.

Cardigan, R. & Green, L. (2015) Thawed and liquid plasma - what do we know? *Vox Sanguinis*, 109(1), 1-10.

Carrier, M., Lazo-Langner, A., Shivakumar, S., Tagalakis, V., Gross, P. L., Blais, N., Butts, C. A. & Crowther, M. (2015) Clinical challenges in patients with cancer-associated thrombosis: Canadian expert consensus recommendations. *Current Oncology*, 22(1), 49-59.

Cekanova, M. & Rathore, K. (2014) Animal models and therapeutic molecular targets of cancer: utility and limitations. *Drug Design Development and Therapy*, 8, 1911-1922.

Chaari, M., Ayadi, I., Rousseau, A., Lefkou, E., Van Dreden, P., Sidibe, F., Ketatni, H., Galea, V., Khaterchi, A. & Bouzguenda, R. (2014) Impact of breast cancer stage, time from diagnosis and chemotherapy on plasma and cellular biomarkers of hypercoagulability. *BMC cancer*, 14(1), 991.

Chen, B., Wu, Y., Ao, Z., Cai, H. W., Nunez, A., Liu, Y. H., Foley, J., Nephew, K., Lu, X. B. & Guo, F. (2019) High-throughput acoustofluidic fabrication of tumor spheroids. *LAB ON A CHIP*, 19(10), 1755-1763.

Chen, C., Skog, J., Hsu, C.-H., Lessard, R. T., Balaj, L., Wurdinger, T., Carter, B. S., Breakefield, X. O., Toner, M. & Irimia, D. (2010a) Microfluidic isolation and transcriptome analysis of serum microvesicles. *Lab on a Chip*, 10(4), 505-511.

Chen, C., Skog, J., Hsu, C. H., Lessard, R. T., Balaj, L., Wurdinger, T., Carter, B. S., Breakefield, X. O., Toner, M. & Irimia, D. (2010b) Microfluidic isolation and transcriptome analysis of serum microvesicles. *Lab on a Chip*, 10(4), 505-511.

Chen, W., Horoszewicz, J., Leong, S., Shimano, T., Penetrante, R., Sanders, W., Berjian, R., Douglass, H., Martin, E. W. & Chu, T. M. (1982) Human pancreatic adenocarcinoma: in vitro and in vivo morphology of a new tumor line established from ascites. *In Vitro Cellular & Developmental Biology-Plant*, 18(1), 24-34.

Chirinos, J. A., Heresi, G. A., Velasquez, H., Jy, W., Jimenez, J. J., Ahn, Y. S., Ahn, E., Horstman, L. L., Soriano, A. O. & Zambrano, J. P. (2005) Elevation of Endothelial Microparticles, Platelets, and Leukocyte Activation in Patients With Venous Thromboembolism. *Journal of the American College of Cardiology*, 45(9), 1467-1471.

Chou, J., Mackman, N., Merrill-Skoloff, G., Pedersen, B., Furie, B. C. & Furie, B. (2004) Hematopoietic cell-derived microparticle tissue factor contributes to fibrin formation during thrombus propagation. *Blood*, 104(10), 3190-3197.

Choudhury, D., Ramsay, W. T., Kiss, R., Willoughby, N. A., Paterson, L. & Kar, A. K. (2012) A 3D mammalian cell separator biochip. *Lab on a Chip*, 12(5), 948-953.

Chu, A. J. (2005) Tissue factor mediates inflammation. *Archives of Biochemistry and Biophysics*, 440(2), 123-132.

Chu, A. J. (2011) Tissue factor, blood coagulation, and beyond: an overview. *International journal of inflammation*, 2011.

Cocucci, E. & Meldolesi, J. (2015) Ectosomes and exosomes: shedding the confusion between extracellular vesicles. *Trends in cell biology*, 25(6), 364-372.

Cointe, S., Judicone, C., Robert, S., Mooberry, M., Poncelet, P., Wauben, M., Nieuwland, R., Key, N., Dignat‐George, F. & Lacroix, R. (2017a) Standardization of microparticle enumeration across different flow cytometry platforms: results of a multicenter collaborative workshop. *Journal of Thrombosis and Haemostasis*, 15(1), 187-193.

Cointe, S., Judicone, C., Robert, S., Mooberry, M. J., Poncelet, P., Wauben, M., Nieuwland, R., Key, N. S., Dignat-George, F. & Lacroix, R. (2017b) Standardization of microparticle enumeration across different flow cytometry platforms: results of a multicenter collaborative workshop. *Journal of Thrombosis and Haemostasis*, 15(1), 187-193.

Combes, V., Simon, A. C., Grau, G. E., Arnoux, D., Camoin, L., Sabatier, F., Mutin, M., Sanmarco, M., Sampol, J. & Dignat-George, F. (1999) In vitro generation of endothelial microparticles and possible prothrombotic activity in patients with lupus anticoagulant. *Journal of Clinical Investigation*, 104(1), 93-102.

Connolly, G. C. & Francis, C. W. (2013) Cancer-associated thrombosis. *ASH Education Program Book*, 2013(1), 684-691.

Connolly, G. C. & Khorana, A. A. (2009) Risk stratification for cancer-associated venous thromboembolism. *Best Practice & Research Clinical Haematology*, 22(1), 35-47.

Connolly, G. C., Phipps, R. P. & Francis, C. W. (2014) Platelets and Cancer-Associated Thrombosis. *Seminars in Oncology*, 41(3), 302-310.

Convery, N. & Gadegaard, N. (2019) 30 years of microfluidics. *Micro and Nano Engineering*.

Costa, E. C., Moreira, A. F., de Melo-Diogo, D., Gaspar, V. M., Carvalho, M. P. & Correia, I. J. (2016) 3D tumor spheroids: an overview on the tools and techniques used for their analysis. *Biotechnology Advances*, 34(8), 1427-1441.

Cote, D. J. & Smith, T. R. (2016) Venous thromboembolism in brain tumor patients. *Journal of Clinical Neuroscience*, 25, 13-18.

Cui, X., Hartanto, Y. & Zhang, H. (2017) Advances in multicellular spheroids formation. *Journal of The Royal Society Interface*, 14(127), 20160877.

Daher, I. N. & Yeh, E. T. H. (2008) Vascular complications of selected cancer therapies. *Nature Clinical Practice Cardiovascular Medicine*, 5(12), 797-805.

Darabi, M. & Kontush, A. (2016) Phosphatidylserine in atherosclerosis. *Current Opinion in Lipidology*, 27(4), 414-420.

Däster, S., Amatruda, N., Calabrese, D., Ivanek, R., Turrini, E., Droeser, R. A., Zajac, P., Fimognari, C., Spagnoli, G. C. & Iezzi, G. (2017) Induction of hypoxia and necrosis in multicellular tumor spheroids is associated with resistance to chemotherapy treatment. *Oncotarget*, 8(1), 1725.

Date, K., Ettelaie, C. & Maraveyas, A. (2017) Tissue factor-bearing microparticles and inflammation: a potential mechanism for the development of venous thromboembolism in cancer. *Journal of Thrombosis and Haemostasis*, 15(12), 2289-2299.

Date, K., Hall, J., Greenman, J., Maraveyas, A. & Madden, L. A. (2013) Tumour and microparticle tissue factor expression and cancer thrombosis. *Thrombosis Research*, 131(2), 109-115.

Davey, H. M. (2003) Flow cytometric techniques for the detection of microorganisms, *Advanced Flow Cytometry: Applications in Biological Research*Springer, 91-97.

Davila, M., Amirkhosravi, A., Coll, E., Desai, H., Robles, L., Colon, J., Baker, C. H. & Francis, J. L. (2008) Tissue factor ‐ bearing microparticles derived from tumor cells: impact on coagulation activation. *Journal of Thrombosis and Haemostasis*, 6(9), 1517-1524.

Demetz, G. & Ott, I. (2012) The interface between inflammation and coagulation in cardiovascular disease. *International Journal of Inflammation*, 2012, 860301-8.

Dikshit, S. (2015) Fibrinogen Degradation Products and Periodontitis: Deciphering the Connection. *Journal of clinical and diagnostic research: JCDR*, 9(12), ZC10.

Donati, M. B., Gambacortipasserini, C., Casali, B., Falanga, A., Vannotti, P., Fossati, G., Semeraro, N. & Gordon, S. G. (1986) CANCER PROCOAGULANT IN HUMAN-TUMOR CELLS - EVIDENCE FROM MELANOMA PATIENTS. *Cancer Research*, 46(12), 6471-6474.

Donnellan, E., Kevane, B., Bird, B. R. H. & Ainle, F. N. (2014) Cancer and venous thromboembolic disease: from molecular mechanisms to clinical management. *Current Oncology*, 21(3), 134-143.

Dutse, S. W. & Yusof, N. A. (2011) Microfluidics-based lab-on-chip systems in DNA-based biosensing: An overview. *Sensors*, 11(6), 5754-5768.

Duval, K., Grover, H., Han, L. H., Mou, Y., Pegoraro, A. F., Fredberg, J. & Chen, Z. (2017) Modeling Physiological Events in 2D vs. 3D Cell Culture. *Physiology*, 32(4), 266-277.

Edmondson, R., Broglie, J. J., Adcock, A. F. & Yang, L. (2014) Three-dimensional cell culture systems and their applications in drug discovery and cell-based biosensors. *Assay and drug development technologies*, 12(4), 207-218.

Edwards, R. L., Rickles, F. R., Moritz, T. E., Henderson, W. G., Zacharski, L. R., Forman, W. B., Cornell, C. J., Forcier, R. J., Odonnell, J. F., Headley, E., Kim, S. H., Odell, R., Tornyos, K. & Kwaan,

H. C. (1987) ABNORMALITIES OF BLOOD-COAGULATION TESTS IN PATIENTS WITH CANCER. *American Journal of Clinical Pathology*, 88(5), 596-602.

Egeblad, M., Nakasone, E. S. & Werb, Z. (2010) Tumors as Organs: Complex Tissues that Interface with the Entire Organism. *Developmental Cell*, 18(6), 884-901.

Elliott, N. T. & Yuan, F. (2011) A Review of Three-Dimensional In Vitro Tissue Models for Drug Discovery and Transport Studies. *Journal of Pharmaceutical Sciences*, 100(1), 59-74.

Ertl, P., Emrich, C. A., Singhal, P. & Mathies, R. A. (2004) Capillary Electrophoresis Chips with a Sheath-Flow Supported Electrochemical Detection System. *Analytical Chemistry*, 76(13), 3749-3755.

Faiz, A. S., Khan, I., Beckman, M. G., Bockenstedt, P., Heit, J. A., Kulkarni, R., Manco-Johnson, M., Moll, S., Ortel, T. L. & Philipp, C. S. (2015) Characteristics and Risk Factors of Cancer Associated Venous Thromboembolism. *Thrombosis Research*, 136(3), 535-541.

Falanga, A., Marchetti, M. & Russo, L. (2015) The mechanisms of cancer-associated thrombosis. *Thrombosis research*, 135, S8-S11.

Falanga, A., Marchetti, M. & Vignoli, A. (2013) Coagulation and cancer: biological and clinical aspects. *Journal of Thrombosis and Haemostasis*, 11(2), 223-233.

Falanga, A., Panova-Noeva, M. & Russo, L. (2009) Procoagulant mechanisms in tumour cells. *Best Practice & Research Clinical Haematology*, 22(1), 49-60.

Falanga, A. & Russo, L. (2012) Epidemiology, risk and outcomes of venous thromboembolism in cancer. *Hamostaseologie*, 32(2), 115-+.

Falanga, A. & Zacharski, L. (2005) Deep vein thrombosis in cancer: The scale of the problem and approaches to management. *Annals of Oncology*, 16(5), 696-701.

Falange, A., Russo, L., Milesi, V. & Vignoli, A. (2017) Mechanisms and risk factors of thrombosis in cancer. *Critical Reviews in Oncology Hematology*, 118, 79-83.

Fatima, F. & Nawaz, M. (2017) Nexus between extracellular vesicles, immunomodulation and tissue remodeling: for good or for bad? *Annals of translational medicine*, 5(6).

Fennema, E., Rivron, N., Rouwkema, J., van Blitterswijk, C. & de Boer, J. (2013) Spheroid culture as a tool for creating 3D complex tissues. *Trends in Biotechnology*, 31(2), 108-115.

Finak, G., Langweiler, M., Jaimes, M., Malek, M., Taghiyar, J., Korin, Y., Raddassi, K., Devine, L., Obermoser, G., Pekalski, M. L., Pontikos, N., Diaz, A., Heck, S., Villanova, F., Terrazzini, N., Kern, F., Qian, Y., Stanton, R., Wang, K., Brandes, A., Ramey, J., Aghaeepour, N., Mosmann, T., Scheuermann, R. H., Reed, E., Palucka, K., Pascual, V., Blomberg, B. B., Nestle, F., Nussenblatt, R. B., Brinkman, R. R., Gottardo, R., Maecker, H. & McCoy, J. P. (2016) Standardizing Flow Cytometry Immunophenotyping Analysis from the Human ImmunoPhenotyping Consortium. *Scientific Reports*, 6.

Fogh, J., Wright, W. C. & Loveless, J. D. (1977) ABSENCE OF HELA-CELL CONTAMINATION IN 169 CELL LINES DERIVED FROM HUMAN TUMORS. *Journal of the National Cancer Institute*, 58(2), 209-214.

Foley, J. H. & Conway, E. M. (2016) Cross talk pathways between coagulation and inflammation. *Circulation research*, 118(9), 1392-1408.

Folkman, J., Klagsbrun, M., Sasse, J., Wadzinski, M., Ingber, D. & Vlodavsky, I. (1988) A HEPARIN-BINDING ANGIOGENIC PROTEIN - BASIC FIBROBLAST GROWTH-FACTOR - IS STORED WITHIN BASEMENT-MEMBRANE. *American Journal of Pathology*, 130(2), 393-400.

Francia, G., Cruz-Munoz, W., Man, S., Xu, P. & Kerbel, R. S. (2011) Mouse models of advanced spontaneous metastasis for experimental therapeutics. *Nature Reviews Cancer*, 11(2), 135-141.

Freyssinet, J. M. (2003) Cellular microparticles: what are they bad or good for? *Journal of Thrombosis and Haemostasis*, 1(7), 1655-1662.

Fuentes-Prior, P., Iwanaga, Y., Huber, R., Pagila, R., Rumennik, G., Seto, M., Morser, J., Light, D. R. & Bode, W. (2000) Structural basis for the anticoagulant activity of the thrombin–thrombomodulin complex. *Nature*, 404(6777), 518.

Furie, B. & Furie, B. C. (2008) Mechanisms of disease: Mechanisms of thrombus formation. *New England Journal of Medicine*, 359(9), 938-949.

Furie, B. C. & Furie, B. (2006) Cancer-associated thrombosis. *Blood Cells, Molecules and Diseases*, 36(2), 177-181.

Gale, A. J. (2011) Continuing Education Course #2: Current Understanding of Hemostasis. Los Angeles, CA: SAGE Publications.

Galley, H. F. & Webster, N. R. (2004) Physiology of the endothelium. *British Journal of Anaesthesia*, 93(1), 105-113.

Geddings, J. E. & Mackman, N. (2013) Tumor-derived tissue factor-positive microparticles and venous thrombosis in cancer patients. *Blood*, 122(11), 1873-1880.

Genschmer, K. R., Russell, D. W., Lal, C., Szul, T., Bratcher, P. E., Noerager, B. D., Roda, M. A., Xu, X., Rezonzew, G., Viera, L., Dobosh, B. S., Margaroli, C., Abdalla, T. H., King, R. W., McNicholas, C. M., Wells, J. M., Dransfield, M. T., Tirouvanziam, R., Gaggar, A. & Blalock, J. E. (2019) Activated PMN Exosomes: Pathogenic Entities Causing Matrix Destruction and Disease in the Lung. *Cell*, 176(1-2), 113-+.

Giannattasio, A., Weil, S., Kloess, S., Ansari, N., Stelzer, E. H. K., Cerwenka, A., Steinle, A., Koehl, U. & Koch, J. (2015) Cytotoxicity and infiltration of human NK cells in in vivo-like tumor spheroids. *Bmc Cancer*, 15.

Giavazzi, R., Foppolo, M., Dossi, R. & Remuzzi, A. (1993) ROLLING AND ADHESION OF HUMAN TUMOR-CELLS ON VASCULAR ENDOTHELIUM UNDER PHYSIOLOGICAL FLOW CONDITIONS. *Journal of Clinical Investigation*, 92(6), 3038-3044.

Gieseler, F., Plattfaut, C., Quecke, T., Freund, A., Ungefroren, H. & Ender, F. (2018) Heterogeneity of microvesicles from cancer cell lines under inflammatory stimulation with TNF-alpha. *Cell Biology International*, 42(11), 1533-1544.

Giesen, P. L. A. & Nemerson, V. (2000) Tissue factor on the loose. *Seminars in Thrombosis and Hemostasis*, 26(4), 379-384.

Giesen, P. L. A., Rauch, U., Bohrmann, B., Kling, D., Roque, M., Fallon, J. T., Badimon, J. J., Himber, J., Riederer, M. A. & Nemerson, Y. (1999) Blood-borne tissue factor: Another view of thrombosis. *Proceedings of the National Academy of Sciences of the United States of America*, 96(5), 2311-2315.

Glynn, J. J., Polsin, E. G. & Hinds, M. T. (2015) Crosslinking decreases the hemocompatibility of decellularized, porcine small intestinal submucosa. *Acta biomaterialia*, 14, 96-103.

Gold, B., Cankovic, M., Furtado, L. V., Meier, F. & Gocke, C. D. (2015) Do Circulating Tumor Cells, Exosomes, and Circulating Tumor Nucleic Acids Have Clinical Utility? *Journal of Molecular Diagnostics, The*, 17(3), 209-224.

Goldenberg, N. A., Everett, A. D., Graham, D., Bernard, T. J. & Nowak-Gottl, U. (2014) Proteomic and other mass spectrometry based "omics" biomarker discovery and validation in pediatric venous thromboembolism and arterial ischemic stroke: Current state, unmet needs, and future directions. *Proteomics Clinical Applications*, 8(11-12), 828-836.

Gonik, A., Rodriguez, A., Zhou, H., Leiserowitz, G. & White, R. (2010) Venous thromboembolism in uterine cancer. *Gynecologic Oncology*, 116(3), S82-S82.

Gopal, S. K., Greening, D. W., Rai, A., Chen, M., Xu, R., Shafiq, A., Mathias, R. A., Zhu, H.-J. & Simpson, R. J. (2017) Extracellular vesicles: their role in cancer biology and epithelial–mesenchymal transition. *Biochemical Journal*, 474(1), 21-45.

Gorgens, A., Bremer, M., Ferrer-Tur, R., Murke, F., Tertel, T., Horn, P. A., Thalman, S., Welsh, J. A., Probst, C., Guerin, C., Boulanger, C. M., Jones, J. C., Hanenber, H., Erdbrugger, U., Lannigan, J., Ricklefs, F. L., El-Andaloussi, S. & Giebel, B. (2019) Optimisation of imaging flow cytometry for the analysis of single extracellular vesicles by using fluorescence-tagged vesicles as biological reference material. *Journal of Extracellular Vesicles*, 8(1).

Green, S. K., Francia, G., Isidoro, C. & Kerbel, R. S. (2004) Antiadhesive antibodies targeting E-cadherin sensitize multicellular tumor spheroids to chemotherapy in vitro. *Molecular Cancer Therapeutics*, 3(2), 149-159.

Guerin, E., Man, S., Xu, P. & Kerbel, R. S. (2013) A Model of Postsurgical Advanced Metastatic Breast Cancer More Accurately Replicates the Clinical Efficacy of Antiangiogenic Drugs. *Cancer Research*, 73(9), 2743-2748.

Haddad, T. C. & Greeno, E. W. (2006) Chemotherapy-induced thrombosis. *Thrombosis Research*, 118(5), 555-568.

Hait, W. N. (2010) Anticancer drug development: the grand challenges. *Nature Reviews Drug Discovery*, 9(4), 253-254.

Han, X., Guo, B., Li, Y. & Zhu, B. (2014) Tissue factor in tumor microenvironment: a systematic review. *Journal of hematology & oncology*, 7(1), 54.

Hanif, S., John, P., Gao, W., Saqib, M., Qi, L. & Xu, G. (2016) Chemiluminescence of creatinine/H2O2/Co2+ and its application for selective creatinine detection. *Biosensors and Bioelectronics*, 75, 347-351.

Haubold, K., Rink, M., Spath, B., Friedrich, M., Chun, F. K. H., Marx, G., Amirkhosravi, A., Francis, J. L., Bokemeyer, C., Eifrig, B. & Langer, F. (2009) Tissue factor procoagulant activity of plasma microparticles is increased in patients with early-stage prostate cancer. *Thrombosis and Haemostasis*, 101(6), 1147-1155.

Heit, J. A. (2015) Epidemiology of venous thromboembolism. *Nature Reviews Cardiology*, 12(8), 464.

Herrmann, J. & Lerman, A. (2014) An update on cardio-oncology. *Trends in Cardiovascular Medicine*, 24(7), 285-295.

Hijmans, J. G., Stockelman, K. A., Garcia, V., Levy, M. a. V., Brewster, L. M., Bammert, T. D., Greiner, J. J., Stauffer, B. L., Connick, E. & DeSouza, C. A. (2019) Circulating Microparticles Are Elevated in Treated HIV‐1 Infection and Are Deleterious to Endothelial Cell Function. *Journal of the American Heart Association*, 8(4), e011134.

Hisada, Y., Auriemma, A. C., Alexander, W., Ay, C. & Mackman, N. (2017) Detection of tissue factor-positive extracellular vesicles by laser scanning confocal microscopy. *Thrombosis research*, 150, 65-72.

Hisada, Y., Grover, S. P., Maqsood, A., Houston, R., Ay, C., Noubouossie, D. F., Cooley, B. C., Wallén, H., Key, N. S. & Thålin, C. (2020) Neutrophils and neutrophil extracellular traps enhance venous thrombosis in mice bearing human pancreatic tumors. *haematologica*, 105(1), 218-225.

Hisada, Y., Thalin, C., Lundstrom, S., Wallen, H. & Mackman, N. (2018) Comparison of microvesicle tissue factor activity in non-cancer severely ill patients and cancer patients. *Thrombosis Research*, 165, 1-5.

Ho, L. W. W., Kam, P. C. A. & Thong, C. L. (2005) Disseminated intravascular coagulation. *Current Anaesthesia & Critical Care*, 16(3), 151-161.

Hoarau-Vechot, J., Rafii, A., Touboul, C. & Pasquier, J. (2018) Halfway between 2D and Animal Models: Are 3D Cultures the Ideal Tool to Study Cancer-Microenvironment Interactions? *International Journal of Molecular Sciences*, 19(1).

Hoffbrand, A. V. & Steensma, D. P. (2019) *Hoffbrand's essential haematology*John Wiley & Sons.

Horsted, F., West, J. & Grainge, M. J. (2012) Risk of Venous Thromboembolism in Patients with Cancer: A Systematic Review and Meta-Analysis. *Plos Medicine*, 9(7).

Horvath, B., Hegedus, D., Szapary, L., Marton, Z., Alexy, T., Koltai, K., Czopf, L., Wittmann, I., Juricskay, I. & Toth, K. (2004) Measurement of von Willebrand factor as the marker of endothelial dysfunction in vascular diseases. *Experimental & Clinical Cardiology*, 9(1), 31.

Hoshi, A., Matsumoto, A., Chung, J., Isozumi, Y. & Koyama, T. (2011) Activation of coagulation by a thalidomide-based regimen. *Blood Coagulation & Fibrinolysis*, 22(6), 532-540.

Hron, G., Kollars, M., Weber, H., Sagaster, V., Quehenberger, P., Eichinger, S., Kyrle, P. A. & Weltermann, A. (2007) Tissue factor-positive microparticles: cellular origin and association with coagulation activation in patients with colorectal cancer. *Thrombosis and haemostasis*, 97(01), 119-123.

Hu, K., Chakrabarty, K. & Ho, T.-Y. (2017) *Computer-aided design of microfluidic very large scale integration (mVLSI) biochips*Springer.

Hussein, M. N. A., Boing, A. N., Biro, E., Hoek, F. J., Vogel, G. M. T., Meuternan, D. G., Sturk, A. & Nieuwland, R. (2008) Phospholipid composition of in vitro endothelial microparticles and their in vivo thrombogenic properties. *Thrombosis Research*, 121(6), 865-871.

Iliescu, F. S., Poenar, D. P., Yu, F., Ni, M., Chan, K. H., Cima, I., Taylor, H. K., Cima, I. & Iliescu, C. (2019) Recent advances in microfluidic methods in cancer liquid biopsy. *Biomicrofluidics*, 13(4), 041503.

Ivascu, A. & Kubbies, M. (2006) Rapid generation of single-tumor spheroids for high-throughput cell function and toxicity analysis. *Journal of Biomolecular Screening*, 11(8), 922-932.

Ivnitski, D., O'Neil, D. J., Gattuso, A., Schlicht, R., Calidonna, M. & Fisher, R. (2003) Nucleic acid approaches for detection and identification of biological warfare and infectious disease agents. *Biotechniques*, 35(4), 862-869.

Jayachandran, M., Miller, V. M., Heit, J. A. & Owen, W. G. (2012) Methodology for isolation, identification and characterization of microvesicles in peripheral blood. *Journal of Immunological Methods*, 375(1-2), 207-214.

Jiang, D., Jiang, Z., Lu, D., Wang, X., Liang, H. S., Zhang, J. F., Meng, Y. P., Li, Y., Wu, D. N., Huang, Y. W., Chen, Y. L., Deng, H. T., Wu, Q., Xiong, J. W., Meng, A. M. & Yu, L. (2019) Migrasomes provide regional cues for organ morphogenesis during zebrafish gastrulation. *Nature Cell Biology*, 21(8), 966-+.

Jin, C., McFaul, S. M., Duffy, S. P., Deng, X. Y., Tavassoli, P., Black, P. C. & Ma, H. S. (2014) Technologies for label-free separation of circulating tumor cells: from historical foundations to recent developments. *Lab on a Chip*, 14(1), 32-44.

Kaiser, J. (2010) Cancer's circulation problem. American Association for the Advancement of Science.

Kalaria, R., Ferrer, I. & Love, S. (2018) Vascular Disease, Hypoxia. *Greenfield's Neuropathology-Two Volume Set*, 59.

Kang, H. G., Jenabi, J. M., Zhang, J. S., Keshelava, N., Shimada, H., May, W. A., Ng, T., Reynolds, C. P., Triche, T. J. & Sorensen, P. H. B. (2007) E-cadherin cell-cell adhesion in Ewing tumor cells mediates suppression of anoikis through activation of the ErbB4 tyrosine kinase. *Cancer Research*, 67(7), 3094-3105.

Kelm, J. M., Timmins, N. E., Brown, C. J., Fussenegger, M. & Nielsen, L. K. (2003) Method for generation of homogeneous multicellular tumor spheroids applicable to a wide variety of cell types. *Biotechnology and bioengineering*, 83(2), 173-180.

Key, N. S., Chantrathammachart, P., Moody, P. W. & Chang, J.-Y. (2010) Membrane microparticles in VTE and cancer. *Thrombosis research*, 125, S80-S83.

Khademhosseini, A., Langer, R., Borenstein, J. & Vacanti, J. P. (2006) Microscale technologies for tissue engineering and biology. *Proceedings of the National Academy of Sciences of the United States of America*, 103(8), 2480-2487.

Khorana, A. A. (2009) Cancer and thrombosis: implications of published guidelines for clinical practice. *Annals of Oncology*, 20(10), 1619-1630.

Khorana, A. A. (2012) Cancer and coagulation. *American Journal of Hematology*, 87, S82-S87.

Khorana, A. A., Ahrendt, S. A., Ryan, C. K., Francis, C. W., Hruban, R. H., Hu, Y. C., Hostetter, G., Harvey, J. & Taubman, M. B. (2007) Tissue factor expression, angiogenesis, and thrombosis in pancreatic cancer. *Clinical Cancer Research*, 13(10), 2870-2875.

Khorana, A. A., Francis, C. W., Culakova, E., Fisher, R. I., Kuderer, N. M. & Lyman, G. H. (2006) Thromboembolism in hospitalized neutropenic cancer patients. *J Clin Oncol*, 24(3), 484-490.

Kim, D. & Herr, A. E. (2013) Protein immobilization techniques for microfluidic assays. *Biomicrofluidics*, 7(4).

Kim, E. J., Lim, K. M., Kim, K. Y., Bae, O. N., Noh, J. Y., Chung, S. M., Shin, S., Yun, Y. P. & Chung, J. H. (2009) Doxorubicin-induced platelet cytotoxicity: a new contributory factor for doxorubicin-mediated thrombocytopenia. *Journal of Thrombosis and Haemostasis*, 7(7), 1172-1183.

Kim, J. S. & Ligler, F. S. (2010) Utilization of microparticles in next-generation assays for microflow cytometers. *Analytical and Bioanalytical Chemistry*, 398(6), 2373-2382.

Kim, Y., Abplanalp, W. A., Jung, A. D., Schuster, R. M., Lentsch, A. B., Gulbins, E., Caldwell, C. C. & Pritts, T. A. (2018) Endocytosis of Red Blood Cell Microparticles by Pulmonary Endothelial Cells is Mediated By Rab5. *Shock (Augusta, Ga.)*, 49(3), 288-294.

Kleinjan, A., Boing, A. N., Sturk, A. & Nieuwland, R. (2012) Microparticles in vascular disorders: How tissue factor-exposing vesicles contribute to pathology and physiology. *Thrombosis Research*, 130, S71-S73.

Koizume, S., Ito, S., Yoshioka, Y., Kanayama, T., Nakamura, Y., Yoshihara, M., Yamada, R., Ochiya, T., Ruf, W., Miyagi, E., Hirahara, F. & Miyagi, Y. (2016) High-level secretion of tissue factor-rich extracellular vesicles from ovarian cancer cells mediated by filamin-A and protease-activated receptors. *Thrombosis and Haemostasis*, 115(2), 299-310.

Koster, T., Blann, A. D., Briet, E., Vandenbroucke, J. P. & Rosendaal, F. R. (1995) ROLE OF CLOTTING FACTOR-VIII IN EFFECT OF VON-WILLEBRAND-FACTOR ON OCCURRENCE OF DEEP-VEIN THROMBOSIS. *Lancet*, 345(8943), 152-155.

Kuenen, B. C., Levi, M., Meijers, J. C. M., Kakkar, A. K., van Hinsbergh, V. W. M., Kostense, P. J., Pinedo, H. M. & Hoekman, K. (2002) Analysis of coagulation cascade and endothelial cell activation during inhibition of vascular endothelial growth factor/vascular endothelial growth factor receptor pathway in cancer patients. *Arteriosclerosis Thrombosis and Vascular Biology*, 22(9), 1500-1505.

Kumar, H. R., Zhong, X., Hoelz, D. J., Rescorla, F. J., Hickey, R. J., Malkas, L. H. & Sandoval, J. A. (2008a) Three-dimensional neuroblastoma cell culture: proteomic analysis between monolayer and multicellular tumor spheroids. *Pediatric surgery international*, 24(11), 1229.

Kumar, H. R., Zhong, X. L., Hoelz, D. J., Rescorla, F. J., Hickey, R. J., Malkas, L. H. & Sandoval, J. A. (2008b) Three-dimensional neuroblastoma cell culture: proteomic analysis between monolayer and multicellular tumor spheroids. *Pediatric Surgery International*, 24(11), 1229-1234.

Lacroix, R. & Dignat-George, F. (2012a) Microparticles as a circulating source of procoagulant and fibrinolytic activities in the circulation. *Thrombosis research*, 129, S27-S29.

Lacroix, R. & Dignat-George, F. (2012b) Microparticles as a circulating source of procoagulant and fibrinolytic activities in the circulation. *Thrombosis Research*, 129(2), S27-S29.

Langer, F., Spath, B., Haubold, K., Holstein, K., Marx, G., Wierecky, J., Brümmendorf, T. H., Dierlamm, J., Bokemeyer, C. & Eifrig, B. (2008) Tissue factor procoagulant activity of plasma microparticles in patients with cancer-associated disseminated intravascular coagulation. *Annals of Hematology*, 87(6), 451-457.

Langhans, S. A. (2018) Three-Dimensional in Vitro Cell Culture Models in Drug Discovery and Drug Repositioning. *Frontiers in Pharmacology*, 9.

Lau, D. H. M., Lewis, A. D., Ehsan, M. N. & Sikic, B. I. (1991) MULTIFACTORIAL MECHANISMS ASSOCIATED WITH BROAD CROSS-RESISTANCE OF OVARIAN-CARCINOMA CELLS SELECTED BY CYANOMORPHOLINO DOXORUBICIN. *Cancer Research*, 51(19), 5181-5187.

Lazzari, G., Couvreur, P. & Mura, S. (2017) Multicellular tumor spheroids: a relevant 3D model for the in vitro preclinical investigation of polymer nanomedicines. *Polymer Chemistry*, 8(34), 4947-4969.

Lechner, D. & Weltermann, A. (2008) Chemotherapy-induced thrombosis: A role for microparticles and issue factor? *Seminars in Thrombosis and Hemostasis*, 34(2), 199-203.

Lee, A. Y. Y. (2010) Thrombosis in Cancer: An Update on Prevention, Treatment, and Survival Benefits of Anticoagulants. *Hematology-American Society of Hematology Education Program*, 144-149.

Lee, B. S. u., Lee, B. S., Cho, Y. W., Kim, G. C., Lee, D. H., Kim, C. J., Kil, H. S., Chi, D. Y., Byun, Y., Yuk, S. H., Kim, K., Kim, I.-S., Kwon, I. C. & Kim, S. Y. (2015a) Induced phenotype targeted therapy: radiation-induced apoptosis-targeted chemotherapy. *Journal of the National Cancer Institute*, 107(2).

Lee, J., Cuddihy, M. J., Cater, G. M. & Kotov, N. A. (2009) Engineering liver tissue spheroids with inverted colloidal crystal scaffolds. *Biomaterials*, 30(27), 4687-4694.

Lee, S. H., Jeong, D., Han, Y. S. & Baek, M. J. (2015b) Pivotal role of vascular endothelial growth factor pathway in tumor angiogenesis. *Annals of Surgical Treatment and Research*, 89(1), 1-8.

Leppert, U. & Eisenreich, A. (2015) The role of tissue factor isoforms in cancer biology. *International Journal of Cancer*, 137(3), 497-503.

Levi, M. (2009) Disseminated intravascular coagulation in cancer patients. *Best Practice & Research Clinical Haematology*, 22(1), 129-136.

Levine, M. N., Gent, M., Hirsh, J., Arnold, A., Goodyear, M. D., Hryniuk, W. & De Pauw, S. (1988) The thrombogenic effect of anticancer drug therapy in women with stage II breast cancer. *New England Journal of Medicine*, 318(7), 404-407.

Li, C. L., Tian, T., Nan, K. J., Zhao, N., Guo, Y. H., Cui, J., Wang, J. & Zhang, W. G. (2008) Survival advantages of multicellular spheroids vs. monolayers of HepG2 cells in vitro. *Oncology Reports*, 20(6), 1465-1471.

Li, J., Zhao, W., Akbani, R., Liu, W. B., Ju, Z. L., Ling, S. Y., Vellano, C. P., Roebuck, P., Yu, Q. H., Eterovic, A. K., Byers, L. A., Davies, M. A., Deng, W. L., Gopal, Y. N. V., Chen, G., von Euw, E. M., Slamon, D., Conklin, D., Heymach, J. V., Gazdar, A. F., Minna, J. D., Myers, J. N., Lu, Y. L., Mills, G. B. & Liang, H. (2017) Characterization of Human Cancer Cell Lines by Reverse-phase Protein Arrays. *Cancer Cell*, 31(2), 225-239.

Lin, H., Li, Q. & Lei, Y. (2017) Three-dimensional tissues using human pluripotent stem cell spheroids as biofabrication building blocks. *Biofabrication*, 9(2), 025007.

Lin, H. C., Chang, H. W., Hsiao, S. H., Chou, M. L., Seghatchian, J. & Burnouf, T. (2015) Platelet-derived microparticles trigger THP-1 monocytic cell aggregation and release of pro-coagulant tissue factor-expressing microparticles in vitro. *Transfusion and Apheresis Science*, 53(2), 246-252.

Lindahl, A. K., Boffa, M. C. & Abildgaard, U. (1993) INCREASED PLASMA THROMBOMODULIN IN CANCER-PATIENTS. *Thrombosis and Haemostasis*, 69(2), 112-114.

Lopez, G. A., Estevez, M. C., Soler, M. & Lechuga, L. M. (2017) Recent advances in nanoplasmonic biosensors: applications and lab-on-a-chip integration. *Nanophotonics*, 6(1), 123-136.

Lovitt, C. J., Shelper, T. B. & Avery, V. M. (2014) Advanced cell culture techniques for cancer drug discovery. *Biology*, 3(2), 345-367.

Ma, H. L., Jiang, Q., Han, S. Y., Wu, Y., Tomshine, J. C., Wang, D. L., Gan, Y. L., Zou, G. Z. & Liang, X. J. (2012) Multicellular Tumor Spheroids as an In Vivo-Like Tumor Model for Three-Dimensional Imaging of Chemotherapeutic and Nano Material Cellular Penetration. *Molecular Imaging*, 11(6), 487-498.

Maacha, S., Bhat, A. A., Jimenez, L., Raza, A., Haris, M., Uddin, S. & Grivel, J.-C. (2019) Extracellular vesicles-mediated intercellular communication: roles in the tumor microenvironment and anti-cancer drug resistance. *Molecular cancer*, 18(1), 55.

Mackman, N. (2006) Role of tissue factor in hemostasis and thrombosis. *Blood Cells Molecules and Diseases*, 36(2), 104-107.

Mackman, N. (2012) New insights into the mechanisms of venous thrombosis (vol 122, pg 2331, 2012). *Journal of Clinical Investigation*, 122(9), 3368-3368.

Mak, I. W. Y., Evaniew, N. & Ghert, M. (2014) Lost in translation: animal models and clinical trials in cancer treatment. *American Journal of Translational Research*, 6(2), 114-118.

Mandala, M., Barni, S., Prins, M., Labianca, R., Tondini, C., Russo, L., Milesi, A., Cremonesi, M., Zaccanelli, M. & Regonesi, C. (2009) Acquired and inherited risk factors for developing venous thromboembolism in cancer patients receiving adjuvant chemotherapy: a prospective trial. *Annals of oncology*, 21(4), 871-876.

Mandalà, M., Reni, M., Cascinu, S., Barni, S., Floriani, I., Cereda, S., Berardi, R., Mosconi, S., Torri, V. & Labianca, R. (2007) Venous thromboembolism predicts poor prognosis in irresectable pancreatic cancer patients. *Annals of oncology*, 18(10), 1660-1665.

Manly, D. A., Boles, J. & Mackman, N. (2011) Role of Tissue Factor in Venous Thrombosis, in Julius, D. & Clapham, D. E. (eds), *Annual Review of Physiology, Vol 73*. Annual Review of Physiology, 515-525.

Manly, D. A., Wang, J. G., Glover, S. L., Kasthuri, R., Liebman, H. A., Key, N. S. & Mackman, N. (2010) Increased microparticle tissue factor activity in cancer patients with Venous Thromboembolism. *Thrombosis Research*, 125(6), 511-512.

Marco, A., Brocal, C. & Marco, P. (2014) Measurement of procoagulant activity of microparticles in plasma: Feasibility of new functional assays. *Thrombosis Research*, 134(6), 1363-1364.

Marcus, A. J., Broekman, M. J., Drosopoulos, J. H. F., Islam, N., Alyonycheva, T. N., Safier, L. B., Hajjar, K. A., Posnett, D. N., Schoenborn, M. A., Schooley, K. A., Gayle, R. B. & Maliszewski, C. R. (1997) The endothelial cell ecto-ADPase responsible for inhibition of platelet function is CD39. *Journal of Clinical Investigation*, 99(6), 1351-1360.

Marik, P. E. & Cavallazzi, R. (2015) Extended Anticoagulant and Aspirin Treatment for the Secondary Prevention of Thromboembolic Disease: A Systematic Review and Meta-Analysis. *Plos One*, 10(11).

Martinelli, I. & De Stefano, V. (2010) Rare thromboses of cerebral, splanchnic and upper-extremity veins. *Thrombosis and Haemostasis*, 103(6), 1136-1144.

Mayer, B., Klement, G., Kaneko, M., Man, S., Jothy, S., Rak, J. & Kerbel, R. S. (2001) Multicellular gastric cancer spheroids recapitulate growth pattern and differentiation phenotype of human gastric carcinomas. *Gastroenterology*, 121(4), 839-852.

Mazzoleni, G., Di Lorenzo, D. & Steimberg, N. (2009) Modelling tissues in 3D: the next future of pharmaco-toxicology and food research? *Genes and Nutrition*, 4(1), 13-22.

McEver, R. P. & Cummings, R. D. (1997) Perspectives series: cell adhesion in vascular biology. Role of PSGL-1 binding to selectins in leukocyte recruitment. *The Journal of clinical investigation*, 100(3), 485-491.

McMichael, M. (2005) Primary hemostasis. *Journal of Veterinary Emergency and Critical Care*, 15(1), 1-8.

Medina-Leyte, D. J., Domínguez-Pérez, M., Mercado, I., Villarreal-Molina, M. T. & Jacobo-Albavera, L. (2020) Use of human umbilical vein endothelial cells (HUVEC) as a model to study cardiovascular disease: A review. *Applied Sciences*, 10(3), 938.

Mege, D., Aubert, M., Lacroix, R., Dignat-George, F., Panicot-Dubois, L. & Dubois, C. (2019) Involvement of Platelets in Cancers. *Seminars in Thrombosis and Hemostasis*, 45(6), 569-575.

Mehta, G., Hsiao, A. Y., Ingram, M., Luker, G. D. & Takayama, S. (2012) Opportunities and challenges for use of tumor spheroids as models to test drug delivery and efficacy. *Journal of Controlled Release*, 164(2), 192-204.

Meikle, C. K., Kelly, C. A., Garg, P., Wuescher, L. M., Ali, R. A. & Worth, R. G. (2017) Cancer and thrombosis: the platelet perspective. *Frontiers in cell and developmental biology*, 4, 147.

Meinardi, M. T., Gietema, J. A., van Veldhuisen, D. J., van der Graaf, W. T. A., de Vries, E. G. E. & Sleijfer, D. T. (2000) Long-term chemotherapy-related cardiovascular morbidity. *Cancer Treatment Reviews*, 26(6), 429-447.

Melki, I., Tessandier, N., Zufferey, A. & Boilard, E. (2017) Platelet microvesicles in health and disease. *Platelets*, 28(3), 214-221.

Metcalf, R. L., Al-Hadithi, E., Hopley, N., Henry, T., Hodgson, C., McGurk, A., Mansoor, W. & Hasan, J. (2017) Characterisation and risk assessment of venous thromboembolism in gastrointestinal cancers. *World journal of gastrointestinal oncology*, 9(9), 363.

Michiels, C. (2003) Endothelial cell functions. *Journal of Cellular Physiology*, 196(3), 430-443.

Mielicki, W., Serwa, J., Kurzawinski, T. & Wierzbicki, R. (1990) PROCOAGULANT ACTIVITY OF HUMAN STOMACH AND COLON CANCERS. *Oncology*, 47(4), 299-302.

Minciacchi, V. R., Freeman, M. R. & Di Vizio, D. (2015) Extracellular vesicles in cancer: exosomes, microvesicles and the emerging role of large oncosomes, *Seminars in cell & developmental biology*. Elsevier.

Mitchell, P. S., Parkin, R. K., Kroh, E. M., Fritz, B. R., Wyman, S. K., Pogosova-Agadjanyan, E. L., Peterson, A., Noteboom, J., O'Briant, K. C., Allen, A., Lin, D. W., Urban, N., Drescher, C. W., Knudsen, B. S., Stirewalt, D. L., Gentleman, R., Vessella, R. L., Nelson, P. S., Martin, D. B. & Tewari, M. (2008) Circulating microRNAs as Stable Blood-Based Markers for Cancer Detection.

Proceedings of the National Academy of Sciences of the United States of America, 105(30), 10513-10518.

Mitrugno, A., Tormoen, G. W., Kuhn, P. & McCarty, O. J. T. (2016) The prothrombotic activity of cancer cells in the circulation. *Blood Reviews*, 30(1), 11-19.

Mitry, M. A. & Edwards, J. G. (2016) Doxorubicin induced heart failure: Phenotype and molecular mechanisms. *IJC heart & vasculature*, 10, 17-24.

Möckl, L., Hirn, S., Torrano, A. A., Uhl, B., Bräuchle, C. & Krombach, F. (2017) The glycocalyx regulates the uptake of nanoparticles by human endothelial cells in vitro. *Nanomedicine*, 12(3), 207-217.

Monagle, P. & Massicotte, P. (2011) Developmental haemostasis: Secondary haemostasis. *Seminars in Fetal and Neonatal Medicine*, 16(6), 294-300.

Moore, K., Andreoli, S. P., Esmon, N., Esmon, C. & Bang, N. (1987) Endotoxin enhances tissue factor and suppresses thrombomodulin expression of human vascular endothelium in vitro. *The Journal of clinical investigation*, 79(1), 124-130.

Moore, R. A., Adel, N., Riedel, E., Bhutani, M., Feldman, D. R., Tabbara, N. E., Soff, G., Parameswaran, R. & Hassoun, H. (2011) High incidence of thromboembolic events in patients treated with cisplatin-based chemotherapy: a large retrospective analysis. *Journal of Clinical Oncology*, 29(25), 3466-3473.

Morel, O., Jesel, L., Freyssinet, J. M. & Toti, F. (2011) Cellular Mechanisms Underlying the Formation of Circulating Microparticles. *Arteriosclerosis Thrombosis and Vascular Biology*, 31(1), 15-26.

Morel, O., Morel, N., Hugel, B., Jesel, L., Vinzio, S., Goichot, B., Bakouboula, B., Grunebaum, L., Freyssinet, J. & Toti, F. (2005) The significance of circulating microparticles in physiology, inflammatory and thrombotic diseases. *La Revue de medecine interne*, 26(10), 791-801.

Muhsin-Sharafaldine, M.-R. & McLellan, A. D. (2018) Tumor-derived apoptotic vesicles: with death they do part. *Frontiers in immunology*, 9, 957.

Nagrath, S., Sequist, L. V., Maheswaran, S., Bell, D. W., Irimia, D., Ulkus, L., Smith, M. R., Kwak, E. L., Digumarthy, S., Muzikansky, A., Ryan, P., Balis, U. J., Tompkins, R. G., Haber, D. A. & Toner, M. (2007) Isolation of rare circulating tumour cells in cancer patients by microchip technology. *Nature*, 450(7173), 1235-1239.

Nelson, K., Tam, M. R., Helton, K., Weigl, B. H., Fu, E., Yager, P. & Edwards, T. (2006) Microfluidic diagnostic technologies for global public health. *Nature*, 442(7101), 412-418.

Noble, S. & Pasi, J. (2010) Epidemiology and pathophysiology of cancer-associated thrombosis. *British Journal of Cancer*, 102, S2-S9.

Nomura, S., Niki, M., Nisizawa, T., Tamaki, T. & Shimizu, M. (2015) Microparticles as biomarkers of blood coagulation in cancer. *Biomarkers in cancer*, 7, BIC. S30347.

Nomura, S. & Shimizu, M. (2015) Clinical significance of procoagulant microparticles. *Journal of Intensive Care*, 3(1), 2.

Nuver, J., Smit, A., Sleijfer, D. T., Van Gessel, A., Van Roon, A., Van Der Meer, J., van den Berg, M., Burgerhof, J., Hoekstra, H. & Sluiter, W. (2004) Microalbuminuria, decreased fibrinolysis, and

inflammation as early signs of atherosclerosis in long-term survivors of disseminated testicular cancer. *European Journal of Cancer*, 40(5), 701-706.

Oppelt, P., Betbadal, A. & Nayak, L. (2015) Approach to chemotherapy-associated thrombosis. *Vascular Medicine*, 20(2), 153-161.

Ording, A. G., Horvath-Puho, E., Lash, T. L., Ehrenstein, V., Borre, M., Vyberg, M. & Sorensen, H. T. (2015) Prostate Cancer, Comorbidity, and the Risk of Venous Thromboembolism: A Cohort Study of 44,035 Danish Prostate Cancer Patients, 1995-2011. *Cancer*, 121(20), 3692-3699.

Orfeo, T., Butenas, S., Brummel-Ziedins, K. E. & Mann, K. G. (2005) The tissue factor requirement in blood coagulation. *Journal of Biological Chemistry*, 280(52), 42887-42896.

Osswald, A., Sun, Z. K., Grimm, V., Ampem, G., Riegel, K., Westendorf, A. M., Sommergruber, W., Otte, K., Durre, P. & Riedel, C. U. (2015) Three-dimensional tumor spheroids for in vitro analysis of bacteria as gene delivery vectors in tumor therapy. *Microbial Cell Factories*, 14.

Otten, H.-M. M., Mathijssen, J., ten Cate, H., Soesan, M., Inghels, M., Richel, D. J. & Prins, M. H. (2004) Symptomatic venous thromboembolism in cancer patients treated with chemotherapy: an underestimated phenomenon. *Archives of Internal Medicine*, 164(2), 190-194.

Owens, A. P. & Mackman, N. (2011) Microparticles in Hemostasis and Thrombosis. *Circulation Research*, 108(10), 1284-1297.

Pabinger, I., Thaler, J. & Ay, C. (2013) Biomarkers for prediction of venous thromboembolism in cancer. *Blood*, 122(12), 2011-2018.

Palabrica, T., Lobb, R., Furie, B. C., Aronovitz, M., Benjamin, C., Hsu, Y.-M., Sajer, S. A. & Furie, B. (1992) Leukocyte accumulation promoting fibrin deposition is mediated in vivo by P-selectin on adherent platelets. *Nature*, 359(6398), 848.

Pampaloni, F., Reynaud, E. G. & Stelzer, E. H. K. (2007) The third dimension bridges the gap between cell culture and live tissue. *Nature Reviews Molecular Cell Biology*, 8(10), 839-845.

Park, K. H. & Song, S. C. (2006) Morphology of spheroidal hepatocytes within injectable, biodegradable, and thermosensitive poly(organophosphazene) hydrogel as cell delivery vehicle. *Journal of Bioscience and Bioengineering*, 101(3), 238-242.

Pellegrino, M., Sciambi, A., Treusch, S., Durruthy-Durruthy, R., Gokhale, K., Jacob, J., Chen, T. X., Geis, J. A., Oldham, W., Matthews, J., Kantarjian, H., Futreal, P. A., Patel, K., Jones, K. W., Takahashi, K. & Eastburn, D. J. (2018) High-throughput single-cell DNA sequencing of acute myeloid leukemia tumors with droplet microfluidics. *Genome Research*, 28(9), 1345-1352.

Pérez-Casal, M., Downey, C., Fukudome, K., Marx, G. & Toh, C. H. (2005) Activated protein C induces the release of microparticle-associated endothelial protein C receptor. *Blood*, 105(4), 1515-1522.

Periayah, M. H., Halim, A. S. & Saad, A. Z. M. (2017) Mechanism action of platelets and crucial blood coagulation pathways in hemostasis. *International journal of hematology-oncology and stem cell research*, 11(4), 319.

Pinsky, D. J., Naka, Y., Liao, H., Oz, M. C., Wagner, D. D., Mayadas, T. N., Johnson, R. C., Hynes, R. O., Heath, M. & Lawson, C. A. (1996) Hypoxia-induced exocytosis of endothelial cell Weibel-Palade bodies. A mechanism for rapid neutrophil recruitment after cardiac preservation. *The Journal of clinical investigation*, 97(2), 493-500.

Poncelet, P., Robert, S., Bailly, N., Garnache-Ottou, F., Bouriche, T., Devalet, B., Segatchian, J. H., Saas, P. & Mullier, F. (2015) Tips and tricks for flow cytometry-based analysis and counting of microparticles. *Transfusion and Apheresis Science*, 53(2), 110-126.

Povero, D., Eguchi, A., Li, H. Y., Johnson, C. D., Papouchado, B. G., Wree, A., Messer, K. & Feldstein, A. E. (2014) Circulating Extracellular Vesicles with Specific Proteome and Liver MicroRNAs Are Potential Biomarkers for Liver Injury in Experimental Fatty Liver Disease. *Plos One*, 9(12).

Prakash, A. R., Amrein, M. & Kaler, K. V. (2008) Characteristics and impact of Taq enzyme adsorption on surfaces in microfluidic devices. *Microfluidics and nanofluidics*, 4(4), 295.

Raghavan, S., Mehta, P., Horst, E. N., Ward, M. R., Rowley, K. R. & Mehta, G. (2016) Comparative analysis of tumor spheroid generation techniques for differential in vitro drug toxicity. *Oncotarget*, 7(13), 16948-16961.

Rajcevic, U., Knol, J. C., Piersma, S., Bougnaud, S., Fack, F., Sundlisaeter, E., Sondenaa, K., Myklebust, R., Pham, T. V., Niclou, S. P. & Jimenez, C. R. (2014) Colorectal cancer derived organotypic spheroids maintain essential tissue characteristics but adapt their metabolism in culture. *Proteome Science*, 12.

Rajendran, P., Rengarajan, T., Thangavel, J., Nishigaki, Y., Sakthisekaran, D., Sethi, G. & Nishigaki, I. (2013) The Vascular Endothelium and Human Diseases. *International Journal of Biological Sciences*, 9(10), 1057-1069.

Rand, M. L., Wang, H., Bang, K. W. A., Packham, M. A. & Freedman, J. (2006) Rapid clearance of procoagulant platelet-derived microparticles from the circulation of rabbits. *Journal of Thrombosis and Haemostasis*, 4(7), 1621-1623.

Rao, L. V. M. & Pendurthi, U. R. (2005) Tissue Factor–Factor VIIa Signaling. *Arteriosclerosis, Thrombosis, and Vascular Biology*, 25(1), 47-56.

Rautou, P.-E., Leroyer, A. S., Ramkhelawon, B., Devue, C., Duflaut, D., Vion, A.-C., Nalbone, G., Castier, Y., Leseche, G. & Lehoux, S. (2011) Microparticles from human atherosclerotic plaques promote endothelial ICAM-1–dependent monocyte adhesion and transendothelial migration. *Circulation research*, 108(3), 335-343.

Razak, A., Binti, N., Jones, G., Bhandari, M., Berndt, M. C. & Metharom, P. (2018) Cancer-associated thrombosis: an overview of mechanisms, risk factors, and treatment. *Cancers*, 10(10), 380.

Repetto, O. & De Re, V. (2017) Coagulation and fibrinolysis in gastric cancer. *Ann NY Acad Sci*, 1404(1), 27-48.

Rodriguez, A. O., Gonik, A. M., Zhou, H., Leiserowitz, G. S. & White, R. H. (2011) Venous Thromboembolism in Uterine Cancer. *International Journal of Gynecological Cancer*, 21(5), 870-876.

Ruf, W. (2012) Tissue factor and cancer. *Thrombosis Research*, 130, S84-S87.

Ruggeri, Z. M. (1997) Mechanisms initiating platelet thrombus formation. *Thrombosis and haemostasis*, 78(01), 611-616.

Schrauder, M. G., Strick, R., Schulz-Wendtland, R., Strissel, P. L., Kahmann, L., Loehberg, C. R., Lux, M. P., Jud, S. M., Hartmann, A., Hein, A., Bayer, C. M., Bani, M. R., Richter, S., Adamietz, B.

R., Wenkel, E., Rauh, C., Beckmann, M. W. & Fasching, P. A. (2012) Circulating micro-RNAs as potential blood-based markers for early stage breast cancer detection. *PLoS ONE*, 7(1), e29770.

Seaman, S., Nelson, A. & Noble, I. (2014) Cancer-associated thrombosis, low-molecular-weight heparin, and the patient experience: a qualitative study. *Patient Preference and Adherence*, 8, 453-461.

Secin, F. P., Jiborn, T., Bjartell, A. S., Fournier, G., Salomon, L., Abbou, C. C., Haber, G. P., Gill, I. S., Crocitto, L. E. & Nelson, R. A. (2008) Multi-institutional study of symptomatic deep venous thrombosis and pulmonary embolism in prostate cancer patients undergoing laparoscopic or robot-assisted laparoscopic radical prostatectomy. *European urology*, 53(1), 134-145.

Shai, E. & Varon, D. (2011) Development, cell differentiation, angiogenesis—microparticles and their roles in angiogenesis. *Arteriosclerosis, thrombosis, and vascular biology*, 31(1), 10-14.

Shao, H., Chung, J., Balaj, L., Charest, A., Bigner, D. D., Carter, B. S., Hochberg, F. H., Breakefield, X. O., Weissleder, R. & Lee, H. (2012) Protein typing of circulating microvesicles allows real-time monitoring of glioblastoma therapy. *Nature Medicine*, 18(12), 1835-1840.

Sheth, R. A., Niekamp, A., Quencer, K. B., Shamoun, F., Knuttinen, M.-G., Naidu, S. & Oklu, R. (2017) Thrombosis in cancer patients: Etiology, incidence, and management. *Cardiovascular Diagnosis and Therapy*, 7(S3), S178-S185.

Sierko, E., Wojtukiewicz, M. Z. & Kisiel, W. (2007) The role of tissue factor pathway inhibitor-2 in cancer biology. *Seminars in Thrombosis and Hemostasis*, 33(7), 653-659.

Sokolova, V., Ludwig, A. K., Hornung, S., Rotan, O., Horn, P. A., Epple, M. & Glebel, B. (2011) Characterisation of exosomes derived from human cells by nanoparticle tracking analysis and scanning electron microscopy. *Colloids and Surfaces B-Biointerfaces*, 87(1), 146-150.

Son, Y. J., Kang, J., Kim, H. S. & Yoo, H. S. (2016) Electrospun Nanofibrous Sheets for Selective Cell Capturing in Continuous Flow in Microchannels. *Biomacromolecules*, 17(3), 1067-1074.

Sørensen, B. & Ingerslev, J. (2004) Whole blood clot formation phenotypes in hemophilia A and rare coagulation disorders. Patterns of response to recombinant factor VIIa. *Journal of Thrombosis and Haemostasis*, 2(1), 102-110.

Soultati, A., Mountzios, G., Avgerinou, C., Papaxoinis, G., Pectasides, D., Dimopoulos, M. A. & Papadimitriou, C. (2012) Endothelial vascular toxicity from chemotherapeutic agents: Preclinical evidence and clinical implications. *Cancer Treatment Reviews*, 38(5), 473-483.

Sousou, T. & Khorana, A. (2009) Identifying cancer patients at risk for venous thromboembolism. *Hamostaseologie*, 29(1), 121-124.

Steppich, B., Mattisek, C., Sobczyk, D., Kastrati, A., Schömig, A. & Ott, I. (2005) Tissue factor pathway inhibitor on circulating microparticles in acute myocardial infarction. *Thrombosis and haemostasis*, 93(01), 35-39.

Sutherland, R. M. (1988) Cell and environment interactions in tumor microregions: the multicell spheroid model. *Science*, 240(4849), 177-184.

Svensson, K. J., Kucharzewska, P., Christianson, H. C., Skold, S., Lofstedt, T., Johansson, M. C., Morgelin, M., Bengzon, J., Ruf, W. & Belting, M. (2011) Hypoxia triggers a proangiogenic pathway involving cancer cell microvesicles and PAR-2-mediated heparin-binding EGF signaling in

endothelial cells. *Proceedings of the National Academy of Sciences of the United States of America*, 108(32), 13147-13152.

Swystun, L. L., Shin, L. Y. Y., Beaudin, S. & Liaw, P. C. (2009) Chemotherapeutic agents doxorubicin and epirubicin induce a procoagulant phenotype on endothelial cells and blood monocytes. *Journal of Thrombosis and Haemostasis*, 7(4), 619-626.

Tan, J. J., Capozzoli, M., Sato, M., Watthanaworawit, W., Ling, C. L., Mauduit, M., Malleret, B., Grüner, A.-C., Tan, R. & Nosten, F. H. (2014) An integrated lab-on-chip for rapid identification and simultaneous differentiation of tropical pathogens. *PLoS neglected tropical diseases*, 8(7), e3043.

Tateo, S., Mereu, L., Salamano, S., Klersy, C., Barone, M., Spyropoulos, A. C. & Piovella, F. (2005) Ovarian cancer and venous thromboembolic risk. *Gynecologic Oncology*, 99(1), 119-125.

Tesselaar, M. E. T., Romijn, F., Van der Linden, I. K., Prins, F. A., Bertina, R. M. & Osanto, S. (2007) Microparticle-associated tissue factor activity: a link between cancer and thrombosis? *Journal of Thrombosis and Haemostasis*, 5(3), 520-527.

Thaler, J., Ay, C., Mackman, N., Bertina, R. M., Kaider, A., Marosi, C., Key, N. S., Barcel, D. A., Scheithauer, W., Kornek, G., Zielinski, C. & Pabinger, I. (2012a) Microparticle-associated tissue factor activity, venous thromboembolism and mortality in pancreatic, gastric, colorectal and brain cancer patients. *Journal of Thrombosis and Haemostasis*, 10(7), 1363-1370.

Thaler, J., Ay, C., Mackman, N., Metz‐Schimmerl, S., Stift, J., Kaider, A., Müllauer, L., Gnant, M., Scheithauer, W. & Pabinger, I. (2013) Microparticle‐associated tissue factor activity in patients with pancreatic cancer: correlation with clinicopathological features. *European journal of clinical investigation*, 43(3), 277-285.

Thaler, J., Ay, C. & Pabinger, I. (2012b) Clinical significance of circulating microparticles for venous thrombo-embolism in cancer patients. *Hämostaseologie*, 32(02), 127-131.

Timp, J. F., Braekkan, S. K., Versteeg, H. H. & Cannegieter, S. C. (2013) Epidemiology of cancer-associated venous thrombosis. *Blood*, 122(10), 1712-1723.

Tkach, M. & Thery, C. (2016) Communication by Extracellular Vesicles: Where We Are and Where We Need to Go. *Cell*, 164(6), 1226-1232.

Trappenburg, M. C., van Schilfgaarde, M., Bredewold, E. O., van Aalderen, M. C., Spronk, H. M., ten Cate, H., Leyte, A. & Terpstra, W. E. (2011) Elevated numbers and altered subsets of procoagulant microparticles in breast cancer patients using endocrine therapy. *Thrombosis research*, 127(4), 363-369.

Truong, J., Yan, A. T., Cramarossa, G. & Chan, K. K. W. (2014) Chemotherapy-Induced Cardiotoxicity: Detection, Prevention, and Management. *Canadian Journal of Cardiology*, 30(8), 869-878.

Unruh, D., Turner, K., Srinivasan, R., Kocatürk, B., Qi, X., Chu, Z., Aronow, B. J., Plas, D. R., Gallo, C. A. & Kalthoff, H. (2014) Alternatively spliced tissue factor contributes to tumor spread and activation of coagulation in pancreatic ductal adenocarcinoma. *International journal of cancer*, 134(1), 9-20.

Vadivelu, R. K., Kamble, H., Shiddiky, M. J. & Nguyen, N.-T. (2017) Microfluidic technology for the generation of cell spheroids and their applications. *Micromachines*, 8(4), 94.

Van de Wouwer, M., Collen, D. & Conway, E. M. (2004) Thrombomodulin-protein C-EPCR system - Integrated to regulate coagulation and inflammation. *Arteriosclerosis Thrombosis and Vascular Biology*, 24(8), 1374-1383.

Van den Berg, Y., Van Den Hengel, L., Myers, H., Ayachi, O., Jordanova, E., Ruf, W., Spek, C., Reitsma, P., Bogdanov, V. & Versteeg, H. (2009) Alternatively spliced tissue factor induces angiogenesis through integrin ligation. *Proceedings of the National Academy of Sciences*, 106(46), 19497-19502.

van den Berg, Y. W., Osanto, S., Reitsma, P. H. & Versteeg, H. H. (2012) The relationship between tissue factor and cancer progression: insights from bench and bedside. *Blood*, 119(4), 924-932.

Van Dreden, P., Elalamy, I. & Gerotziafas, G. T. (2017) The role of tissue factor in cancer-related hypercoagulability, tumor growth, angiogenesis and metastasis and future therapeutic strategies. *Critical Reviews™ in Oncogenesis*, 22(3-4).

Versteeg, H. H., Spek, C. A., Peppelenbosch, M. P. & Richel, D. J. (2004) Tissue factor and cancer metastasis: The role of intracellular and extracellular signaling pathways. *Molecular Medicine*, 10(1-6), 6-11.

Viator, J. A., Gupta, S., Goldschmidt, B. S., Bhattacharyya, K., Kannan, R., Shukla, R., Dale, P. S., Boote, E. & Katti, K. (2010) Gold Nanoparticle Mediated Detection of Prostate Cancer Cells Using Photoacoustic Flowmetry with Optical Reflectance. *Journal of Biomedical Nanotechnology*, 6(2), 187-191.

Vinci, M., Gowan, S., Boxall, F., Patterson, L., Zimmermann, M., Lomas, C., Mendiola, M., Hardisson, D. & Eccles, S. A. (2012) Advances in establishment and analysis of three-dimensional tumor spheroid-based functional assays for target validation and drug evaluation. *BMC biology*, 10(1), 29.

Wahba, J., Natoli, M., Whilding, L. M., Parente-Pereira, A. C., Jung, Y., Zona, S., Lam, E. W.-F., Smith, J. R., Maher, J. & Ghaem-Maghami, S. (2018) Chemotherapy-induced apoptosis, autophagy and cell cycle arrest are key drivers of synergy in chemo-immunotherapy of epithelial ovarian cancer. *Cancer Immunology, Immunotherapy*, 67(11), 1753-1765.

Wakefield, T. W., Myers, D. D. & Henke, P. K. (2008) Mechanisms of venous thrombosis and resolution. *Arteriosclerosis Thrombosis and Vascular Biology*, 28(3), 387-391.

Walker, A. J., Baldwin, D. R., Card, T. R., Powell, H. A., Hubbard, R. B. & Grainge, M. J. (2016) Risk of venous thromboembolism in people with lung cancer: a cohort study using linked UK healthcare data. *British journal of cancer*, 115(1), 115-121.

Walker, A. J., Card, T. R., West, J., Crooks, C. & Grainge, M. J. (2013) Incidence of venous thromboembolism in patients with cancer–a cohort study using linked United Kingdom databases. *European journal of cancer*, 49(6), 1404-1413.

Walsh, J., Wheeler, H. R. & Geczy, C. L. (1992) MODULATION OF TISSUE FACTOR ON HUMAN MONOCYTES BY CISPLATIN AND ADRIAMYCIN. *British Journal of Haematology*, 81(4), 480-488.

Wang, Y. J., Qin, C. N. & Witarsa, F. (2018) Clarifying configurations of reaction rate constant for first-order and Monod-type kinetics: A comparative manner and a pursuit of parametric definition. *Waste Management*, 77, 22-29.

Warsinke, A. (2009) Point-of-care testing of proteins. *Analytical and Bioanalytical Chemistry*, 393(5), 1393-1405.

Watanabe, M., Kenmotsu, H., Ko, R., Wakuda, K., Ono, A., Imai, H., Taira, T., Naito, T., Murakami, H., Abe, M., Endo, M., Nakajima, T., Koh, Y. & Takahashi, T. (2018) Isolation and molecular analysis of circulating tumor cells from lung cancer patients using a microfluidic chip type cell sorter. *Cancer Science*, 109(8), 2539-2548.

Watson, S. P. (2009) Platelet Activation by Extracellular Matrix Proteins in Haemostasis and Thrombosis. *Current Pharmaceutical Design*, 15(12), 1358-1372.

Weigelt, B. & Bissell, M. J. (2008) Unraveling the microenvironmental influences on the normal mammary gland and breast cancer, *Seminars in cancer biology*. Elsevier.

Weiswald, L.-B., Bellet, D. & Dangles-Marie, V. (2015) Spherical cancer models in tumor biology. *Neoplasia*, 17(1), 1-15.

Welsh, J., Smith, J. D., Yates, K. R., Greenman, J., Maraveyas, A. & Madden, L. A. (2012) Tissue factor expression determines tumour cell coagulation kinetics. *International Journal of Laboratory Hematology*, 34(4), 396-402.

Welsh, J. A., Holloway, J. A., Wilkinson, J. S. & Englyst, N. A. (2017) Extracellular Vesicle Flow Cytometry Analysis and Standardization. *Frontiers in Cell and Developmental Biology*, 5.

Whitesides, G. M. (2006) The origins and the future of microfluidics. *Nature*, 442(7101), 368-373.

Williams, M. R., Azcutia, V., Newton, G., Alcaide, P. & Luscinskas, F. W. (2011) Emerging mechanisms of neutrophil recruitment across endothelium. *Trends in immunology*, 32(10), 461-469.

Wilson, J. L. & McDevitt, T. C. (2013) Stem cell microencapsulation for phenotypic control, bioprocessing, and transplantation. *Biotechnology and bioengineering*, 110(3), 667-682.

Wojcik, T., Buczek, E., Majzner, K., Kolodziejczyk, A., Miszczyk, J., Kaczara, P., Kwiatek, W., Baranska, M., Szymonski, M. & Chlopicki, S. (2015) Comparative endothelial profiling of doxorubicin and daunorubicin in cultured endothelial cells. *Toxicology In Vitro*, 29(3), 512-521.

Wojtukiewicz, M. Z., Sierko, E., Klement, P. & Rak, J. (2001) The hemostatic system and angiogenesis in malignancy. *Neoplasia*, 3(5), 371-384.

Wolf, P. (1967) The nature and significance of platelet products in human plasma. *British journal of haematology*, 13(3), 269-288.

Wu, M., Ouyang, Y., Wang, Z., Zhang, R., Huang, P.-H., Chen, C., Li, H., Li, P., Quinn, D. & Dao, M. (2017) Isolation of exosomes from whole blood by integrating acoustics and microfluidics. *Proceedings of the National Academy of Sciences*, 114(40), 10584-10589.

Wysoczynski, M. & Ratajczak, M. Z. (2009) Lung cancer secreted microvesicles: Underappreciated modulators of microenvironment in expanding tumors. *International Journal of Cancer*, 125(7), 1595-1603.

Xu, R., Simpson, R. J. & Greening, D. W. (2017) A protocol for isolation and proteomic characterization of distinct extracellular vesicle subtypes by sequential centrifugal ultrafiltration, *Exosomes and Microvesicles*Springer, 91-116.

Yamada, K. M. & Cukierman, E. (2007) Modeling tissue morphogenesis and cancer in 3D. *Cell*, 130(4), 601-610.

Yanez-Mo, M., Siljander, P. R. M., Andreu, Z., Zavec, A. B., Borras, F. E., Buzas, E. I., Buzas, K., Casal, E., Cappello, F., Carvalho, J., Colas, E., Cordeiro-da Silva, A., Fais, S., Falcon-Perez, J. M., Ghobrial, I. M., Giebel, B., Gimona, M., Graner, M., Gursel, I., Gursel, M., Heegaard, N. H. H., Hendrix, A., Kierulf, P., Kokubun, K., Kosanovic, M., Kralj-Iglic, V., Kramer-Albers, E. M., Laitinen, S., Lasser, C., Lener, T., Ligeti, E., Line, A., Lipps, G., Llorente, A., Lotvall, J., Mancek-Keber, M., Marcilla, A., Mittelbrunn, M., Nazarenko, I., Nolte-t' Hoen, E. N. M., Nyman, T. A., O'Driscoll, L., Olivan, M., Oliveira, C., Pallinger, E., del Portillo, H. A., Reventos, J., Rigau, M., Rohde, E., Sammar, M., Sanchez-Madrid, F., Santarem, N., Schallmoser, K., Ostenfeld, M. S., Stoorvogel, W., Stukelj, R., Van der Grein, S. G., Vasconcelos, M. H., Wauben, M. H. M. & De Wever, O. (2015) Biological properties of extracellular vesicles and their physiological functions. *Journal of Extracellular Vesicles*, 4.

Yates, K. R., Welsh, J., Echrish, H. H., Greenman, J., Maraveyas, A. & Madden, L. A. (2011) Pancreatic cancer cell and microparticle procoagulant surface characterization: involvement of membrane-expressed tissue factor, phosphatidylserine and phosphatidylethanolamine. *Blood coagulation & fibrinolysis*, 22(8), 680-687.

Yau, J. W., Teoh, H. & Verma, S. (2015) Endothelial cell control of thrombosis. *Bmc Cardiovascular Disorders*, 15.

Yu, L., Ng, S. R., Xu, Y., Dong, H., Wang, Y. J. & Li, C. M. (2013) Advances of lab-on-a-chip in isolation, detection and post-processing of circulating tumour cells. *Lab on a Chip*, 13(16), 3163-3182.

Yunis, A. A., Arimura, G. K. & Russin, D. J. (1977) HUMAN PANCREATIC CARCINOMA (MIA PACA-2) IN CONTINUOUS CULTURE - SENSITIVITY TO ASPARAGINASE. *International Journal of Cancer*, 19(1), 128-135.

Zhang, H. (2015) Apatinib for molecular targeted therapy in tumor. *Drug design, development and therapy*, 9, 6075.

Zhang, Z. & Nagrath, S. (2013) Microfluidics and cancer: are we there yet? *Biomedical microdevices*, 15(4), 595-609.

Zhu, H., Sarkar, S., Scott, L., Danelisen, I., Trush, M. A., Jia, Z. & Li, Y. R. (2016) Doxorubicin redox biology: redox cycling, topoisomerase inhibition, and oxidative stress. *Reactive oxygen species (Apex, NC)*, 1(3), 189.

Zuchowska, A., Kwapiszewska, K., Chudy, M., Dybko, A. & Brzozka, Z. (2017) Studies of anticancer drug cytotoxicity based on long-term HepG2 spheroid culture in a microfluidic system. *Electrophoresis*, 38(8), 1206-1216.